# JOURNAL OF APPLIED PHYSICS

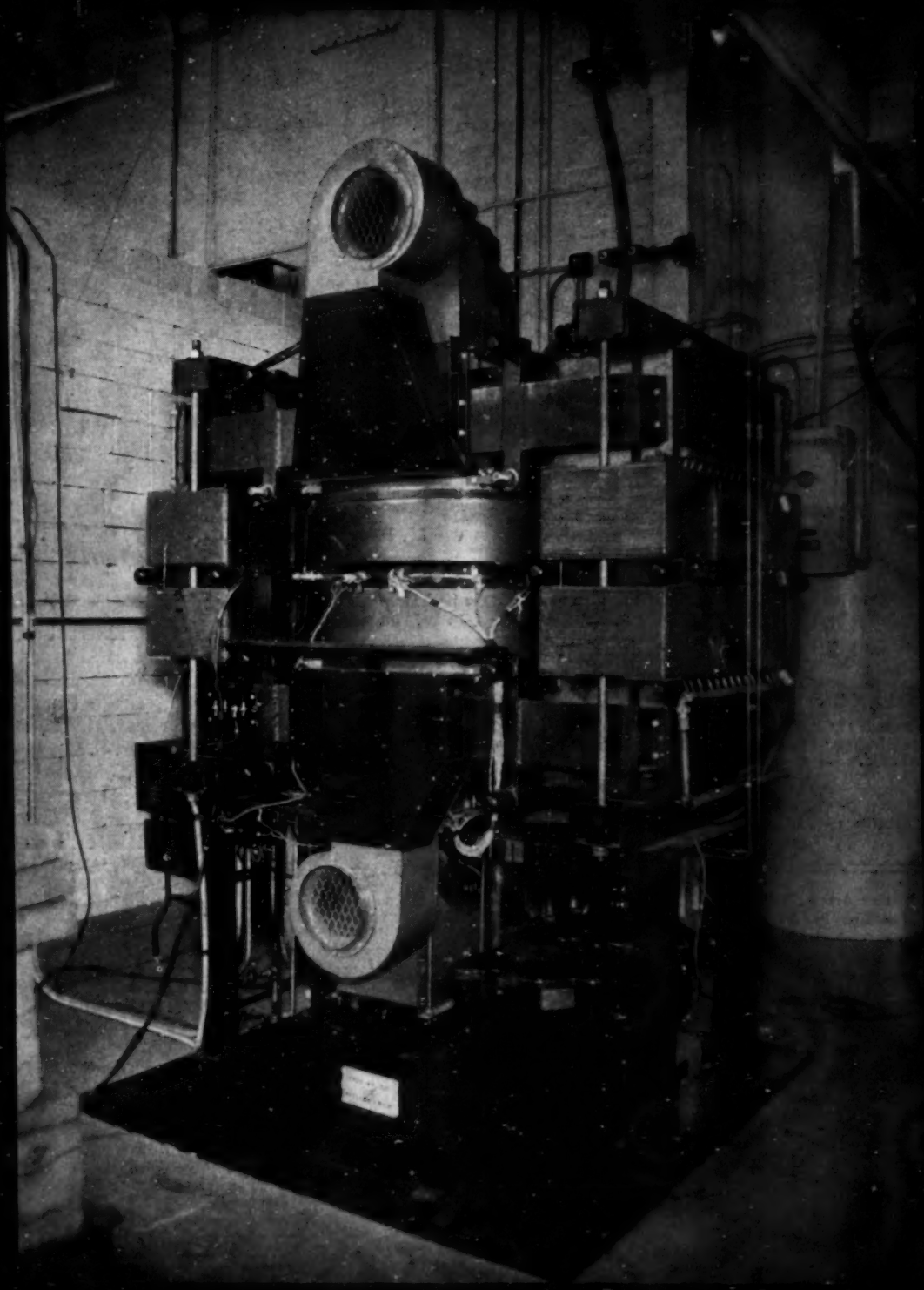

# JOURNAL OF APPLIED PHYSICS

Vol. 18, No. 2 FEBRUARY, 1947


## *In This Issue*


| | | Page |
|---|---|---|
| **Physics in 1946** | PHILIP MORRISON | 133 |
| *Contributed Original Research* | | |
| **Effect of Electron Bombardment upon Carbon Black** | JOHN L. WATSON | 153 |
| **On Cavity Formation in Water** | E. NEWTON HARVEY, WM. D. MCELROY, AND A. H. WHITELY | 162 |
| **New Magnetic Material of High Permeability** | O. L. BOOTHBY AND R. M. BOZORTH | 173 |
| **Apparatus and Techniques for Practical Chemical Identification by X-Ray Diffraction** | C. S. SMITH AND R. L. BARRETT | 177 |
| **Charts for Computation of *d*-Values in X-Ray Diffraction Chemical Analysis** | O. E. BROWN | 191 |
| **Streamlines for Subsonic Flow of a Compressible Fluid Past a Sphere** | E. R. VAN DRIEST | 194 |
| **Minimum Sparking Potentials of Barium, Magnesium, and Aluminum in Argon** | H. JACOBS AND A. P. LAROCQUE | 199 |
| **Fatigue of Ag-$Cs_2O$, Ag-Cs Photoelectric Surfaces** | S. PAKSWER | 203 |
| **Measurement of Elasticity in Fluids of Low Viscosity** | J. R. VAN WAZER AND H. GOLDBERG | 207 |
| **On Creep and Relaxation** | B. GROSS | 212 |
| **Parallel Plate Optics for Rapid Scanning** | S. B. MYERS | 221 |
| **Space Charge Frequency Dependence of Magnetron Cavity** | W. E. LAMB AND M. PHILLIPS | 230 |
| **Reduction of Microphonics in Triodes** | A. H. WAYNICK | 239 |
| **Effect of Hydrostatic Pressure on the Fracture of Brittle Substances** | P. W. BRIDGMAN | 246 |
| **Addendum and Erratum: Thermoluminescence and Conductivity of Phosphors** | R. C. HERMAN AND C. F. MEYER | 258 |
| **Letters to the Editor:** | | |
| **On the Action of Cutting Oils** | G. P. BREWINGTON | 260 |
| **Approximation for Absorption Displacement in X-Ray Diffraction by Highly Absorbing Cylindrical Samples** | ZIGMOND W. WILCHINSKY | 260 |
| *In Every Issue* | | |
| **Here and There** | | 262 |
| **Calendar of Meetings** | | 262 |



**BOARD OF EDITORS**

ELMER HUTCHISSON, *Editor*

*Associate Editors*

R. BOWLING BARNES
OTTO BEECK
W. F. BUSSE
SELIG HECHT
W. JAMES LYONS
PHILIP MORRISON
PAUL E. SABINE
FREDERICK SEITZ
J. R. TOWNSEND
JOHN VON NEUMANN

**Publication of the American Institute of Physics**

**ADMINISTRATIVE STAFF**

HENRY A. BARTON, *Director*
MARGARET S. GRIFFIN, *Publications Manager*
THEODORE VORBURGER, *Business Manager*
JOHN T. TATE, *Adviser on Publications*

**GOVERNING BOARD**

PAUL E. KLOPSTEG, *Chairman*
WALLACE WATERFALL, *Secretary*
GEORGE B. PEGRAM, *Treasurer*
R. B. DOW
L. A. DUBRIDGE
W. F. FAIR, JR.
FLOYD A. FIRESTONE
HARVEY FLETCHER
R. C. GIBBS
K. S. GIBSON
W. H. MARKWOOD, JR.
A. H. PFUND
JOHN T. TATE
L. W. TAYLOR
A. G. WORTHING



The JOURNAL OF APPLIED PHYSICS, published monthly at Prince and Lemon Sts., Lancaster, Pa., is devoted to physics in its role as the science basic to other natural sciences and to the arts and industries. Previous to 1937 this publication was known as PHYSICS. The JOURNAL OF APPLIED PHYSICS publishes editorials, news of physicists, and reviews, as well as technical papers of applied physics.

**Manuscripts** should be submitted to Elmer Hutchisson, Editor, Case School of Applied Science, Cleveland 6, Ohio.

**Subscriptions** and orders for back numbers should be addressed to Prince and Lemon Streets, Lancaster, Pa. or to the American Institute of Physics, 57 East 55 Street, New York 22, N. Y.

**Subscription Price**

| | U.S. AND CANADA | ELSEWHERE |
|---|---|---|
| To members and associate members of the American Institute of Physics | $5.00 | $5.70 |
| To all others | 7.00 | 7.70 |

**Back Number Prices**

Complete set: Vol. 1, July, 1931–Vol. 17, 1946—$108.50
Yearly back number rate: **$7.70**
Single copies: **$0.70** each.

**Changes of address** and proofs should be addressed to the Publications Manager.

**Advertising rates** supplied on request. Orders, advertising copy, and cuts should be sent to the American Institute of Physics.

Entered as second class matter January 22, 1937, at the Post Office at Lancaster, Pennsylvania, under the Act of March 3, 1879.
Accepted for mailing at the special rate of postage provided for in the Act of February 28, 1925, authorized May 2, 1932.



Copyright 1947, by the American Institute of Physics.

Journal
of
Applied Physics

Volume 18, Number 2 February, 1947

# Physics in 1946

BY PHILIP MORRISON

*Cornell University, Ithaca, New York*

NINETEEN forty-six was the first year of peace. Throughout the world, and especially in the United States, the generally difficult problems of reconversion began in earnest. Reconversion meant much for physics and physicists. The strange symbols of wartime work—the SCR-584 radars, the HVAR rockets, the VT fuzes, the compounds of tuballoy—began to lose their compelling interest and their jealously-guarded secrecy. The great "amateur" wartime laboratories, where academic physicists and their industrial and engineering colleagues had worked so hard and so successfully on war program, began to dwindle. The publication of volumes of reports began. And physicists went back, a little rustily, to the problems of the days before the war. Most of those problems were still there, for not much fundamental progress had been made during the war years. But gone was the reluctance to do big things, gone the sometimes valuable, sometimes hampering isolation of the research worker. Physics, especially nuclear physics and its related frontier fields, had grown up. It was pretty well organized, in the wake of the OSRD and the Manhattan Project.

The work of the year very much reflected the problems of the physicist. Much work was begun, but not very much completed. People had plans, often great and exciting ones, but still only plans. Some wits began to talk of the latest "Physical PREview." Teaching loads were heavy, and the flood of students, good and serious and deserving students, drew many research workers away from problems they had almost begun to remember. New laboratories had sprung up, like Oak Ridge and the Argonne, and in the first postwar year began to make their mark on public research.

Most striking of all was the essential disappearance of the peacetime international community of physics. The United States, tired enough by years of war but still incredibly rich by the standards of Europe and Asia, was preeminently the home of physics. Our once good communication with the rest of world had atrophied with the secrecy and the contingencies of wartime. By the end of the year, only a beginning had been made towards a return of the days when physics was truly international. Few physicists hoped more wistfully for anything than for the full restoration of the ways of peace in travel, in publications, and in the spirit of a world-wide science.

The present account is for all these reasons a fragmentary account, mainly of "work in progress," and mainly of work here in America. But it is work of the highest promise for physics, work carried on with the highest hope that in 1947 and the years ahead the best of the old spirit will come to employ the great new tools which are the legacy of war.

## SUPERCONDUCTIVITY

One of the most spectacular results of the year was in the tradition of the world before the war. Professor Richard A. Ogg, working essentially alone in the Chemistry Department of Stanford University, discovered a substance which is electrically superconducting at liquid-air temperatures and even above.[1] This statement has little in common with the dramatic discoveries of new particles, but this work may be as fundamental a step towards the understanding of the strange phenomenon of superconductivity as was the finding of the neutron to nuclear physics.

For decades it has been known that some metals and alloys cooled to very low temperatures lost all electrical resistivity. Resistances of many ohms dropped by twelve or fourteen orders of magnitude when the transition temperature was reached. Strange electrical and thermal experiments could be performed with such extraordinary solids. By moving a ring of the material out of a magnetic field in which it was cooled, a current was induced. This current died away with a time constant given by the inductance and the extremely small resistance of the cold metal. It is told that the Leyden laboratory workers delighted to prepare such persistent currents, and to send the loop, still cold in its Dewar, to a distant place where the lecturer could demonstrate that the current was still flowing, hours or even days after it had been started up! Such conductors demonstrated Lenz's law with a vengeance: their low resistivities meant that the induced currents cancelled the external fields to a T, and magnetic fields thus cannot be set up within superconductors. They are almost perfectly diamagnetic.

The large scale theory of such phenomena is fairly clear, but it is quite unsure what is the electronic and atomic mechanism by which the state of superconductivity is caused. Only one thing seemed essential: extremely low temperatures. No superconductor was known which showed the effect above ten degrees absolute.

Ogg had long been interested in a famous and strange set of substances, the solutions of the alkali metals in liquid ammonia. For twenty years these materials have provided work for physical chemists concerned with the nature of ionization in solution. The example which proved so interesting was the dilute solution of sodium in ammonia, in concentrations of twenty or thirty grams of metal per liter of solvent. That solutions of this kind are sufficiently strange in their other properties was well known. They look like metals, with a quickly-frozen solution having a metallic steely blue luster. At $-50°C$ or so, the homogeneous solution separates in two differently-colored phases, bronze and blue, if slowly cooled. It is not hard to prepare the material. In one method, an annular glass trap is employed, attached to a vacuum line.[2] Water and air must of course be kept out. The sodium metal is placed in the system, and anhydrous ammonia brought into contact with the metal. The system is kept cool, below the boiling point of the ammonia, at $-34°C$, and the solution forms. To demonstrate the superconductivity it is enough to place the liquid solution in its vessel inside a solenoid coil, and to freeze it in liquid air within a matter of ten seconds or so. When the frozen ring is removed from the liquid air, it is placed near a flip coil, and the magnetic field of the ring detected by a galvanometer deflection. A magnetic field will repel the ring strongly, because of the very large *negative* susceptibility of the substance. Such tests seem to prove the superconducting nature of the substance.

It is not quite so simple as that, as usual. Out of a few score preparations, only a few are successful. Apparently the large volume change on freezing causes the solid to crack seriously, and the resistance is the resistance of the cracks and not of the solid itself. One must be patient to find the effect. Two attempts[3,4] to confirm Ogg's work failed to do so, probably for this reason, but it has been confirmed by at least one other worker.

Why the interest? One more superconductor for the handbooks does not sound exciting. But there is a vast difference. This material is a superconductor not at 5 or 10 degrees absolute temperature, but at more than 90°K. Recall that thermodynamically the gap between these tem-

[1] R. A. Ogg, Phys. Rev. **69**, 243 (1946).

[2] J. W. Hodgins, Phys. Rev. **70**, 568 (1946).

[3] Boorse, Cook, Pontius, and Zemansky, Phys. Rev. **70**, 92 (1946).

[4] Daunt, Désirant, Mendelssohn, and Birch, Phys. Rev. **70**, 219 (1946).

peratures is much greater than the gap between the temperature of liquid air and room temperature. Consider, for instance, the amount of work required to remove a given amount of heat energy, say by the use of a mechanical refrigerator. If the region to be cooled is at liquid-air temperature and the condenser of the refrigerator at room temperature, less than one-third as much work is required as if the heat had to be moved from a region at 10°K to a condenser cooled by liquid air. Thus Professor Ogg's solutions hold the suggestion that a superconductor can perhaps be made at room temperature. One cannot predict such a result, of course, but it would be a foolhardy statement now to deny its possibility. A little speculation on what would happen to laboratory apparatus and indeed to all electrical devices if fairly large current density could be achieved *without appreciable ohmic loss* is worth while. Even if no such near-fantastic result ever ensues, the first superconductor at temperatures so "high" as those of liquid air is sure to prove a challenge and a stimulus to the theory of this strange phenomenon.

Ogg predicted this property of the sodium-ammonia system from his own theory[5] of the structure of this unusual substance. His theory is formally strange and unconventional to most physicists, and is unconvincing to this author at least. It involves the notion of paired electrons which move in cavities in the solvent, after escaping from the valence bonds of the alkali metal. These paired electrons have no resultant spin and satisfy a condition years ago proposed to explain superconductivity as an effect bound to occur with particles which have no spin. The stability of these arrangements and the order-of-magnitude of concentrations and temperatures do not appear evident from Ogg's so far preliminary theory. It is to be hoped that the next year will bring wider interest in this remarkable problem both from the experimental and the theoretical side. There is hardly a laboratory which cannot make a superconductor now! Liquid hydrogen generators and the rest of the special techniques of cryogeny are no longer needed.

[5] R. A. Ogg, Phys. Rev. 69, 668 (1946).

## THE PUSH TOWARD HIGH ENERGY

The one most characteristic feature of nuclear physics is the high energy per atom involved in the reactions. Where chemical reactions release a few electron volts for each atom involved, the reactions of nuclear physics release or require millions. The very fact of such high specific energies makes it possible to do experiments in which only individual atoms take part, observability following only from the highly energetic nature of the motions and transformations of the reactants. Nuclear physics—with of course the spectacular and decisive exception of the chain reaction of uranium—does not often work with macroscopic amounts of matter.

But to give even single atoms the millions of electron volts they need often requires large scale apparatus. The engineering which is so typical of such laboratories today began in the first efforts to concentrate a few million volts in ions of hydrogen and heavy hydrogen. Since Rutherford's Cavendish days, this has been done by simply setting up a few million volts potential difference in the laboratory (with a.c., as in a surge transformer set, with electrostatically-generated d.c., as in the familiar Van de Graaff machines) and letting the ions fall through the potential difference in a vacuum tube. Always the demand was for higher energy.

The first energy barrier which it was sought to overcome was the electrostatic barrier, the energy required to bring one positively-charged projectile very near the positively-charged nucleus. One wanted the charges near enough so that the nuclear matter could touch and "stick," to produce new radioactive nuclei and to initiate nuclear reactions. The size of this barrier is easy to compute: the energy of repulsion is $Zze^2/r$, where $ze$ is the charge of the projectile (generally $e$ or $2e$ for protons, deuterons, or alphas), $Ze$ the charge of the target nucleus, ranging to $94e$ for the heaviest known, and the distance $r$ is the nuclear radius, never much larger than $10^{-12}$ cm. The answer turns out to be some ten million electron volts needed to cross the barrier for the most difficult cases. No one has yet established a potential difference above six million or so. But the desire to produce particles with such energies has led to ingenious solutions.

The most famous of these is the cyclotron, in which a modest radiofrequency potential difference of a hundred or two kilovolts is applied again and again to the moving particle which is bent into a spiral path by a large magnetic field. Successive passages across the r-f drop occur uniformly spaced in time and, "resonant" with the r-f frequency, lead to high final energies. The Crocker cyclotron at Berkeley, the largest machine of its kind, is capable of making forty million-volt alpha-particles, which cross any nuclear barrier with energy to spare, and make possible many complicated reactions. Why go further?

The answer is, of course, that there are still more remote objectives. The probing of nuclear matter by bringing the "test charge" which is the rapidly moving projectile closer and closer to the nucleus has given us information about distances of the order of $10^{-12}$ cm or somewhat less; we would like to look at matter even more intimately. The closer the impact, the more energy transferred, the finer the detail of exploration. We learned many years ago that there were particles of very short life, which we cannot find in our laboratories, but which stream in to the earth in the cosmic rays. These objects, known now as mesotrons, because of their mass of 200 electron masses (intermediate between that of electron and proton), are believed on quite general grounds to be associated with those extraordinary attractive forces which make nuclear matter sticky, which bind together the neutrons and protons of the nucleus. The argument for the connection is essentially this: The electromagnetic forces are by now familiar. They are long range forces, falling off as the inverse square of the distance between two interacting particles. Now, these forces, which propagate, of course, with the finite velocity of light can be thought of as caused by the transfer of quanta between the moving charges. This is quite evident for the transverse electromagnetic waves, but it is true at least formally for the static Coulomb field as well. From this point of view electric charges are surrounded by quanta. If there is energy available, these quanta may be set free to go as far as they will. Otherwise they must be emitted, last a very short while, and then be reabsorbed by the particle which emitted them or by another particle nearby. By analogy the same mechanism is used to account for nuclear forces by the exchange of mesons, It turns out that the Compton wave-length, $\lambda = h/mc$, of the particles transferred determines the effective range of the forces. Thus, for quanta, the rest mass is zero, and the "Compton wave-length" infinite, and the range infinite. The force decreases only for geometrical reasons, and is simply inverse-square. But the nuclear forces act only at short range, about $2 \times 10^{-13}$ cm. The rest mass corresponding to such a range is about two hundred electron masses, just that observed for the mesons of cosmic rays. The inference is strong that around nuclear particles there is a transient cloud of mesons, and that if one supplies enough energy by collision or even by energetic "light" quanta, such mesons can be set free. The study of this mechanism would correspond for the nuclear forces to the study of Maxwell's equation, and could lead to the understanding of the nuclear forces in detail. It must be said that since the first suggestion of Yukawa in 1936 that such mesons might exist, reinforced by their discovery in the cosmic rays two years later, the best theorists have worn thin their patience on this theory. No consistent description has yet been given of the properties of nuclear forces. All the more has this challenged experimenters to make mesons in the laboratory and there to study them in the number and the detail which is impossible while their source is still only the cosmic ray.

How much energy does one need? No one knows. There are clues. Certainly at least 100 Mev is needed, just for the rest energy, known to be 200 times the 0.51 Mev which is the electron rest energy. Perhaps they can be made only in positive and negative pairs, as are electrons in the field of a nucleus. Then at least 200 Mev is needed. More will be required to make them in some quantity, for one must do more than merely tickle the threshold of the reaction. So a popular target for the ingenious builders of machines has been 300 Mev. There are some who think that many mesons must be made at once really to study the details of their creation; these pessimists (or optimists) are planning in billions of volts, but still for some years in the future!

The first postwar year saw active construction

on large machines and smaller prototypes, all shooting at the 300-Mev target, or thereabouts.[6] Most direct attack was that planned long ago at Berkeley, where a giant cyclotron had been built. This seventeen-foot magnet was built in 1940, and used during the war in the experiments which led to the construction of the great electromagnetic separation plant at Oak Ridge. By simply extending the cyclotron design to real California scale, 200-Mev deuterons were expected, somewhat short of the popular goal, the more because such particles directed at nuclear particles have an effective velocity not much more than half of that in the laboratory system of reference. The transferrable energy is given by the velocity with which the particles are brought together computed in the frame of reference in which their center of gravity is at rest. Even this energy is most difficult to get with a cyclotron. In the cyclotron, the particles must all spiral out in step, at constant phase, returning in each circuit to the region between the $D$'s, where the high r-f voltage is applied. The familiar resonance condition is that $2\pi f = eH/mc = \omega$, where $e$ and $m$ are the charge and relativistic mass of the particle, i.e., $m = \dfrac{(\text{rest energy} + \text{kinetic energy})}{c^2}$, $H$ the constant magnetic field, $f$ the frequency of the r-f oscillator and $\omega$ the angular velocity of the particle. This implies that the particles at all radii have the same resonant frequency, though some go fast and others slow. This is the key to the success of the machine. But the mass value, hence the resonant frequency, is not, in fact, constant, if the relativistic variation of mass with velocity be considered. For 200-Mev deuterons this is not a small effect. The hope was, however, that by running up the highest possible r-f voltage, several million volts, some particles could be gotten out in spite of their having fallen a little out of phase on each step, for the number of times they need circle in the machine is only a hundred. The giant cyclotron has indeed been operating at Berkeley since November 1, producing its deuterons as planned, but the principle of operation is quite changed, and the deuterons make not a hundred circles in their spiral path, but nearer to ten thousand. And the r-f oscillator is not a giant device producing thousands of kilowatts but an oscillator which would be considered small even for an ordinary-sized cyclotron.

The story of this change is also a story of 1946. It began, of course, much earlier. The start was probably the development of the betatron in which the accelerating voltage is not applied by any electrodes, but is simply the induced e.m.f. caused by the changing magnetic flux in the a.c. magnet, acting on the electrons in their vacuum doughnut as if they were the secondary turns of a transformer. The total induced voltage in present design is only some seventy-five volts per turn, but the electrons come out with a hundred million volts in the General Electric betatron. These particles have circled the primary about a million times, traveling something like a thousand miles in the vacuum tube. The key to this machine is evidently the stability of the electron orbits, so that a chance disturbance from stray fields or by collision with a gas molecule does not throw too many electrons against the glass walls of the vacuum tube. This is a good machine for energies up to several hundred million volts. The 100-Mev General Electric model produced the first man-made radiation of such high energy, but, in spite of hopes and even the illusion of success, probably has made no mesons. Professor Kerst is now engaged in constructing a 300-Mev model, of quite advanced design, at the University of Illinois in Urbana.

In 1945 Professor E. M. McMillan, then at Los Alamos, of the University of California, proposed a new type of acceleration. Actually, the same proposal had been published months earlier and completely independently by the Soviet physicist V. Veksler. The McMillan-Veksler idea[7] stems in a way from the demonstration in the betatron that it was not foolhardy to plan for very long paths in the vacuum tube, if the conditions of stability are properly fulfilled by the design of the machine. The fact that one could count on geometrical stability had been proved in the betatron. McMillan began to think of the use of radiofrequency accelerating electrodes, as in the cyclotron, with stability in

[6] L. Schiff, Rev. Sci. Inst. **17**, 6 (1946).

[7] E. McMillan, Phys. Rev. **68**, 143 (1945); V. Veksler, J. Phys. (USSR) **9**, 153 (1945).

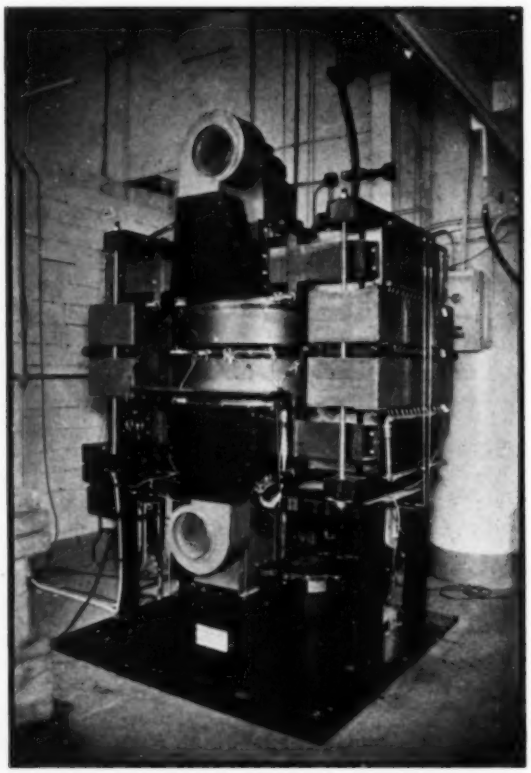

FIG. 1. The first synchrotron to operate in America. This device is installed at the General Electric Research Laboratory at Schenectady, and is under the supervision of Dr. H. C. Pollock. The vacuum tube is visible between the magnet poles.

time, or, as he calls it, phase stability. With such a condition, the resonance condition of the cyclotron might be far from satisfied by all particles, and yet eventually after many turns, the particles might gain a large energy.

For definiteness, think of a particle in the cyclotron at perfect resonance. Each time it reaches the gap between the accelerating electrodes the r-f voltage has reached its maximum. If the particle happened to arrive a little early, the r-f voltage has not yet climbed to its maximum and the particle gets a little less energy than it should have gotten. It will then make the next turn in the field with a somewhat too high angular velocity (the equivalent mass is too small) and arrive still earlier next time. Such a particle lacks phase stability and will gradually fall more and more out of step. It will never gain much energy. Now consider a very different case, that of a particle which arrives when the r-f voltage drop across the gap between electrodes—the accelerating field—has fallen to zero. This particle is just 180 electrical degrees out of phase with the r-f voltage. It will be in resonance, but it will gain no energy in passing the gap. There are two such nodes in the complete cycle. Let us consider the one in which the voltage across the gap is changing from being slightly accelerating through zero to be slightly decelerating. (The other node will not provide stability.) Now suppose the out-of-phase particle arrives just a bit early. It will feel a small amount of an accelerating electric field. It will gain energy, its equivalent mass will increase, its angular velocity go down, it will begin to lag, and next time it will be more nearly 180 degrees out of phase again. If it came a bit late, it would cross a small decelerating potential drop, and be reduced in energy. The mass would go down, the angular velocity go up, and it would come more closely to the 180 degree phase. A particle exactly out-of-

FIG. 2. An oscillogram showing operation of the 75-Mev GE synchrotron. The trace is cut off every 100 microsec. (1) marks the time of electron injection. At this time the machine is operating as a betatron. At (2) the r-f voltage is turned on. The electrons have by now about two-Mev energy. At (3) the r-f is turned off and at (4) is a signal from a photo-multiplier tube placed in the x-ray beam. For this trace the energy was about 20 Mev.

FIG. 3. Another oscillogram of synchrotron operation. The length of the sweep is 1000 microseconds. The trace begins at the time the r-f was turned off, and the electrons soon begin to strike the internal target. The irregular signal shown is taken from the output of a photo-multiplier tube placed in the emergent x-ray beam. Note the complex structure of the beam. This effect is still unclear. The machine is operating between 60 and 70 Mev.

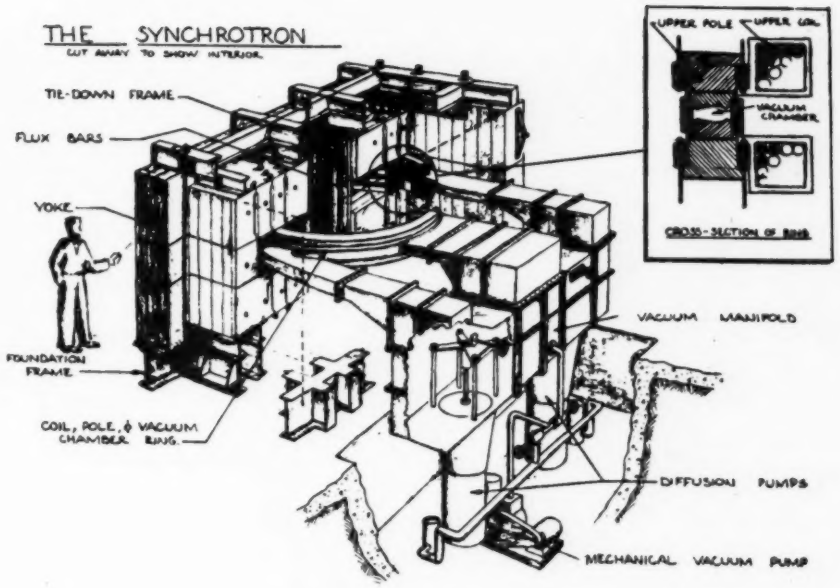


FIG. 4. The synchrotron being built at Berkeley for 300-Mev electrons by the group under Professor E. M. McMillan. The flux bars referred to bars of iron which saturate at a modest field. Until they saturate they strengthen the central field of the machine so that the electrons will accelerate under betatron conditions. When they saturate the electrons are moving at a modest energy, and the synchrotron r-f voltage is turned on.

phase then will have phase stability; it will tend to maintain this condition both at low and at relativistic velocities. Now suppose either the magnetic field or the alternating frequency be slowly increased, changing a little, but only a little, during the time the particle is making its turn in the magnetic field. The stability in phase will act to insure that the particle increases its mass to keep resonant with the increased frequency. The particle will cross the gap just enough before the time when the electric field is zero so that it gains energy sufficient to keep it near resonance. As long as the frequency or magnetic field changes slowly, the particle will oscillate in phase back and forth across the 180 degree time, gaining on the average just enough energy to be resonant under the new conditions. Thus after many turns, picking up a very small amount of the available accelerating energy on each turn, the particle can reach high energy. The frequency may be varied with constant magnetic field, and the particle will spiral out as its energy increases. Or the r-f frequency and orbit radius may stay constant or nearly so and the magnetic field increased. Or combined changes may be made. In all such devices the particles will not be accelerated in a steady stream as in a cyclotron, but in pulses, repeating as rapidly as the frequency is varied or the magnetic field made to increase.

These devices, of which there is clearly a large family, are generically called "synchrotrons." The name is based on the analogy between the motion of the particles and that of the rotor of a synchronous motor. The rotor spins at exactly the synchronous speed with no load. But loading the shaft does not change the speed. The phase slips behind far enough so that the field differences will supply the needed energy to the load. In the same way the particles in the synchrotron slip out of exact phasing, "hunting" in fact for the node, but gaining energy just enough to compensate for the changing frequency or magnetic field.[8]

The first American synchrotron completed is a seventy-five million volt electron machine, Fig. 1. The pulses of fast electrons from this machine are shown in Fig. 2. A synchrotron was made even earlier in Britain[9] by placing a small electrode for the r-f voltage inside a betatron doughnut. The output of the machine went from four millions to more than double that, since the saturation of the central part of the magnet core in the betatron limits the field at the orbit to less than half of practical design saturation values. The stability of orbits in the betatron demands that the central flux change be larger by a

[8] D. Bohm and L. Foldy, Phys. Rev. **70**, 249 (1946); H. C. Pollock, Phys. Rev. **69**, 125 (1946).
[9] Goward and Barnes, Nature **158**, 413 (1946).

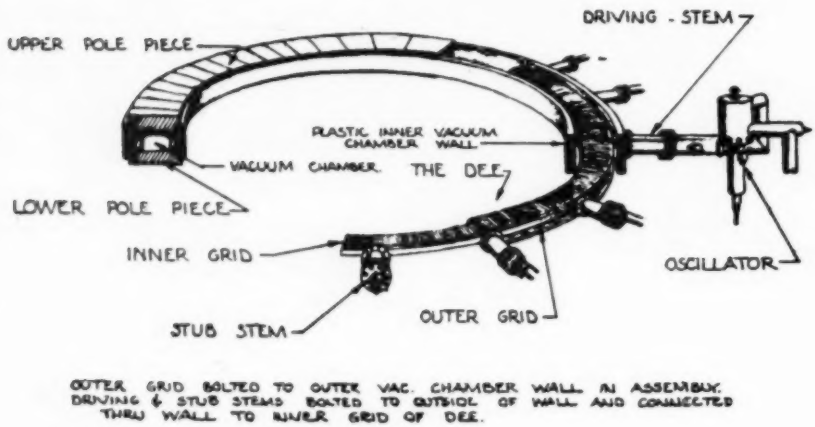
SYNCHROTRON VACUUM CHAMBER ASSEMBLY
EACH POLE PIECE COMPOSED OF FORTY SECTORS. EACH SECTOR LAMINATED OF .014 INCH THICK SPECIAL STEEL SHEET CEMENTED WITH INSULATING & VACUUM-PROOF "REDUX". INDIVIDUAL SECTORS ARE SEPARATED WITH 1/8 INCH RUBBER GASKETS.
DRIVING - STEM
UPPER POLE PIECE
PLASTIC INNER VACUUM CHAMBER WALL
VACUUM CHAMBER
THE DEE
LOWER POLE PIECE
INNER GRID
OSCILLATOR
STUB STEM
OUTER GRID
OUTER GRID BOLTED TO OUTER VAC. CHAMBER WALL IN ASSEMBLY. DRIVING & STUB STEMS BOLTED TO OUTSIDE OF WALL AND CONNECTED THRU WALL TO INNER GRID OF DEE.

FIG. 5. The vacuum assembly for the Berkeley synchrotron. Note the r-f electrode "dee." It is constructed as a grid instead of as a solid electrode to reduce eddy-current losses and fields which would be set up by the strong a.c. magnetic field. The r-f energy is supplied by a pulsed water-cooled oscillator at about 48 megacycles. The stubs are provided to adjust the position of the nodes on this rather high impedance structure.

definite factor than that at the orbit. Synchrotron stability does not require any such condition, for the voltage gain comes from the r-f field imposed by electrodes, and not from the transformer effect except incidentally. The GE machine actually begins the acceleration of its electrons as a betatron; then, when they have reached an appropriate starting energy, the r-f is turned on.

The giant cyclotron is working now accelerating heavy particles not as a conventional cyclotron, but as a synchrotron, or as it is sometimes called, a synchro-cyclotron. Frequency modulation of the r-f supply accomplished by a rapidly rotating condenser in the plate tank of the r-f oscillator brings out the high energy beam, after thousands of turns, with a modest amount of r-f power. The synchrotron principle maintains resonance acceleration in spite of the relativistic variation of mass.[10] The synchro-cyclotron accelerates deuterons, which are caused so far to strike an internal beryllium target, producing a beam of very fast neutrons. The first operation of the machine was on schedule, November 1, 1946, and experiments with the new fast neutrons are already in progress. No mesons have

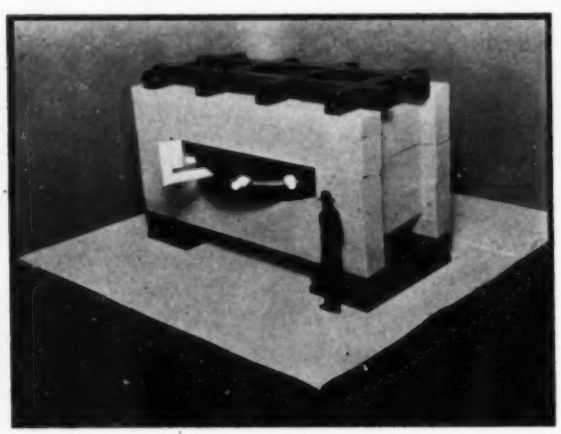

FIG. 6. Photograph of a model of the Berkeley synchrotron showing the driving stem and stubs.

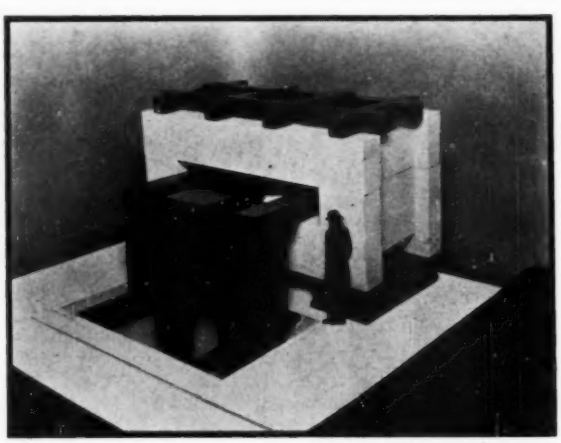

FIG. 7. The other side of the synchrotron model, showing the vacuum pumps in their pit, and the large vacuum manifold.

[10] Richardson, MacKenzie, Lofgren, and Wright, Phys. Rev. 69, 669 (1946).

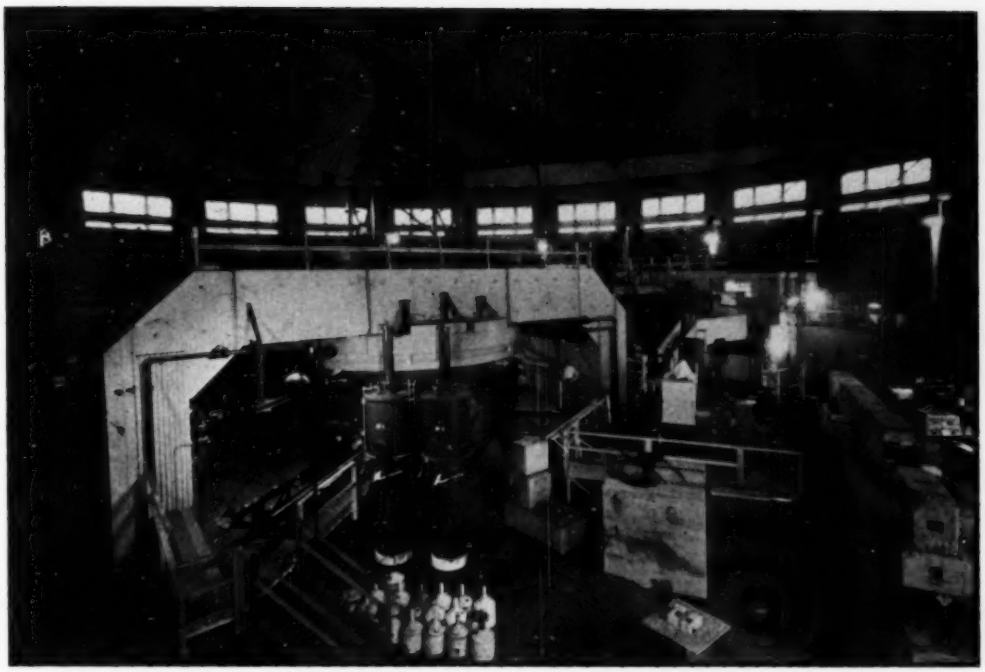

FIG. 8. A general view of the giant Berkeley cyclotron, now operating for 200-Mev deuterons as a synchro-cyclotron. Note the large radial crane of thirty-ton capacity overhead, the magnet with its 184″ pole pieces (there is a man visible against the right leg of the magnet yoke), the two 32″ oil diffusion pumps used for evacuating the vacuum "can," whose thick iron walls are visible between the pole pieces, and the rails, to the left of the pumps, used for removing the ion source. The temporary concrete block shielding wall and a cloud-chamber set-up are seen at the right. (The photographs of this machine were furnished through the kindness of Professor R. L. Thornton, in charge of the giant cyclotron group at Berkeley.)

yet been seen; but important results on the nature of nuclear forces seem sure already (December 15, 1946). It is planned to bring the deuteron beam itself out of the machine in the near future.

Michigan,[11] Massachusetts Institute of Technology, Cornell, the General Electric Laboratory, Berkeley, and no doubt other laboratories are now engaged in design and construction of synchrotron-type electron accelerators of the 300-Mev size, in a variety of ingenious exemplifications of the same principle. The mechanical and electrical engineering problems involved in such work are not small, and many a design variant may have its own special advantages. General problems like starting the particles in their orbits, removing the particles from the machine after acceleration, detection methods specially suited to these pulsed sources, and many others may be expected to build up a whole science of very high energy physics in the next year or two.

One simple and elegant achievement of the year in this field was the first successful removal of a high energy electron beam from the Urbana betatron, at about 20 Mev.[12] The device which did the work is simply a piece of iron shaped like a U-channel, mounted in the vacuum doughnut in the right position. The electrons enter the U-shaped slot, where the iron walls shield them from most of the magnetic field, and shoot out in the field-free space in a straight line to a target or a thin window outside the machine. The success of this device should make possible many experiments with fast electrons, up till now never available in a well-directed beam.

The idea of bending the fast particles in circular orbits and causing them to retrace their steps is evidently economical. But if the magnet grows

[11] H. R. Crane, Phys. Rev. **69**, 542 (1946); Phys. Rev. **70**, 800 A (1946); Pollock *et al.* Phys. Rev. **70**, 798 (A) (1946).

[12] Skaggs, Almy, Kerst, and Lanzl, Phys. Rev. **70**, 95 (1946).

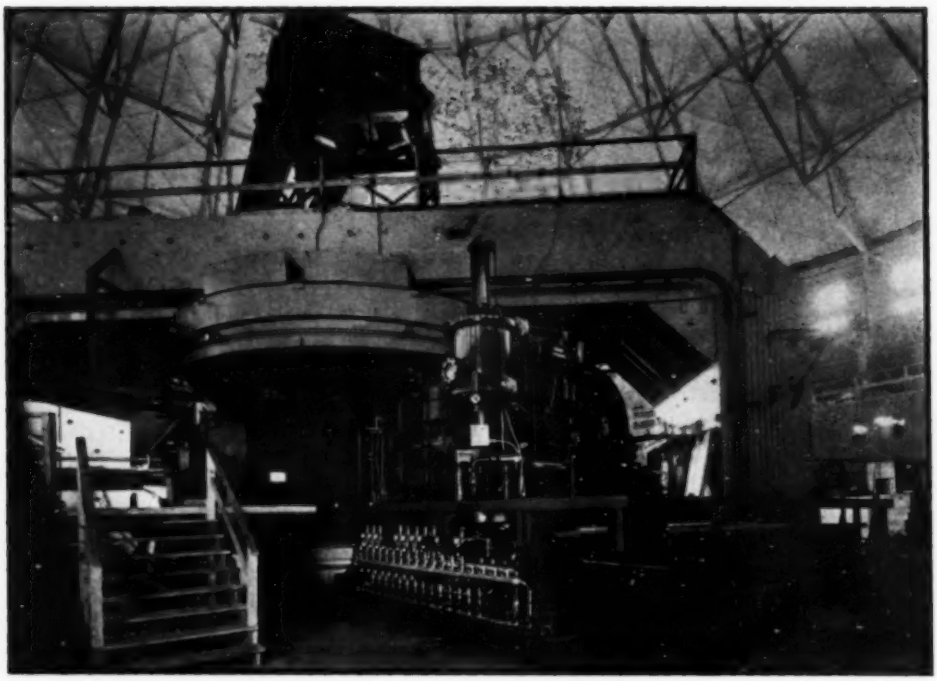

FIG. 9. A view of the big cyclotron from the side opposite to that shown in Fig. 8. In the right foreground, on the truck which moves on rails in the floor, are mounted the round vacuum housing for the rotating condenser, its associated vacuum pump, behind them the oscillator housing. The vacuum chamber is here shown clearly in operating position in the field. To the left may be seen the horizontal rod, which extends into the vacuum chamber holding the internal beryllium probe against which the beam is made to strike. Neutrons were produced at 100 Mev or more on November 1, 1946.

to be very large the economy of the scheme begins to seem less obvious. Perhaps it is better to let the particles fly in a straight line down a long tube. If one can set up a certain electric field strength, the cost of the linear accelerator goes up about as its length (the parts are simply repeatedly placed end-to-end); but if a large magnet needs to be scaled up with the magnetic field kept constant, the volume, weight, and hence the major part of the cost will go up as the cube of the radius. But the energy of particles in their equilibrium orbits goes up only as the radius or, if they are still moving much more slowly than light, as the square of the radius. Thus for sufficiently high energy a linear accelerator will be cheaper than a scaled-up magnetic device. The idea is an old and unsuccessful one; but the familiarity with microwave techniques gained in wartime makes it appear practical once more. Professor Alvarez at Berkeley is now engaged in building a large linear accelerator for protons. Protons enter the machine with a few million volts energy, from a one-step accelerator, in this case a Van de Graaff machine. The vacuum tube down which they fly is one long resonator, made of many resonant cavities placed back-to-back and so driven by individual but phased microwave oscillators at 150 cm that the moving protons enter each cavity in phase with an accelerating electric field. By the time they cross the cavity, one cycle has elapsed, the field behind has dropped to zero, and the next cavity is beginning to acquire an accelerating electric field. There is one difficulty with this simple picture. The protons do not move with uniform velocity, but constantly increase in velocity. If the cavities are driven, as they must be, by an oscillation of one frequency, some trick must be used to keep the protons in step. This is done by adjusting the repeat length of the resonant cavities $l$ so that $l/\sigma = \lambda/c$ where $\lambda$ is the wave-length of the driving oscillator and $\sigma/c$ the velocity of the particle relative to that of light. If the outside cavity diameter is held fixed, the cavities must be

modified in shape to keep them resonant, though of different lengths. In transmission line language the line is a loaded line. A short coaxial cylinder is placed inside the outer cavity cylinder, and the protons move down the axis of the whole cavity. Adjusting the diameter of these central tubes keeps resonance. Each cavity will during half the cycle be decelerating: the electric field will point the wrong way. During this time the proton must be inside the central tubes, and shielded from the wrongly-directed field. The tubes are hence called drift tubes, because within them the protons "drift" under no field.[13] To maintain phase stability and geometrical focusing, it is necessary to place conductors athwart the drift tubes, through which the protons must pass. Thin beryllium foils have been developed for this work. In trials more than a million volts per foot has been developed in a cavity. As yet no coupled cavities have been tried for acceleration, but the first forty-foot unit is soon to be tried out. It is expected that it will be delivering protons at more than thirty-two million volts by February, 1947. New high power radar oscillators have been developed for the job, using the pulsed magnetron principle. Here again the output beam will be pulsed at a rather slow audiofrequency, for the sake of magnetron cooling and performance.

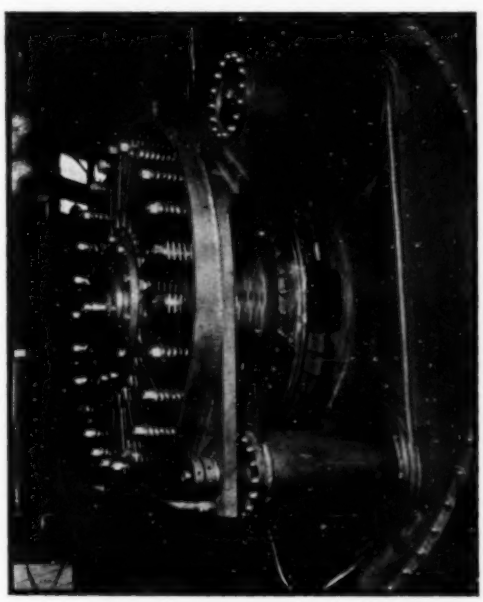

FIG. 10. A close-up of the rotating vacuum condenser whose housing is seen in Fig. 9. The many teeth which produce the varying capacity are plainly visible. The oscillator frequency, which is in the neighborhood of 10 Mc, is varied about 20 percent at a modulation rate of a few hundred times per second by means of this device.

[13] Oppenheimer, Johnston, and Richman, Phys. Rev. **70**, 447 A (1946); L Alvarez, Phys. Rev. **70**, 799 A (1946).

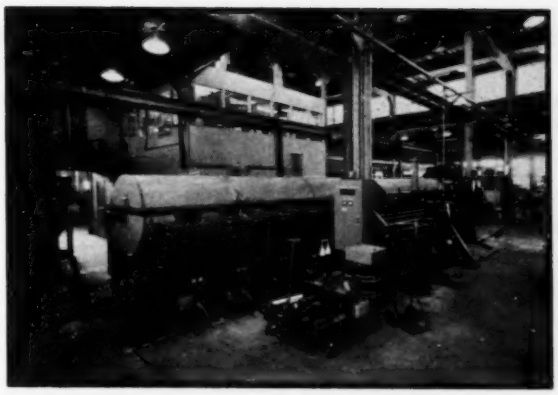

FIG. 11. The forty-foot linear accelerator at Berkeley. Note the large tank of the horizontal pressure Van de Graaff machine at the far right. This is the ion source for the machine. The outer steel tank for the linear accelerator tube itself is conspicious, flanked by the thirty-odd war surplus 1.5-m radar oscillators on either side. Protons in the thirty-to-forty-million volt range are expected by February, 1947. New high power magnetrons are under construction to replace the many oscillators shown here. Only a few of the new magnetrons would be needed for a forty-foot section. (Photo from Professor L. W. Alvarez, heading the linear accelerator group.)

A similar linear accelerator but without the drift tubes and without phase stability can be built for particles moving near the speed of light.[14] High energy electrons are planned for at M.I.T. and at Purdue by groups working on the design of such a device.

If mesons are not made in 1947, it will not be for want of effort! It is to be hoped that enough leisure will be left to plan the experiments which these machines will make possible.

## THE LEGACY OF THE WAR

The year was marked by the widespread if delayed publication of results of the key war projects in physics, and above all, by the return to their old laboratories of hundreds of war-experienced physicists, brimful of information about what had been done, and confident in their understanding of whole fields of technique which had been vague general possibilities in 1940.

[14] J. Slater, Phys. Rev. **70**, 749 A (1946).

## 1. Radar

To this author one of the most fascinating parts of microwave radar has been the duplication in the radio spectrum of the familiar results of physical optics. The "optics" of microwaves—mirrors, gratings, diffraction at openings—are by now familiar to everyone. Not so familiar is the microwave lens.[15] An optical lens works, of course, because the phase velocity of the electromagnetic wave is reduced by the coherent scattering of the bound electrons in the dielectric. Shaping the lens is a matter of adjusting the delay introduced along each ray path to produce a net wave front with the form desired, usually changing the radius of curvature while leaving a spherical incoming wave still approximately spherical. No one has made bound electrical oscillators on a larger scale for microwave optical glass. But the fact has been used that the propagation of a wave in a wave guide, a region bounded by conducting walls, proceeds with an increased phase velocity, *greater* than that of light in free space. (If the reader is worried about relativity, he should review the distinction between wave and group velocity.) By spacing a set of copper plates, their planes parallel to the direction of propagation of the wave, a half-wave-length apart, a change in the phase velocity of the microwave can be secured. Shaping these plates in forms not unlike those of ordinary optics (but with a refractive index always less than one) microwave lenses can be made which quite successfully act as condensing lens, and even produce a fairly sharp focus. They are of course good only for one wave-length. "Chromatic aberration" is large!

Quite the opposite point of view has been used with good effect in recently-reported experiments using microwave radar technique. These experiments were really experiments in measuring the absorption spectrum of water vapor molecules in the region of wave-lengths from 7 mm to about 1.7 cm. An absorption line was found at 1.34 cm and its shape measured as a function of the pressure. The same line could be predicted roughly from the older work on the rotational fine structure in the infra-red region around 20 microns wave-length. Absorption is of course a quantum phenomenon, and it is satisfying to see that the analysis of the instrument—the "spectroscope"—employed came very naturally if one remembered the quantum nature of microwaves.[16]

The instrument consisted of an eight-foot cubical box of copper, arranged to be filled with moist air. Through the box were strung, at random, the detectors, in this case thermocouples. The box was coupled to a pulsed magnetron oscillator—several were used to get points at several wave-lengths—and the space-and time-averaged energy density measured as proportional to the thermoelectric e.m.f. This energy density for a constant excitation is compared with and without the water vapor. The oscillator pumps a fixed number of quanta into the box each second. These quanta are eventually absorbed, either by the walls of the box, the thermocouples, solder, air, and fingerprints of any actual experiment, or by the molecules of water vapor in the box. Since the thermocouple reading is proportional to the density of quanta built up in the box, all that is required is to compare the rate of loss due to the water vapor with some known absolute rate of loss of quanta, and the absorption of water vapor is known for that particular wave-length. But how to get an absolute loss rate? It is difficult to compute such a quantity for walls of a copper cube, the more because of the actual complex nature of the experimental geometry. But the quantum idea gives a direct method. It is necessary only to make a hole in the side of the box. All the quanta that strike the hole must leave the box. This number can be calculated just as the number of molecules leaving an orifice to form a molecular beam can be calculated. The expression is just the familiar kinetic theory formula: the number of quanta leaving through a hole of area $A$ per second is given by $\frac{1}{4}nc$, where $n$ is the number of quanta per unit volume and $c$, of course, their mean velocity—the velocity of light. The whole method of procedure was checked both by experiment and by the more complicated exact calculations of wave theory.

Randomness had to be guaranteed. No standing wave pattern could be allowed. This was as-

[15] W. E. Kock, Proc. I. R. E. **34**, 828 (1946).

[16] W. E. Lamb, Phys. Rev. **70**, 309 (1946); Becker and Autler, Phys. Rev. **70**, 300 (1946).

FIG. 12. A face of the shielding wall of the graphite-moderated pile at the Clinton Laboratories at Oak Ridge. The operation shown is that of exposing a sample to a strong neutron flux, for the production of a radio isotope. The sample in an aluminum holder is being inserted into a hole in a graphite block can be pushed back along a slot into the interior of the pile. The slot is then filled with more graphite blocks to complete the structure, and the shield hole is then plugged. Note the many removable "stringers" of graphite for which shield openings are provided.

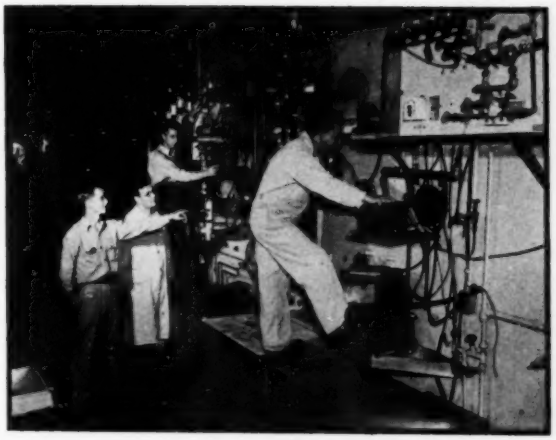

FIG. 13. A face of the "hot lab" at the Clinton Laboratories. This is a concrete cubicle fitted to permit the remote operation of chemical plant adequate for the inorganic separations needed to produce pure radio isotopes from fission product. The air and steam valves and lines, the thermocouple potentiometer, plainly seen in the right foreground are typical for any chemical operation. The periscopes through which the operators are watching the reaction behind the concrete wall are the evidence of the special problems met in the handling of kilogram equivalents of radium.

sured by the slow rotation of some copper-bladed fans within the enclosure, which changed the geometry and made it sure that a random set of normal modes was excited. Diffraction effects were small, because the hole was made large compared to the wave-length. Apertures up to several hundred square centimeters in area were used. The whole experiment not only gave results and pioneered a method sure to be useful for the study of molecular structure, but formed a beautiful illustration of the unity of our dual picture of radiation.

A number of other gas absorption studies have been made at microwave frequencies, using more conventional techniques, like attenuation in a wave guide, or using the atmospheric propagation itself.[17]

## 2. Atomic Energy

The chain reaction of uranium and its consequences are too well known and too extensive to give any general account here. The slow but steady publication of the results of this project will eventually form a sizeable branch of nuclear physics, as they now do in secrecy. The great continuing laboratories at Chicago, Oak Ridge, Los Alamos, and Berkeley, as well as the new regional laboratory at Brookhaven, Long Island, and the power development laboratory at Schenectady will become an integral part of American physics. Some topics selected out of the many possibilities from the Manhattan project will be sketched here.

### *a. Isotopes*

Some hundreds of separate lots of artificial radioactive isotopes have been sold to research workers already by the Isotope Section, Research Division, Manhattan Engineer District, PO Box E, Oak Ridge, Tennessee. This activity will surely continue and expand under the newly formed Atomic Energy Commission, which took over control of the great project from the Army on January 1, 1947. The long-lived soft beta-emitter, $C^{14}$, made in the high neutron flux of the Clinton graphite pile by the reaction $N^{14}(n,p)C^{14}$ which goes well with thermal neutrons, is the material of greatest interest as a tracer in biological studies. The two-week beta-emitter, $P^{32}$, is also in demand, chiefly for its therapeutic value in some cases of leukemia and related diseases. It is made by neutron capture in the

[17] Beringer, Phys. Rev. **70**, 53 (1946); Dicke *et al.*, Phys. Rev. **70**, 340 (1946); Townes, Phys. Rev. **70**, 665 (1946).

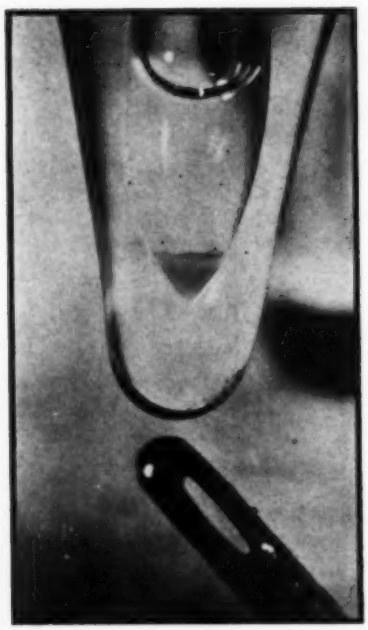

FIG. 14. A microphotograph of the first sample of the new element americium ($Z$-95) ever isolated. The lower part of the photograph shows the eye of an ordinary needle to fix scale. Above it is a small glass capillary, which is the test tube for this sort of chemistry. In the capillary can be seen the curved meniscus of the supernatant solution. At the bottom tip of the *inside* of the glass capillary is the grayish precipitate of americium hydroxide. (Photo furnished by Professor G. T. Seaborg, discoverer of Am.)

normal phosphorus isotope, $P^{31}$. A third popular product is $I^{131}$, which is a fission product, produced in the exposed uranium metal slugs of the pile. These three are only examples, but they indicate the three types of reactions which go with ease in the reacting pile. The technique of separating a particular radioactive isotope out of the complicated mixture which may be formed by bombardment is well shown in Figs. 12 and 13. It always involves remotely controlled chemical operations, with all personnel protected from the radiation emitted by thousands or tens of thousands of curies of activity. The handling of large amounts of radioactive substances is now a well-developed branch of engineering.

### *b. The Transuranic Elements*

The element of highest atomic number and highest atomic weight which is found in nature is of course uranium. But the periodic table now goes well beyond that. In the year 1946 the disclosure and naming of the transuranics had progressed through neptunium, number 93, and plutonium, 94, to americium, 95, and curium, 96.[18] In 1942 plutonium was produced only by cyclotron bombardment beginning with natural uranium. It was obtained in microgram amounts, and the extraordinary techniques developed by the radio chemists to handle such ultra-microchemistry have been admired widely by now. The elements at the top of the table are still made in microgram amounts by cyclotron bombardment. But the starting point may now be the man-made element plutonium, available in kilogram lots! It is interesting that the chemistry of the transuranics, especially of trivalent curium and americium, seems to prove that a new rare earth like series of the periodic table begins with actinium, atomic number 90, and that successive elements essentially are made by adding electrons, not to the outermost 7*s* shell, but to fill the 5*f* shell. This is in close analogy to the rare earths, which may be called the lanthanides, for at lanthanum the 4*f* shell begins to be filled. The transuranics we should call actinides.

It is appropriate here to say that identity and name are now suggested, though not yet officially, for all the elements of the table up to curium, 96.[18] The blanks are to be filled in this way, all by known radioactive isotopes of the element in question: Element 43 will be named by Professor Segrè of Berkeley, probably to be called technesium, from *techne-* art, to indicate that it is artificial only. It has no stable isotopes. The previous identification of a stable 43, called masurium, is certainly in error. Element 61 is now known to be a rare earth fission product. No name has been suggested as yet. Element 85, an unstable halogen, will be called by the beautiful name astasine, from *a-* not, and *stasis-* standing still. Element 87 is known from radioactive work only, not chemically, and on these not quite complete grounds may be named francium, since it was discovered in this sense by a French radio chemist, and is believed to be a homologue of cesium.[19]

[18] Seaborg, Science (Oct. 25, 1946).

[19] See, for example: Seaborg and Segrè, Phys. Rev. **55**, 808 (1939) for element 43, Corson, MacKenzie, and Segrè, Phys. Rev. **57**, 459, 1087 (1940) for element 85, Perey, J. de phys. et rad. **10**, 453 (1939) for element 87. Private communications from E. Segrè, D. Corson, C. Coryell, and A. Turkevitch.

### c. The Pile as an Instrument

The chain-reacting pile forms an excellent device for the determination of the probability of neutron absorption, especially for thermal neutron absorption, by any material. The substance is placed into the reacting structure at a point where the neutron density is fairly high. At such a place, evidently, the absorption of neutrons will have an important effect on the criticality of the whole structure. Since the time required for the neutron density to double in a barely-critical pile is approximately proportional to the difference between the actual reproduction factor of the structure and unity, careful measurements of pile level changes with and without samples introduced provide a very sensitive way of measuring neutron absorption. Macroscopic samples are used, of course, and the cross section per atom can be measured at least relatively with high accuracy. This method has been applied to many elements—all that could be tried—and even, for engineering purposes, to manufactured materials. By oscillating the sample to and fro, from one point of the pile to another where the neutron density was quite different, sinusoidal change in neutron level of the whole pile is produced.[20] This allows the elimination of slow drifts and the amplification of the effects by the use of resonant galvanometer systems. In the hands of the group at Oak Ridge this has become a method suitable for both precision measurement of absorption cross sections, in favorable cases, and in the detection of very small cross sections. A general review of all the neutron cross sections over the whole periodic table is in preparation based on the extensive project work. The pile work was mainly done at the Argonne Laboratory in Chicago and the Clinton Laboratory at Oak Ridge; very beautiful work in the region of fast neutrons was done mainly at Los Alamos; and neutron spectroscopy, with cyclotron velocity selectors or with crystals (see below) at all these places and by sub-contract at Cornell and Columbia. Much of this work is in the press for release; some has appeared this past year.[21]

[20] E. O. Wollan, in press.

[21] For example: Bailey *et al.*, Phys. Rev. **70**, 583 (1946); Barschall, Battat, and Bright, Phys. Rev. **70**, 458 (1946); Rainwater and Havens, Phys. Rev. **70**, 136, 154 (1946); H. H. Goldsmith, a survey article in press.

### d. The Pile as a Source of Neutrons

A well-collimated beam of thermal neutrons defined by cadmium slits only millimeters wide and meters apart was long a dream of neutron physicists. When the intensity in addition leaves little to be desired, real progress has been made. This was made clear in 1946 by the experiments reported from the Manhattan Project—still only fragmentarily—in which the beam of neutrons from a pile was put to work. The Bragg crystal diffraction of neutrons is not a new effect. It has been somewhat obscurely demonstrated in several laboratories. A neutron moving with the energy corresponding to thermal equilibrium in the lattice of the block of graphite in which it has been slowed has a wave-length of a few angstroms. This is just right to give strong low order diffraction maxima from natural crystal gratings. The effect has been put to work in the construction of crystal spectrometers,[22] using not x-ray tubes, sources of the diffracted waves, brass slits, and photographic plates for detectors, but cadmium slits defining a sharp beam of thermal neutrons from the pile, and boron-filed ionization chambers as detectors. The apparatus has had many uses. At Chicago[22] the neutrons have been used to investigate the scattering of neutrons from crystalline compounds. The neutron is scattered with different phase and amplitude by different nuclei. The intensity of scattering

FIG. 15. Another section of the face of the Clinton pile. This suggests at least the kind of geometry applicable to the production of a strong collimated neutron beam. A beam is here emerging from a small hole in the pile face (the opening marked *20*) and being caught in the large lead brick housing in the center of the photo.

[22] Abstracts by Fermi, Zinn, Sturm, Turkel, and L. Marshall, Phys. Rev. **70**, 103 (1946); Borst *et al.*, Phys. Rev. **70**, 557 (1946).

FIG. 16. A German-built V-2 rocket being made ready for flight at the proving grounds in the White Sands region of New Mexico. Note the truck at the left evidently supplying the liquid oxygen fuel to the rocket.

determines the probability of the process, or the scattering cross section. This has long been investigated. But the interference of the scattered amplitudes from the planes of differing nuclei in crystals, or even in molecules, gives a way to measure the hitherto unmeasured phase shifts in the scattered neutron wave. They show up in the relative intensities of the different orders of diffraction from various crystal planes, for example. This effect has no parallel in x-ray diffraction, where the wave is electromagnetic and its phase shift uniform. When this complication is unravelled, use of the neutron diffraction as a supplement to x-ray crystal analysis is likely to interest the workers in this field. Neutrons feel the effect of hydrogen and especially deuterium atoms much more than do x-rays, which are capable of interaction only with the electron cloud. This may lead to the study of the hydrogen atom location in some compounds with the aid of neutrons. The neutrons which have been thermalized leak out of the pile with a velocity distribution just that of a molecular beam of hydrogen leaking out of a chamber at a little above room temperature. Collimated and directed suitably against a crystal of salt or calcite or what you will, a spectrum of the neutrons will be spread out in angle, according to the well-known Bragg law, $n\lambda = d\sin\theta$. Here $\lambda$ is the deBroglie wave-length, $\lambda = h/mv$, and thus the distribution in angle is a distribution in velocity. Putting absorbers in the diffracted beam at any angle will serve to produce the attenuation for the energy of neutrons present at that angle of deflection. This is a physically monochromatic beam of neutrons, not simply a device for selecting the effects of a particular velocity group, like all the familiar time-modulated schemes. Energy resolution and range of usable energies is about as good as the best time-modulation schemes, and—apart from the pile—very much simpler. This scheme has been responsible already for the mapping of several resonance peaks in neutron absorption, for example those of In, Rh, Sm, Eu, and Gd.

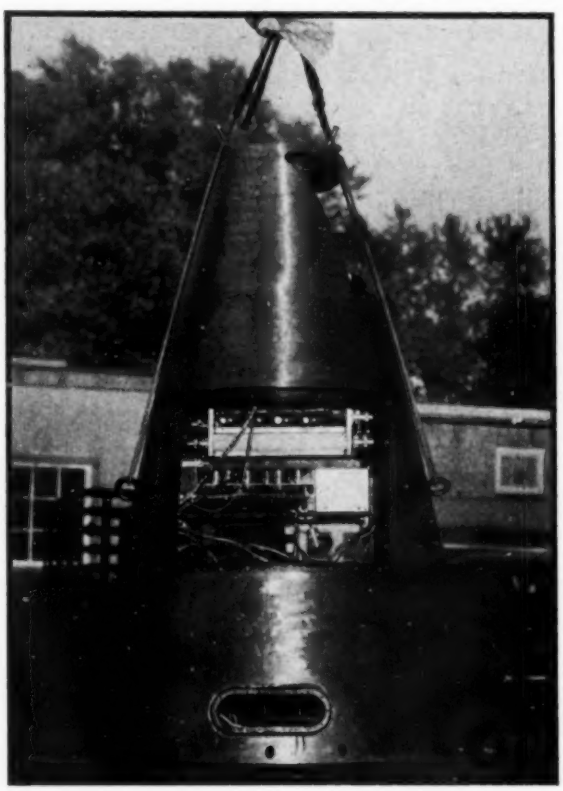

FIG. 17. A war-head of the V-2 fitted with research apparatus, in this case the electronic circuits of a cosmic-ray telescope whose Geiger-Muller tubes "look" through the openings in the war-head. This installation was made by the Applied Physics Laboratory of Johns Hopkins, at Silver Springs, Maryland.

The strong beam has given us one result of decisive importance, a precision re-measurement of the magnetic moment of the neutron.[23] At the Argonne Laboratory, the heavy-water moderated pile, which produces a strong thermal beam, was used as the source for an experiment measuring the magnetic moment of the neutron by polarizing and analyzing the neutrons with ferromagnets through which they passed. The magnetic moment was obtained by observing the resonant frequency at which the polarized beam was partly depolarized by induced transitions in a magnetic field, coming from the Larmor precession of the neutron magnetic moment. (This is the exact experiment of Alvarez and Bloch, an analog to those of Rabi with molecular and atomic beams.) The proton and deuteron moments were measured as calibrating data in the same magnetic field, using the method of nuclear induction in one form (see below). The result was given a conservatively estimated precision of one part in fifteen hundred. To this accuracy the magnetic moment of the deutreron is shown now to be just that of the free neutron plus that of the free proton plus a small calculable contribution arising from the non-spherically symmetric motion of the proton in the deuteron, the known slightly cigar-shaped distribution of charge. No effect of the binding on the nuclear particles themselves is found, to a rather high accuracy. This point is a long debated one in the theory of the lightest nuclei, and sets a necessary condition to be met by any meson theory of the future.

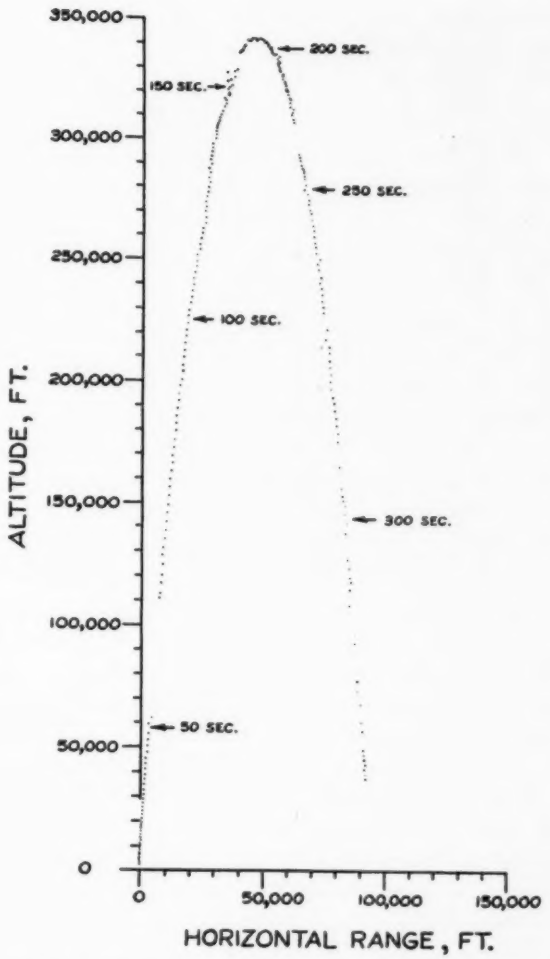


FIG. 18. The graph of the spectacular trajectory of a successful V-2 flight. The high altitude data were obtained by radar tracking. Note that about four minutes is passed in regions beyond the reach of balloons or planes, above 100,000 feet. Not long, but something!

### 3. Rockets

The great technical development of the Axis Powers during the war was certainly the V-2 rocket. For the first time it was possible to launch a projectile of some size into the region beyond the atmosphere. This wartime feat again has meaning for physics. Last year two dozen rockets were launched in New Mexico, most of them reaching altitudes of fifty miles or more. The flight lasts for several minutes, and up to a ton of apparatus can be carried aloft. In cooperation with the ordnance and industrial teams engaged in studying the rockets as weapons, several laboratories have taken advantage of the chance to study the region beyond the atmosphere. Here are the cosmic-ray primary particles, not yet complicated by cloudbursts of secondary particles which they cause on striking the atmosphere. Here may be measured the spectrum of the sun and of the stars, not through the dark glass of the air, but as they come through empty space. Both spectra and cosmic-ray measurements have been made with interesting results.[24] Too little has yet been done to draw any valid conclusions, but it is certain that the exploration

[23] Arnold and Roberts, Phys. Rev. **70**, 766 (1946); cf. Alvarez and Bloch, Phys. Rev. **57**, 111 (1940).

[24] Golian, Krame, and Perlow, Phys. Rev. **70**, 776 (1946); private communication from Applied Physics Laboratory, Silver Springs, Maryland.

of space beyond the air will have real importance for more than one field of physics.

## THE MASS OF THE MESON

For the years since its discovery, the meson has been examined in the cosmic ray in an effort to measure all its properties. Most fundamental, after its charge, is perhaps its rest mass. If the cosmic-ray meson is that predicted in connection with nuclear force theories, its mass should be somewhere between 150 and 250 times that of the electron. Up until 1946 about twenty-five mesons had been observed with sufficient accuracy to make possible some measurement of their mass. The spread in values was great, and it was by no means sure that the meson had only one definite mass. Perhaps the meson was not a unique particle but a whole family.

An excellent experiment just reported[25] seems to have shown that the ordinary meson which makes up the penetrating component of cosmic rays at sea level has one mass, about $202 \pm 5$ times the electron rest mass.

This measurement was made by a very careful and successful application of the usual technique. The method of measuring the mass is ordinarily this: The momentum of the meson can be measured by measuring the curvature of its path as made visible in a cloud chamber across which there is applied a known constant magnetic field. This measurement is made difficult by the accidental deflections of the track of droplets caused by the irregular and turbulent motion of air in the cloud chamber. Then the ionization which the particle produces is measured, by counting the droplets left in the chamber gas, or by seeing what thickness of matter it will penetrate before it comes to rest. This gives the rate at which the particle loses energy by interaction with the electrons of matter, and this is known as a function of the velocity of the particle. The scheme then is to measure the curvature of the track and on the same particle to determine what thickness of lead it will penetrate. The experiment here reported divided up these measurements between two cloud chambers. The upper chamber was free of any obstacles, and carefully controlled in temperature. Track curvature could be measured with minimum difficulty from turbulence. A second chamber mounted two feet below the first and in the same plane was expanded simultaneously, and photos were taken of both chambers. The lower chamber was crossed by eight half-inch sheets of lead. By observing in which plate the track appeared to end the range in lead could be gotten to fair accuracy, and the velocity calculated. The particles observed could be assigned a momentum with a spread due to the error in curvature measurement, and a range with the error coming from the finite plate thickness and other sources. The particles then could each be assigned a mass and a definite error. The spread of values was from 142 to 264 electron masses. Statistical analysis of the data gives the result that a unique mass of 202 $m$ is quite consistent with the data. The observations agree among themselves just as well as can be expected from their individual estimated errors. These mesons have the single mass 202 $m$.

[25] W. B. Fretter, Phys. Rev. **70**, 625 (1946).

## NUCLEAR INDUCTION

For some years the magnetic moment which is intrinsic to nuclear particles and to their motion within the nucleus has been an important object of study. This is a very small magnetic moment indeed, roughly two thousand times less than that associated with a single atom. First evidence for and some measurements of these tiny magnetic dipoles were spectroscopic. They interacted with the current respesented by the orbital motion of the electrons around the nucleus in the atom, and the different orientations the nuclear magnetic moment assumed in the magnetic field resulting from the electrons' motion gave rise to atomic energy levels. These levels are very close together: the energy difference is very small, and the difference in frequency and hence wavelength of the emitted spectral lines very small indeed. Lines which originate in this way are said to be lines of the hyperfine structure of spectra. About ten years ago another and more elegant method was devised, which reached its present form in the work of Professor Rabi and his co-workers at Columbia. Here the nuclei are examined as they stream in molecular beams. Such beams are made to pass through strong inhomogeneous magnetic fields. The nuclear mag-

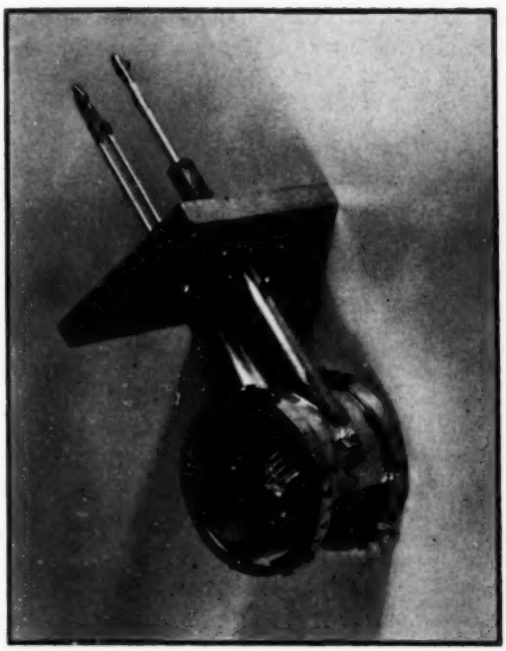

FIG. 19. The receiver-transmitter coils first used to measure the nuclear magnetic moment by nuclear induction. The four heavy turns are the transmitter coil, and the more finely-wound receiver coil is seen within, its axis at right angles to the transmitter coil. Within the receiver coil is placed the sample encased in a half-inch spherical glass bulb. The whole arrangement is shielded heavily. Openings in the shield allow the installation of a rotating copper paddle for adjusting stray fields from without. (Photograph by Professor Felix Bloch of Stanford University, where this work was done.)

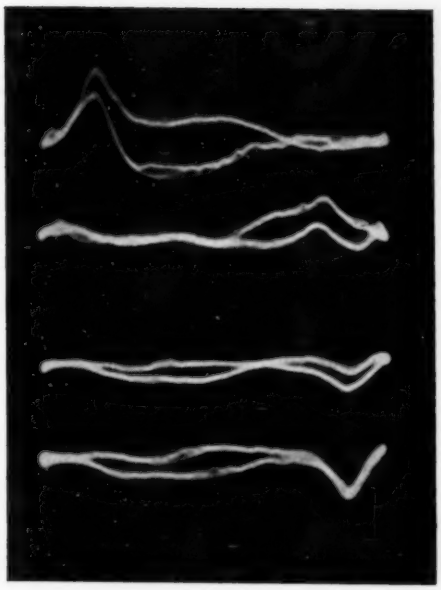

FIG. 20. Oscilloscope traces of the nuclear induction signal. The vertical deflection is proportional to the precessing magnetic moment (or its component in the direction of the axis of the receiver coil), the horizontal deflection to the applied d.c. magnetic field, which has a small, 60-cycle variation in magnitude. The traces shown are those of the proton signal from a water sample. In the top trace the applied field is above the resonance field on the average. The d.c field was lowered in about a second's time to a value below resonance. The proton signal decreased slowly. The next three traces were taken at successive five-second intervals after the reduction of the d.c. field. Note that the signal slowly reverses to a below-resonance condition, though no external change is now going on. This time lag, or "memory," is the consequence of the time it takes for the small nuclear magnets to realign themselves into thermal equilibrium with the new applied field. The time is clearly a few seconds in the case of water. (The double trace is a result of stray 60-cycle pick-up, which separated the forth- and back sweep in the camera exposure.)

netic dipoles feel a force which will depend upon their quantized orientation in space, and the molecular beam will split into several components. These components are each deflected by a different amount, and the deflection may be measured. The deflections one gets with any realizable magnetic fields are small, of the order of hundredths of a millimeter. The method could not by the nature of things be very precise. An elegant adaptation of the molecular beam technique was made by Rabi. He used two equal but oppositely directed inhomogeneous fields. The beam passes through the first and is split into its components. Then the beam is reunited by passage through the second, and strikes a detector. But between the analyzer and the second field there is placed a third region. Here a uniform magnetic field is produced, and also a small radiofrequency magnetic field. The large uniform field has of course no effect on the nuclear dipoles. But the radiofrequency "quanta" may be absorbed whenever their frequency reaches a value such that the quantum energy $h\nu$ equals the energy difference between one orientation of the nuclear magnet in the uniform field and another one. Classically one writes $h\nu = \mu H$, where $H$ is the uniform field strength and $\mu$ the magnetic moment of the nucleus. Fields around a thousand gauss correspond to resonant frequencies of a few megacycles for typical nuclei. Now the nucleus which "absorbs" the quantum is flopped over to a new orientation, cannot be refocused in the second field, and never reaches the detector. By measuring the detector response as frequency or magnetic field are varied, the shapes of the lines corresponding to resonance

with the nuclear magnetic moment can be found. This leads to precision comparisons of nuclear moments, depending only upon frequency measurements, always easy to do well. No nuclear quantities are known with the precision with which nuclear magnetic moments can be found in this way. But the apparatus is delicate and the skill and patience required great. Nor can every substance be gotten into a molecular beam and detected.

It was exciting, then, when not only one but two investigators suggested methods by which the same phenomenon—the flip of the nuclear magnets when they feel an oscillating field of the right frequency—could be detected with no fancy molecular beam techniques. For the first time the macroscopic effect of the nuclear magnets on the magnetic polarization of bulk material was taken into account. Think of a sample of material placed in a magnetic field. The nuclear magnets will line up in the magnetic field to get into the state of minimum potential energy. But of course the thermal agitation of the molecules will act to disorient the magnets. The net result will be given by the usual Curie-Langevin law: the resultant nuclear moment per cc at thermal equilibrium will be approximately $n\mu(\mu H/kT)$, where $n$ is the number of nuclei per cc with magnetic moment $\mu$ per nucleus, $H$ is the applied magnetic field, and $kT$ is Boltzmann's constant times temperature. This is a small contribution to the paramagnetism at best. For protons in water in even pretty high fields it is almost unobservable. What is measured is not the d.c. effect, but a resonant effect at radio-frequency. In one experiment, a resonant cavity was made for about 30 mc.[26] It was filled with paraffin, and was placed in a strong magnetic field, at about 7000 gauss. A weak r-f magnetic field in the cavity was kept perpendicular to the d.c. field. The d.c. field was slowly varied until a sharp resonance absorption was observed. The absorption of r-f energy had changed the $Q$ of the cavity, reduced its output, and affected a detector which had been balanced out off resonance. The same advantages can be claimed for this method as for the molecular beam.

An even simpler technique was applied somewhat later. Here the effect observed is the precession of the resultant nuclear magnetic moment as resonance is approached.[27] The observation is made, not of the reaction upon the driving circuit, but of the e.m.f. induced directly by the precessing nuclear magnets in a pick-up coil in which all e.m.f. had been balanced out off resonance. The nuclear-induced precessing field has a component perpendicular both to the constant field and to the r-f field. It is this component which is observed. No more is needed than a radio oscillator, a lecture table magnet, a transmitter-receiver coil arrangement, and appropriate radiofrequency amplifiers and oscillograph circuits. The coils of Fig. 19 are the heart of the apparatus.

It should be noted that the methods of nuclear induction, as they are called, depend upon the nuclear magnets reaching thermal equilibrium, with their moments oriented not at random, but with the equilibrium resultant value. It is just the macroscopic want of cancellation which makes the whole effect. But the mechanism by which the nuclei come to thermal equilibrium is complex and little-known. If it took weeks for equilibrium to arise, the experiment would be very difficult. The time taken will be a function of the chemistry of the compound and of many atomic features. A whole new subject in atomic physics is opened up by this technique, as well as a simple new supplement to the existing study of magnetic moments. The use of the technique for isotope analysis without any destruction of the sample, isotope analysis by radio, so to speak, may prove of great importance in tracer work with stable isotopes. The whole subject is a good example of how new ideas may arise in fields believed already carried to their highest development. The world of physics is surely infinite.

This sketchy review of the first year of peace is full of promise. The promise will be fulfilled only if physicists can share with all men the prospect which carries all our hopes, the prospect of the many years of peace that lie ahead.

I am glad to acknowledge the kind cooperation of all the busy men who answered letters and supplied photographs to make this account possible.

[26] Purcell, Torrey, and Pound, Phys. Rev. 69, 37 (1946).

[27] F. Bloch, Phys. Rev. 70, 460 (1946) (theory); Bloch, Hansen, and Packard, Phys. Rev. 70, 474 (1946) (exp't).

# Contributed Original Research

## An Effect of Electron Bombardment upon Carbon Black

JOHN H. L. WATSON
*Plant Research Department, Shawinigan Chemicals Limited, Shawinigan Falls, Quebec*
(Received September 9, 1946)

A significant change is reported in mean particle size and shape characteristics of carbon black due to specimen contamination while under examination in electron microscopes. The effect is described for a number of well-known commercial blacks and examples are given in graphical form to illustrate expected variations in mean particle size with continued bombardment at normal focusing intensities. The effect is observed in other materials but is more pronounced in carbon black. Suggestions are made for minimizing the effect.

A CHANGE in any specimen in an electron microscope resulting from the effect of either vacuum or electron bombardment is of interest to electron microscopists both for itself and for the information which may be gained for interpretation of electron micrographs. Very few effects of vacuum upon electron microscope specimens have been reported, although an evaporation of sulphur crystals has been observed. Some modification of specimens in the electron microscope due to shrinkage or evaporation, is discussed in a recent article by L. Marton *et al.*[1] Artifacts introduced into electron images by electron bombardment of a specimen object are also rare. Dulling of sharp crystal corners and edges by bombardment has been noted and charging effects are common, but permanent deformations are not often seen. One notable exception involves the phenomenon of the deposition of insulating films upon metal surfaces under electron beams.[2]

The particular effect reported here is an increase in the mean size of carbon black with bombardment as measured by the methods of electron microscopy. This was observed first with a filmless[3] preparation where the increase is very pronounced. This increase in mean particle size is important from the point of view of its explanation and from the practical standpoint of its influence upon the problem of carbon black particle size and shape determinations.

A qualitative description of the change in appearance of Shawinigan Acetylene Black under bombardment can be described best from an examination of Fig. 1. This figure shows the appearance of a particular field of a filmless sample as the time of bombardment increases. Bombardment times for each exposure are given in the figure caption and refer to the total elapsed period relative to the first exposure. As the bombardment continues the original crystalline appearance of the particles is lost and almost all become round or oval after a few minutes, where previously they were predominantly crystalline and straight-edged. The particles not only change shape, but they increase in size, and fewer are distinguishable. There is a lessening of contrast over the image, less structure is visible in both chains and particles, and the chains become clumps. The change in mean particle size and in appearance is considerable over even short periods of 15 or 30 seconds, but occurs slowly enough that the eye can distinguish it only after discrete intervals. Over the usual times allowed for examination of a specimen in the electron microscope the changes may be unnoticed qualitatively but will be of sufficient magnitude to materially affect particle size frequency distributions and observations of shape characteristics.

The effect has been checked for many preparations of Shawinigan Acetylene Black and has been observed to some extent in all samples studied.

[1] L. Marton, N. N. Das Gupta, and C. Marton, Science **104**, 35–36 (1946).
[2] R. L. Stewart, Phys. Rev. **45**, 488–490 (1934).
[3] J. H. L. Watson, J. App. Phys. **17**, 121–127 (1946).

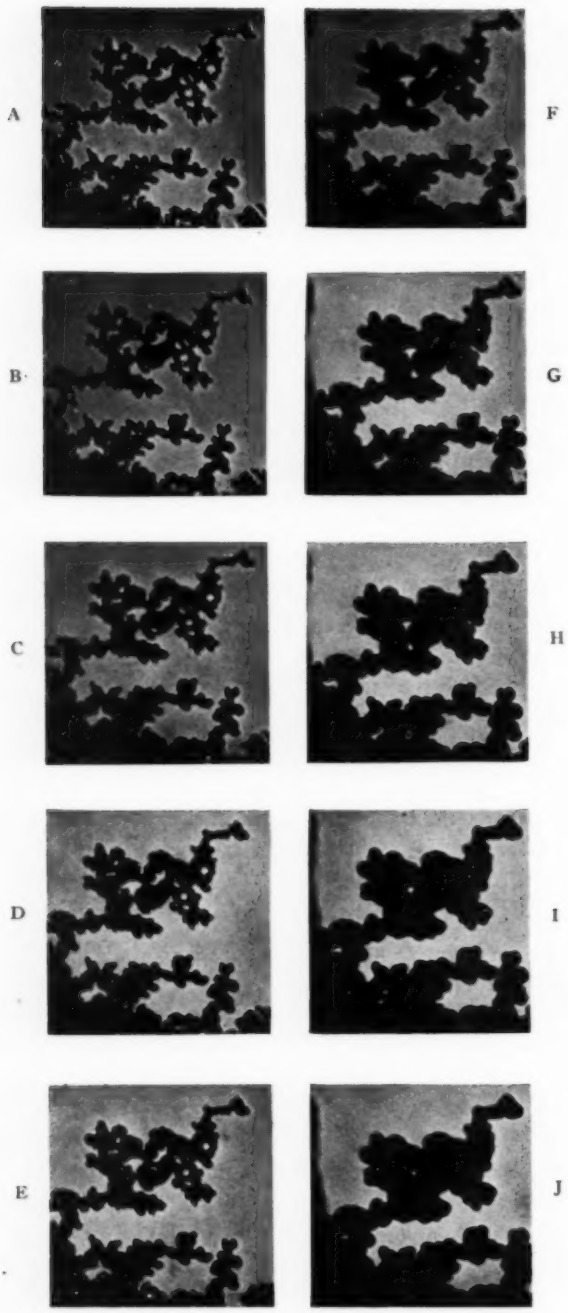


FIG. 1. Shawinigan Acetylene Black under continued bombardment in the electron microscope, filmless preparation ×20,000. Bombardment times are: A, zero; B, 1 min.; C, 2 min.; D, 3 min.; E, 4 min.; F, 5 min.; G, 7 min.; H, 9 min.; I, 11 min.; J, 12 min. relative to the first exposure.

Figure 1 is representative. In general, depending upon intensity, the increase in mean particle size for this black in a filmless preparation is of the

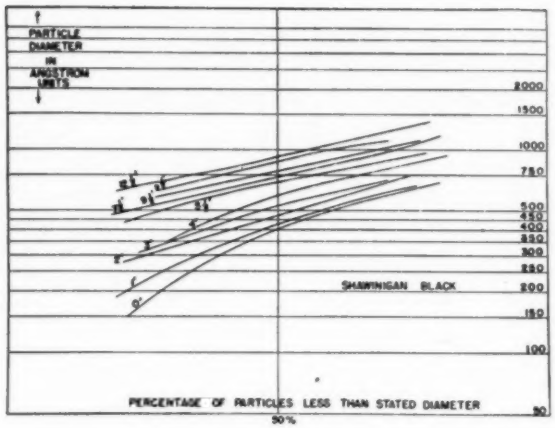


FIG. 2. Particle size frequency distribution curves for each of the exposures in Fig. 1, respectively.

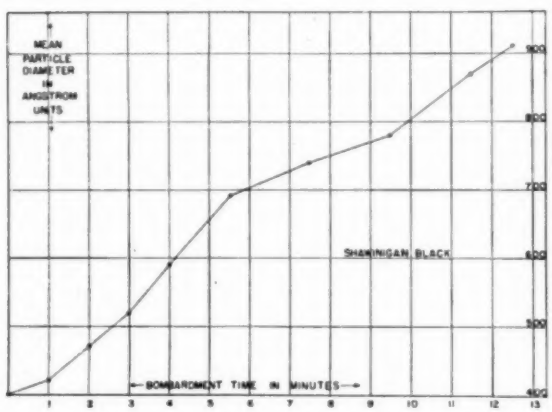


FIG. 3. Mean particle size for each of the exposures in Fig. 1, respectively, plotted against time of bombardment relative to the first exposure Fig. 1A.

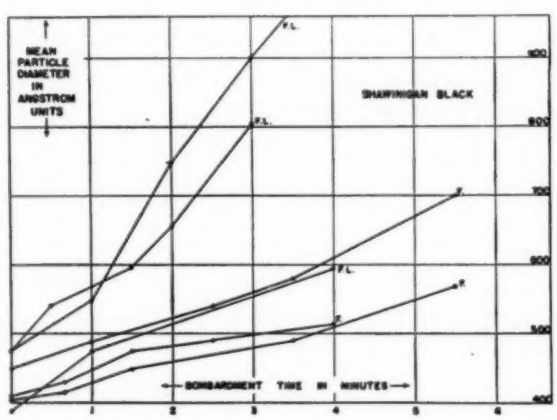


FIG. 4. Other typical increases of mean particle size with bombardment time for filmless and film preparations of Shawinigan Acetylene Black. F., film preparation; F.L., filmless preparation.

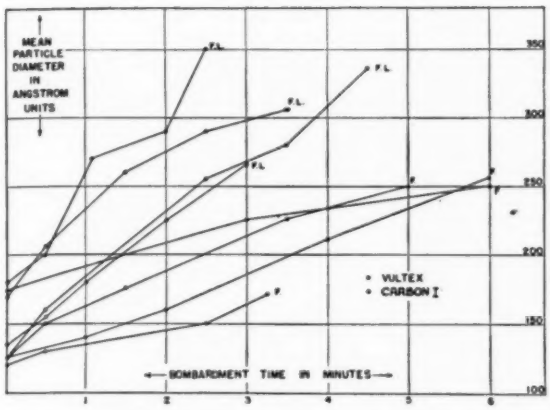


FIG. 5. Typical increases of mean particle size with bombardment time for filmless and film preparations of Voltex and Carbon I. F., film preparation; F.L., filmless preparation.

order of at least 70 percent after 5 minutes bombardment. This is easily a significant value for the type of counting procedure involved. At fairly high, although not focused intensities, the particle size usually will have changed significantly (i.e., say more than 5 percent) in 30 or sometimes in as little as 15 seconds.

In studying a bombardment time series, the same field is photographed after discrete intervals and particle size frequency distributions are obtained from each exposure for comparison. As an example, the frequency distributions, plotted upon logarithmic probability paper[4] (the distributions being negatively skewed), are given in Fig. 2 for each of the exposures in Fig. 1, respectively. In the exposures of this series, too few particles are visible to give good straight lines. The mean particle diameters thus obtained are plotted against time to give the graph in Fig. 3. Other typical increases for acetylene black are shown in Fig. 4. The mean values in the first exposures are within ±10 percent of their arithmetic mean which is fair agreement considering the fact that but one field of the specimen is under study in each case and the number of particles counted is necessarily low. These curves are labeled as being from either filmless or film preparation.* For any particular field, if the intensity is kept constant throughout a run, the relationship between mean particle diameter and bombardment time follows a straight line.

Similar bombardment experiments have been carried out using specimens of such well-known colloidal carbon blacks as Micronex, Voltex, Statex, and P-33. These are structureless carbons as compared with acetylene black which is characterized particularly by its chain structure. Micronex and Voltex are representative of channel blacks of very small diameter. Statex is close to Shawinigan in mean size but is a combustion furnace black, where Shawinigan is formed by a process of thermal decomposition. P-33 is a large diameter black formed by a thermal furnace process. Table I gives (a)—particle sizes for each black represented, (b)—a brief description of the process by which the black is made, and (c) a summary of average values in angstrom units of the increases which can be expected for film and filmless preparations over a 3-minute bombardment period at normal focusing intensity. This table is merely intended to give the reader some idea of expected variation in particle sizes. Other than this it has little significance since the contamination is dependent, as will be discussed later, on several factors which it is difficult to control. Figure 5 gives several curves for mean particle diameter *versus* bombardment time for Carbon I and Voltex. Again, the mean sizes reproduce well from the *first* exposures of the series. Figure 6 shows a typical sequence of Voltex under the electron beam for a film preparation, and

TABLE I. Average increase in mean particle diameter after three minutes of bombardment at normal focusing intensity. The distance of the material from the wire of the grid is unknown.

| Sample | Process of manufacture | Mean* particle diameter | Film mounting | Filmless mounting |
|---|---|---|---|---|
| | | (A) | (A) | (A) |
| Carbon I | Channel Black | 140 | 55 | 155 |
| Voltex | Channel Black | 155 | 110 | 155 |
| Micronex W-6 (EPC) | Channel Black | 295 | 90 | 200 |
| Statex | Furnace Combustion Black | 400 | 115 | 240 |
| Shawinigan | Thermal Decomposition of Acetylene | 430 | 115 | 345 |
| P-33 | Furnace Thermal Black | 1050 | Negligible except at high intensities | |

* The mean particle diameters published here are calculated as an average of the values obtained in these experiments from the particle measurements made on the *first* exposures of the series. The *longest* diameters are taken when measuring a particle. The effect of distortion has been kept as far as possible at a minimum.

[4] J. M. Dallavalle, *Micromeritics* (Pitman Publishing Corporation, New York, 1943), p. 47.

* The term "filmless preparation" is described under reference 3. "Film" preparation referred to here involves blowing the dry carbon from a de Vilbuss atomizer toward a Formvar film over a usual electron microscope specimen holder.

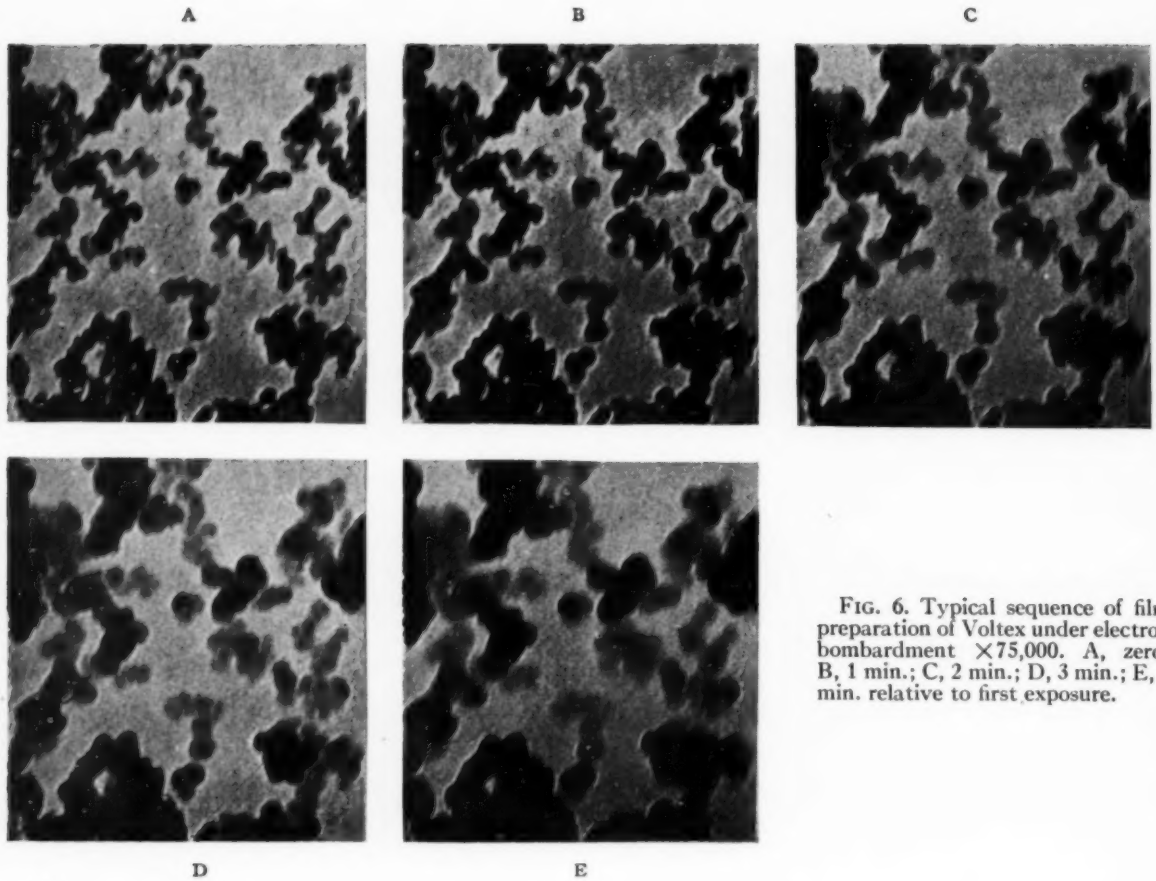


FIG. 6. Typical sequence of film preparation of Voltex under electron bombardment ×75,000. A, zero; B, 1 min.; C, 2 min.; D, 3 min.; E, 4 min. relative to first exposure.

Fig. 7 for a filmless one. Increases of well over 100 percent may be recorded for film specimens of the finest carbons such as Carbon I and Voltex in 3 minutes. From filmless preparations of these two carbons it is difficult to secure particle diameters at all after a few minutes since the clumps seem to coalesce and single particles are no longer visible.

Similar changes are observed with Statex samples and to a marked lesser degree with P-33. However, with very intense bombardment of P-33, large changes are recorded. In general, as would be expected, the percentage increase in mean particle diameter is greatest for blacks of smaller particle size.

Several general observations have been made concerning the relative magnitude of the effect under different conditions of specimen examination. It is more pronounced in a filmless rather than a film mounting. It is zero when the specimen is incorporated into the body of a Formvar film. It is most pronounced at high intensities and may be made negligible if the intensity is lowered sufficiently. With prolonged bombardment of carbon black the effect does not clean up but is permanent, and becomes progressively more pronounced as shown in Fig. 1. The effect is of equal magnitude regardless of whether the sample is on the filament side of the supporting film, or on the reverse side. The carbon "grows" only in that area where the specimen is being bombarded.

That a contaminant surface is deposited, is easily demonstrated by bombardment of a Formvar film which has holes through its surface. The film thickens noticeably and contrast between film and hole space is enhanced by the bombardment, see Fig. 8. Figure 8B was taken after a 3-minute bombardment with all operating conditions and photographic processes, the same as for Fig. 8A. This film thickening will lower resolution and contrast over the specimen but not to a sufficient extent in short times to account for the pronounced increases in mean particle size recorded here. The holes in the Formvar are

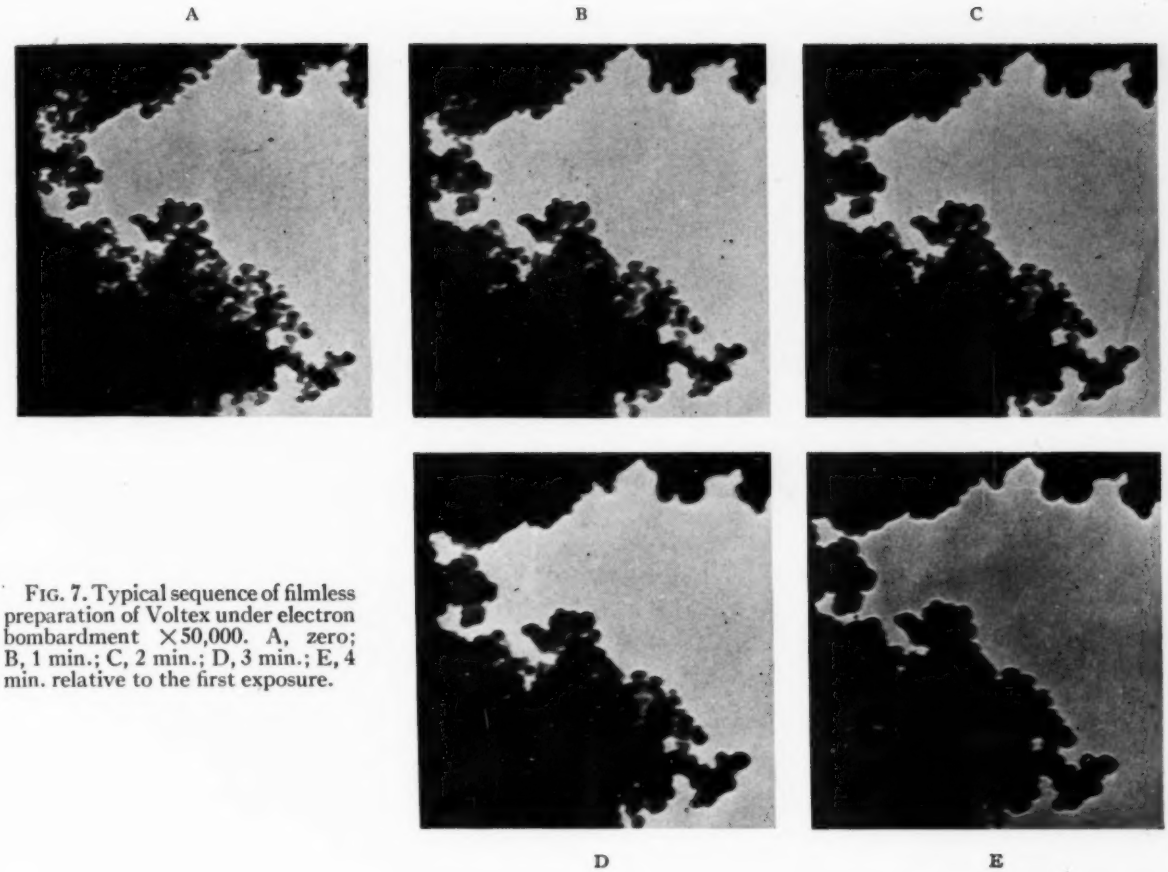


FIG. 7. Typical sequence of filmless preparation of Voltex under electron bombardment ×50,000. A, zero; B, 1 min.; C, 2 min.; D, 3 min.; E, 4 min. relative to the first exposure.

measurably smaller after bombardment; a decrease of about 8 percent occurring in 5 minutes.

It has been pointed out already that a greater contamination effect is observed in filmless than in film preparations. In a filmless one a field is usually chosen which is quite near the metal of the specimen grid. Upon further investigation, it is observed that in either type of specimen preparation, the closer the bombarded area is to the grid wire the greater is the effect of contamination. Figures 9 and 10 are offered to illustrate this. These were taken of the *same* specimen of Shawinigan Black mounted on a filmless holder. Figures 9 A and B were taken of a field in the center of one of the holes, as far from the wire as possible. No change was noted after a bombardment of six minutes. Figures 10 A and B were taken of a field immediately adjacent to the wire. There is an 81 percent change in mean particle size between these two figures after one minute bombardment. The mean particle size changes from 470 to 850 A.

An attempt is being made to relate percentage change in mean particle size with distance from the screen. From preliminary experiments it appears that the very pronounced contamination falls off rapidly and only occurs in a region distant about 8$\mu$ from the wire. This distance will vary with different specimens and electron intensities. In regions further than this from the screen the contaminant builds up more slowly. In order to keep the effect at a minimum, fields for examination should be chosen as far as possible from the metal grid.

The observations cited support an explanation based upon specimen contamination occasioned by the deposition of a hydrocarbon material under electron bombardment after the manner described in reference 2. The mechanism of this hydrocarbon formation in the electron microscope is related to the well-known phenomenon of polymerization and condensation of organic vapors and gases, and certain other gaseous products, under electron or other charged-particle

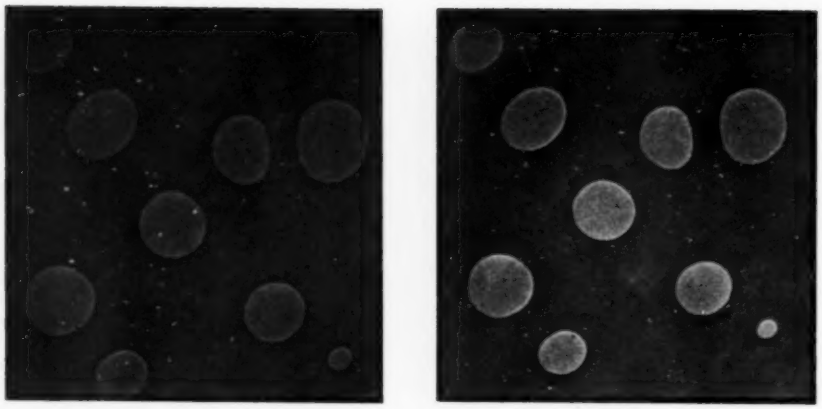

A B

FIG. 8. A, Formvar film before bombardment. B, Same field after three-minutes bombardment ×25,000.

bombardment.[5,6] Theoretically these contaminant surfaces may originate either from organic materials in the metal body of the microscope itself, from grease used to a limited extent on vacuum seals, or from impurities present in the specimen holder and supporting grid. It is con-

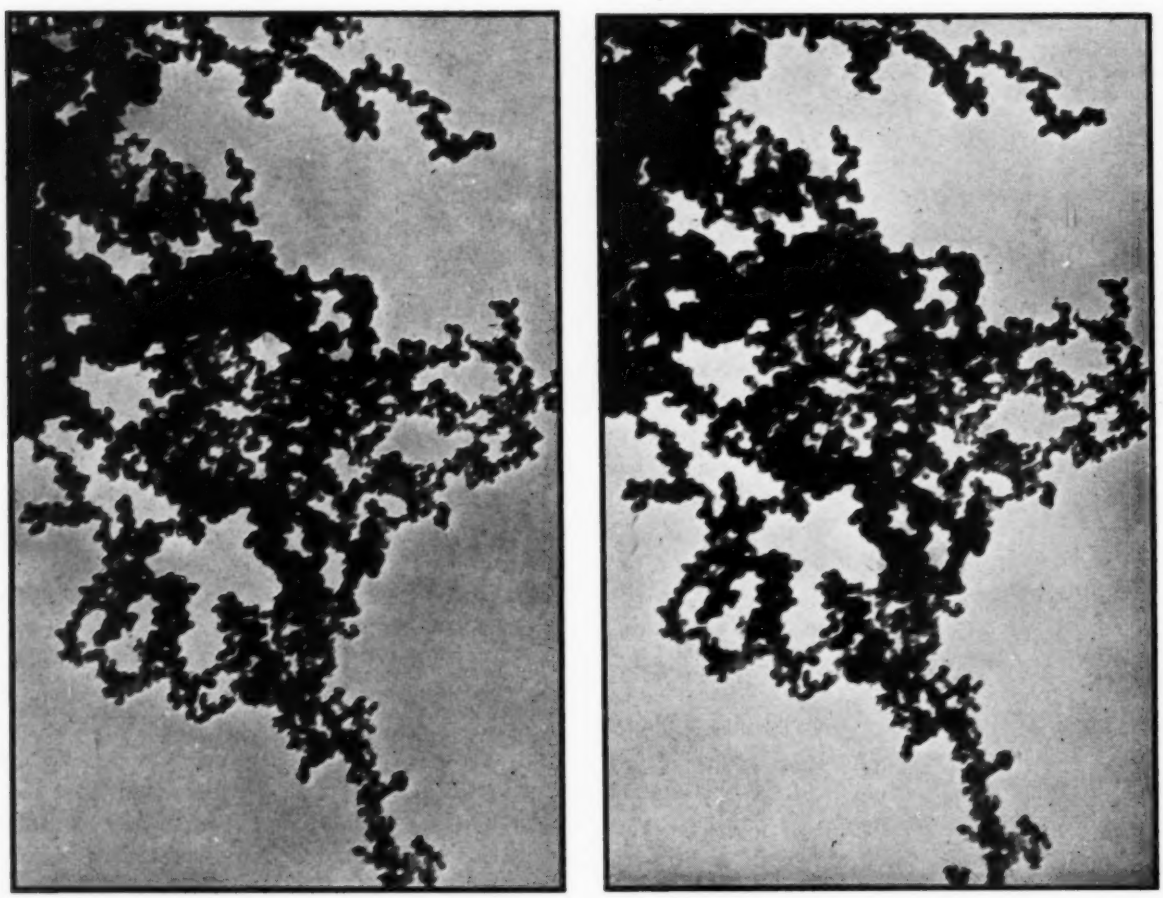

A B

FIG. 9. Shawinigan Carbon Black, filmless preparation, micrograph taken of a field which was as far from the metal wire of the grid as possible. A, no bombardment. B, after 6 minutes of bombardment.

[5] George Glockler and Alvin E. Walz, Trans. Electrochem. Soc. **88**, 151–160 (1945).
[6] J. C. McLennan, M. W. Perrin, and H. J. C. Ireton, Proc. Roy. Soc., **A125**, 246 (1929).

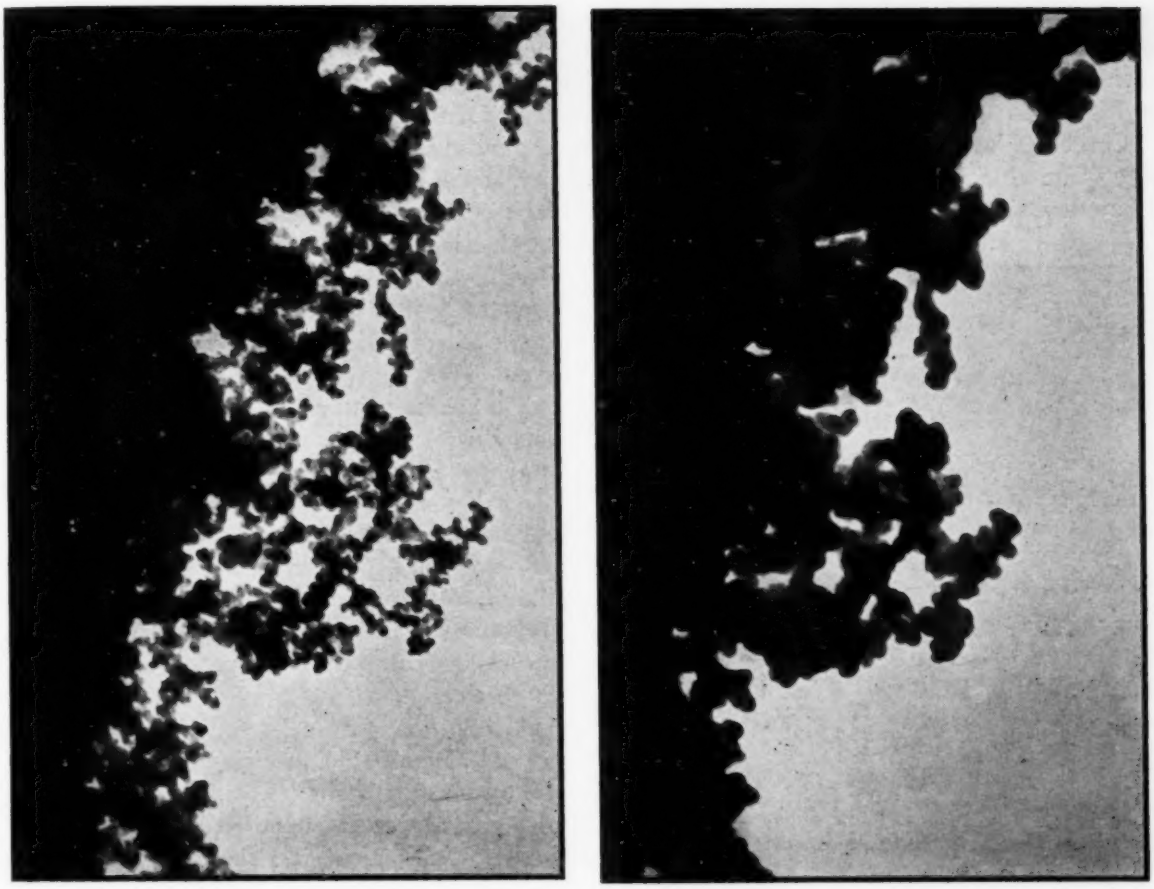

A B

FIG. 10. Same specimen as Fig. 9, micrograph taken under same conditions as Fig. 9 of a field immediately adjacent to the grid. A, no bombardment. B, after 1-minute bombardment.

ceivable also that organic substances present in the object could be distributed as a vapor under the beam and be redeposited upon the particles; but it is known that the percentage of volatile material in these blacks bears no relation to the magnitude of the change.

If we assume that the explanation for the contamination lies in the above paragraph, a reason for the more pronounced effect near the grid can be advanced. The formation of the polymer can be explained from Lind and Glockler's[7,8] experiments upon alpha-ray bombardment and consequent polymerization of acetylene and other hydrocarbons. They suggest that when the molecules in gaseous or vapor state are bombarded by charged particles they are ionized and that they then attract neutral molecules to themselves to form a cluster-ion. When this finally is neutralized a large molecule is formed.[9] This neutralization and resulting deposition of the contaminant will occur most easily upon electron microscope specimens at or near the *conducting* grid.

In order to test this explanation a conductive film of chromium metal was deposited over a Formvar film preparation of Voltex Carbon, by use of shadow casting methods. Under these conditions, marked contamination was observed over the specimen regardless of position relative to the grid. Figures 11 A and B are reproduced of a field

[7] S. C. Lind, and G. Glockler, *The Electrochemistry of Gases and Other Dielectrics* (John Wiley and Sons, Inc., New York, 1939).

[8] G. Glockler and S. C. Lind, J. Am. Chem. Soc. **53**, 3355 (1931).

[9] J. H. L. Watson and K. Kaufmann, J. App. Phys. **17**, 996 (1946).

approximately in the center of a grid hole. The normal degeneration of contrast over the specimen and increase in mean particle size is observed in Fig. 11 B.

Carbon black, and especially Shawinigan Acetylene Black, is particularly conductive. Heavy contaminant deposits would be expected therefore to form upon it. Whereas it is always possible with carbon black to demonstrate a rapid increase in size under bombardment, it has not been found possible in this laboratory to do so to the same extent with other materials.

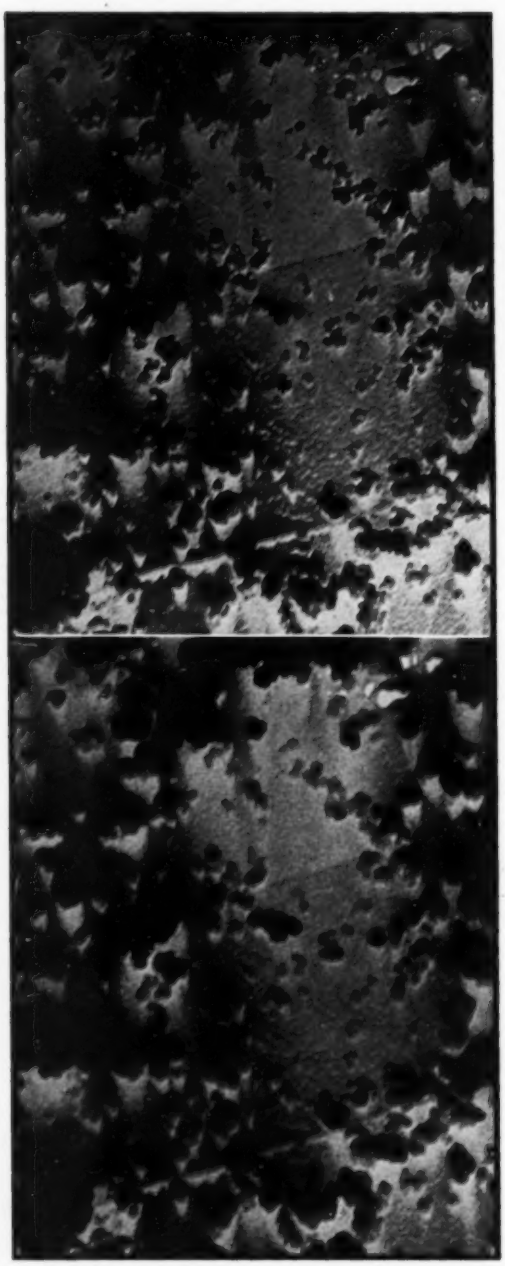


FIG. 11. A chromium shadow cast specimen of Voltex. A, no bombardment. B, after a 4-minute bombardment. The field was chosen far from the grid wire.

The loss of contrast over the specimen and the lack of detail are explainable on a basis of contamination of both the film and the specimen itself. Likewise masking of the small particles; growth of all the particles; and loss of original shape characteristics could be caused by contamination.

That as large an effect is not noted with other substances as with carbon black may be significant also as an indication that the surface of the black has a certain activity for attracting and holding the contaminant permanently so that it will not clear up under continued bombardment. This would conform with the known activity of carbon surfaces in other regards[10] such as their adsorbent, catalytic, and unsaturated electron properties.

Recognition of the existence of the effect points out at least one way in which values from particle size frequency distribution curves can be secured with greater accuracy and reproducibility. Since increases in particle sizes similar to these but of less magnitude have been found to occur to some extent with other materials under bombardment, precautions for minimizing the effect should be followed in all particle size determinations made with electron microscopes.

The change takes place so rapidly with finer carbons that in any micrograph where there is a possibility that it has occurred the *original shape* of the particles is masked almost certainly. Therefore it may distort not only particle size determinations but it may lead to wrong conclusions concerning particle shape and through these to incorrect calculations of specific surfaces. In Shawinigan Acetylene Black for example, the fine, platelet particles appear as round or oval units after a few minutes. In experiments to date the finest carbons such as Carbon I and Voltex appear to be "feathery" in the original uncontaminated condition but rapidly become small, distinct spheres under bombardment. The feathery appearance may be caused wholly by

[10] U. Hofmann and W. Höper, Naturwiss. **32**, 225–226 (1944).

lack of resolution but the possibility exist that some of these extremely fine carbon particles possess crystalline properties and straight-edged shapes in their original condition, much in the manner of Shawinigan Acetylene Black. The shape characteristics however would be within, or near, the limit of resolution, and would not be seen except insofar as they lend the feathery appearance to the image.

The effect may be made zero by incorporating the black samples into the supporting film. However, the sample manipulation required in effecting this type of mounting will tend to change the appearance of the carbon from what it was originally, causing structure breakdown and making interpretation of results more difficult and less reliable. In this laboratory it is desirable to study the black as much in its normal state as possible and therefore dry mounts are essential. It is in these that the change under bombardment is considerable. Therefore it becomes a necessity that conditions in the microscope be kept such that a minimum of change is possible. To do this the following rules of procedure are followed: (1)—the intensity is kept at a minimum, (2)—micrographs are taken as rapidly as is practically possible, (3)—focusing is often carried out using a part of the field which is not to be photographed, and (4)—fields are photographed which are as far as possible from the metal of the specimen grid. If a black is bombarded at fairly high intensity, (focusing intensity) for any length of time longer than 15 seconds a correction downward in particle size should be applied. It is impossible to give a value for this correction here as it will depend upon the time taken for focusing and the intensity used by the individual microscopists.

Many of the observations and much of the information concerning contamination is contradictory and incomplete. Since it is becoming an increasingly important problem in electron microscopy an exchange of information on the subject in publication is needed in order to clarify many aspects of it.

# On Cavity Formation in Water*

E. Newton Harvey, Wm. D. McElroy, and A. H. Whiteley
*Department of Biology, Princeton University*

(Received October 28, 1946)

Phenomena involving the tensile strength of water have been studied by a kinetic method—high speed motion photography of the rapid movement of a blunt glass rod (5 mm diameter) in a narrow (16 mm inside diameter) glass tube of water. Special precautions have been taken to remove all hydrophobic patches and small gas masses (gas nuclei) but to retain the dissolved gas (air at one atmosphere) in the water. If the rod surface contained gas nuclei, or was hydrophobic and free of gas nuclei, cavitation occurred at the rear end when the velocity was less than 3 meters/sec., but if completely hydrophilic and free of gas nuclei, the velocity could be 37 meters/sec. or 83 miles/hour without cavitation. Addition of a detergent (diactyl sodium succinate) to the water did not prevent cavitation at a low velocity with the hydrophobic rod free of gas nuclei. Movement of a rod in pure corn syrup (viscosity 20.1 poises), free of gas nuclei, left a large cylindrical cavity that collapsed in a matter of hundredths of a second. It is not possible to calculate the tensions developed in these experiments, but it is pointed out that the velocities attained without cavitation are far higher than previously observed for movement of bodies in an aqueous medium, a result believed to be owing to the absence of all gas phases and hydrophobic surfaces.

## INTRODUCTION

DURING a study of bubble formation in the blood and tissues of animals—a condition leading to such symptoms of decompression sickness as the "bends"—the conclusion was reached that a decrease in hydrostatic pressure, i.e., a tension in the tissues, was one of the primary factors involved. Favoring this view is the observation that straining movements and muscular exercise at simulated high altitudes greatly increase the incidence of bends in men or of bubbles in animals.[1] This work led to investigation of the tensile strength of pure water containing dissolved air, and it is the purpose of this paper to describe the method and certain observations in connection with the experiments. Calculation of the actual tensions involved has not been attempted, but all relevant data are given.

There is a general belief that water under tension can be easily torn apart; that it is only necessary to reduce the pressure to that of water vapor in order to obtain profuse bubbling and boiling. Actually, the boiling which occurs at the vapor pressure is because of the presence of minute gas pockets adhering to dust particles in the water or on the walls of the container. The gas phase serves as a gas nucleus to start the cavitation. It is a simple matter to show that if gas nuclei are removed, water in non-capillary spaces can be subjected to high vacua or can be heated to over 206°C without boiling,[2] although evaporation from the surface is rapid (Harvey *et al.*[3]).

Many experiments, recently reviewed by Vincent[4] and discussed by Dean[5] indicate that a water column in a well-cleaned container can be subjected to a tension measured in atmospheres without breaking. The maximum values for this tension have been obtained by means of the thermal contraction method. In this method a glass tube, *completely* filled with the liquid at a higher temperature, is slowly cooled. The differential contraction of liquid and container then exerts the tension that finally pulls liquid from the walls with a sudden click. Dixon[6] obtained 150 atmospheres and Vincent[4] 157 atmospheres, using this method.

Both values are far short of the 10,000 atmos-

* The work described in this paper was done under a contract recommended by the Committee on Medical Research, between the Office of Scientific Research and Development and Princeton University.

[1] For a general discussion of decompression sickness and bubble formation, see E. N. Harvey, Bull. N. Y. Acad. Med. **21**, 505 (1944).

[2] The vapor pressure of water at 206°C is 17.3 atmospheres and at 270°C, the highest temperature to which Kenrick, Gilbert, and Wismer, J. Phys. Chem. **28**, 1297 (1924) could superheat water, is 54 atmospheres.

[3] E. N. Harvey, A. H. Whiteley, W. D. McElroy, D. C. Pease, and D. K. Barnes, J. Cell. Comp. Physiol. **24**, 23 (1944).

[4] R. S. Vincent, Proc. Phys. Soc. London **53**, 126 (1941) and **55**, 41 (1943).

[5] R. B. Dean, J. App. Phys. **15**, 446 (1944).

[6] H. H. Dixon, Proc. Roy. Dublin Soc. **14** (N.S.), 229 (1914).

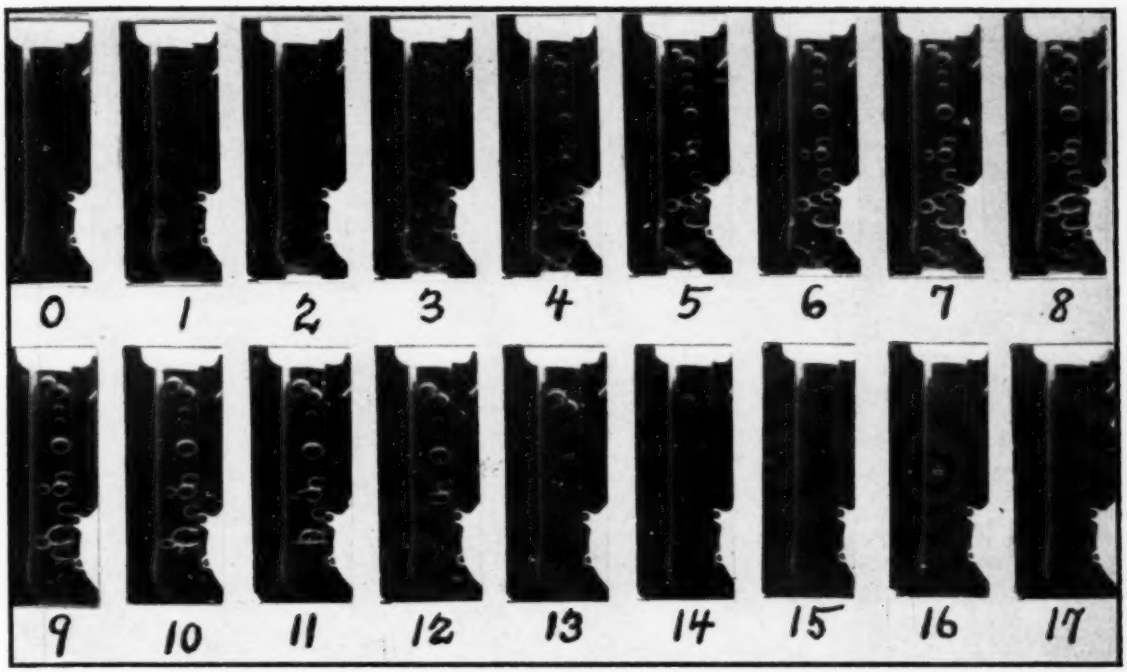


FIG. 1. Moving picture of cavity formation due to a pressure pulse (with negative pressure component) which arises when the bottom of a glass tube containing highly evacuated water (vapor pressure = 19 mm Hg) is struck a blow with a wooden block. The block appears in frame 1 and disappears in frame 10. Note that the cavities, which have enlarged from gas nuclei, first become of maximum size near the bottom of the tube and last longest near the top of the tube. Tube diameter 19.3 mm, 140 frames per second. Exp. 6-9-43.

pheres for the mutual attraction between the water molecules, or the "intrinsic pressure" within the liquid, possibly because breaking is not simultaneous across a unit cross-sectional area. On the other hand, the variation in experimental values from 5 to 157 atmospheres that have been obtained by different workers, may be a reflection of insufficient removal of small gas masses.* In every experimental investigation of the tensile strength of water the container is as important as the water. Not only must there be no gas nuclei on the walls but also no hydrophobic surfaces must be present, since water does not adhere to these surfaces and readily separates from them. Both these conditions indicate that a relatively small amount of water and a minimum surface area of easily cleaned hydrophilic material is essential for experimental work. Glass is unquestionably ideal for the surface since the water-glass contact angle is zero.

In addition to the previously mentioned thermal contraction method of exerting tension on water, kinetic methods are also available. In one of these the bottom of a tall glass tube filled with water, which has been exhausted to the vapor pressure, is struck a sudden blow. The blow moves the glass wall of the tube sufficiently to start a pressure pulse with a negative component. The cavitation and bubble formation under those conditions are well known. In Fig. 1 is reproduced a series of prints from a high speed moving picture which show the resulting cavitation when the bottom of a tube of evacuated water (vapor pressure = 19 mm Hg) is hit with a wooden block. The cavities have started from gas nuclei.

Another method of developing tension is to move a long tube of water rapidly in the direction of its open end and suddenly bring it against a rigid barrier or stop. The momentum of the moving water tends to pull it apart.

Although the above two procedures have readily caused cavitation and bubble formation if gas nuclei were present, after the removal of

* Additional references on the tensile strength of water which have recently come to the attention of the author are: A. L. King, Proc. Nat. Acad. Sci. **30**, 155 (1944) and H. N. V. Temperley and L. G. Chambers, Proc. Phys. Soc. London **58**, 420, 436 (1946).

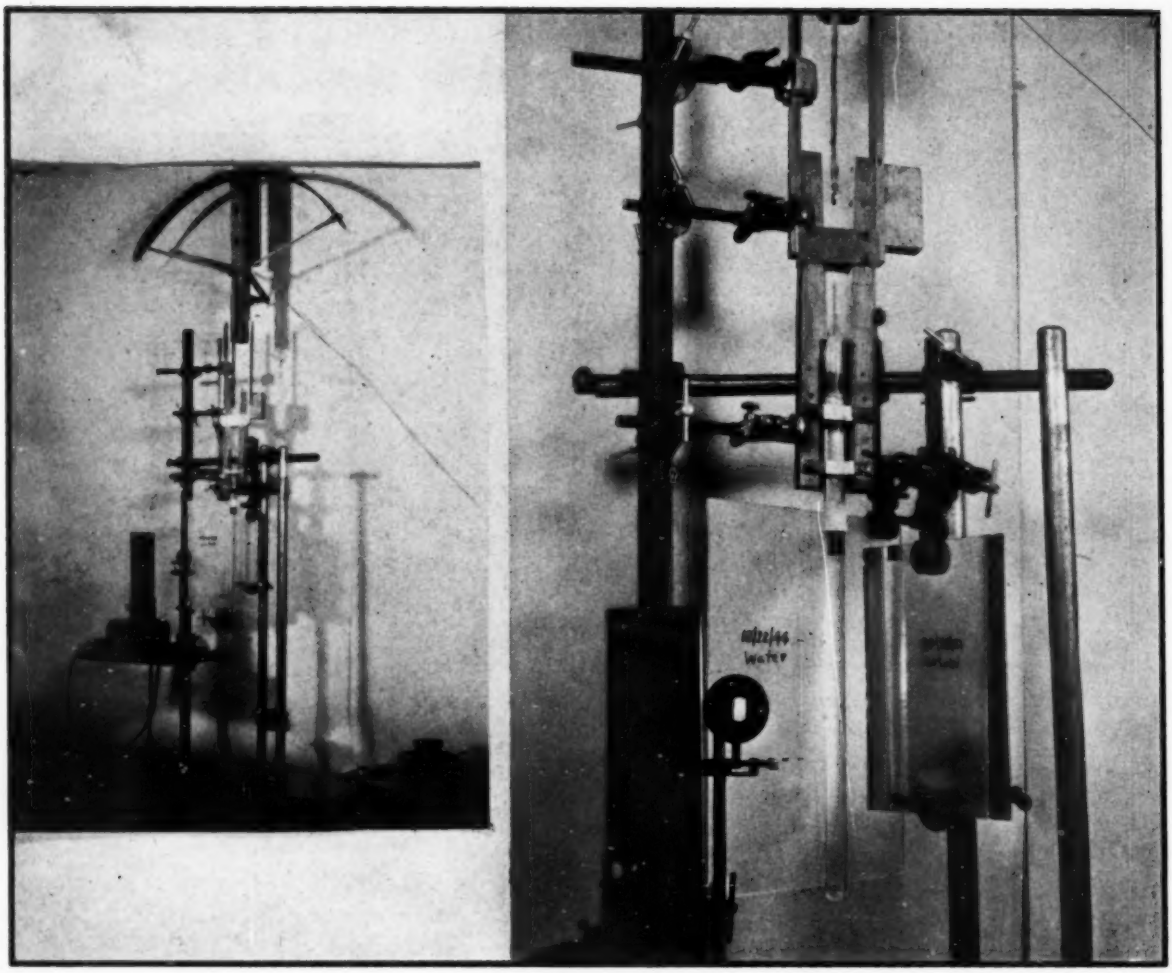

FIG. 2. A far (left) and near (right) view of the apparatus for rapidly moving a glass rod vertically in water. The steel bow appears above and the sodium lamp (with a circular mirror) on right. This lamp flashes 120 times a second and is used for timing the frames. In the near view, the Cellophane covering of the tube to protect against dust and a large mirror to allow a view of the cavitation at right angles to the camera is plainly seen.

the gas nuclei the blow to the tube or the velocity of the movement necessary to cause cavitation were so great as frequently to break the tube. Likewise we have found that cavitation of water, caused by the passage of high frequency sound waves, ceased when gas nuclei were previously removed, although a fairly high intensity of sound was employed (Harvey *et al.*[3]).

Flow methods of reducing pressure, which depend on the principle of Bernouilli (a Venturi or a Reynolds tube, Fig. 6) or the flow past a fixed body in the stream, are not feasible because of the large amount of water necessary and the problem of removing gas nuclei from such a volume. However, by moving a surface rapidly through stationary water similar regions of low pressure develop. The rear end of a moving object, such as a rod, exerts a continuous pull on the surrounding medium, which attempts to follow the rod and close the potential space. This method has been adopted in the experiments described below.

## TECHNIQUE

In order to study the tearing of water from a glass surface moving with high speed, conditions most favorable for the development of tension were selected, namely, a cylindrical glass rod cut squarely across at one end and moved rapidly through a small volume of water in a narrow

glass container. The walls of the container were near enough to those of the rod to give the additional suctional effect of a leaky piston. Rod and container cannot be too close, as the contact of one surface with another supplies the conditions for immediate cavity and bubble formation (Harvey *et al.*[7]).

To make certain that no hydrophobic spots remained on the glass surface, cleaning was accomplished by washing with soap and water, followed by hot trisodium phosphate and then hot concentrated sulphuric acid-bichromate mixture. Dust particles were removed by centrifuging (800×g for 30 minutes) the water used in the experiment. Our experiments differ from those of previous workers in that attempts were made to remove completely all gas nuclei, but to leave the dissolved air (at a tension of one atmosphere) in the water.

The method for removing gas masses was that of high hydrostatic pressure treatment (Harvey *et al.*[3]) which forces gas nuclei into solution. The glass tube, 16.0 mm inside diameter and about 41 cm long, with its contained water (distilled) and glass rod in position, with wire attached for pulling the rod, was covered with dialyzing Cellophane tubing tied both to the wire and to the glass tube end to prevent the entrance of dust, as shown in Fig. 2. This assembly was then placed in water in a long steel pressure chamber and subjected to 16,000 lbs./in.$^2$ hydrostatic pressure for from 15 to 120 minutes.

After the cleaning and pressure treatment, the tube, rod, and water were tested by evacuation to the vapor pressure of water to see if bubbles would arise. In no case was bubbling observed. The assembly was then mounted in a frame and the rod connected by its wire either to a coiled wire spring (in earlier experiments) or a bow, fabricated from a steel auto spring leaf, for rapid movement of the rod.

The lower part of the tube and rod were arranged in position before an Eastman 16 mm high speed moving picture camera, the maximum speed of which is 3000 frames per second. Behind the tubes there was a ground glass, illuminated by two No. 2 photo-flood lamps, run on 130 volts in a reflector. This intensity of transmitted light was found to give proper exposure for 2000 frames per second with $f = 3.5$ and a camera distance of three feet. In some experiments a mirror was so arranged that a view of the moving rod at right angles, in addition to the direct view, was recorded by the camera. The bow or spring was stretched and locked in position with a trigger release that was activated when about 35 feet of a 50-foot roll of Eastman super XX panchromatic film had passed behind the camera lens. The film was developed in D11 for 5.5 minutes. Just before the motion picture of the moving rod was taken, the Cellophane cover, which protects from dust, was loosened around the edge of the glass tube but left attached to the rod wire, thereby moving upward with the rod. No dust could enter the water until after the rod had moved out of the camera field of view.

Two sizes of Pyrex glass rod have been used, both about 29 cm long, one 5 mm in diameter, and one 10 mm in diameter. The end of the 5-mm rod was fire polished while the end of the 10-mm rod was ground and polished with rouge to make a right angle. The larger rod was introduced to increase the suction and tension on the water. The wall clearance between the 10-mm rod and tube (16-mm internal diameter) is only 3 mm, and the ratio of cross-sectional area of rod (78.5 mm$^2$) to cross-sectional area of tube (201 mm$^2$) is 0.39. It is not feasible to increase this ratio further because scraping of glass on glass causes bubble formation in gas supersaturated solutions or in a liquid under reduced hydrostatic pressure. Such a scraping of glass rod on glass wall has never occurred in our experiments but would undoubtedly result in cavitation.

## EXPERIMENTS

To demonstrate the tearing of water from a hydrophobic surface, dry clean glass rods 5 mm in diameter were covered with a thin film of paraffin or a thin layer of General Electric repellent varnish[8] (two experiments). The special cleaning procedure could not be applied to these surfaces. They were placed in the tube containing

[7] E. N. Harvey, K. W. Cooper, and A. H. Whiteley, "Bubble formation from contact of surfaces," J. Am. Chem. Soc. 68, 2119 (1946).

[8] We express our thanks to Dr. F. J. Norton, of the General Electric Co. for a sample of this varnish.

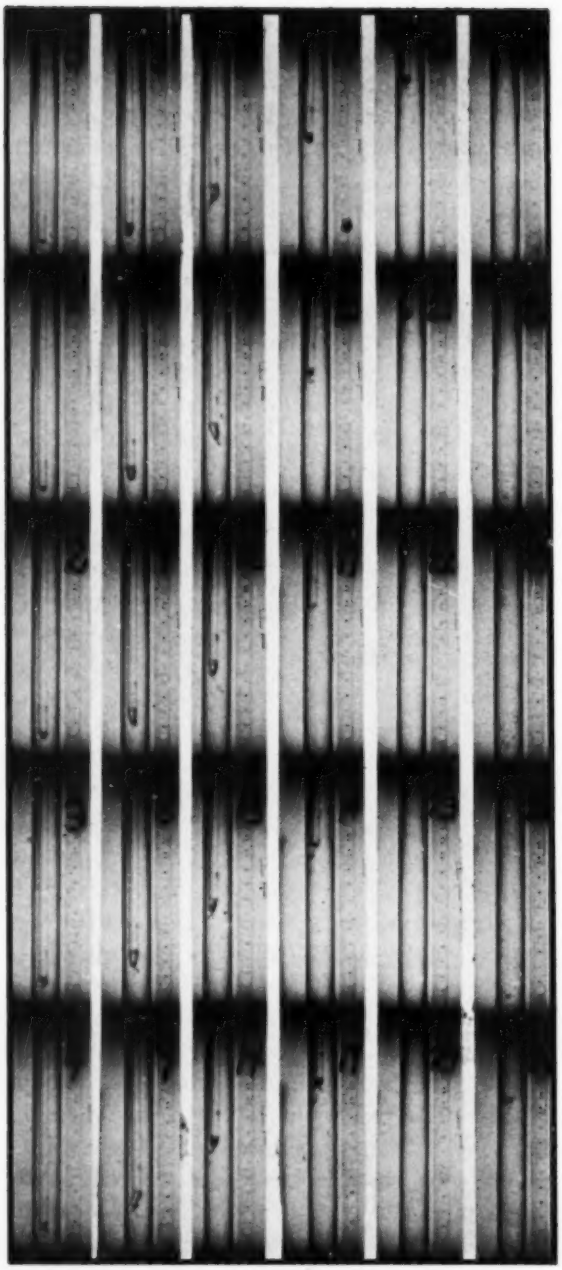

FIG. 3. Moving picture (2280 frames/sec.) of a paraffin tipped rod (5-mm diameter) moved through gas nucleus-free water at a final maximum speed of about 16 meters a second. Note the abundant cavitation, characteristic of hydrophobic surfaces, which appears in the first frame when the velocity was less than 3 meters a second. Cavitation disappears in frame 17, to reappear and again disappears in frame 22, with subsequent periodicity. Scale in centimeters. Exp. 9-7-44.

water and pressurized at 16,000 lbs./in.$^2$ for from 30 to 90 minutes. When tested at the vapor pressure of water (20 mm Hg) no bubbles arose from the glass surfaces or from the water. However, motion pictures of the movement of the hydrophobic rods through water showed cavitation on the first frame when the velocity was less than 3 meters/sec., and a misty trail of fine cavities in succeeding frames, as shown in Fig. 3. The water in the tube after the rod was drawn out was observed to be full of fine bubbles. On the other hand, completely hydrophilic rods, 5 mm in diameter, have been drawn through the water with a velocity of 37 meters/sec. without a sign of cavitation. A plot of rod velocity *vs.* time is shown in Fig. 4 and will illustrate the rapid acceleration attained with our type of bow.

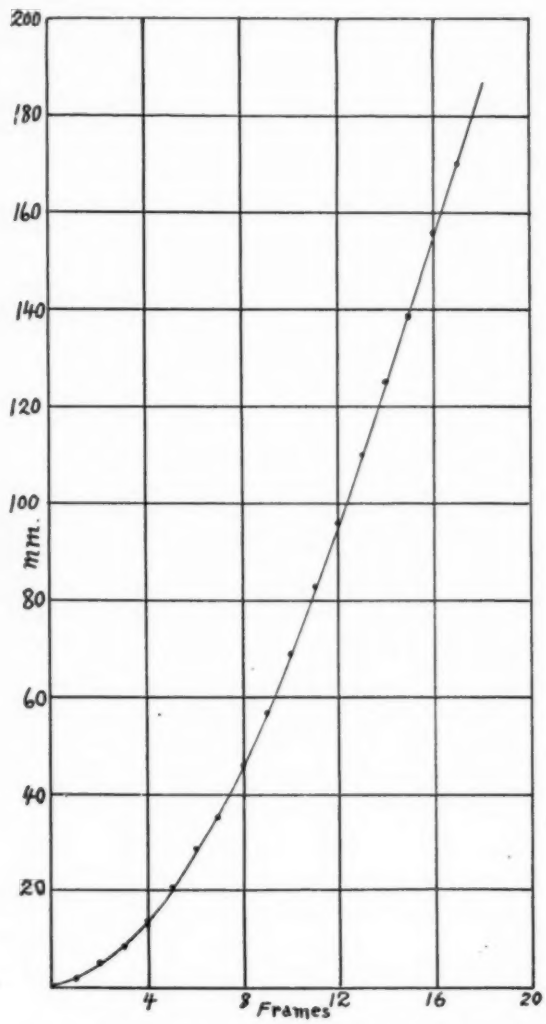


FIG. 4. A plot of the acceleration of a 5-mm glass rod in gas nucleus-free water. Exp. 12-14-44. 2400 frames/sec. The final velocity was 36.7 meters/sec., yet no cavitation appeared at this speed.

The question arises whether the presence of a detergent in the water, that might cover hydrophobic surfaces, leaving an outwardly directed hydrophilic layer of molecules, might not prevent this ready cavitation. Accordingly, one of the water repellent varnish covered rods (5-mm diameter) was moved rapidly in water containing 0.5 percent aerosol OT (dioctyl sodium succinate). Cavitation appeared practically from the start of movement. It is very possible, however, that movement of the rod tears detergent molecules away from the surface, thereby exposing hydrophobic spots.

The bubble formation on the paraffined rod is very similar to that which is observed if the rod and tube have not been subjected to the cleaning and pressure treatment, i.e., if gas nuclei have not been removed. Again the first frame shows a fine mist of cavitation at the end of the rod, when the velocity may be only 3 meters/sec.

In some of the early experiments, where cleaning of glass surfaces involved soaking in cold concentrated sulphuric-bichromate mixtures only, and the tube was not protected from dust particles, cavitation occurred when the 5-mm rod had reached a high velocity. In one case, shown in Fig. 5, two small cavities appeared on the end of the rod at the 9th frame when the velocity was 18 meters per second. These enlarged until the 12th frame, when they disappeared, but reappeared on the 14th, 15th, and 16th frames. This periodic formation and disappearance of cavities is frequently observed during cavitation, and is particularly well seen in a Venturi nozzle. The sound during such Venturi cavitation is caused by periodic formation and collapse of cavities which were photographed by Hunsaker,[9] using the Edgerton high speed technique. In Fig. 6 are reproduced prints from a 2000 frames per second film of cavitation in a small glass Reynolds tube (a glass tube with an abruptly constricted region), taken with our Eastman high speed camera. The burst of cavitation is periodic although the rate of picture taking is not sufficient to follow the complete cycle.

As in the Reynolds tube, the periodic nature of cavitation below the rod is because of the fact that cavity formation relieves the tension in the water, with consequent collapse of the cavity; then further tension develops with cavity formation, followed again by collapse. The process is

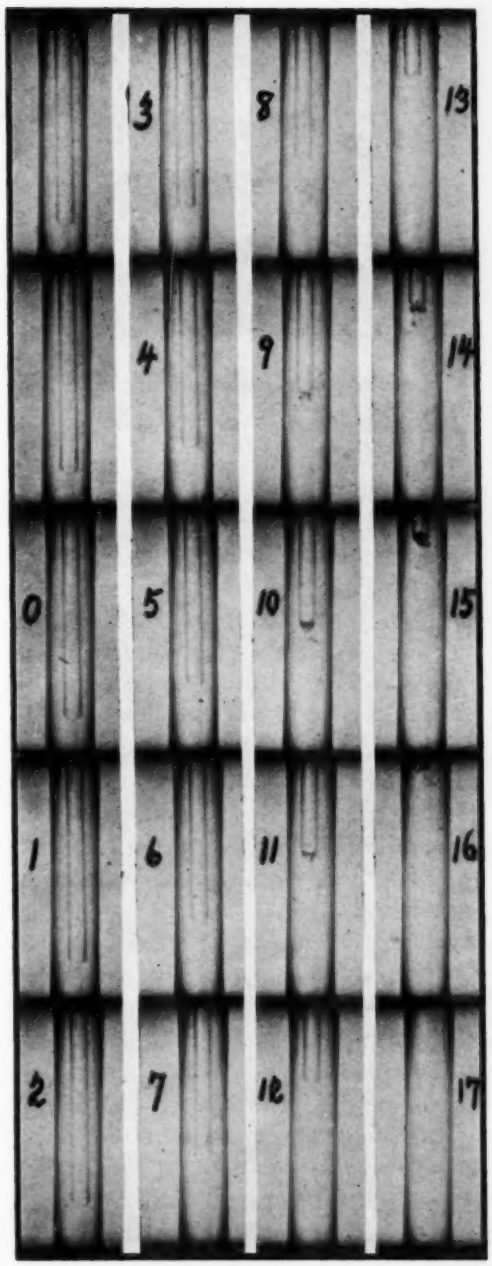


FIG. 5. Moving picture (2280 frames/sec.) of a 5-mm diameter glass rod moved through water in which cavitation first appeared (frame 9) when the velocity was 18 meters/sec. Note disappearance of cavitation in frames 12 and 13, with reappearance in frame 14. External diameter of tube 19.5 mm. Exp. 7-9-44.

[9] J. C. Hunsaker, Mech. Eng. **57**, 211 (1935).

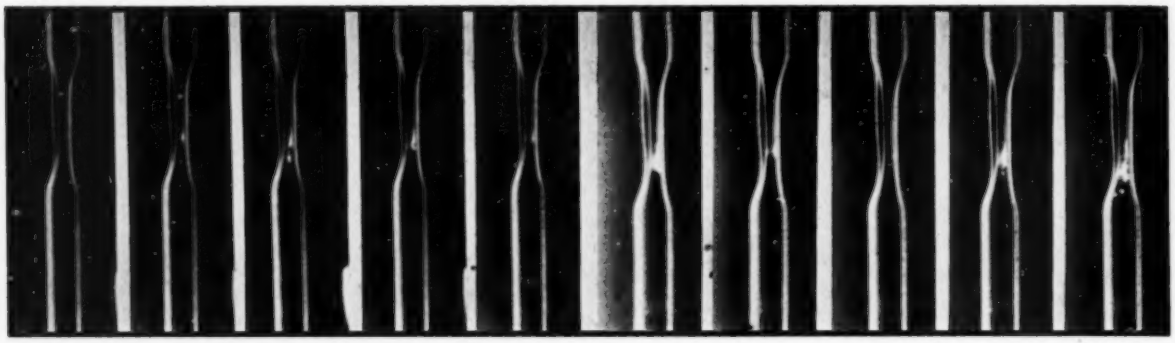

FIG. 6. Negative prints from a moving picture (1680 frames/sec.) showing cavitation in a Reynolds tube (8.3-mm large diameter) from flow (top to bottom) of water through a constriction. Note the periodic cavitation (white in appearance) which always begins at a particular spot on the narrow region of the tube.

repeated as long as the conditions for development of tension persist.

Whenever cavities appear under a rod, they are greatly disturbed by the turbulence and frequently look like a fine mist. If hydrophobic dust particles with air films have fallen into the pressurized water (or are purposely placed there) isolated bubbles may form at a distance from the rod, as shown in Fig. 7. The bubbles may appear almost immediately or after the rod has reached a certain speed. Sometimes they are attached to the wall and sometimes free in the tube. If near the rod, they may enter vortices at the end as the rod passes in the water, and a trail of misty cavitation will follow. Isolated bubbles are also observed to pulsate, appearing for several frames and then disappearing again, reflecting the periodic pressure changes in the tube.

In order to study the effect of viscosity, two 5-mm rods have been drawn from concentrated sugar solutions (Staley's crystal white syrup) at a temperature of 23°C, where the syrup viscosity is 20.1 poises, as compared with a viscosity of 0.00936 poise for water at 23°C. Density of the syrup is 1.383 at 20°C. One rod was of glass and one of aluminum. Since aluminum tends to dissolve in water, this rod might contain films of hydrogen which could not be removed by prepressurization. However, when tested at the vapor pressure of water, the aluminum rod was found to contain no gas nuclei that grew to bubbles. The moving picture film, reproduced in Fig. 8A showed that at the very start of movement (1st frame) several minute cavities appeared at the end and side of the rod and in succeeding frames grew into a long cylindrical cavity the width of which remained approximately that of the rod. Finger-like processes reflecting the initial cavities were present at the lower end where rod movement starts. The cylindrical cavity remained static during the movement of the rod out of the syrup and then started to collapse (Fig. 8B). The collapse occurred along the long axis of the tube from top down, not from side to side, and proceeded at a uniform speed of 940 cm/sec. It was as if the rod had left an impression of itself in the syrup. When the collapse finally occurred, several smaller cavities appeared and oscillated several times before subsiding. The glass rod drawn from the syrup behaved in a similar way, but lacked the several fingers at the tip of the cavity, only one cavity tip appearing.

However, in two experiments, glass rods 5 mm in diameter, moved in 75 percent syrup at temperatures of 25°C and 27°C, failed to cause the development of a cavity, although their velocity reached 18 meters/sec. The viscosity of 75 percent syrup at 25°C is 0.56 poise. There was also no cavitation in citrated cat blood plasma at 18 meters/sec. The viscosity of plasma is only slightly greater than water.

Since the 5-mm rods failed to cavitate in clean pressurized water at the highest velocity (37 meters/sec.) attainable with the steel bow. 10 mm diameter rods were substituted. Both because of the greater cross-sectional surface area at the end of the rod and the greater suction effect in the glass tube, a much greater tension is to be expected for a given speed. In three

experiments, 10-mm diameter glass rods, the ends of which had been polished with rouge and cleaned thoroughly by the procedure previously described, were moved through centrifuged water at a maximum speed of 24 meters/sec.[10] In all three cases, cavitation occurred somewhere in the tube. In one experiment cavitation appeared at the end of the rod when the velocity was 16 meters/sec. In another, an isolated bubble formed below and at a distance from the rod in the first frame, followed by additional bubbles when the velocity was 21 meters/sec., as shown in Fig. 9. The first isolated bubble expanded to a large size and later collapsed so suddenly that the glass tube was broken by the water hammer effect. Cavitation may thus appear at the end of the rod despite the presence of a large bubble cavity in the tube. In the third experiment no cavitation formed on the end of the rod, but after the rod had attained its maximum velocity of 24 meters/sec. and disappeared from the camera field of view, bubbles appeared and expanded into a large cavity, the collapse of which again broke the glass tube.

## DISCUSSION

In the three experiments with a 10-mm diameter glass rod, despite rigorous cleaning, high hydrostatic pressure treatment, and every precaution to remove and protect from hydrophobic dust particles, cavitation occurred at some point in the tube before the maximum velocity of 24 meters per second was reached. The suction of the 10-mm rod in the 16-mm glass tube must have been considerable, as evidenced by the large size of cavity, but no figures for the tension can be given until the problem of calculation is solved. It is possible that in the short time intervals involved, negative pressures of the order of 100 atmospheres are developed. The experiments are described in detail, because of the interesting phenomena involved, which could only be detected by the high speed photographic technique.

In most experiments by other workers on cavitation at the surface of moving bodies, the water has not been freed of gas nuclei and cavitation occurs at a relatively low velocity. It is therefore of considerable interest to find that in the case of experiments with the 5-mm diameter rod moving in a 16-mm tube, the velocity reached

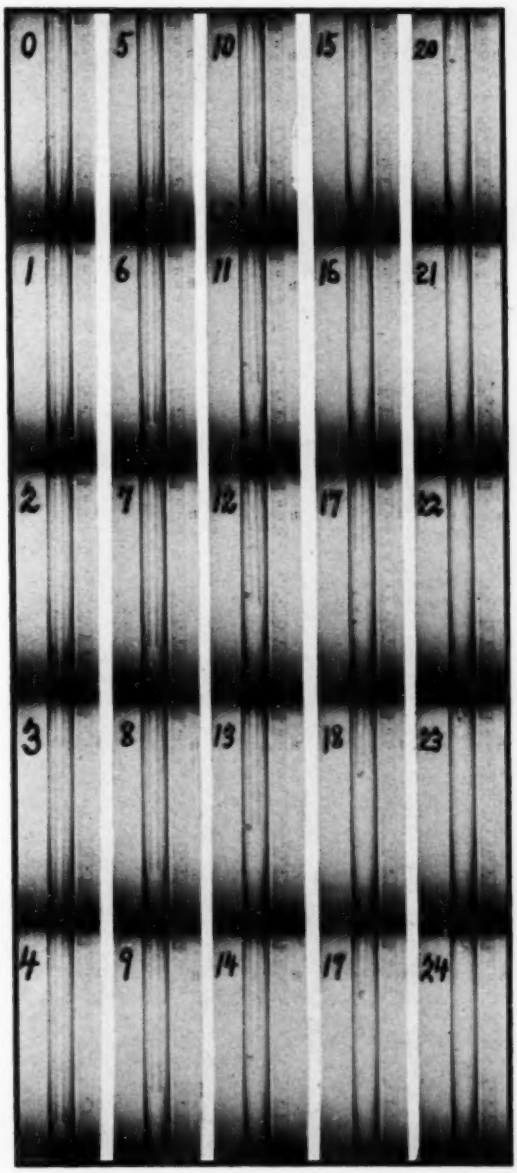


FIG. 7. Moving picture (2160 frames/sec.) of a 5-mm diameter glass rod moving in water at a maximum speed of 16 meters a second. No cavitation appears on the end of the rod until frame 18 but in earlier frames (1, 8, 10) bubbles form away from the rod and grow in size. They probably come from hydrophobic dust particles, as the Cellophane protective covering of the tube was not used in this experiment. Scale in centimeters. Exp. 9-2-44.

[10] This rod, which weighed 53.3 grams, when moved with the steel bow in air, attained a maximum speed of 26 meters/sec.

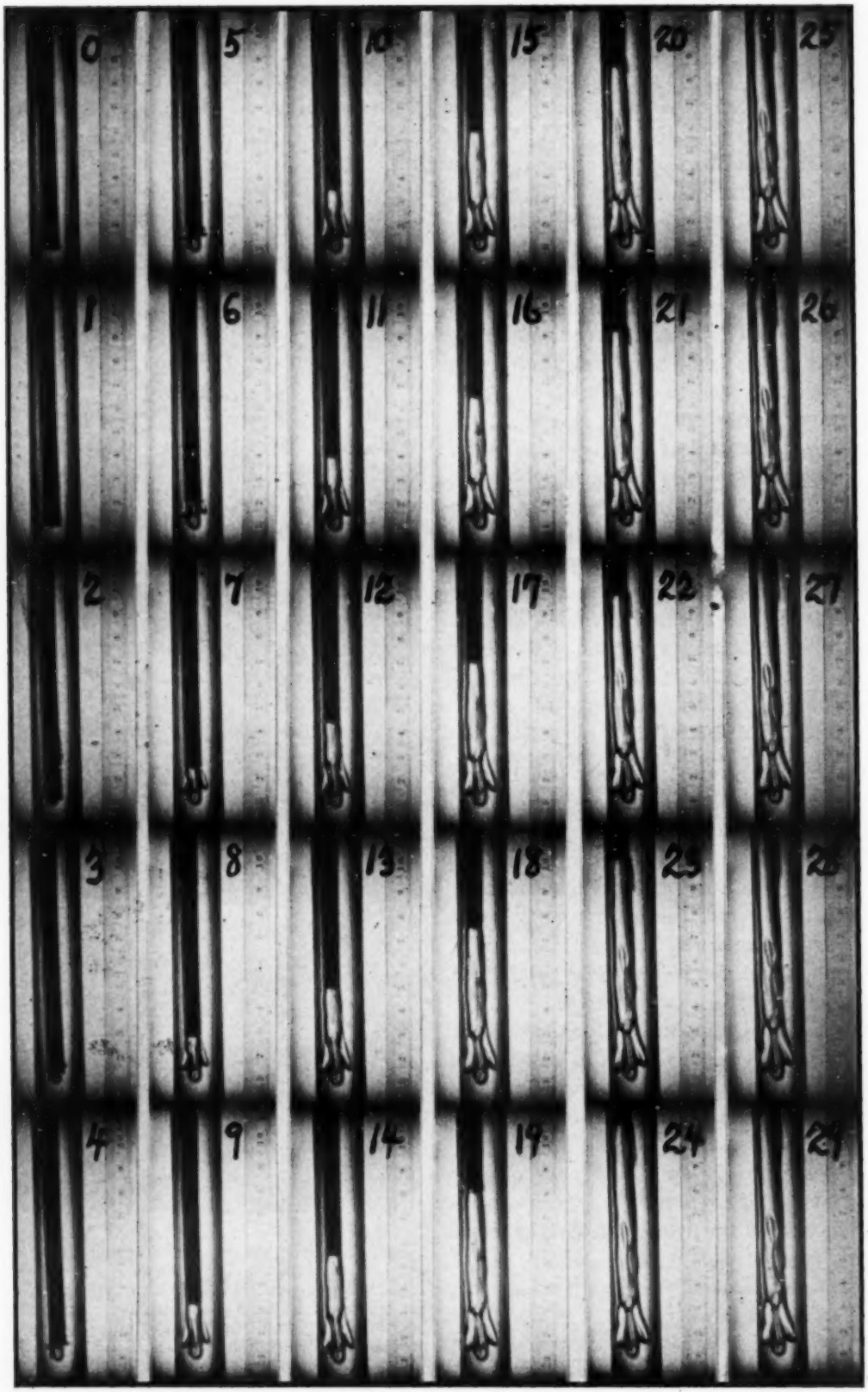


A

FIG. 8. A and B. Moving pictures of a 5-mm diameter aluminum rod moving in gas nucleus-free corn syrup (viscosity, 20.1 poises; density, 1.383; temperature 23°C) at a maximum speed of 12.2 meters per second. Since the high viscosity of the syrup prevents its filling the space behind the rod, a large

B

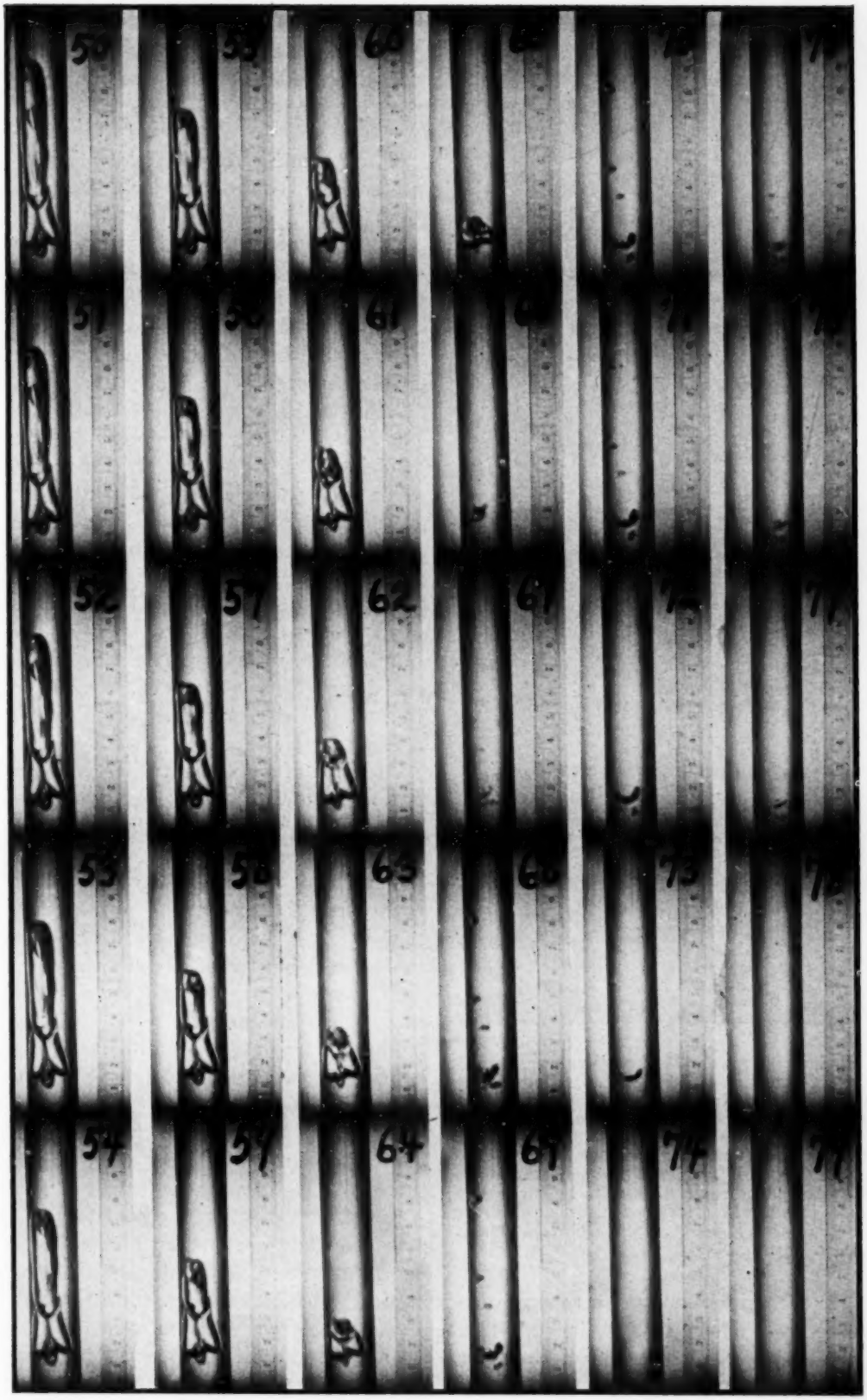

cavity forms from a number of initial points which remain as fingers. In B the collapse of the cavity is shown, beginning with frame 50. Note that collapse is from above downward and that the remnants of the cavity disappear in frame 74 and then reappear again. They oscillate several times before subsiding. Scale in centimeters. Exp. 8-23-44.

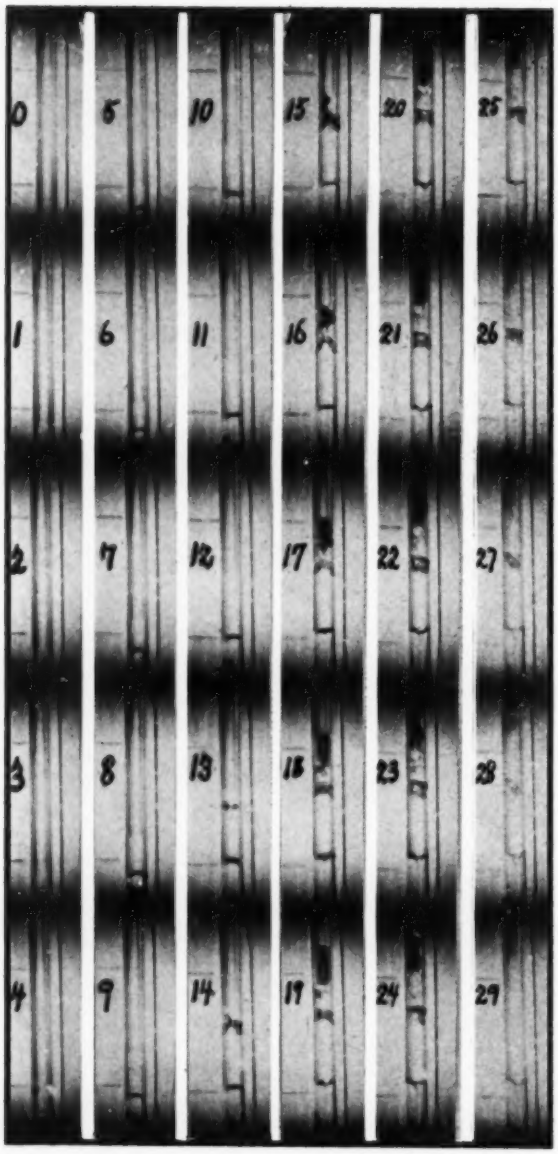


FIG. 9. Moving picture of a 10-mm diameter glass rod, moving in a 16-mm internal diameter tube containing gas nucleus-free water with a maximum speed of 23.2 meters/sec. Note that no cavitation forms on the end of the rod until frame 15 (speed 23.2 meters/sec.) but that a bubble appears below the rod in frame 1 (speed less than 3 meters/sec.) and grows into a large cavity. Bubbles also appear below the rod in frame 13 (speed 21 meters/sec.) and then grow into a mist of cavitation. Collapse of the large cavities broke the glass tube. The two horizontal lines are 10 cm apart. Exp. 12-21-44.

37 meters per second without cavitation appearing anywhere, even at the rear of the rod. This velocity can be better compared with other speeds in water if converted into the English system when it becomes about 83 miles an hour, or 1.38 miles a minute, truly a remarkable figure for cavitationless motion in a liquid medium.

## SUMMARY

Phenomena involving the tensile strength of water have been studied by a kinetic method—high speed motion photography of the rapid movement of a blunt glass rod in a narrow (16-mm inside diameter) glass tube of water.

Special precautions have been taken to remove all hydrophobic patches and small gas masses (gas nuclei) but to retain the dissolved gas (air at one atmosphere) in the water.

If the rod (5-mm diameter) surface contained gas nuclei, or was hydrophobic and free of gas nuclei, cavitation occurred at the rear end when the velocity was less than 3 meters/sec., but if completely hydrophilic and free of gas nuclei, the velocity could be 37 meters/sec. or 83 miles/hour without cavitation.

When improperly cleaned rods (5-mm diameter) were used, isolated cavities formed at intermediate velocities. These cavities appeared and disappeared as the rod movement proceeded, in a manner similar to the periodic cavitation in a Reynolds tube.

Addition of a detergent (diactyl sodium succinate) to the water did not prevent cavitation at a low velocity with the hydrophobic rod (5-mm diameter) free of gas nuclei.

Movement of a rod (5-mm diameter) in pure corn syrup (viscosity 20.1 poises), free of gas nuclei, left a large cylindrical cavity that collapsed in a matter of hundredths of a second. In 75 percent corn syrup (viscosity 0.56 poise) no cavitation occurred.

Large glass rods (10-mm diameter) could not be moved more than 24 meters/sec. within a glass tube (16-mm internal diameter) containing clean gas-nucleus free water without the appearance of cavitation at some place in the liquid, though not necessarily at the end of the rod.

It is not possible to calculate the tensions developed in these "leaky piston" experiments but it may be pointed out that the velocities attained without cavitation are far higher than previously observed for movement of bodies in an aqueous medium, a result believed to be owing to the absence of all gas phases and hydrophobic surfaces.

# A New Magnetic Material of High Permeability

O. L. Boothby and R. M. Bozorth
*Bell Telephone Laboratories, Murray Hill, New Jersey*
(Received November 18, 1946)

This paper describes the preparation, heat treatment, and properties of *supermalloy*, a magnetic alloy of iron, nickel, and molybdenum. In the form of 0.014 in. sheet it has an initial permeability of 50,000 to 150,000, a maximum permeability of 600,000 to 1,200,000, coercive force of 0.002 to 0.005 oersted, and a hysteresis loss of less than 5 ergs/cm³/cycle at $B=5000$. Transformer cores made of insulated 0.001 in. tape, spirally wound, have about the same initial permeability and a maximum permeability of 200,000 to 400,000. The alloy has a Curie point of 400°C and appears to have an order-disorder transformation temperature somewhat above 500°C.

DURING the last few years a magnetic alloy has been made in these laboratories that has an initial permeability several times as high as that of molybdenum permalloy and mumetal, alloys now in general use. The new material has been named "supermalloy" (su-perm'-al-loy). Its preparation, heat treatment, and properties are described briefly in this article. It has already been made in considerable quantities for use in apparatus supplied to the U. S. Navy. When in the form of 0.001 in. insulated tape, used in transformer cores, it has an initial permeability of 50,000 to 120,000; this is to be compared to molybdenum permalloy of the same thickness, having an initial permeability in the range 10,000 to 20,000. The use of supermalloy in communication transformers permits a threefold increase in the range of frequencies transmitted, and a pulse duration three times that heretofore obtained.

Supermalloy constitutes the latest step in the development of the high nickel alloys for use at low inductions. The important previous steps are shown graphically in Fig. 1, where the initial permeability is plotted on a logarithmic scale against the year of discovery.

It is interesting to mention briefly the novelty of each of these steps, regarding them in the light of present day knowledge and theory. The addition of silicon to iron, by Hadfield, neutralized partially the bad effect of the carbon always present as an impurity. The high permeability of the iron-nickel alloys, discovered by Elmen,[1] is attributed primarily to their low magnetostriction, as pointed out by McKeehan.[2] The next improvement, due to rapid cooling or "permalloy treatment," is now believed to be associated with the atomic ordering of iron and nickel atoms in the alloy. The addition[3] of one or more elements such as chromium, molybdenum, and copper, lowered the optimum cooling rate so that it could easily be attained in practice. In Neumann's 1040 alloy[4] the beneficial effect of purification of the material with respect to non-

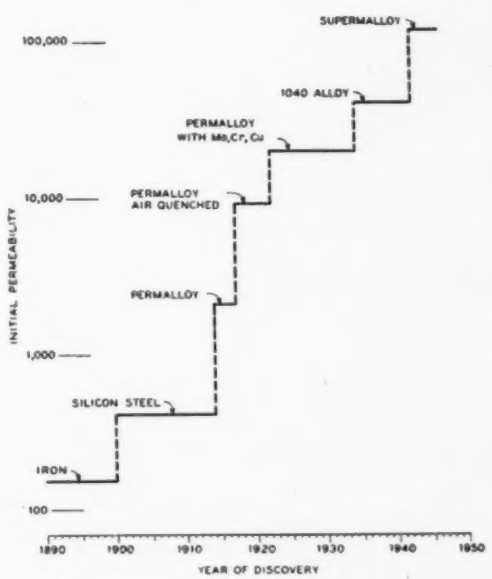


FIG. 1. Initial permeabilities of some useful materials plotted against the year of discovery. Note logarithmic scale.

[1] H. D. Arnold and G. W. Elmen, J. Frank. Inst. **195**, 621 (1923).

[2] L. W. McKeehan, Phys. Rev. **26**, 948 (1925).

[3] G. W. Elmen, Elec. Eng. **54**, 1292 (1935); W. F. Randall, J. Inst. Elec. Eng. **80**, 647 (1937).

[4] H. Neumann, Arch. Tech. Messen **4**, Z913 (1934).

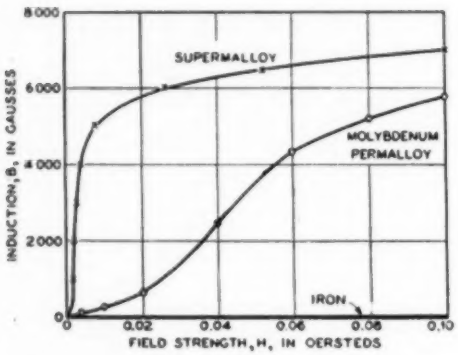


FIG. 2. Magnetization curves for supermalloy, molybdenum permalloy, and iron, in low fields.

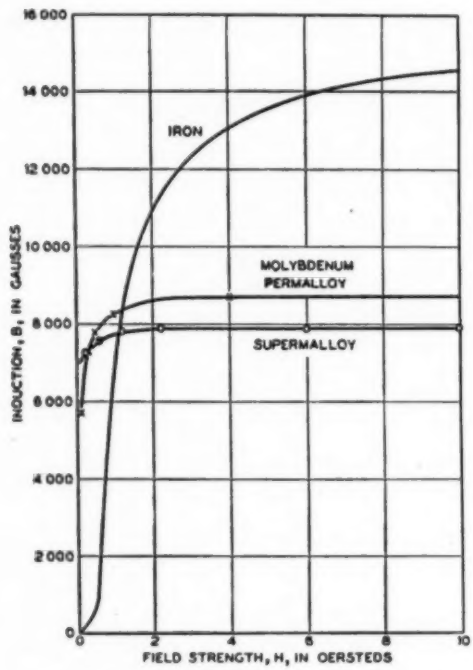


FIG. 3. Magnetization curves in higher fields.

metallic substances such as carbon and oxygen, as developed by Yensen,[5] Cioffi,[6] and others, was also used to advantage.

Although the physical reasons for the success of the supermalloy process are still not known in detail, the work so far accomplished indicates that there are two main considerations: (1) the presence of certain impurities or combinations of impurities, usually found in commercial alloys, will prevent the attainment of high permeability following the procedure now used; and (2) a definite cooling rate must be used below the temperature at which atomic ordering begins, or the specimen must be held for a definite time at a temperature between about 400 and 500°C. The hypothesis is made that, when a critical amount of ordering is present, the magnetostriction and the magnetic crystal anisotropy both tend to disappear at the same time in the alloy of proper composition and that high permeability then occurs in the polycrystalline material. These properties are now under investigation.

## PREPARATION AND HEAT TREATMENT

The composition of supermalloy is about 79 percent nickel, 5 percent molybdenum, 15 percent iron, and 0.5 percent manganese. Impurities such as silicon, carbon, sulfur, etc., are lower than in most commercial alloys. Materials are melted in vacuum in an induction furnace of about 30 lbs. capacity, and poured in helium or nitrogen at atmospheric pressure.

Ingots are hot and cold rolled by commercial methods to any thickness down to 0.00025 in. The tape is wound spirally to form toroidal specimens. When insulation is desired a thin film of magnesia is applied in carbon tetrachloride suspension so that a film about 0.00005 in. in thickness is left on each side of the tape. Trans-

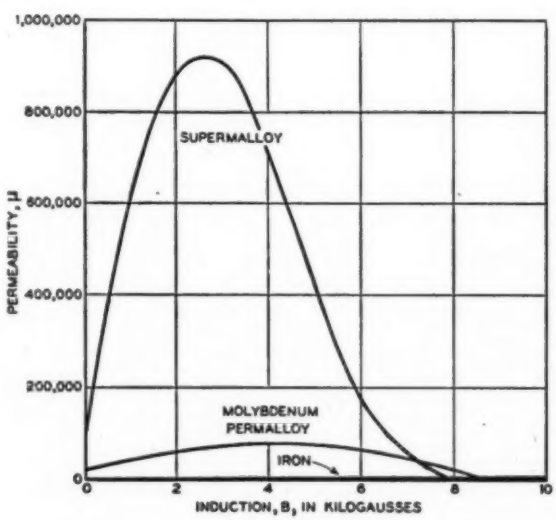


FIG. 4. Permeability *vs.* induction curves of supermalloy in the form of 0.014 in. sheet. Curves for other materials are for comparison.

[5] T. D. Yensen, Trans. A.I.E.E. **33**, 451 (1914).
[6] P. P. Cioffi, U.S.P. **2**, 110, 569 (1938).

former cores are made in this manner. Heat treatment consists of maintaining at 1300°C in pure dry hydrogen, and cooling through the temperature range 600° to 300°C at a critical rate appropriate to the composition.

## PROPERTIES

Magnetic properties are given for (a) 0.014 in. uninsulated and (b) 0.001 in. insulated material. Magnetization curves of the former are compared, in Figs. 2 and 3, with curves of molybdenum permalloy and iron. The ratio of permeabilities of supermalloy and molybdenum permalloy varies with induction from about 5 at $B=20$ to about 10 at $B=3000$ (maximum permeability). At inductions of 7000 to 8000 the permeability of supermalloy has decreased markedly and is less than that of molybdenum permalloy or iron; saturation is at $B_s=7900$. Figure 4 shows typical permeability *vs.* induction curves for supermalloy, molybdenum permalloy, and iron.

The permeability in very low fields is shown in Fig. 5 for a representative specimen of supermalloy, and for materials previously known. Finally, hysteresis loops for supermalloy and molybdenum permalloy are shown in Fig. 6.

When thin tape is *insulated* before heat treatment, the permeability in low fields is affected

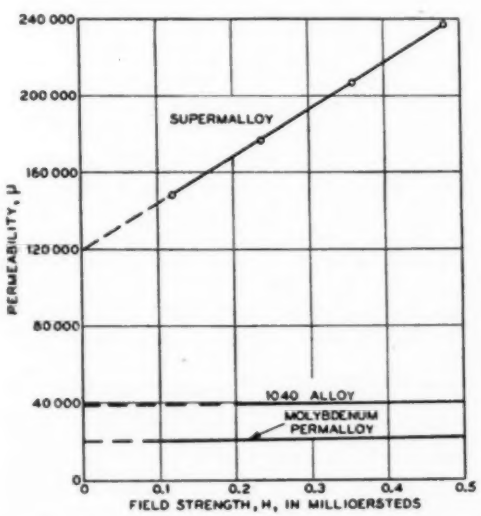


FIG. 5. Permeability *vs.* field strength curves for low fields, for representative specimens of 0.014 in. sheet of three materials of high permeability.

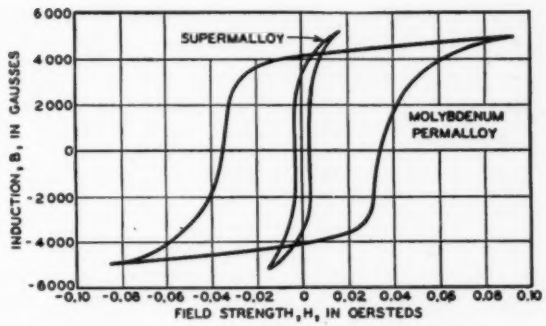


FIG. 6. Hysteresis loops of supermalloy (5 ergs/cm³/cycle) and molybdenum permalloy (50 ergs/cm³/cycle) for $B_m=5000$, in 0.014 in. sheet.

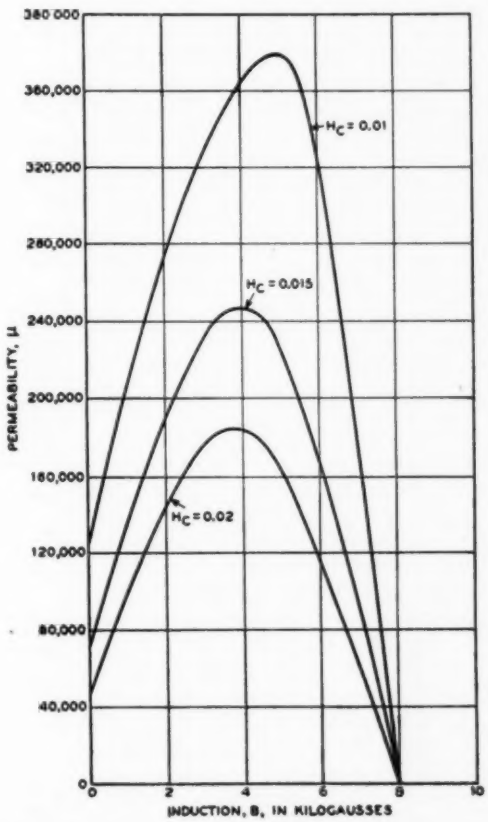


FIG. 7. Representative permeability curves for good, average, and marginal specimens of supermalloy made from insulated 0.001 in. tape.

but slightly. However, the curves of Fig. 7 indicate that the maximum permeability of 0.001 in. insulated tape is considerably lower than that of thicker tape. Insulated 0.004 in. tape has a maximum permeability about twice as large as that of insulated 0.001 in. tape; its permeability is therefore intermediate between the 0.001 in.

insulated and the 0.014 in. uninsulated tape. The middle curve of Fig. 7 is near to the average of a lot of several thousand cores of 0.001 in. tape, made in the early stages of development of the material.

The resistivity of supermalloy is about 65 microhm-cm.

The high permeability of supermalloy opens the way toward further improvements in transformers operating at frequencies common in communication engineering, in much the same way that the various permalloys led to the improvements described a decade ago.[7]

We are indebted for cooperation and assistance to many members of the Laboratories and the Western Electric Company. Messrs. D. H. W. Wenny and H. C. Theuerer should be specially mentioned for helping to solve many of the metallurgical problems connected with the development of the material.

[7] A. G. Ganz and A. G. Laird, Elec. Eng. **54**, 1367 (1935).

# Apparatus and Techniques for Practical Chemical Identification by X-Ray Diffraction

CHARLES S. SMITH, *Department of Physics, Case School of Applied Science*

AND

RICHARD L. BARRETT,* *Department of Mineralogy and Geology, Case School of Applied Science, Cleveland, Ohio*

(Received August 30, 1946)

The method of chemical identification by means of x-ray diffraction is reviewed from the point of view of apparatus and techniques recently made commonly available, with particular emphasis on the use of long wave-length x-radiation. Experience in using the A.S.T.M. card index file of x-ray diffraction data is reported. The discussion is designed especially for the person who wishes to make use of this important analysis tool but who is not an expert in x-ray diffraction.

## I. INTRODUCTION

WHEN Hull in 1919 described the powder method of x-ray diffraction, he observed that the method should be a potent tool for the identification of crystalline substances. Hull pointed out, "That every crystalline substance gives a pattern; that the same substance always gives the same pattern; and that in a mixture of substances, each produces its pattern independently of the other, so that the photograph obtained with a mixture is the superimposed sum of photographs that would be obtained by exposing each of the components separately for the same length of time."[1] The new method immediately began to be used by mineralogists and chemists but at first its usefulness was limited by the fact that standard patterns of known substances were needed for comparison. In 1938 Hanawalt[2] and some of his co-workers at the Dow Chemical Company published tables giving the diffraction patterns of 1000 substances and showed that the data could be indexed in such a way that the identity of any listed substance could usually be found by reference to the three strongest lines in its diffraction pattern. The availability of this table of standard patterns, including as it did most of the more important inorganic compounds, made x-ray diffraction a practical means of quick identification of an unknown substance. Following Hanawalt's publication the American Society for Testing Materials made available a card index comprising the substances he had listed plus additional ones obtained from other sources and arranged essentially according to the indexing system suggested in his paper. More recently the A.S.T.M. has issued a supplementary set of cards greatly amplifying the scope of the index so that it now includes some 3000 substances. This card index, which makes available in useful form the patterns of the commoner inorganic salts, most of the important minerals, and even many organic substances, enables the x-ray diffraction method to take its place along with the spectroscope and the polarizing microscope among the potent physical tools for chemical research.

In his 1938 paper Hanawalt described in detail the technique used in the Dow Chemical Laboratories and his co-workers and others have amplified the description in subsequent papers.[3–5] The Dow technique employs molybdenum radiation, large radius quadrant cameras, and a multiple diffraction unit which permits the exposure of 24 samples simultaneously. It is perhaps particularly adapted to large industrial laboratories where considerable numbers of samples are being run on a day to day basis. However exposures of some six hours are required and the particular apparatus used is no longer being manufactured.

In the last several years the writers have had occasion to examine a considerable number of

* Now at the New Mexico College of Agriculture and Mechanic Arts, State College, New Mexico.

[1] A. W. Hull, J. Am. Chem. Soc. **41**, 1168 (1919).

[2] J. D. Hanawalt, H. W. Rinn, and L. K. Frevel, Ind. Eng. Chem. Anal. Ed. **10**, 457 (1938).

[3] L. K. Frevel, Ind. Eng. Chem. Anal. Ed. **14**, 687 (1942).

[4] L. K. Frevel, Ind. Eng. Chem. Anal. Ed. **16**, 209 (1944).

[5] W. P. Davey, J. App. Phys. **10**, 820 (1939).

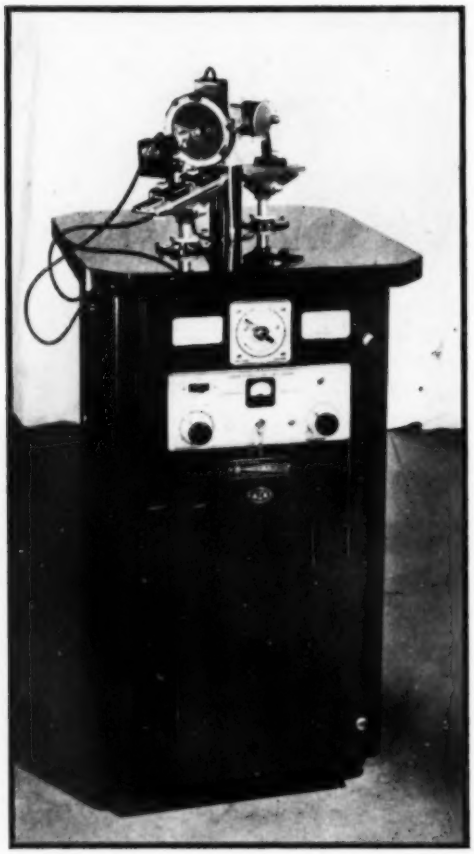

FIG. 1. An example of a modern self-contained x-ray diffraction outfit (Courtesy of the Picker X-Ray Corporation).

industrial samples and, in common with many other workers in x-ray diffraction, have come to prefer a somewhat different technique employing a smaller radius camera of the full circle type, and copper, iron, cobalt, or chromium radiation which makes possible satisfactory resolution of lines with the small camera. Although numerous papers have been published describing details of camera design, special methods of sample preparation, improvements in x-ray tubes, etc., the chemist or mineralogist who is not himself an x-ray specialist has remained dependent for a general treatment of the subject upon the papers of Hanawalt and his co-workers. It is the purpose of the present writers to describe for the non-specialist the practical considerations involved in modern x-ray methods, employing the more modern apparatus now available commercially. While in a general way the technique to be described will be familiar to x-ray crystallographers some details based upon the writers' experience may be new and it is hoped that the present paper may be helpful to chemists and technologists who have not previously employed x-ray diffraction in taking advantage of this extremely useful tool.

In what follows it will be assumed that the reader has a general knowledge of the physics of x-rays and of x-ray diffraction such as may be obtained in a standard text.[6] It is also assumed that the reader is familiar with the general method of x-ray diffraction chemical identification as presented in the 1938 paper of Hanawalt.

## II. APPARATUS

In the past ten years a number of manufacturers have introduced lines of x-ray diffraction equipment built around the recent American development of efficient diffraction tubes, particularly those with long wave-length targets. In general this equipment is excellent and our intention here is to point out only the practical details in choosing equipment for chemical identification work. The writers' own experience has been in a laboratory primarily devoted to instruction and research and they accordingly have had the benefit of a variety of versatile equipment. They have found it best however to do most chemical identification work with the standard forms of commercial apparatus, employing the available research apparatus only on the rare problems of a difficult or special nature. It is certain that the laboratory doing routine problems will do well to standardize on convenient commercial apparatus chosen for the particular field of identification involved.

### Power Supplies

The available commercial power supplies are designed for use with a particular manufacturer's tube, Fig. 1, and are all uniformly good, incorporating the necessary electrical controls, high voltage, and x-ray protection for the operator and water and electrical failure protection for the apparatus. For identification work alone x-ray tubes of all types can be run at 40 kv and hence the high potential controls are strictly unneces-

[6] A new book which presents an excellent treatment is C. S. Barrett, *Structure of Metals* (McGraw-Hill Book Company, Inc., New York, 1943).

sary. Full wave rectification is desirable, and half-wave rectification somewhat less so but neither is necessary. The writers have used for some time a homemade power supply which merits description not because of its originality but because it emphasizes how simple and convenient such equipment can be.

The apparatus employs a ray proofed diffraction tube mounted horizontally on a wide, high wood table. Screens are provided for high voltage protection, but these would be unnecessary were the tube also shockproof and equipped with a shockproof cable. The electrical apparatus consists simply of a high voltage transformer and a filament transformer (both the usual second-hand radiographic equipment), a Variac, milliameter, and voltmeter. The high voltage transformer has a 35-kv secondary and is powered directly from the a.c. line through an ordinary toggle switch which is the only high voltage control. The transformer is located under the table and is protected, the high potential being led by a shielded cable to the tube through the millimeter. The tube filament is powered and controlled by the sequence, a.c. line, Variac, filament transformer. The latter is mounted on the table at the screened cathode end of the tube and supports the filament voltmeter and the milliameter. The cooling water for the tube is carried by Saran tubing, and is run off through a small standpipe in which is immersed a one-ampere fuse which carries the primary current for the high voltage transformer. This water fuse has been effective protection against water or memory failure. The whole outfit is obviously inexpensive, it is simple in its controls, two switches and a Variac; and the horizontal mounting of the tube and the large table area has permitted the easy use of a variety of x-ray cameras.

## Tubes

It has already been mentioned that diffraction apparatus is built around the tube that is used. The diffraction tube is therefore the item on which the choice of apparatus turns and while most features of diffraction tubes, such as a line focus, two or four radiation ports, rated voltage and current, etc., are now standard, there are a few features which vary among tubes and which should be considered in choosing apparatus for chemical identification. Chief among these are window material, effective tube radius, and target material. The first two items determine the x-ray intensity available at the camera, and the choice of the third is influenced by the field of the identification work.

At the present time Lindemann glass and beryllium are used for x-ray tube windows. For Mo target tubes ($\lambda = 0.71$ kX) the difference between these two window materials is not important because the transmission of either is near to one. These window materials were developed for the softer radiation from targets of Cu ($\lambda = 1.54$ kX), Co ($\lambda = 1.79$ kX), Fe ($\lambda = 1.93$ kX) and Cr ($\lambda = 2.29$ kX) where x-ray transmission is inherently low especially with Cr, and here the difference between the two materials is significant, the advantage being with the beryllium.[7]

The effective radius of an x-ray diffraction tube should be as small as possible because one deals always with an inverse square law of radiation intensity. The effective radius is determined by how close one can place the diffraction camera to the center of the tube focal spot. Beryllium window tubes enjoy two advantages here: the camera can be placed in contact with the window if desired, and the window can be placed close to the target, beryllium being a good thermal and electrical conductor.

It has been indicated that the writers have found it advantageous to use characteristic radiations other than the Mo$K\alpha$ recommended by the A.S.T.M. practice.[8] Radiations such as Cr, Fe, Co, and particularly Cu have long been used extensively by crystallographers and metallurgists and now that high intensity tubes with these targets are available in this country, their use in identification problems has become more common. These radiations are all much longer wave-length than Mo, and the choice of the particular one to use will depend strongly on the fluorescence considerations discussed below. Because Cu targets can be safely loaded to higher values than Cr, Fe, and Co targets, Cu-radiation is by far the most commonly used of the group

[7] R. R. Machlett, J. App. Phys. **13**, 398–401 (1942).

[8] "Tentative Recommended Practice for Identification of Crystalline Materials by Hanawalt X-ray Diffraction Method," A.S.T.M., Philadelphia, Pennsylvania, 1942.

in crystallography and in our own practice. The advantages of long wave-length radiation will therefore be discussed in terms of Cu$K\alpha$; the same remarks will apply to the other radiations with minor changes.

An important advantage of Cu-radiation is the short exposure time required. There are several obvious factors such as necessary camera diameter and film sensitivity which greatly favor Cu-radiation in this respect, but there are also a number of less obvious and equally important factors some of which favor short wave-length radiation. We shall not try to assign a reason therefore but merely state the well known empirical result that for equal dispersion and resolution, a 15-minute Cu exposure is equivalent to one of several hours with Mo-radiation. Such short exposures have made it possible for the writers to supply useful answers to identification problems when the longer exposure would have been prohibitive, and it would seem that workers closer to industrial problems would very frequently find short exposure an advantage.

Since the wave-length of Cu$K\alpha$ is approximately twice that of Mo$K\alpha$ much greater angular dispersion results, the diffraction pattern of most materials being spread through the full 90° range of Bragg angle in contrast to the range of $\theta$ of from 0 to 30° found with Mo$K\alpha$. This fact may be used to help shorten exposures through decreased camera diameter as noted above, or the large dispersion of long wave-length radiation may be used for better observation of those $d$ values lying in the range from 3 to 8 kX. Many materials, especially mineralogical and organic materials, have strong lines, and what is important, discriminating lines, in this region. The writers have found that this $d$ region is indeed a critical one and merits close attention.

In chemical identification work it is seldom necessary to resort to precision determination of $d$ values or lattice parameters. Some specialized problems however are profitably studied by such determinations which are not particularly difficult to make by means of well-known back reflection methods. Back reflection methods necessarily employ long wave-length radiation.

These factors influence us strongly to the use of long wave-length radiation and it is apparent from the availability of the equipment that other workers are so influenced also. There are disadvantages in the use of long wave-length radiation, notably the fluorescence difficulty and the fact that much existing data lists intensities in terms of Mo-radiation. The effect of these difficulties will be discussed, but we are left with a strong preference for long wave-length, and particularly for Cu-radiation, the most generally useful of all.

The fluorescence difficulty may be stated as follows: the characteristic radiation from a given target in the long wave-length group (wave-lengths listed above) is capable of exciting $K$ fluorescence in specimen atoms which have an atomic number less than that of the target by two or more. The resulting $K$ fluorescence radiation ($L$ fluorescence is seldom troublesome) produces a general background on the diffraction pattern which is exceedingly strong if the specimen contains a substantial portion of material located 2, 3, or 4 places below the target material in atomic number. Fluorescence may thus involve an important group of elements, e.g., Co, Fe, and Mn in the case of a Cu target tube, and Mo-radiation possesses the advantage that few important elements are located immediately below Mo in the atomic number.

It is evident then that the choice of the particular long wave-length radiation must be made with the field of the identification work in mind. Thus metallurgists dealing exclusively with ordinary steels use Co- or Fe-radiations; those dealing with high alloy steels would be well advised to use Cr-radiation; chemists concerned only with iron corrosion products should use Co- or Fe-radiation. The person confronted with materials which range the periodic table will find, however, that Cu-radiation is the most generally useful, the number of problems involving Co, Fe, and Mn in such a case being statistically not too numerous, and these problems being susceptible to techniques pointed out below.

The ideal solution in the general case for the fluorescence difficulty is to have available a choice of long wave-length tubes. The writers have fallen back on this expedient upon occasion, but most frequently they actually have found it more convenient to use Cu-radiation and to accept the fluorescence background. The reasons

for this procedure may be discussed in terms of Cu-radiation and a specimen known to contain Fe. Four cases arise depending on whether the material is single phase or polyphase, and on whether the phases are simple or complex crystallographically. A single simple phase such as Fe or FeO being high in Fe will produce strong fluorescence when exposed to Cu-radiation, but being simple, it will in general produce a strong diffraction pattern, and we have found such patterns easily identifiable in spite of the background. The same remark applies to a lesser degree to a polyphase mixture of simple materials. Single phase specimens involving crystallographically complex materials will in general give a weak diffraction pattern, but also in general the proportion of Fe and hence the fluorescence will be low. Polyphase and crystallographically complex materials will usually be difficult, and so, of course, would be the detection of any minor phase in the presence of a high Fe major phase. In the Cu–Fe situation and in similar situations the fluorescence background can be reduced by the use of filters discussed below, but this technique is not nearly so effective as when the fluorescence is caused by elements considerably below the target element in atomic number.

Elements five places or more below the target element also produce fluorescence, but in this case the excitation is not nearly so strong, and since the fluorescence wave-length is considerably longer than that of the target radiation, it can be effectively filtered out of the radiation striking the film. Filtration can be effected by placing between the sample and the film sheets of aluminum or better still, sheets of the $K\beta$ filter appropriate to the radiation used. In this manner identifiable patterns of $MnO_2$, and excellent patterns of $TiO_2$ can be made with Cu-radiation. Because fluorescence radiation may be excited by radiation from the tube other than the characteristic radiation which creates the diffraction pattern, the use of the $K\beta$ filter in this fashion is generally desirable and should be standard practice. Since the filter used in this way should not be in contact with the film and because filter materials are difficult to handle, some sort of jig or other holding device is desirable. It would be helpful if camera manufacturers built in such devices in the future.

### Filters

The purpose of the $K\beta$ filter is to reduce to a negligible amount the intensity of the characteristic and monochromatic $K\beta$-radiation relative to the intensity of the $K\alpha$-radiation of the target element. In the case of the long wave-length targets this can be done by inserting in the x-ray beam a filter composed predominantly of the element one lower in atomic number than the target element; for Mo-radiation a proper filter is Zr. Such filters may be the proper pure element and in the case of Ni for Cu-radiation this is convenient[9] but in the case of other $K\beta$ filters the active element is more easily used in the form of a compound. Such filters made with the proper concentration of active elements are now available in any desired size.[10] The filter will serve its designed purpose when a small piece is inserted in the primary x-ray beam, but as indicated above, the $K\beta$ filter will in addition act as a fluorescence filter when introduced in the proper sized sheet between the film and the specimen. Since the $K\beta$ filter does not eliminate the $K\beta$-radiation but merely reduces it relative to the $K\alpha$-radiation, the identification worker will do well to assess its effectiveness by making long exposure trial patterns of a simple substance.

### Camera Design

At the Dow Chemical Laboratories quarter-circle cameras of 8-inch radius are used on an apparatus which permits exposing 24 samples at one time. However the exposure time runs about six hours. Where molybdenum radiation is used, the quarter-circle camera gives all of the pattern that is useful for identification purposes. With longer wave-length radiation, it is profitable to employ a full circle camera which permits recording of back reflection lines and gives a symmetrical pattern which doubles the accuracy of measurement of the angle $\theta$.

Cameras of the full circle type are commerci-

[9] Nickel foil of the proper thickness (0.0004 in.) may be obtained from the General Electric X-ray Corporation.

[10] Manufactured by the Patterson Screen Company, Towanda, Pennsylvania, and available through representatives of the leading x-ray apparatus manufacturers.

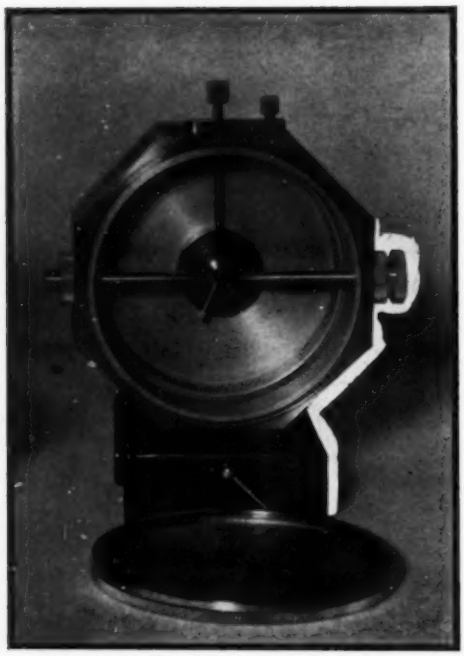

FIG. 2. An example of an x-ray diffraction camera particularly suitable for identification work. The collimating system is entirely within the camera. Two desirable features shown are the specimen centering device and the primary x-ray beam outlet shield (Courtesy of Otto von der Heyde, Newton Highlands, Massachusetts).

ally available from several of the manufacturers of x-ray equipment and also from some of the independent instrument makers. These cameras differ among themselves in a number of details, and the purchaser of new x-ray equipment will do well to investigate a number of makes with a view to getting the most suitable equipment for his purpose. The design of powder cameras for general use has been extensively treated recently in an excellent paper in this journal.[11] We shall mention here points particularly pertinent in chemical identification.

The diameter of the camera should preferably be some integer multiple of 57.26 mm in order that linear measurement on the film will be easily convertible to angular measurement in degrees. This greatly reduces the amount of routine calculation in determining $d$ values. The writers have used a camera of 57.26-mm diameter with considerable satisfaction and have found it to give sufficient accuracy for most routine identification work. With copper radiation, exposures run from 10 to 20 minutes. However, we are of the opinion that if only one camera is to be purchased and speed is not too important a consideration, it would be best to select one of 114.52-mm diameter. This camera size used with copper radiation permits somewhat greater accuracy of measurement than the large radius quadrant cameras employed by Hanawalt when used with molybdenum radiation. By using the back reflection lines, lattice parameters for cubic crystals can be calculated with considerable precision. At the same time exposure times are not unduly large. Cameras of still greater size may be useful on occasion, but should not be needed for routine identification work.

Some provision for rotating the sample during exposure is made on practically all modern cameras. The purpose of sample rotation is to increase effectively the randomicity of crystalline orientations in the specimen. In the case of large grained, difficult-to-grind specimens, rotation saves much time and labor. The writers prefer the type of apparatus for rotation with a belt driven pulley attached to the sample holder rather than the built-in motor type. The reason is that the sample can be rotated by hand while the alignment of the x-ray beam is being adjusted, thus checking the centering of the sample. We prefer not to rotate the sample if the sample size is adequate, and the particle size small enough to give a smooth pattern without rotation. It is very important that the sample should be accurately centered in the camera and coaxial with the rotating mechanism. While a number of permanently centered cameras are on the market, the type with centering screws for making this adjustment is to be preferred.

All modern cameras have a fluorescent window in the exit portal for use in aligning the camera in the x-ray beam, and the centering of the sample can be finally checked by watching the shadow of the sample in the window while the sample is rotated by hand. The design of the collimating system is of utmost importance in obtaining clean films with a minimum of background darkening. It is desirable for intensity reasons that the collimating system should be within the camera itself with the final opening as near as possible to the sample. Some cameras have as a highly desirable feature a shield or trap

[11] M. J. Buerger, J. App. Phys. 16, 501–510 (1945).

which protects the film from radiation scattered from the collimating system and from the air near the exit portal, Fig. 2.

The camera must be provided with a flexible and convenient mounting arrangement so that it can be easily aligned in the x-ray beam. It should also be possible to remove the camera for loading and unloading films and replace it in accurate alignment without readjustment. A little time saved on these routine operations will mount up if much work is done.

### Film

At the present time x-ray film is available with thick, double emulsions, which film compares favorably in speed with older emulsions used with intensifying screens. Such film sold variously under the names No-Screen, Non-Screen, etc., is best for diffraction work. The writers always use this type of film and in routine work make no attempt to correct for dimensional changes caused by the film processing, finding it readily possible to achieve the accuracy inherent in the A.S.T.M. data without correction. The only precaution taken is to dry the film thoroughly before measurement.

It is proper here to mention the Straumanis technique which has come into common use. The Straumanis technique is essentially a method of eliminating errors owing to camera diameter uncertainty and film dimension changes[12] by an ingenious method of loading the film. Two holes are punched in the film instead of the customary one hole for the exit beam. The two holes are spaced a camera half-circumference apart and the film is loaded so that the beam enters through one hole and leaves through the other. If back reflection lines are present on the pattern, appropriate measurements on the processed film will serve to determine the effective camera diameter. This scheme will fulfill the purpose for which it was designed only when properly used. The technique inherently demands precision positioning of the specimen and, therefore, requires an accurately made camera equipped with specimen centering cross motions. The Straumanis method of loading the film is to be recommended regardless of whether the diameter determination is carried through. No extra effort is involved, and as has been pointed out[11] a complete record of the diffraction pattern results, which can at any latter time be used for diameter correction and/or back reflection measurements.

[12] M. J. Buerger, *X-Ray Crystallography* (John Wiley and Sons, Inc., London, 1942), pp. 394–396.

### Geiger Counter Method

There has recently appeared an excellent Geiger counter spectrometer[13] which has valuable application in the field of x-ray diffraction chemical identification. Because the instrument yields directly and quickly x-ray intensities, it opens wide the field of quantitative diffraction analysis, and it would appear to be especially valuable in routine control operations. While the instrument possesses ample angular precision for identification purposes, the writers are not convinced by the literature statements that the instrument "is capable of angular measurements and resolutions beyond that attainable by means of photographic cameras."[14] The published intensity curves and comparable microphotometer records do not support the part about angular measurements, and it is well known that microphotometer traces are an exceedingly poor way of exhibiting photographic resolution and the detectability of a diffraction line. The instrument will have many applications but we feel that these will be complementary to photographic methods in the general identification laboratory.

## III. TECHNIQUE

### Preparation of the Sample

Probably there are almost as many ways of preparing the diffraction sample as there are x-ray workers. The ideal sample would consist wholly of the substance to be identified without either a container or a binder. The specimen should be small enough for good resolution and to avoid absorption effects and yet large enough for reasonable exposures and for practicable handling. Finally the specimen must contain enough crystals to give a smooth line pattern. These ideals can seldom all be attained simultaneously in practice except in the case of metals which can be drawn into wires.

[13] North American Philips Company, Inc., 100 East 42 Street, New York 17, New York.

[14] H. Friedman, Electronics (April 1945).

The size of the specimen to be exposed to the x-ray beam is a matter of compromise primarily between x-ray line resolution and practicable handling. Consensus of opinion among x-ray workers seems to favor a sample diameter of 0.4 mm. For the small 57.3-mm diameter camera, this is certainly an upper limit for good resolution, and the writers have found it necessary to employ smaller sample diameters in many cases.

Specimens which are the proper size but which absorb x-rays highly will produce systematic small errors in $d$ value and large errors in intensity. The cure is reduction in specimen size, error correction, or dilution. Most sample preparation techniques involve a binder which allows qualitative dilution to be made. The writers have never found it practical to follow a schedule of dilution, although this is possible.

Samples should be ground to 200-mesh or finer to help insure that the sample contains enough crystals to produce a smooth line diffraction pattern. Many identification samples have small enough crystal size naturally but must be ground to insure homogeneity and for effective mixing with the binder. Small "sillimanite" mortars are very convenient for grinding and mixing the identification specimen which is often itself quite tiny. Such mortars are so inexpensive that a number can be kept at hand to avoid the necessity of repeated washing, and even to store the specimen for other tests.

Frequently 200-mesh specimens do not produce smooth diffraction lines. In this case the specimen must be rotated, and in some cases should be scanned along its length in order to increase the effective number of crystals. Buerger[11] has discussed the design of rotation devices and of an ingenious scanning device. The latter, unfortunately, is not available commercially to our knowledge. The point to be kept in mind about rotation is that it demands accurate specimen centering; scanning imposes such alignment demands as to be of questionable practicability in routine identification work. The writers prefer not to rotate if it can be avoided by further grinding. An interesting sidelight to rotation is that occasionally in identification work the lines of two phases may be separated by their differing spottiness.

In the Dow Chemical Laboratories, samples are loaded in thin Pyrex capillary tubes having an internal diameter of 0.40 mm. Where molybdenum radiation is employed, glass capillaries are not greatly objectionable, but even very thin glass is quite absorptive of x-rays and most workers who use softer radiations, such as copper or iron, must avoid it. Plastic capillaries have been used by some workers but they are not readily available at the present time. It is quite possible to prepare suitable tubes of Cellophane by rolling it around a mandrel of proper size.[15] The tubes are made as short as the sample holder will permit and the ends are closed with wax after filling. Other workers prefer to mix the sample with collodion diluted with amyl acetate and ether and coat it on a thin thread obtained by untwisting a piece of sewing thread. Another method is to place the sample in a drop of collodion on a glass slide and when the collodion is nearly dry to roll it into the shape of a thin rod incorporating the sample.[16] If only a little sample is available, all of it can be quite conveniently concentrated in one end of the rod. Rubber cement can be used in the same way. Another technique is to mix the sample with a suitable binder such as library paste, dilute collodion, or glyceryl phthalate and then extrude the mixture through a simple die.[17] The die itself with the attached extrusion can be made to fit directly in the sample holder. Probably the beginner in x-ray work will do well to try several of these methods and then adopt the one that pleases him best. It must be remembered that all tubes or binder materials absorb some x-rays and produce more or less background darkening on film, and many of them produce a diffraction pattern of their own. It is desirable to run a blank film on the container or binder without any sample in order to determine whether any diffraction pattern is produced.

### Measurement of Films

After the exposed film has been developed and dried, it may be conveniently studied on a light box with a sloping opal glass front. Some workers use more or less elaborate film measuring devices, but the writers prefer to measure routine films

[15] A. A. Burr, Rev. Sci. Inst. **13**, 127 (1942).
[16] G. A. Harcourt, Am. Mineralogist **27**, 63 (1942).
[17] J. S. Lukesh, Rev. Sci. Inst. **11**, 200 (1940).

made in the 57.26-mm diameter camera by setting a pair of sharp pointed dividers on corresponding lines and reading the distance on a good celluloid scale graduated in half-millimeters. Successive readings seldom differ by more than one or two tenths of a millimeter, and errors as large as this are likely to occur in setting any of the measuring devices in use.

When very weak lines must be found and measured, as is sometimes necessary in polyphase samples, the characteristics of the human eye play an important part.[18] The cross line slider with which some measuring devices are equipped has a definite tendency to cause weak lines to vanish, apparently, as the setting is being made. The simple divider technique avoids this difficulty and the detection of weak lines can be made easier by providing the viewing box with a Variac to lower the level of illumination. It is sometimes an advantage to clip or tape the film to a piece of plain glass which can be placed some distance from the opal illuminator and which can be tilted with respect to it. If a device with a slider is used, we prefer a pointed indicator to the cross line type.

If the camera diameter is some simple multiple of 57.26 mm, interlinear measurements are easily converted into angular measurement in degrees by simply dividing by the appropriate factor. $d$ values are calculated from the Bragg formula $d=\lambda/2\sin\theta$. Repeated performance of this routine calculation is time consuming and can be avoided by the use of a very convenient graphical chart prepared at the suggestion of the writers by O. E. Brown.[19] This chart is intended particularly for identification work and covers a range suitable for use with the A.S.T.M. tables. The chart covers copper, cobalt, iron, chromium, and molybdenum radiations which are the ones most valuable for identification work. To use it, the measured $\theta$ value is found under the appropriate horizontal line and the corresponding $d$ value read off above the line.

The intensity of x-ray diffraction lines is most easily estimated by eye and noted on a scale of 1 to 10. Apparently most workers use such a method as do the writers. The method is recommended in the majority of problems for its speed, but some problems may require a more careful method. Hanawalt's method is to use a comparison strip, which is a film containing lines of graded exposure. The comparison method is certainly accurate enough for all identification work, and once the comparison strip is prepared the use of it is nearly as rapid as simple estimation. It is to be hoped that one of the x-ray manufacturers will make comparison strips available commercially.

[18] It may be pointed out here that the eye is a far more sensitive instrument for such purposes than a microphotometer.

[19] Orley E. Brown, J. App. Phys. **18**, 191 (1947).

## IV. INTERPRETATION

The result of the purely experimental side of x-ray chemical identification is a table of $d$ values and the corresponding relative intensities. The interpretation of these data may follow several courses, depending on the complexity of the problem and the comparison data available. Identification work has long been carried out by simple comparison of the unknown film with films of known substances, and much work can be and is done in this way even yet. Such a method fails in the case of polyphase materials or where only a limited library of standards is available. The great contribution of Hanawalt and the A.S.T.M. has been to place in the literature a volume of identified data arranged in a systematic fashion.

### Examples

A great volume of identification problems deal with questions such as "What manganese compound is present in this sample?," "What oxide of lead is this?," or "This substance is predominately one phase; what is the phase?" Where the problem is a simple one of this type, with auxiliary information available, the data for 1000 common materials published by Hanawalt[2] are the rapid and effective means of making the identification. An example is described below in which this interpretation technique was used, and in which also a modified experimental approach was used.

On one occasion the writers were asked to identify a very thin white coating on the inside of a glass tube. The conditions under which the coating had been formed suggested the probability that it was a copper compound. The

FIG. 3. X-ray diffraction pattern made with Cu$K\alpha$-radiation of an unknown identified as $CaSO_4 \cdot \frac{1}{2}H_2O$ and $CaCO_3$. The line labeled $B$ is a superposition of strong lines from each phase. The $K\beta$-filter (a sheet of nickel foil) was placed between the sample and the film. The sharply defined blackening occurs where the filter did not meet and is caused by calcium fluorescence radiation.

thinness of the coating made it infeasible to prepare a sample in the ordinary way. Instead, the tube was broken, and a small piece of the glass was mounted in the center of the camera in such a way that a pencil of x-rays struck the coated surface with a very small glancing angle. A pattern consisting of only four rather weak lines was obtained. The $d$ values were computed and the data of Hanawalt[2] were inspected, the search being confined to the simple copper compounds. The data matched perfectly with the principal lines of the pattern for $CuCl_2$. Since the presence of chlorine in the system had not previously been suspected, the information proved highly useful and the determination required less than an hour of elapsed time. Other modifications in technique will be suggested by the ingenuity and experience of the worker. The small 57-mm camera is ideal for problems of this general type, where precision and resolving power are not particularly needed, and where speed may be useful.

The more complex problems involve polyphase samples, or samples consisting of an uncommon single phase. In the former case the interpretation approach described above is often effective with the dominant phase, but the minor phases which may be represented by only a few lines each must be attacked by using a systematic method employing as large a volume of standard data as possible. The A.S.T.M. card index file of x-ray diffraction data provides such a method.

The A.S.T.M. card index file, including the recent supplement, contains data for roughly 3000 substances. A given substance is represented by three cards, one for each of its three strongest lines and their relative intensity, and the card for the strongest line carries, in addition, the data for the entire pattern plus auxiliary information and references. All cards are arranged in order of decreasing $d$ value.[20] To use the card file one simply searches the cards in the vicinity of the $d$ value of the strongest unknown line, allowing reasonable limits of error. One looks for a card that shows *other* strong lines matching other strong unknown lines, and which corresponds with a substance which is reasonable on the grounds of the other evidence available. When a match of strongest lines is found, the card corresponding with the strongest line of the tentative identification is looked up and all the unknown lines are compared. If all unknown lines match, the identification is complete; if the match is not good, a further search must be made; if the unknown accounts substantially for all the lines of the tentative identification and unknown lines are left over, a second phase must be sought for. The complex situation involving several phases and superposition of lines is best described by example.

Such an example is one which the writers invented for students in an x-ray laboratory class to solve, and the reasoning used by one of the better students is presented below. The sample consisted of equal parts by weight of $CaSO_4 \cdot \frac{1}{2}H_2O$ and precipitated $CaCO_3$, and the students were given no advance information except that of their eyes telling them that the unknown was a white fluffy powder.

The sample was prepared by grinding in a small "sillimanite" mortar, mixing with collodion-ether-amyl acetate and coating on a fine cotton thread. The film was loaded in the Straumanis manner and a filter of nickel foil 0.0004 in. thick was placed in the camera between the sample and the film. In this particular instance a 72-mm camera manufactured by the Picker X-Ray

[20] This statement applies to the cards as furnished by the A.S.T.M. Other arrangements within subgroups of cards are possible.

Corporation was used and the exposure was 30 minutes with copper radiation and without rotation of the sample. The resulting pattern, Fig. 3, contained one very strong line, about ten medium lines, and many weak lines. The lines were measured with dividers and scale, the camera diameter was determined from the film, and the $\theta$ values were computed. $d$ values were determined by the use of O. E. Brown's chart.[19] Intensity values were estimated visually. The resulting data are listed in Table I.

Since the line at $d=3.02$ kX is by far the strongest line on the film the student began his attempted identification by searching in the card file from $d=3.00$ to $d=3.04$ kX for cards which also listed a strong line at either $d=5.9\pm0.1$ kX *or* $d=2.80\pm0.02$ kX. When such a card was found, the third listed line was checked against the data for the unknown sample. Those cards on which all three strongest lines did not correspond to lines in the data for the unknown (three cases) were returned to the file. The one case where correspondence occurred for all three lines was the card for $CaSO_4\cdot\frac{1}{2}H_2O$. Accepting this as a tentative identification, all of the lines listed for this substance were compared with the data for the unknown, the cases of correspondence being shown in Table I. It will be seen that the strongest five lines listed for $CaSO_4\cdot\frac{1}{2}H_2O$ as well as some of the weaker lines occur in the data for the unknown. The identification of $CaSO_4\cdot\frac{1}{2}H_2O$ is thus confirmed, but it was clear that an additional phase must be present since so many lines in the unknown were not accounted for. This being the case, the fact that some of the weaker $CaSO_4\cdot\frac{1}{2}H_2O$ lines were missing from the unknown was correctly ascribed to the effects of dilution.

The next step was to identify the as yet unknown phase or phases. At this point the student reasoned that although the line $d=3.02$ is by far the strongest line on the film, it is listed as only the second strongest in the data for $CaSO_4\cdot\frac{1}{2}H_2O$ and consequently there must be a strong line for the unknown phase superimposed upon it. Accordingly he again searched the file in the $d=3.02$ region, this time seeking cards which list a strong line at $d=2.48\pm0.02$ *or* $d=2.28\pm0.02$. This search led to the $CaCO_3$ card which listed as its third strongest line $d=2.28$ and as its second strongest $d=1.92$ which is also found in the data for the unknown. The comparison is completed in Table I which exhibits the fact that all of the experimental $d$ values are accounted for by the identified phases. Conversely the experimental data account for all the strong and medium lines listed in the card file for the two phases except $d=2.13$ for $CaSO_4\cdot\frac{1}{2}H_2O$. Examination of the film revealed that the $d=2.09$ line is in fact broadened toward the high $d$ side suggesting that the $d=2.13$ line was missed because of partial superposition. The intensity agreement is rough but satisfactory. Any doubts on this score are resolved when reference is made to cards which give duplicating data for the two phases from different sources. The experimental data agree with any one card as well as the cards agree with each other.

This example was chosen intentionally to present the student with the difficulty caused by superposition of strong lines from the two phases contained in the sample. Yet the identification was correctly made in a minimum of time. The fact that all the stronger lines for both phases appear on the film would have justified the further inference that both phases are present in major amount. Any further quantitative inferences would not be justified without prepa-

TABLE I. X-ray diffraction data for an unknown specimen compared with the card file data of the identified phases.

| | Experimental data | | Card No. 2438 $CaSO_4\cdot\frac{1}{2}H_2O$ | | Card No. 2438 $CaCO_3$ | |
|---|---|---|---|---|---|---|
| Line | Relative intensity (estimated) | $d$ value in kX | $d$ value | Relative intensity (measured) | $d$ value | Relative intensity (measured) |
| | 4 | 5.96 | 6.0 | 0.40 | | |
| | 3 | 3.87 | | | 3.86 | 0.08 |
| *A* | 3 | 3.46 | 3.48 | 0.30 | | |
| *B* | 10 | 3.02 | 3.00 | 0.60 | 3.04 | 1.00 |
| *C* | 4 | 2.80 | 2.80 | 1.00 | | |
| *D* | 4 | 2.48 | | | 2.49 | 0.20 |
| | | | 2.34 | 0.02 | | |
| *E* | 4 | 2.28 | | | 2.28 | 0.24 |
| | | | 2.13 | 0.18 | | |
| *F* | 4 | 2.09 | | | 2.09 | 0.20 |
| | 3 | 1.92 | | | 1.92 | 0.32 |
| *G* | 3 | 1.86 | | | 1.87 | 0.24 |
| | 3 | 1.84 | 1.85 | 0.60 | | |
| | | | 1.74 | 0.02 | | |
| *H* | 1 | 1.68 | 1.69 | 0.10 | | |
| *I* | 2 | 1.595 | | | 1.60 | 0.16 |
| | | | 1.53 | 0.04 | | |
| *J* | 2 | 1.514 | | | 1.51 | 0.12 |
| *K* | 1 | 1.469 | 1.470 | 0.02 | 1.475 | 0.05 |
| | | | 1.445 | 0.02 | | |
| *L* | 2 | 1.432 | | | 1.439 | 0.08 |

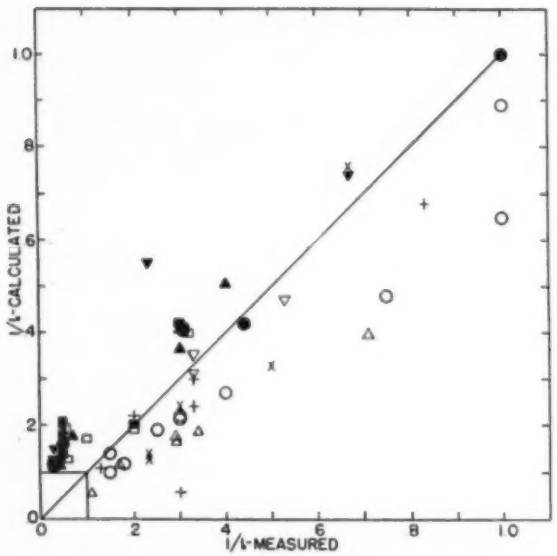


FIG. 4. Calculated theoretical relative intensities are plotted against relative intensities measured by the comparison method by Hanawalt and co-workers. The experimental data all come from the A.S.T.M. card file. The numerous data in the small square are not plotted.

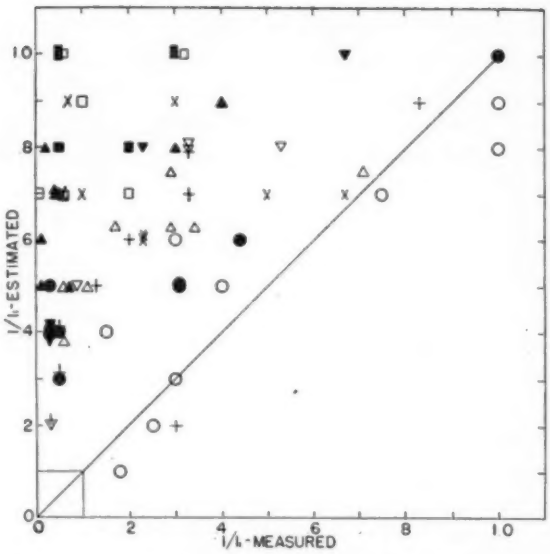


FIG. 5. Estimated relative intensities are plotted against measured intensities for the same substances as Fig. 4. Data are from duplicate entries in the A.S.T.M. card file.

□ Columbium
○ Cadmium oxide
△ Tungsten
▽ Copper
+ Sodium chloride
■ Tantalum
● Cuprous oxide
▲ Aluminum
▼ Lithium fluoride
× Calcium fluoride

ration of standard films from the two substances for comparison.

## V. AGREEMENT OF DATA

The Hanawalt scheme of chemical identification is based on the empirically demonstrated fact that the *d* values of the three strongest lines of a phase identify that phase nearly uniquely. Completely unique identification implies agreement of all *d* values and in addition substantial agreement of intensities. While *d* value agreement, within allowable limits, must occur intensity agreement often does not occur even in the case of the three strongest lines. Often, too, different sources will disagree on the actual presence of a fairly important line.

Table I lists three sets of data for the same substance, taken from the A.S.T.M. card file, and illustrating these three effects. These data are the work of skilled workers, and there is little likelihood of chemical impurity of the sample examined. It is highly probable that the reader will find as many deviations in his own data as among the ones quoted. The agreement among *d* values is about as good as could be expected considering technical limitations. *d* value results similar to the third set of data quoted *may* occur because of excessive sample size and absorption, poor sample position or possibly film shrinkage, all effects which should be eliminated in standardized technique. The situation with regard to "missing" lines is an interesting one of not infrequent occurrence, the reasons for which are too varied for a general explanation to be attempted here. The very existence of such discrepancies in the card file means that one need not be too disconcerted when it occurs in practice. Of course, a reason and sometimes a significant reason for such effects exists, but if the work has been carefully done the "difficulty" may just as well be in the literature data or literature material.

The discrepancies in intensities of Table II are disturbing at first sight and the writers have made an inspection of published data in an attempt to discover the source of the difficulty. The details of the study need not be given here but the results of the comparison will be of interest to the user of the card file data and are summarized in Figs. 4 and 5.

Duplicate sets of data for 10 simple substances are compared in the figures. Since the chosen substances are simple, reliable calculations of

theoretical intensity are readily made by the accepted methods. Figure 4 is a composite plot comparing the relative intensities as measured by Hanawalt by his simple method of visual comparison with prepared standards, against the calculated theoretical intensities. The calculated and measured values agree as well as is usually the case with x-ray diffraction intensities. The comparison is presented here to give added reliance on the measured values and to indicate the degree of intensity agreement to be expected generally.

Figure 5 gives a comparison of intensities as measured by Hanawalt with intensities obtained by the commonly employed method of visual estimation on the basis of an arbitrary scale of one to ten. The data are all from the card file and the number of observers is large enough to eliminate the personal factor. It is clear that the estimated intensities differ rather radically from the measured ones and that the method of estimation tends to exaggerate the relative intensity of the weaker lines. The disagreement is large enough that an identification cannot be expected to show intensity agreement except in a highly qualitative fashion when intensities are estimated. Actually in straight identification work, the disagreements are not as important as they appear. The intensity values themselves are less important than the *order* of intensities and this is quite reliably determined by visual comparison.

Since one of the purposes of the present paper is to recommend the use of long wave-length radiations in identification work, it is pertinent to inquire how the relative intensities on long wave-length patterns compare with the intensities on patterns made with Mo$K\alpha$. Frevel has given an answer for Cu$K\alpha$ on a semi-empirical, semi-theoretical basis,[21] in the form of a table of conversion factors. This table shows that Cu$K\alpha$ intensities should not differ from Mo$K\alpha$ intensities by more than 25 percent, as long as the Cu$K\alpha$ Bragg angle is less than 45°. This difference is certainly not an important one. At Bragg angles greater than 45°, Cu$K\alpha$ relative intensities are very much higher than the relative intensities of lines of the same $d$ value on a Mo$K\alpha$ pattern. There may be as much as a factor of 5 at high Bragg angle, arising from the Lorentz polarization factor. Because the most intense lines generally arise from the large $d$ values which occur at small Bragg angle, it would seem that the wave-length effect on intensities could as a first approximation be neglected.

The above remarks and conclusion have necessarily been made on the basis of theory and apply to intensity *measurements*. Intensity estimates with Cu$K\alpha$ will of course be as good or as bad as Mo$K\alpha$ estimates. In addition there is the effect of absorption by the sample which can be

[21] Quoted in the "Alphabetical Index of X-ray Diffraction Patterns," A.S.T.M., Philadelphia, Pennsylvania.

TABLE II. Comparison x-ray diffraction data taken from A.S.T.M. card file for anatase ($TiO_2$). The number of the card is given, II denoting a card from the First Supplement—1945. The third pair of columns is stated to represent data from two sources, in good agreement, with the symbol $n$ denoting lines not given by both sources.

| Card 1406 Mo$K\alpha$-radiation | | Card II-876 Mo$K\alpha$-radiation | | Card II-911 Mo$K\alpha$-radiation | |
|---|---|---|---|---|---|
| $d$ | $\frac{I}{I_1}$ measured | $d$ | $\frac{I}{I_1}$ estimated | $d$ | $\frac{I}{I_1}$ estimated |
| 3.52 | 1.00 | 3.508 | 1.0 | 3.47 | 1.0 |
| | | 2.425 | .1 | 2.39 | .4 |
| 2.37 | .24 | 2.372 | .5 | 2.35 | .4*n* |
| | | 2.333 | .1 | 2.305 | .2*n* |
| 1.88 | .40 | 1.887 | .9 | 1.878 | .9 |
| 1.70 | .28 | 1.696 | .7 | 1.689 | .7 |
| 1.66 | .24 | 1.662 | .7 | 1.654 | .7 |
| 1.480 | .24 | 1.447 | .7 | 1.472 | .6 |
| 1.362 | .08 | 1.361 | .6 | 1.358 | .3 |
| 1.335 | .08 | 1.335 | .6 | 1.332 | .4 |
| 1.262 | .11 | 1.261 | .7 | 1.258 | .6 |
| | | 1.247 | .2 | 1.242 | .4*n* |
| 1.164 | .06 | 1.163 | .6 | 1.159 | .4*b* |
| | | 1.158 | .1 | | |
| | | 1.054 | .1 | | |
| 1.045 | .03 | 1.0488 | .5 | 1.044 | .3 |
| | | 1.0407 | .5 | 1.038 | .6*n* |
| | | 1.0155 | .5 | 1.014 | .2 |
| | | 1.0043 | .2 | 1.002 | .2 |
| | | .9939 | .1 | | |
| .950 | .02 | .9528 | .7 | .951 | .3 |
| | | .9437 | .6 | .943 | .4 |
| .913 | .02 | .9167 | .7 | .916 | .6 |
| | | .9114 | .7 | .912 | .3 |
| .894 | .02 | | | .892 | .1*n* |
| | | | | .876 | .1*n* |
| | | | | .843 | .1*n* |
| | | | | .824 | .1*n* |
| | | | | .806 | .1*n* |
| | | | | .795 | .1*n* |
| | | | | .740 | .1*n* |
| | | | | .702 | .1*n* |
| | | | | .668 | .1*n* |

important with long wave-lengths. The effect of absorption is to reduce the intensity of high $d$ lines, and because these are generally the strong lines, to raise effectively all relative intensities. That this effect is present to a significant degree is entirely supported by eight cases of duplicate card file data involving both Mo$K\alpha$ and Cu$K\alpha$.

All of the above remarks for Cu$K\alpha$ intensity apply with much more force to the longer wave-lengths such as Fe$K\alpha$ and Cr$K\alpha$. With these radiations the absorption factor is exceedingly important, and further the important lines begin to occur at large Bragg angle where they are enhanced by the Lorentz polarization factor. Three cases have been found in the card file literature where Mo$K\alpha$ intensity measurements are duplicated by estimates on patterns of the same material made with Ni$K\alpha$, Fe$K\alpha$, and Cr$K\alpha$. The long wave-length intensities show only small differences from line to line, while the Mo$K\alpha$ intensities for corresponding lines show radical differences.

## VI. LIMITATIONS AND ADVANTAGES

The x-ray diffraction method of chemical identification is obviously limited to materials listed in the standards library available which ordinarily excludes solid solutions, and, of course, eliminates non-crystalling materials. In addition the method suffers the major limitation that it is not very sensitive to small *concentrations* of a given phase. The minimum concentration that will be detectable will depend upon the substance and also in part, upon the other substances present. Hanawalt states that the minimum may be as low as 1.0 percent or less, or more than 50.0 percent. Perhaps a representative figure would be around 10.0 percent. In general only experiments with known mixtures of the substances to be detected will definitely decide the minimum detectable concentration. However, it is clear that substances giving several lines of high absolute intensities will be detectable in smaller concentration than those yielding only weak lines.

Not uncommonly in industrial work a sample must be studied which contains four or five phases, some of which may be present in such small concentration as to show only one or two of their strongest lines. Clearly in cases of this kind a positive identification cannot be made by x-ray means alone. However, in practical cases some information is usually available to suggest some of the possible substances whose presence the x-ray pattern may confirm. Even in the most difficult cases the diffraction pattern usually yields some information which supplements that obtained from other methods and justifies the effort involved.

The x-ray method also fails to give complete identification in several minor instances. For example, there are numerous oxides of the type $AB_2O_4$ which have the same structure, the spinel type, and of these materials many have lattice parameters that are nearly the same. In addition then to nearly identical $d$ values, the intensities turn out to be similar. Clearly an identification beyond that of the structure type is difficult in such a case. The spinel situation emphasizes that the x-ray method identifies *structures*, from which rigid chemical analyses must not be inferred.

The x-ray diffraction method has unique advantages. Like the petrographic microscope it identifies the phases present and not merely the elements of which they are composed. Dimorphous forms of the same substance are as easily distinguished as different substances, an exceedingly important fact. Unlike the microscope it is not sensitive to very small concentrations of a minor phase but it is particularly successful with opaque materials and very finely divided samples.

Other major advantages of the x-ray method are that only a small sample is needed and the accuracy necessary is easy to achieve. The sample which is used is not destroyed so that it is available for chemical or spectroscopic study later. The x-ray method can upon occasion rival the companion electron diffraction method with respect to its ability to obtain results from a small amount of specimen.

## VII. AUXILIARY PROCEDURES

X-ray diffraction will not displace other means of examination but it does supplement them with information not otherwise obtainable and in some cases it may yield the same information with less effort. In difficult cases it is most helpful to have supplemental information obtained by spectroscopic or conventional chemical analysis. The major cation constitution is particularly

useful in interpretation as well as being a time saver if the cations are such as to cause fluorescence. Industrial clients are occasionally reluctant to furnish such analytical and source information as they already possess regarding a sample, with the result that the x-ray worker is greatly handicapped in interpreting his results.

The writers prefer to give each sample a preliminary examination under the petrographic microscope. Sometimes this makes x-ray examination unnecessary. It is frequently possible to tell at a glance whether the sample is homogeneous or not and at times the presence of a minor phase may be revealed which would be overlooked by x-ray examination alone. Where several phases are present it may be desirable to make a preliminary separation by magnetic means, by heavy liquids, by washing or some other physical means and then examine the fractions separately by x-rays.

It has been stated on certain occasions that the x-ray diffraction method permits chemical identification work to be done with untrained personnel. Probably this is true where a certain number of routine determinations of the same type are to be done over and over again. However, it cannot be too strongly stressed that good x-ray diffraction work demands a high degree of experience and judgment, and at least a reasonable background in x-ray theory and crystallography, together with an understanding of the industrial problems to which the work is being applied. It will be completely futile for any laboratory to purchase an expensive x-ray diffraction outfit and expect to "hire a boy" to operate it.

---

## Charts for Computation of $d$-Values in X-Ray Diffraction Chemical Analysis*

ORLEY E. BROWN
*Department of Mathematics, Case School of Applied Science, Cleveland 6, Ohio*
(Received October 16, 1946)

IN chemical identification by x-ray diffraction, Bragg's equation

$$2d = \lambda \csc\theta,$$

in which $d$ represents the crystallographic interplanar spacing, $\lambda$ the x-ray wave-length, and $\theta$ the Bragg angle, must be repeatedly solved to find the $d$-value which corresponds to a known $\lambda$-value and an observed $\theta$-value. Whereas this equation lends itself to conventional treatment graphically, it is not convenient to secure the accuracy required by the ordinary graphical methods.

Since only five different values of $\lambda$, one for each of five different x-ray targets, are commonly used, these five values were assigned and a doubly graduated scale was prepared for each of the five resulting equations. This type of chart has the advantage of being constructable for any desired accuracy and of being immune to damage due to paper shrinkage or distortion in reproduction.

To use one of the charts, locate the $\theta$-value on the lower side of the scale and read off the corresponding $d$-value from the upper side.

The plates used in printing these charts are being retained, and if the demand warrants, arrangements will be made with a commercial concern to supply reprints of the charts in quantity.

* These charts were undertaken at the suggestion of Richard L. Barrett. See paper in this issue by Smith and Barrett, p. 177.

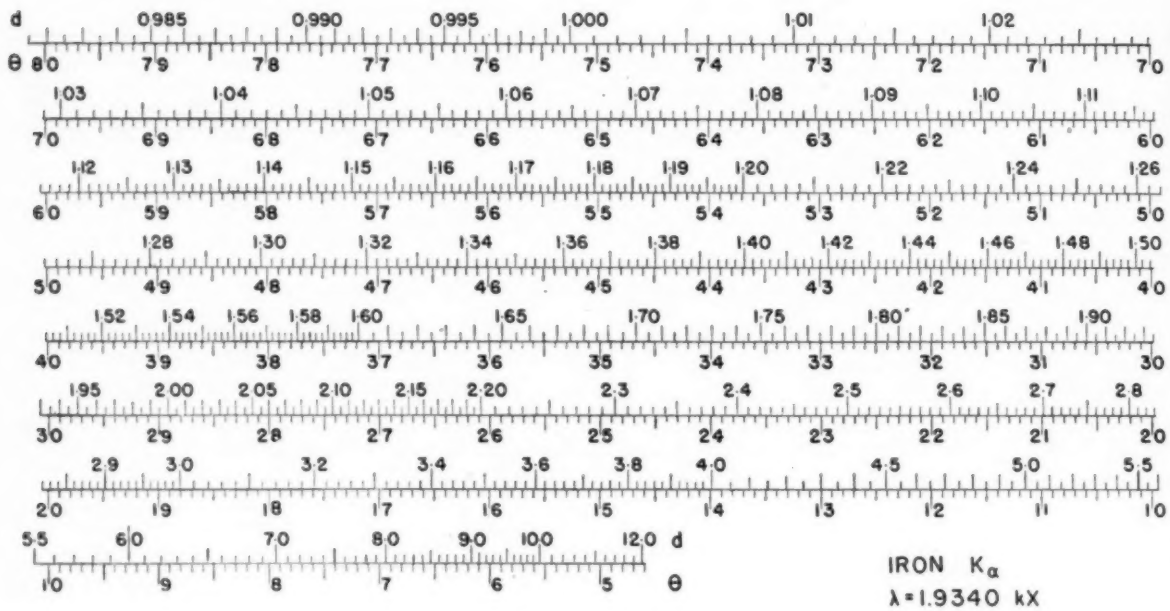
d
θ
IRON $K_\alpha$
λ = 1.9340 kX

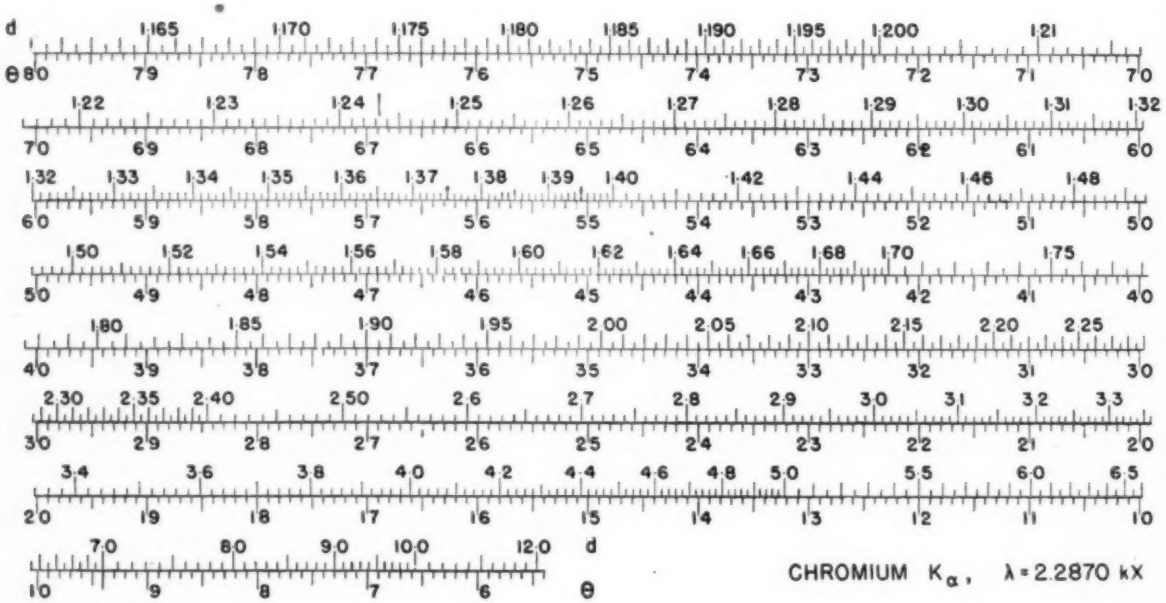
d
θ
CHROMIUM $K_\alpha$, λ = 2.2870 kX

## Charts for Computation of *d*-Values in X-Ray Diffraction Chemical Analysis

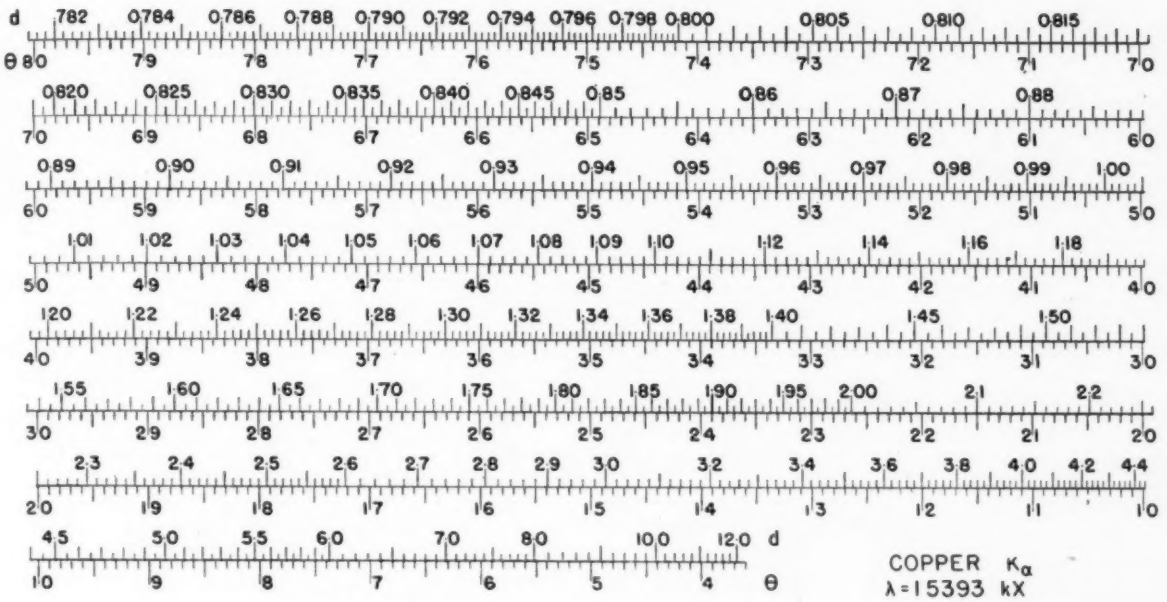


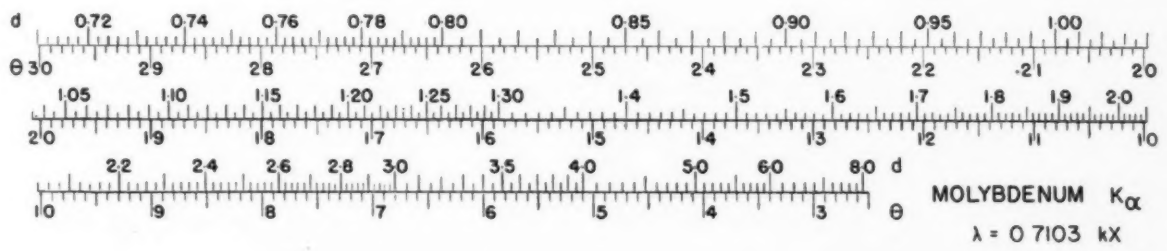


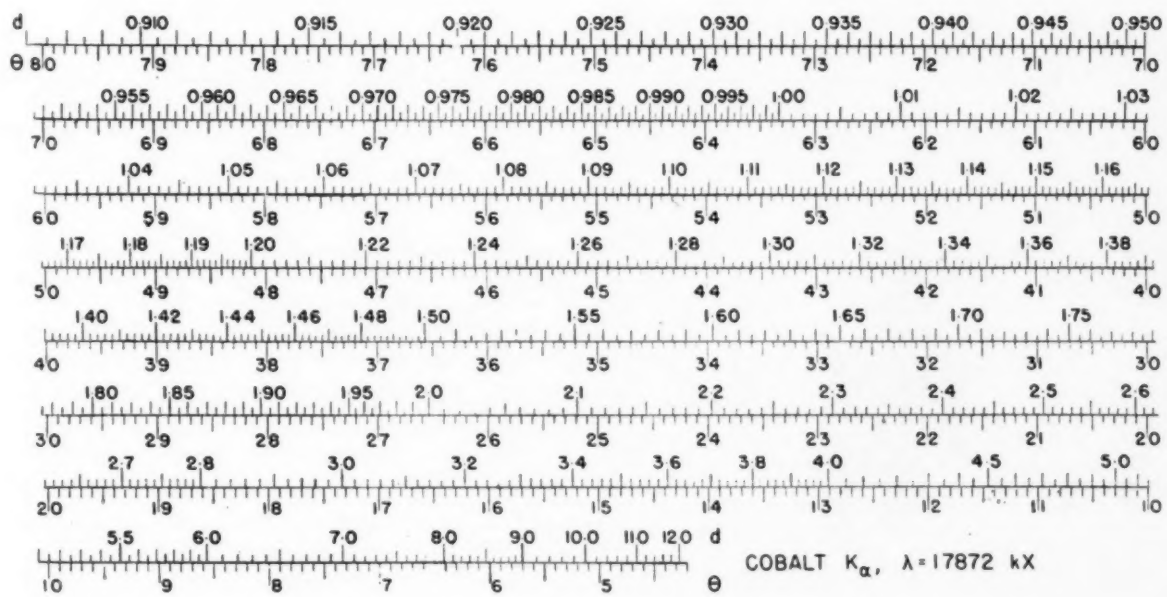

# Streamlines for the Subsonic Flow of a Compressible Fluid Past a Sphere

E. R. Van Driest*
*Massachusetts Institute of Technology, Cambridge, Massachusetts*
(Received June 28, 1946)

The second approximation to the velocity potential for the irrotational flow of a compressible fluid past a sphere, derived independently by Tamada and Kaplan, is used to calculate the subsonic streamlines for the flow of air at a Mach number of 0.5 past a sphere. Comparison is made between these streamlines and those for the irrotational flow of an incompressible fluid. Velocity and pressure comparisons are also shown.

## INTRODUCTION

THE subsonic irrotational flow of a compressible fluid past a sphere has been studied extensively by Lord Rayleigh,[1] K. Tamada,[2] and C. Kaplan.[3] Designating the flow of an incompressible fluid past a sphere as the zero approximation to a solution expressed in ascending powers of $M^2$ for the flow of a compressible fluid about the same object, the first approximation was obtained by Lord Rayleigh and the second by Tamada and Kaplan. Inasmuch as the work of Tamada and Kaplan included the comparison of velocity and pressure distribution on the surface of the sphere for compressible fluid flow with the corresponding distributions for the incompressible flow, the author thought it would be also worth while to make a comparison of the streamlines for the two cases. The present paper therefore shows the second approximation to the streamlines for the flow of air at a Mach number of 0.5 and the corresponding streamlines when the fluid is considered incompressible.

## THE SECOND APPROXIMATION TO THE POTENTIAL FUNCTION

In the case of the steady adiabatic frictionless flow of a perfect gas, the local velocity of sound is given by

$$c^2=c_0^2\left[1+\frac{\gamma-1}{2}M^2\left(1-\frac{V^2}{U^2}\right)\right], \tag{1}$$

where $U$ is the velocity of the undisturbed stream, $c_0$ the velocity of sound corresponding to the undisturbed stream, $M$ the Mach number for the undisturbed stream ($=U/c_0$), $\gamma$ the ratio of the specific heats of the fluid, and $V$ the local velocity of the fluid.

Furthermore, assuming irrotational motion, combination of the equations of motion and continuity takes the form

$$\Delta\phi=\frac{\partial^2\phi}{\partial x^2}+\frac{\partial^2\phi}{\partial y^2}+\frac{\partial^2\phi}{\partial z^2}$$
$$=\frac{1}{2c^2}\left(\frac{\partial\phi}{\partial x}\frac{\partial V^2}{\partial x}+\frac{\partial\phi}{\partial y}\frac{\partial V^2}{\partial y}+\frac{\partial\phi}{\partial z}\frac{\partial V^2}{\partial z}\right), \tag{2}$$

where $\phi$ is the velocity potential. When the motion has axial symmetry as for the flow past a sphere, Eq. (2) becomes in polar coordinates $(r, \theta)$

$$\Delta\phi=\frac{\partial^2\phi}{\partial r^2}+\frac{2}{r}\frac{\partial\phi}{\partial r}+\frac{1}{r^2\sin\theta}\frac{\partial}{\partial\theta}\left(\sin\theta\frac{\partial\phi}{\partial\theta}\right)$$
$$=\frac{1}{2c^2}\left(\frac{\partial\phi}{\partial r}\frac{\partial V^2}{\partial r}+\frac{1}{r^2}\frac{\partial\phi}{\partial\theta}\frac{\partial V^2}{\partial\theta}\right), \tag{3}$$

in which

$$V^2=\left(\frac{\partial\phi}{\partial r}\right)^2+\frac{1}{r^2}\left(\frac{\partial\phi}{\partial\theta}\right)^2. \tag{4}$$

By reason of the extreme complexity of Eq. (3), methods for approximate solution have been resorted to. As stated in the introduction, a first approximation was obtained by Lord Rayleigh; he took the well-known solution for incompressible flow as the zero approximation, substituted it into the right-hand side of Eq. (3), placed $c=c_0$, and then obtained a solution of the new equation.

* Assistant Professor of Mechanical Engineering.

[1] Lord Rayleigh, "On the flow of compressible fluid past an obstacle," Phil. Mag. **32**, No. 187, 1–6 (July, 1916).

[2] K. Tamada, "On the flow of a compressible fluid past a sphere," Proc. Phys.-Math. Soc., Japan **21**, 743–752 (1939).

[3] C. Kaplan, "Flow of a compressible fluid past a sphere," N. A. C. A. Tech. Note, No. 762 (May, 1940).

The second approximation to the compressible fluid flow, accomplished by Tamada and Kaplan, was carried out under the assumption that $\phi$ can be expanded as a power series in $M^2$, thus

$$\phi=\phi_0+\phi_1M^2+\phi_2M^4+\cdots. \tag{5}$$

Substituting Eq. (5) into Eq. (3) and equating terms of like powers of $M$ on both sides, there results

$$\Delta\phi_0=0, \tag{6}$$

$$\Delta\phi_1=\frac{1}{2U^2}\left(\frac{\partial\phi_0}{\partial r}\frac{\partial V_0^2}{\partial r}+\frac{1}{r^2}\frac{\partial\phi_0}{\partial\theta}\frac{\partial V_0^2}{\partial\theta}\right), \tag{7}$$

$$\Delta\phi_2=\tfrac{1}{2}(\gamma-1)(V_0^2-1)\Delta\phi_1+\frac{1}{2U^2}\left(\frac{\partial\phi_0}{\partial r}\frac{\partial V_1^2}{\partial r}+\frac{1}{r^2}\frac{\partial\phi_0}{\partial\theta}\frac{\partial V_1^2}{\partial\theta}\right)+\frac{1}{2U^2}\left(\frac{\partial\phi_1}{\partial r}\frac{\partial V_0^2}{\partial r}+\frac{1}{r^2}\frac{\partial\phi_1}{\partial\theta}\frac{\partial V_0^2}{\partial\theta}\right). \tag{8}$$

It will be noted that the solution of the first equation represents the incompressible fluid case, *viz.*,

$$\phi_0=U\left(r+\frac{a^3}{2r^2}\right)P_1, \tag{9}$$

wherein $a$ is the radius of the sphere and $P_1$ is the Legendre polynomial of the first order (of argument $\cos\theta$). The second equation leads to the first-order correction to the velocity potential as obtained by Lord Rayleigh, i.e.,

$$\phi_1=a^3U\left[\left(\frac{1}{3}\frac{1}{r^2}-\frac{1}{5}\frac{a^3}{r^5}+\frac{1}{24}\frac{a^6}{r^8}\right)P_1+\left(-\frac{3}{10}\frac{1}{r^2}+\frac{27}{55}\frac{a^2}{r^4}-\frac{3}{10}\frac{a^3}{r^5}+\frac{3}{176}\frac{a^6}{r^8}\right)P_3\right]. \tag{10}$$

The third equation yields the second-order correction as given by Tamada and Kaplan:

$$\begin{aligned}\phi_2=a^3U(\gamma-1)&\left[\left(\frac{599}{16800}\frac{1}{r^2}-\frac{3}{70}\frac{a^3}{r^5}+\frac{1}{24}\frac{a^6}{r^8}-\frac{13}{560}\frac{a^9}{r^{11}}+\frac{13}{2800}\frac{a^{12}}{r^{14}}\right)P_1+\left(\frac{83133}{3665200}\frac{a^2}{r^4}-\frac{1}{10}\frac{a^3}{r^5}+\frac{15}{176}\frac{a^6}{r^8}\right.\right.\\&\left.\left.-\frac{57}{1960}\frac{a^9}{r^{11}}+\frac{23}{6800}\frac{a^{12}}{r^{14}}\right)P_3+\left(\frac{1}{7}\frac{a^3}{r^5}-\frac{50517}{276640}\frac{a^4}{r^6}+\frac{3}{52}\frac{a^6}{r^8}-\frac{9}{1120}\frac{a^9}{r^{11}}+\frac{5}{8512}\frac{a^{12}}{r^{14}}\right)P_5\right]\\&+a^3U\left(\frac{1325952}{4065600}\frac{1}{r^2}-\frac{49}{150}\frac{a^3}{r^5}-\frac{243}{1925}\frac{a^5}{r^7}+\frac{1049}{3080}\frac{a^6}{r^8}+\frac{5589}{84700}\frac{a^8}{r^{10}}-\frac{3049}{18480}\frac{a^9}{r^{11}}+\frac{7789}{369600}\frac{a^{12}}{r^{14}}\right)P_1\\&+a^3U\left(-\frac{53}{150}\frac{1}{r^2}+\frac{70620063}{95295200}\frac{a^2}{r^4}-\frac{61}{150}\frac{a^3}{r^5}-\frac{156}{275}\frac{a^5}{r^7}+\frac{28}{55}\frac{a^6}{r^8}+\frac{1137}{7150}\frac{a^8}{r^{10}}-\frac{12631}{64680}\frac{a^9}{r^{11}}+\frac{929}{56100}\frac{a^{12}}{r^{14}}\right)P_3\\&+a^3U\left(\frac{5}{42}\frac{1}{r^2}-\frac{6}{11}\frac{a^2}{r^4}+\frac{2}{3}\frac{a^3}{r^5}+\frac{135921}{640640}\frac{a^4}{r^6}-\frac{60}{77}\frac{a^5}{r^7}+\frac{253}{728}\frac{a^6}{r^8}+\frac{87}{1540}\frac{a^8}{r^{10}}-\frac{997}{18480}\frac{a^9}{r^{11}}+\frac{85}{29568}\frac{a^{12}}{r^{14}}\right)P_5.\end{aligned} \tag{11}$$

## DETERMINATION OF THE STREAMLINES

The potential and stream functions are connected by the relations

$$\frac{1}{r}\frac{\partial\phi}{\partial\theta}=-\frac{1}{\rho r\sin\theta}\frac{\partial\psi}{\partial r}, \tag{12}$$

$$\frac{\partial\phi}{\partial r}=\frac{1}{\rho r^2\sin\theta}\frac{\partial\psi}{\partial\theta}, \tag{13}$$

in which

$$\rho=\rho_0\left[1+\frac{\gamma-1}{2}M^2\left(1-\frac{V^2}{U^2}\right)\right]^{1/(\gamma-1)} \tag{14}$$

where $\rho_0$ is the density of the undisturbed stream.

From Eqs. (12), (14), and (4), there results

$$\rho_0\left\{1+\frac{\gamma-1}{2}M^2\left[1-\frac{1}{U^2}\left(\frac{\partial\phi}{\partial r}\right)^2-\frac{1}{U^2r^2}\left(\frac{\partial\phi}{\partial\theta}\right)^2\right]\right\}^{1/(\gamma-1)}\sin\theta\frac{\partial\phi}{\partial\theta}=-\frac{\partial\psi}{\partial r}, \tag{15}$$

or, absorbing $\rho_0$ in $\psi$,

$$\left\{1+\frac{\gamma-1}{2}M^2\left[1-\frac{1}{U^2}\left(\frac{\partial\phi}{\partial r}\right)^2 - \frac{1}{U^2r^2}\left(\frac{\partial\phi}{\partial\theta}\right)^2\right]\right\}^{1/(\gamma-1)} \sin\theta\frac{\partial\phi}{\partial\theta}+=-\frac{\partial\psi}{\partial r}. \quad (16)$$

For the particular case of $M=0.5$ and $\gamma=1.405$ for air, Eq. (16) becomes

$$\left\{1+0.0506\left[1-\frac{1}{U^2}\left(\frac{\partial\phi}{\partial r}\right)^2 - \frac{1}{U^2r^2}\left(\frac{\partial\phi}{\partial\theta}\right)^2\right]\right\}^{2.465} \sin\theta\frac{\partial\phi}{\partial\theta}=-\frac{\partial\psi}{\partial r}. \quad (17)$$

Now the simplest way of integrating Eq. (17) is by graphical means, i.e., for certain values of $\theta$, the left-hand side can be computed at various values of $r$, and the area under the curve can be calculated to give corresponding values of $\psi$. The graph relating $\psi$ and $r$ can then be used to determine the radial distance $r$ for certain preassigned values of $\psi$. This process can of course be carried out to any degree of accuracy.

Upon differentiation of Eq. (5) and substitution of $M=0.5$,

$$\frac{\partial\phi}{\partial\theta}=\frac{\partial\phi_0}{\partial\theta}+\frac{1}{4}\frac{\partial\phi_1}{\partial\theta}+\frac{1}{16}\frac{\partial\phi_2}{\partial\theta}. \quad (18)$$

Substitution of Eqs. (9)–(11) into Eq. (18) then yields, when $a=1$,

$$\begin{aligned}\frac{\partial\phi}{\partial\theta}=&-U\sin\theta(r+0.5699r^{-2}+0.0556r^{-4}\\&-0.0995r^{-6}+0.0020r^{-8}-0.0326r^{-7}\\&+0.0525r^{-8}+0.0087r^{-10}-0.0166r^{-11}\\&+0.0019r^{-14})\\&-U\sin3\theta(-0.1760r^{-2}+0.2899r^{-4}\\&-0.1560r^{-5}+0.0071r^{-6}-0.1064r^{-7}\\&+0.0909r^{-8}+0.0215r^{-10}-0.0272r^{-11}\\&+0.0023r^{-14})\\&-U\sin5\theta(0.0183r^{-2}-0.0840r^{-4}\\&+0.1116r^{-5}+0.0212r^{-6}-0.1200r^{-7}\\&+0.0570r^{-8}+0.0087r^{-10}-0.0088r^{-11}\\&+0.0005r^{-14}). \quad (19)\end{aligned}$$

Furthermore,

$$\frac{\partial\phi}{\partial r}=\frac{\partial\phi_0}{\partial r}+\frac{1}{4}\frac{\partial\phi_1}{\partial r}+\frac{1}{16}\frac{\partial\phi_2}{\partial r},$$

so that

$$\begin{aligned}\frac{\partial\phi}{\partial r}=&U\cos\theta(1-1.1394r^{-3}-0.2224r^{-5}\\&+0.4975r^{-6}-0.0121r^{-7}+0.2280r^{-8}\\&-0.4201r^{-9}-0.0866r^{-11}+0.1822r^{-12}\\&-0.0266r^{-15})\\&+U\cos3\theta(0.1181r^{-3}-0.3870r^{-5}\\&+0.2595r^{-6}-0.0142r^{-7}+0.2481r^{-8}\\&-0.2416r^{-9}-0.0716r^{-11}+0.0996r^{-12}\\&-0.0106r^{-15})\\&+U\cos5\theta(-0.0073r^{-3}+0.0671r^{-5}\\&-0.1116r^{-6}-0.0255r^{-7}+0.1679r^{-8}\\&-0.0915r^{-9}-0.0174r^{-11}+0.0194r^{-12}\\&-0.0013r^{-15}). \quad (20)\end{aligned}$$

This is all the further that the process can be reduced. The remaining work is pure computation. In this paper, streamlines were located to the nearest one-thousandth of the unit for each of the following nine angles of $\theta$: $\tan^{-1}1/15$, $\tan^{-1}1/8$, $\tan^{-1}1/4$, $\tan^{-1}4/10$, $\pi/6$, $\pi/4$, $\pi/3$, $\tan^{-1}11/3$, and $\pi/2$.

Figure 1 shows the streamlines for both the compressible and incompressible fluid flow. Also in this figure are plotted the corresponding velocities in the field at $\theta=\pi/2$ and the corresponding pressures on the surface of the sphere. (Note that in the figure $u_0=U$, and $u=V$ in the field at $\theta=\pi/2$.) The pressure distribution for the compressible fluid case is given by the formula

$$\frac{p-p_0}{\frac{1}{2}\rho_0U^2}=\frac{1}{(\gamma/2)M^2} \times\left\{\left[1+\frac{\gamma-1}{2}M^2\left(1-\frac{V^2}{U^2}\right)\right]^{\gamma/(\gamma-1)}-1\right\}, \quad (21)$$

where $p_0$ is the pressure in the undisturbed

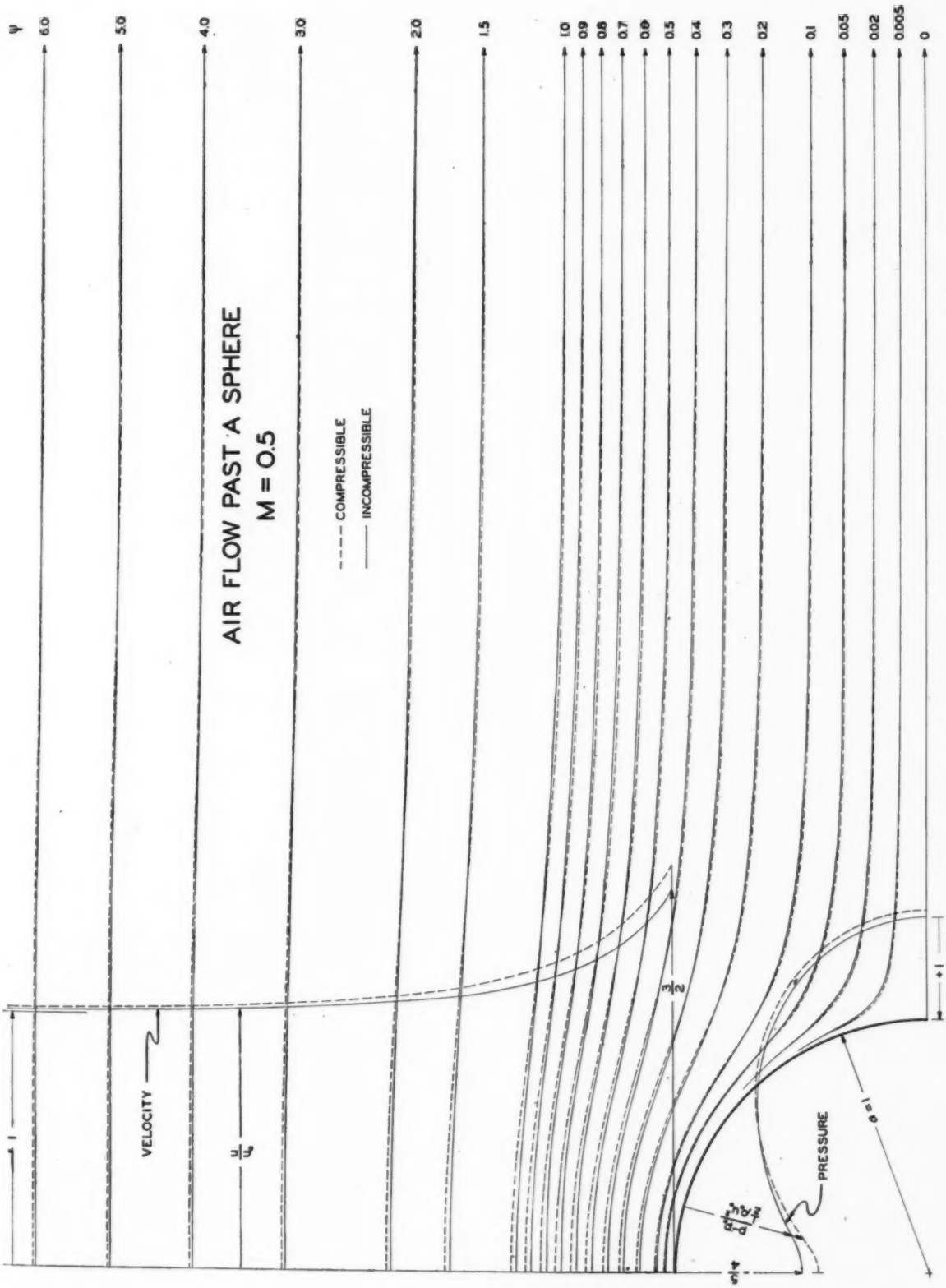


FIG. 1. Streamlines for the flow of both a compressible and an incompressible fluid past a sphere.

TABLE I.

| | on surface of sphere | | | | in field at $\theta=\pi/2$ | | |
|---|---|---|---|---|---|---|---|
| | $\frac{p-p_0}{\frac{1}{2}\rho_0 U^2}$ | | $\frac{V}{U}$ | | | $\frac{V}{U}$ | |
| $\theta$ | comp. | incomp. | comp. | incomp. | $r$ | comp. | incomp. |
| 0 | +1.070 | +1.000 | 0 | 0 | 1.0 | 1.600 | 1.500 |
| $\tan^{-1}1/15$ | +1.058 | +0.990 | 0.093 | 0.100 | 1.1 | 1.464 | 1.376 |
| $\tan^{-1}1/8$ | +1.030 | +0.965 | 0.174 | 0.186 | 1.2 | 1.368 | 1.289 |
| $\tan^{-1}1/4$ | +0.930 | +0.867 | 0.342 | 0.364 | 1.4 | 1.241 | 1.182 |
| $\tan^{-1}4/10$ | +0.751 | +0.689 | 0.528 | 0.557 | 1.8 | 1.120 | 1.086 |
| $\pi/6$ | +0.496 | +0.437 | 0.719 | 0.750 | 2.2 | 1.069 | 1.047 |
| $\pi/4$ | −0.098 | −0.125 | 1.049 | 1.061 | 3.0 | 1.029 | 1.019 |
| $\pi/3$ | −0.736 | −0.688 | 1.331 | 1.299 | 4.0 | 1.012 | 1.008 |
| $\tan^{-1}11/3$ | −1.218 | −1.093 | 1.526 | 1.447 | | | |
| $\pi/2$ | −1.416 | −1.250 | 1.600 | 1.500 | | | |

stream, or

$$\frac{p-p_0}{\frac{1}{2}\rho_0 U^2}=5.695\left\{\left[1+0.0506\left(1-\frac{V^2}{U^2}\right)\right]^{3.465}-1\right\} \quad (22)$$

for the air flow at Mach number 0.5.

Table I gives the velocity and pressure data for the two flows.

It is seen that in the case of the compressible fluid the point on the sphere at which the pressure is equal to the pressure in the undisturbed stream is at a location different from that for the incompressible fluid. For the compressible fluid flow the point is located by placing $-U=(1/r)(\partial\phi/\partial\theta)$, substituting Eq. (19) for $\partial\phi/\partial\theta$, putting $r=1$, and then solving the resulting equation, *viz.*,

$$1.5419\sin\theta-0.0539\sin3\theta+0.0045\sin5\theta=1. \quad (23)$$

The solution of Eq. (23) is $\theta=43°\,38'$. For the incompressible fluid case, the point of zero pressure difference is located at $\theta=41°\,49'$.

The local Mach number is greatest at the top of the sphere. This number can be computed using Eq. (1), thus

$$M_l=\frac{V}{c}=\frac{V}{c_0\left[1+\frac{\gamma-1}{2}M^2\left(1-\frac{V^2}{U^2}\right)\right]^{\frac{1}{2}}}, \quad (24)$$

or, since $c_0=U/M$,

$$M_l=\frac{V/U}{\left[\frac{1}{M^2}+\frac{\gamma-1}{2}\left(1-\frac{V^2}{U^2}\right)\right]^{\frac{1}{2}}}. \quad (25)$$

At the top of the sphere where $V/U=1.600$, $M_l=0.833$, and therefore there is no shock in the field of flow. This is to be expected since the critical Mach number of the undisturbed flow for shock establishment is approximately 0.55 as indicated in another paper by Tamada.[4]

[4] K. Tamada, "Further studies on the flow of a compressible fluid past a sphere," Proc. Phys.-Math. Soc., Japan, **22**, 519–525 (1940).

# Minimum Sparking Potentials of Barium, Magnesium, and Aluminum in Argon

HAROLD JACOBS AND ARMAND P. LAROCQUE
*Sylvania Electric Products Inc., Kew Gardens, New York, New York**
(Received August 21, 1946)

Minimum sparking potentials of barium, magnesium, and aluminum in argon are found to be 93±½ v, 123±1 v, and 155±1 v, respectively. Utilizing the data in measuring the minimum sparking potentials, the ratios of electrons emitted from the cathode per bombarding positive ion ($\gamma_m$) are determined and found to be .149±.001 for barium, .089±.033 for magnesium, and .045±.002 for aluminum. A relationship is found such that, at a given field per unit pressure, a lower work function indicates a lower sparking potential and a higher $\gamma_m$ indicates a lower sparking potential, for the case of the three metals studied. A graphical method is proposed for predicting the minimum sparking potentials for metals, whose sparking potential values have not been determined, based upon the values of $\gamma_m$ or the work function $\phi$.

WHEN considering the design and manufacture of electron tubes which contain gases at reduced pressure, it has been found that the surface phenomenon plays a major role in successful operations and applications. For instance, the sparking potential of many gas tubes has been found to be a function of the cathode surface as well as the gas in the region of the minimum sparking potential. Similarly, the voltage drop across the gas tube while in operation is a function of the surface as well as the gas.

In spite of the large number of applications of gas tubes, relatively little is known concerning the actual mechanism of operation of these devices. This is probably due to the large number of variables which are possible in gas tubes, and to the fact that techniques of measurement have not been adequately developed. For instance, it has been found that small traces of mercury,[1] oil vapors, and oxygen in the gas or adsorbed by the surfaces in a tube will cause great alterations in the behavior of the tube. Thus, reproduceable results have been difficult to obtain, and, actually, it has only been in recent years that any valid data has been obtained.

One of the problems concerning gas tubes, then, is the effect of surfaces in gases upon sparking potential. In the following experiments, the surfaces of Ba, Mg, and Al were studied in reduced pressures of argon and the minimum sparking potentials obtained. From this data, various interpretations have been made including the deduction of the ratio of emitted electrons released by bombarding positive ions and the importance of this ratio upon the sparking potential.

## EXPERIMENTAL METHOD

Tubes were constructed as sketched in Fig. 1. It should be noted that these tubes consisted of two electrodes and a getter container which held the metal to be studied. Each of the two electrodes were made of nickel and shaped in the

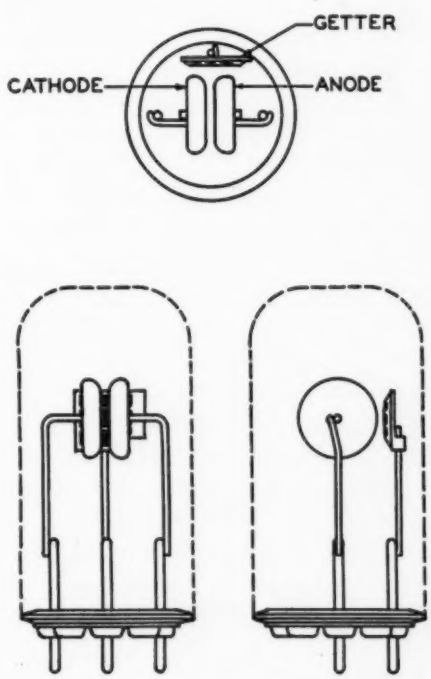


FIG. 1. Experimental tube.

* This work was undertaken in association with the Applied Physics Laboratory of the Johns Hopkins University under Section T series contract NOrd 7872 sponsored by the Bureau of Ordnance, United States Navy.
[1] W. E. Bowls, Phys. Rev. **53**, 293 (1938).

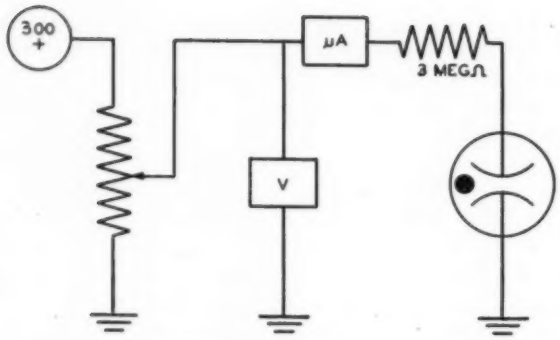


FIG. 2. Circuit for measuring sparking potentials.

manner of "Rogowsky electrodes."[2] That is, the electrodes were shaped such that surfaces facing each other followed equipotential lines. This was done to prevent concentrations of field at the edges and would make quantitative measurements of the field readily accessible. The tube to be studied was placed on exhaust together with a "dummy tube" containing only a barium-aluminum getter. This second tube was used as a reservoir to down any impurities in the argon, i.e., $O_2$, $N_2$, $H_2$ which was to be later admitted.

The nickel electrodes and getter container were then degassed as well as possible and the metal to be studied was evaporated on the nickel surface. In the case of barium, an iron clad barium getter was used and was electrically flashed. Magnesium powder was used for the Mg surface and aluminum powder for the Al surface. These reactions in no way depend upon reducing agents and hence the chance for impurity was greatly reduced. Argon was then admitted to the system from a standard Airco argon bottle (99.9+ percent pure). Liquid air was used at all times between the mercury manometer and the vacuum system. The electrical circuit used was such as sketched in Fig. 2. The criteria for sparking was such that a sudden rise in current would indicate the "breakdown" through the tube. In all cases, tests were conducted for stability of the surface before measurements were made. This was done by allowing $3\mu a$ current to pass through the tube. If current and voltage conditions were constant with respect to time, the surface was assumed to be stable. No measurement was made of the thickness of the metal deposited on the nickel cathode.

[2] J. D. Cobine, *Gaseous Conductors* (McGraw-Hill Book Company, Inc., New York, 1941), 171–181.

## DATA

The curves in Fig. 3 indicate the results of measuring sparking potential in relation to pressure times distance. In the case of Ba, Mg, and Al in argon, it was found that the minimum sparking potentials were $93\pm\frac{1}{2}$, $123\pm1$, and $155\pm1$ volts, respectively.

## PREVIOUS DATA CONCERNING COLD CATHODES

Before attempting to interpret the above data, it would be of interest to consider the work of previous experimenters in the field of cold cathodes.

It has been demonstrated,[3] that in tubes such as studied in these experiments, the following relation exists

$$i=i_0\frac{e^{ax}}{1-\gamma(e^{ax}-1)}. \qquad (1)$$

$i$ = total current,
$i_0$ = constant,[4]
$x$ = distance between electrodes,
$\alpha$ = ratio of ions formed to electrons in a unit distance,
$\gamma$ = roughly, ratio of secondary emission from the cathode to the ions bombarding the cathode.

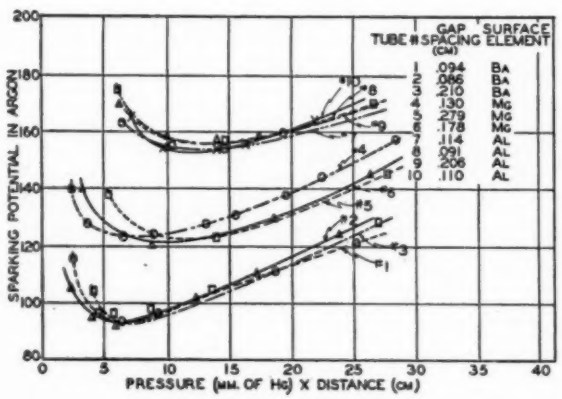


FIG. 3. Sparking potentials of barium, magnesium, and aluminum in argon *vs.* pressure×distance. The ordinate identifications should read 0, .5, 1.0, 1.5, 2.0, 2.5, 3.0, 3.5, and 4.0.

[3] L. B. Loeb, *Fundamental Processes of Electrical Discharge in Gases* (J. Wiley & Sons, Inc., New York, 1939), 378.

[4] The symbol $i_0$ which is the initial photoelectric current leaving the cathode is not truly constant and for very large values of $i$, there is found to be a slight drop in the

Now, this equation has been used by some experimenters as a criteria for determining or predicting sparking potentials. That is, if the denominator goes to zero, the current goes to infinity. Hence, a criteria for sparking may be:

$$1-\gamma(e^{\alpha x}-1)=0,\ \gamma=\frac{1}{e^{\alpha x}-1}. \qquad (2)$$

As we shall see later, the higher the value of $\gamma$, the lower is the sparking potential in a given gas. Thus, the constant is extremely important from the point of view of any quantitative work on low pressure cold cathode discharge tubes. The exact interpretation of $\gamma$ has not been well developed, but it should be emphasized that although $\gamma$ is roughly the ratio of emitted electrons per positive ion bombarding the cathode, it also contains the ratio of electrons per quanta of light producing photoelectrons, and possibly several other sources of electrons which have been assumed to be small in comparison with the first ratio. Because of the importance of $\gamma$ in gas discharge work, there has been some research in recent years to determine the nature of $\gamma$ and the mechanism involved.

As late as 1938, Bowls[5] opened many questions concerning the constant $\gamma$. He utilized a mercury free vacuum system, platinum and sodium cathodes, and nitrogen gas. He obtained his values of $\gamma$ not by sparking but by measuring current and computing $\gamma$ from the following equation.

$$i=i_0\frac{(\alpha-\beta)e^{(\alpha-\beta)x}}{\alpha-\beta e^{(\alpha-\beta)x}}, \qquad (3)$$

where

$$\beta/\alpha=\gamma.$$

Three very important discoveries were brought to light.

1. There was an "anomalous" peaking of $\gamma$ at low $X/p$ values. This had never been observed by sparking potential measurements.

2. When Hg was introduced to the system, radically different results occurred as to the value of $\gamma$. Thus, it appears that all work done previously without safeguards as to mercury contamination may have been in serious error.

3. In nitrogen, the Na cathode had a lower $\gamma$ than the Pt cathode. This is contrary to what would be expected since the lower work function cathode should have the higher $\gamma$ and hence the lower sparking potential.

sparking potential. However, for very small currents ($<1\ \mu a$) such as used in the experiments above, the effect is small and has not been detected experimentally. For further comment, see L. B. Loeb, reference 3, pp. 420–425.

[5] W. E. Bowls, reference 1, 293.

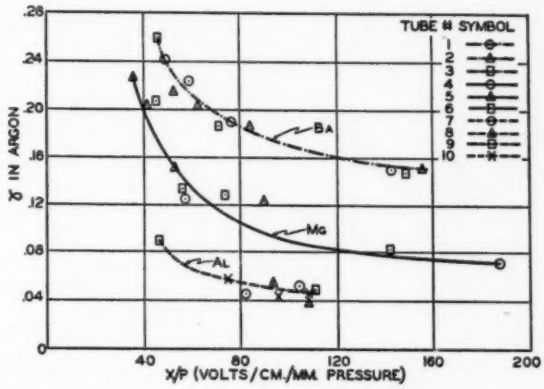


FIG. 4. $\gamma$ of barium, magnesium, and aluminum in argon *vs.* field per unit pressure.

In 1939, Hale[6] continued this work, but this time made measurements in hydrogen instead of nitrogen. His results again indicated:

1. An "anomalous" peaking in $\gamma$ appeared at very low $X/p$ values. (Pt: $X/p=125$; NaH: $X/p=10$.)

2. The presence of Hg could alter the characteristics of the surface completely.

3. Except at very low $X/p$ ratios, the $\gamma$ of the sodium was less than that for platinum.

Now, in this work, it was thought that the anomalous peaking was caused by a photoelectric phenomenon. That mercury vapor could change the surface was well established. The question of work function *versus* $\gamma$ was by no means settled and still remains open to question. In the experiments of Bowls and Hale, it is possible that the nitrogen and hydrogen combined with the Na surface in such a manner as to create a high work function surface. The answers to this question will be revealed by further experiments in inert gases.

In 1939, Huxford[7] studied Cs-Ag-O surfaces in photo-tubes filled with argon. He measured $\gamma$ by two methods, using the sparking criteria method as indicated above and also the method of measuring current prior to discharge and calculating the $\gamma$-values by means of Eq. (1). He obtained very good agreement using both methods.

Another piece of work is described by Loeb[8]

[6] D. H. Hale, Phys. Rev. **55**, 815 (1939).
[7] W. S. Huxford, Phys. Rev. **55**, 754 (1939).
[8] L. B. Loeb, reference 3, p. 53.

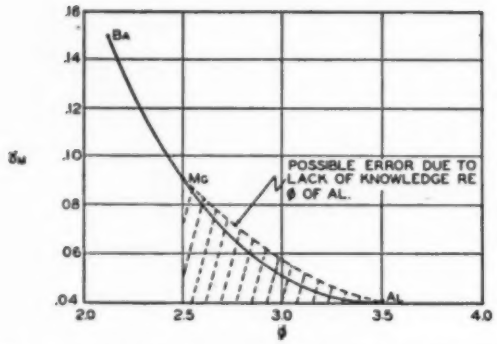


FIG. 5. $\gamma_m$ (ratio of emitted electrons per bombarding positive ion at the minimum sparking potential) *vs.* work function.

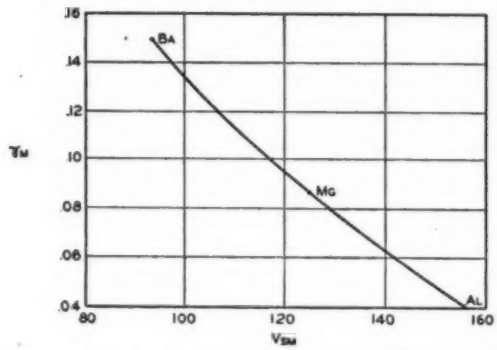


FIG. 6. $\gamma_m$ (ratio of emitted electrons per bombarding positive ion at the minimum sparking potential) as a function of the minimum sparking potential.

concerning some work done by Engstrom[9] on barium cathodes in argon. Here, also, good agreement is obtained between the two methods of measuring $\gamma$ except that the sparking method provides a smoother line. In other words, it is claimed that when measuring by sparking methods, the anomalies are wiped out and a more continuous value of $\gamma$ is obtained as a function of $X/p$.

## INTERPRETATION OF DATA

With the above background in mind, we can now return to the data concerning Ba, Mg, and Al in argon. Utilizing Eq. (2) again:

$$\gamma=\frac{1}{e^{\alpha x}-1}, \quad X=\frac{V_s}{x}, \tag{4}$$

$$\therefore \quad \gamma=\frac{1}{e^{\alpha V_s/X}-1}, \quad \gamma=\frac{1}{e^{(\alpha/p)\cdot(p/X)V_s}-1}.$$

$V_s$ = sparking potential,
$X$ = field (volts/cm),
$x$ = distance (cm),
$p$ = pressure (mm).

The values for $\gamma$ as determined by Eq. (4) are shown in Fig. 4. The $\gamma_m$ values (at the minimum sparking potential) were found to be $.149\pm.001$ for barium, $.089\pm.033$ for magnesium, and $.045\pm.002$ for aluminum.

Having evaluated $\gamma$, we are in a position to draw certain conclusions. The work functions of Ba,[10] Mg,[11] and Al[11] are 2.1 electron volts, 2.42 electron volts, and $3.57(2.5-3.6)$ electron volts, respectively.

We can therefore conclude from the data in Fig. 4, that, at any of the given values of $X/p$ in the range we have observed, and in the case of the metallic surfaces studied, a lower work function indicates a higher $\gamma$. And, in addition, from the data in Fig. 3, a lower work function will indicate a lower minimum sparking potential.

One may wonder, then, why Bowls obtained a lower $\gamma$ in a large region of $X/p$ for platinum than was obtained for sodium. The answer may well be that the Na was not free on his cathode surface, but was, in fact, combined to form a composite cathode with nitrogen.

We should emphasize that in the case of Ba, Mg, and Al we were dealing with pure metal surfaces. As yet, there are no available data concerning the effects of $\gamma$ and $\phi$ on composite cathodes in gas tubes.

Knowing $\gamma$ and the $\phi$ of the surfaces in argon, it may be possible to predict the $V_{sm}$ (minimum sparking potential) of a cold cathode gas tube. If these predictions are valid, the designer would take a tube with a given sparking requirement and estimate the region of sparking potential by considering the published values of the work functions of the surfaces. Loeb[12] gives the following formula for minimum sparking potentials.

$$V_{sm}=\frac{3B_4}{A_4}\log\frac{1}{\gamma_m}+\frac{B_4}{A_4}\frac{1}{\log\left(\frac{1}{\gamma_m}\right)}. \tag{5}$$

[9] L. B. Loeb, reference 3, p. 407; R. W. Engstrom, Phys. Rev. 56 (1939).
[10] A. L. Reimann, *Thermionic Emission* (J. Wiley & Sons, Inc., New York, 1934), p. 80–1.
[11] J. D. Cobine, reference 2, p. 109.
[12] L. B. Loeb, reference 3, p. 414.

$B_4$ and $A_4$ are constants which could be evaluated. However, at best, this is an empirical formula and does satisfy a requirement which can be fulfilled more rapidly and simply by graphical methods.

In the first graph, we have $\gamma_m$ *versus* $\phi$. (Figure 5.)

Then by either knowing $\gamma_m$ or $\phi$, we may estimate $V_{sm}$ of a surface in argon by Fig. 6.

As an example of the use of these charts, suppose we calculate the $V_{sm}$ of sodium. The $\phi$ of sodium is given as 2.46−1.90 volts.[13] This is roughly a $\gamma_m$ in argon of from .08 to slightly more than .15 using Fig. 5. Now, turning to Fig. 6, this is roughly between 90 volts and 125 volts. According to Loeb,[14] the $V_{sm}$ of a Na surface in argon is 95 volts, or in the expected region.

We realize our range is limited and more samples may be desirable in future work, but the indications are that this may be a fruitful method for utilizing data concerning cold cathodes.

Acknowledgment should be made to Mr. Gerald Rich, Sylvania Electric Products, Inc., Kew Gardens, New York, for his discussions and help relating to this work.

[13] J. D. Cobine, reference 2, p. 109.

[14] L. B. Loeb, reference 3, p. 414.

## Fatigue of Ag-$Cs_2O$, Ag-Cs Photoelectric Surfaces

S. Pakswer
*Continental Electric Company, Geneva, Illinois*
(Received August 8, 1946)

Fatigue of Ag-$Cs_2O$, Ag-Cs surfaces has been observed in blue and red light. In blue light the long wave threshold shifts to shorter wave-length and the long wave maximum increases and sometimes shifts to shorter wave-length. Rise of temperature at the cathode counteracts the phenomena. In red light temperature effects are dominating. The observed phenomena are in line with de Boer's theory of the photoelectric effect on such surfaces as the formation of positive ions on the surface causes polarization of the neighboring Cs-atoms and a change in their selective absorption.

SURFACES with *S*1* spectral sensitivity have been commonly manufactured for a number of years and the technique of their production is well known. There is, however, little agreement concerning the mechanism of the photoelectric emission. The spectral sensitivity characteristic of the *S*1 surface shows two main maxima—one at approximately 3500A and the other around 8000A corresponding probably to two different emission processes. It has not yet been definitely established where these electron emission processes take place.

According to the ideas developed by J. H. deBoer,[1,2] the sensitivity maximum at 8000A is caused by cesium atoms adsorbed at so-called "active" spots on the surface of a semi-conductive layer containing $Cs_2O$ and interspersed with Cs and Ag metal atoms. The surface layer of the semi-conductor polarizes the atoms of Cs and thus reduces their work function. The emitted electrons are supplied by diffusion through the layer of the semi-conductor.

Timofeev,[3] in a series of experimental investigations, emphasizes the importance of the formation of positive charges on the surface of the semi-conductive layer, and their influence on the photoelectric and secondary electron emission of Ag-Cs cathodes.

Other authors[4–6] believe that the photo-ionization takes place inside the layer of the semi-conductor as an "inner" photoelectric effect and that the electrons have to break through the

* *S*1 and *S*4 spectral sensitivity are RMA designations for "red" and "blue" sensitive tubes, respectively.

[1] J. H. deBoer, *Electron Emission and Adsorption Phenomena* (Cambridge University Press, England, 1935).

[2] J. H. deBoer and M. C. Teves, Zeits. f. Physik **83**, 521 (1933).

[3] Timofeev, J. Tech. Phys. U.S.S.R. **6**, 340 (1944).

[4] H. Teichmann, Zeits. f. Electrochemie **44**, 602 (1938).

[5] G. Maurer, Zeits. f. Physik **60**, 170 (1941).

[6] N. S. Chlebnikov, Bull. Acad. Sci. U.S.S.R. Ser. Phys. **8**, 286 (1944).

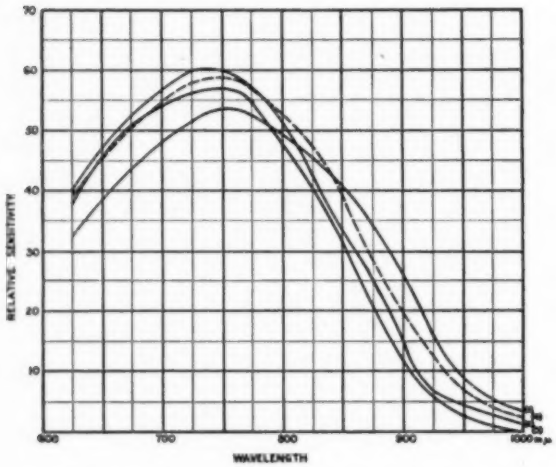


FIG. 1. Tube No. 10 type CE-1 vacuum exposed to blue light (200 w at 1′+filter 554) curve 1: 0 hr., curve 2: 1 hr., curve 3: 48 hr. illumination, curve 4 (———): 78 hr. in the dark.

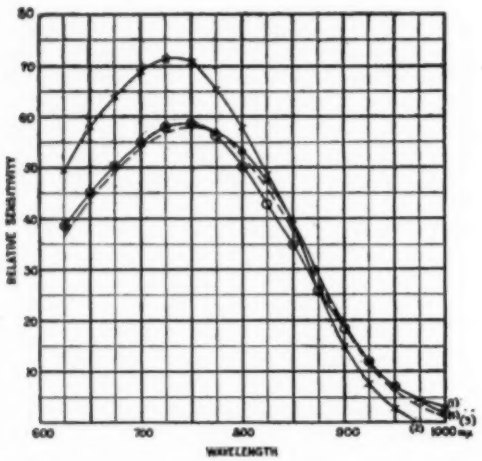


FIG. 2. Tube No. 10 type CE-1 vacuum exposed to blue light (500 w at 12″+filter 554) curve 1 (0): 0 hr., curve 2 (X): 1 hr., curve 3 (△): 24 hr. illumination, curve 4 (———): 50 hr. in the dark.

potential barrier at the surface, possibly at "active" spots.[5]

Experiments tend to support the deBoer conception[7] particularly the behavior in polarized light, the high velocity of emitted photoelectrons and the low quantum yield. The semi-conductor theory is supported by experience won on the secondary emission, by the spectral characteristic of the inner photo-effect[4] and by the influence of the thickness of the oxide layer on the sensitivity and the spectral characteristic of *S*1 surfaces.[8] Electron microscopic study of *S*1 surfaces,[9] showing spotty, non-uniform distribution of electrons emitted under illumination by light of 6000A, can be explained by both theories.

An insight into the mechanism of photoelectric emission can be obtained by a study of the fatigue of *S*1 surfaces. DeBoer[10] observed that tubes irradiated with blue light, without voltage applied, dropped in sensitivity to white incandescent light more than tubes irradiated with green light, and that red light and infra-red rays not only did not cause fatigue, but regenerated the original sensitivity of tubes which lost sensitivity. With voltage applied and a white light source, the drop of sensitivity was a function of the applied voltage and the illumination on the cathode. The fatigue phenomena increased at low temperature (−196°C) and decreased at higher temperature. In tubes exposed to white light of .15 lumen, the infra-red threshold was shifted considerably to shorter wave-lengths and the response in the maximum was lower and the maximum itself was shifted slightly to shorter wave-lengths.

To explain these phenomena deBoer assumed that the positive cesium ions recombine with electrons diffusing to them from the conductivity levels of the semi-conductor. The rate of recovery from fatigue is given by the rate of diffusion. Illumination with infra-red rays or rise of temperature increase the thermal agitation of

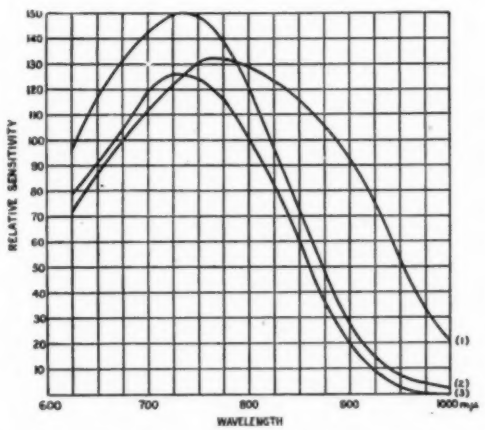


FIG. 3. Tube No. 4 CE-1 gas-filled exposed to blue light (200-w lamp at 1′+filter 554) $V_A = 22.5$ v curve 1: 0 hr., curve 2: 3 hr., curve 3: 264 hr. illumination.

[7] G. Lewin, Trans. Electrochem. Soc. **87**, (1945), preprint.
[8] P. M. Morosov and M. M. Butslov, Bull. Acad. Sci. U.S.S.R., Ser. Phys. **8**, 291 (1944).
[9] Yosimaro Morija, Electrotech. J. (Japan) **1**, 65 (1937).
[10] J. H. deBoer and M. C. Teves, Zeits. f. Physik **74**, 604 (1932).

the lattice, and thus the amount of electrons diffusing toward the surface. If voltage is applied, positive cesium ions migrate toward the cathode into the layer and must be replaced by cesium atoms migrating from the layer to the surface. A decrease of free alkali atoms at the surface has also been observed by Timofeev and Kondorskaya[11] who found that the time variation in fatigue phenomena is a series of exponentials.

It was felt that the data given in literature do not give a complete picture of fatigue phenomena. Following observation of the influence of different parameters on the stability and the fatigue of Ag-Cs photo-tubes, it was, therefore, decided to obtain additional data. As sensitivity measurements in white light give only integrated values, it seemed that a study of spectral distribution would give a better picture of the phenomena.

Measurements of the distribution of spectral sensitivity were made with a Coleman spectrophotometer Model 10S, calibrated against a VanCittert monochromator and a thermopile. The instrument was a Leeds & Northrup galvanometer. The plate voltage was 22.5 v. The color temperature of the lamp in the photometer was 2870°K. All tests were made on tubes of the type CE-1/918, vacuum and gas-filled, with silver-plated copper cathode and also on gas-filled 918 tubes with massive silver cathode.

## TESTS IN "BLUE" LIGHT

The tubes were exposed to the light of a 200-w lamp at 12″ distance filtered by a Corning filter 554; only blue and ultraviolet radiation fell on the cathode. In some tests the 200-w lamp was replaced by a 500-w projection lamp. The intensity of the radiation in this case, as measured with a blue-sensitive CE-61 tube was increased three times.

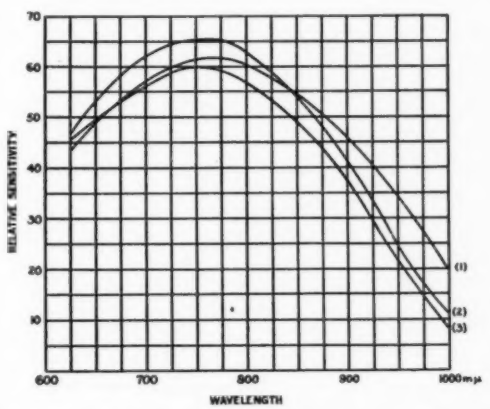


FIG. 4. Tube No. 3a. 918 gas-filled exposed to blue light (200-w lamp at 12″ filter 554) $V_A = 22.5$ v curve 1: 0 hr., curve 2: 3 hr., curve 3: 264 hr. illumination.

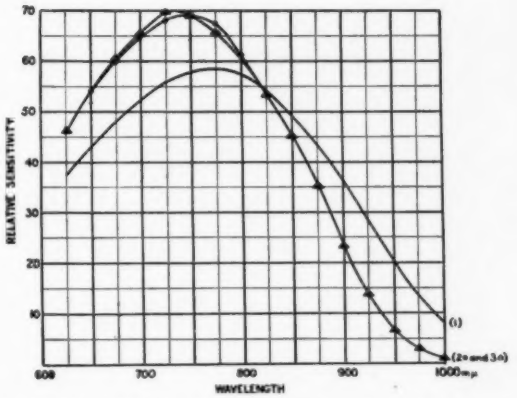


FIG. 5. Tube No. 16 CE-1 vacuum, curve 1: 0 hr., curve 2: exposed 1 hr. to blue light (500-w lamp at 1′+filter 554), curve 3: 2 hr. in dark at −80°C.

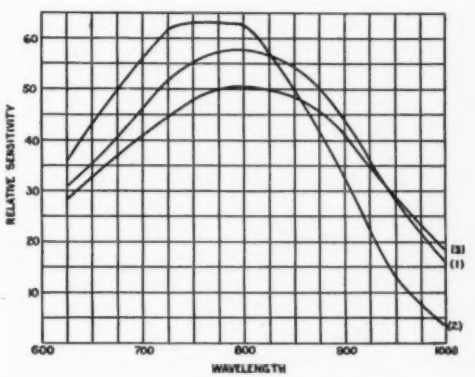


FIG. 6. Tube No. 17 CE-1 vacuum, curve 1:0 hr., curve 2: 1 hr. exposed to blue light (500-w lamp at 1′+filter 554), curve 3: 2 hr. in dark at +90°C.

In Figs. 1 and 2 are represented typical distribution curves. In Fig. 1 curve 1 is the original curve. After 1-hour illumination by the 200-w lamp without any plate current on, the sensitivity in the maximum surprisingly increased considerably and the threshold shifted to shorter wave-lengths (curve 2). After a protracted period of time the sensitivity at the maximum decreased slightly (curve 3, after 48 hr.) and the threshold was shifted still further. The tube was now kept in the dark. After 78 hours (curve 4) the increase at the maximum still persisted

[11] Timofeev and Kondorskaya, Physik. Zeits. Sovjetunion 9, 683 (1936).

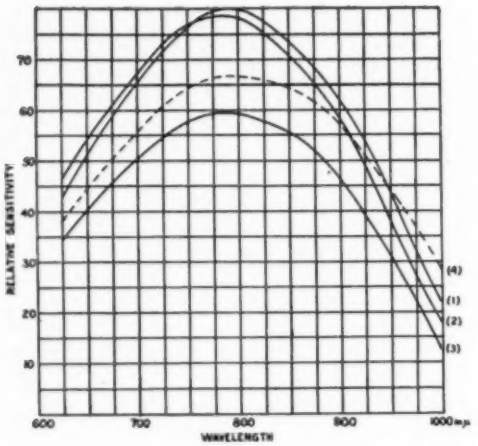


FIG. 7. Tube No. 15 type CE-1 vacuum exposed to red light (500-w lamp at 1′+filter 244) curve 1: 0 hr., curve 2: 1 hr., curve 3: 24 hr., curve 4: 50 hr. in the dark.

but the threshold moved back to longer wave-lengths.

This tube was now subjected to the light of the 500-w lamp (Fig. 2). After 1 hour the maximum had greatly increased (curve 2) but fell down rapidly (curve 3); the tube was heated up to about 50°C. After 50 hours in the dark (curve 4) the maximum and the threshold shifted to longer wave-lengths.

All other tubes investigated, gas-filled and vacuum, silver and silver plated, showed this initial increase in the maximum. Sometimes a shift in the maximum could be observed (Fig. 3). In Fig. 4 is shown the response of a tube with a silver cathode.

It was thought that these tests indicated the influence of three separate processes:

1. A process in blue light leading to a shift and an increase of the maximum and a shift of the threshold.
2. A process due to the rise of temperature which decreases the maximum.
3. A process in the dark which shifts the threshold back to longer wave-lengths.

To investigate further, separately, the influence of light and temperature two tubes were exposed to light of the 500-w lamp for 1 hour (curve 2, Figs. 5 and 6). Then one tube was kept for two hours in a mixture of solid $CO_2$ and acetone (−80°C) (curve 3, Fig. 5) and the other at +90°C for the same period of time (curve 3, Fig. 6). In the first tube the initial changes persisted while in the second tube the sensitivity in the maximum decreased considerably and the sensitivity on the long wave side recuperated completely.

## TESTS IN "RED" LIGHT

The same lamps were used in conjunction with Corning filter 244 transmitting red-infra-red radiation. With the 200-w lamp the curves showed a small drop of sensitivity in all wave-lengths. With the 500-w lamp (Fig. 7) where the heat development on the cathode was considerable, the sensitivity in the maximum went down considerably after 24 hours (curve 3). A large amount of sensitivity, especially at long wave-lengths, was recuperated after 50 hours in the dark.

## CONCLUSION

It can be easily understood that changes of spectral sensitivity, combining with the energy distribution of an incandescent lamp, will cause variations of output current which will appear as "instability." Parameters affecting the long wave end of the sensitivity curve will have a relatively greater effect than parameters affecting the maximum. This will explain why "blue" light or high plate voltage cause a higher drop of sensitivity than red light. By proper choice of the color temperature of the lamp, the temperature, the applied voltage, and the intensity of the light, it is possible to balance the different influences out and obtain stable operation.

It is difficult to explain the observed phenomena solely by the recombination of positive ions and electrons. It can be easily shown that fatigue and recovery would follow exponential or hyperbolic laws in case of recombination and depending on its mechanism.

The increase and the shift of the maximum and the shift of the threshold indicate changes in the electrical state of the Cs-atoms on the surface due to the formation of positive charges. This polarization of atoms next to an ion, and the change of selective absorption of light following the Franck-Condon principle, have been described by deBoer in his book,[1] mainly on pages 193, 228, 280, and 333.

Acknowledgment is made to Mr. John A. Loeber, who performed most of the experiments described above.

# The Measurement of Elasticity in Fluids of Low Viscosity

JOHN R. VAN WAZER* AND HERBERT GOLDBERG**
*Department of Manufacturing Experiments, Eastman Kodak Company, Rochester, New York*
(Received August 19, 1946)

By means of an apparatus applying an alternating shearing motion to a liquid, it was shown that fluids with a viscosity of around one poise have elastic properties. A discussion of the variation of the resonance maxima with the amount of damping is given, and the shear modulus and damping viscosity are calculated for some dilute solutions of high polymeric materials.

## INTRODUCTION

ALTHOUGH all forms of matter exhibit elastic behavior upon the application of hydrostatic force, it is customary to think of only solids and rather thick gels as being elastic on the application of force in shear or extension. This viewpoint is based on the concept that the relaxation time of the structural bonds holding a liquid together is of the order of $10^{-8}$ sec. However, a different state of affairs exists in many fluids. When a close-knit gel of a high polymer is diluted, the interlocking molecular chains to which the elasticity in shear is attributed are gradually separated and broken. It thus appears that the shear modulus of such a gel will decrease upon dilution until there are not enough continuous polymer chains reaching from wall to wall to give a measurable elastic effect. This type of elasticity can be observed experimentally when the time in which interpolymer bonds make or break is greater than or of the same order of magnitude as that of the experiment—that is to say, when the relaxation time is measurably long.

Kendall[1] has shown that some high polymeric solutions can be diluted to very low concentrations and still exhibit elastic recoil in shear. Although Kendall's method is very sensitive, it suffers from the difficulties of interpretation inherent in transient measurements. In the study reported below, the oscillatory method of Goldberg and Sandvik[2] has been adapted to the measurement of shear elasticity in fluids of low viscosity. This latter method appears to be as sensitive as that of Kendall and is, of course, more easily interpreted.

## EXPERIMENTAL PROCEDURE

The apparatus used in these experiments consisted primarily of a pair of concentric cylinders between which was placed the liquid under study. The outer cylinder was made from a piece of glass tubing selected for regularity of bore. It had a diameter of 1.240 cm. This cylinder was held in the apparatus so that it could be made to oscillate about its axis at a given amplitude and any chosen frequency. The frequency was adjusted by changing the speed of a variable speed motor which drove the oscillating cylinder through a cam and rocker-arm device. Photographic study showed that the rotatory oscillations of the outer cylinder were pure sine waves. The frequency of rotation of the outer cylinder was measured by a strobotac lamp.

The hollow inner cylinder (4.55 cm long with a diameter of 1.174 cm), having a low moment of inertia (4.12 g-cm$^2$) about its major axis, was suspended from a thin fiber. This low moment of inertia was achieved by building the cylinder of thin-walled tubing affixed to a heavy central shaft which served to weight the cylinder so that it would not float. A phonograph needle was used as a bottom bearing for the inner cylinder. Before an experiment was started, the cylinders were aligned by adjusting the support holding the suspension thread; then the inner cylinder was lifted slightly away from its bearing. A mirror was attached to the central rod of the inner cylinder so that a beam of light could be used to amplify its motion. The suspension fiber consisted of a single strand of untwisted silk approximately 15 cm long. Thus, the elasticity of the fiber was so slight that its contributions to the

* Now in the Research Laboratory, Rumford Chemical Works, Rumford, Rhode Island.
** Member of the Research Department, Eastman Kodak Company.
[1] Rheol. Bull. 12, 26 (1941).
[2] To be published.

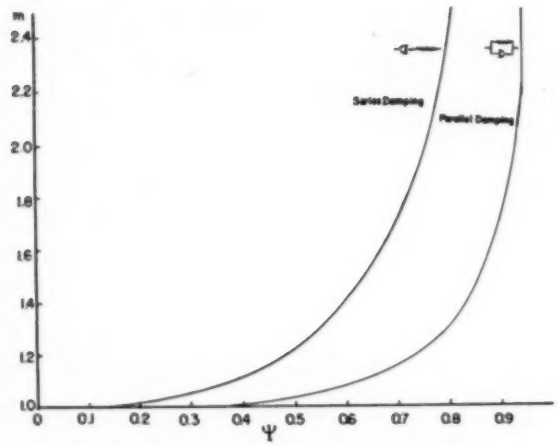


FIG. 1. Calculated variation of $\psi$ with $m$ at resonance for an elastic element with series or parallel damping.

observed elastic effects were negligible. In the studies reported below, end effects were negligible since the layer of liquid at either end of the inner cylinder was approximately 20 times thicker than that in the annular space between the two cylinders.

To make a measurement, the outer cylinder was filled with the solution under study, and then the inner cylinder was carefully inserted so that no air bubbles were entrapped between the two cylinders. After the cylinders were aligned, the outer cylinder was set in oscillation, and the amplitude of rotation of the inner cylinder was measured by the path of a beam of light reflected from its mirror onto a screen which was usually placed several meters from the instrument. Thus, any slight drifting of the inner cylinder with respect to the outer one was greatly amplified with the result that a slow erratic drifting was superimposed upon the oscillatory motion of the light spot. This necessitated "on the fly" measurement of the amplitude of oscillation with a caliper. When a non-elastic liquid was placed between the two cylinders, the inner cylinder had the same amplitude of rotation as that of the outer cylinder at low frequencies; and there was a gradual decrease in amplitude as the frequency was raised until at extremely high frequencies the inner cylinder remained practically motionless. When an elastic liquid was being studied, the amplitude of rotation of the inner cylinder was the same as that of the outer cylinder at very low frequencies and became negligibly small at high frequencies. However, at an intermediate frequency the amplitude of rotation of the inner cylinder was greater than that of the outer cylinder because of the phenomenon of resonance. It should be noted that the existence of mechanical resonance means that there is an elastic restoring force resisting distortion of the liquid. Therefore, the studies reported in this paper cannot be interpreted on the basis of thixotropy, simple non-Newtonian flow, or any other of the multitudinous rheological classifications which are concerned with changes in the internal friction of a substance.

The amplitude of rotation of the outer cylinder could be measured in two ways: first, by extrapolating the plot of amplitude *vs.* frequency of the inner cylinder to zero frequency, and secondly, by rigidly joining the two cylinders together and observing the light beam. The same value for the amplitude was always obtained by both of these methods.

The modulus of rigidity can be calculated from the following easily derived equation:

$$G_0=\frac{2\pi I}{r_1 L}\left(\frac{1}{r_1}-\frac{1}{r_2}\right)f_{\max}^2 \qquad (1)$$

where $G_0$ is the modulus of rigidity assuming no damping, $f_{\max}$ the resonance frequency, $L$ the length of the inner cylinder, and $r_1$ and $r_2$ are the radii of the inner and outer cylinders respectively.

The magnification factor, $m$, can be defined as the ratio of the amplitude of oscillation of the inner cylinder to that of the outer cylinder.

TABLE I. A comparison of elastic data from recoil and resonance studies.

| Material | Approximate viscosity (poises) | Kendall's resilient effect | Resonance data: Shear modulus (dynes/cm²) | Resonance data: Type of damping | Resonance data: Damping viscosity (poises) |
|---|---|---|---|---|---|
| Lucite in dichlorobenzene | 1 | Very large | 80 | Series | 1 |
| Rubber cement in benzene | 1 | Large | 0.28 | Parallel | 0.028 |
| Boiled linseed oil | | None | No resonance maximum | | |
| Glucose in water | 1 | None | No resonance maximum | | |

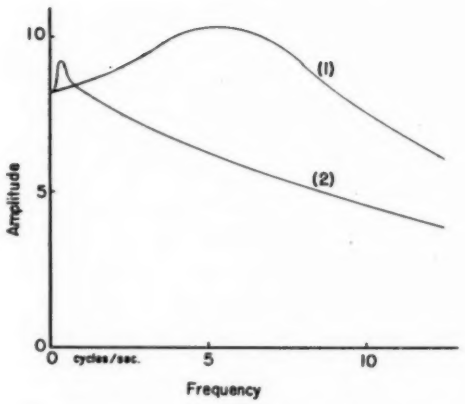


FIG. 2. Resonance curves: (1) methyl methacrylate polymer in dichlorobenzene; (2) rubber cement in benzene.

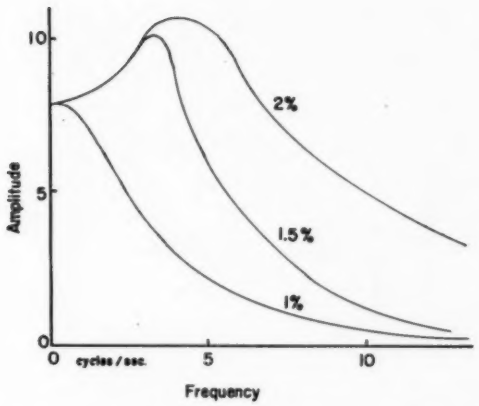


FIG. 3. Resonance curves for various concentrations of napalm in gasoline.

When the magnification factor is smaller than two or three, the modulus of rigidity computed from the previous equation is too small, because the damping causes a pronounced shift in the resonance frequency, and the equation is derived for an undamped system. It is impossible to compute the shift of the resonance maximum due to damping, unless a model for the system is assumed. We have calculated this shift for two models: a spring with parallel damping, and a spring with series damping. The calculations which are based on the direct electrical analog[3] are given in the appendix, and a graph of the ratio of the resonance frequency with damping to the resonance frequency that would be found, if the spring were not damped, *vs.* the magnification factor, is to be found in Fig. 1. From this graph the shear modulus as determined from the above equation can be corrected as follows:

$$G = G_0/\psi^2 \qquad (2)$$

where $G$ is the real shear modulus (assuming that the model is correct); $G_0$ is the shear modulus calculated from Eq. (1); and $\psi$ is the ratio of the frequencies taken from the graph. It is possible to compute the variation of $m$ with $\psi$ for the more complex model of a spring with a series and parallel dashpot, but instead of one $m-\psi$ curve, a family of curves will result depending on the relative values of the damping constants. However, this procedure was not followed because the apparent increase in accuracy of interpretation should not be accepted without fitting the whole frequency-amplitude curve.

The damping viscosity can be computed for the assumed models since the ratio of the damping viscosity to the shear modulus is related to the resonance frequency and magnification factor by means of Eqs. (2), (3), (6), and (9) in the Appendix, for the spring with either series or parallel damping. If the damping viscosity as calculated for series damping is much less than the viscosity determined in a conventional viscosimeter, the predominant damping is in parallel with the elastic element. If the calculated series viscosity is equal to the regular viscosity, the damping is in series with the elastic element. The calculated series viscosity cannot be greater than the regular viscosity. Thus, by comparison of the viscosity as calculated from the models with the regular viscosity, it is possible to find the predominant type of damping and thus the most correct value of the shear modulus as computed for a given fluid. In this discussion of damping, anomalous viscosity has been neglected since most fluids of low viscosity are only slightly non-Newtonian.

## DATA AND DISCUSSION

Several substances studied by Kendall were used with this apparatus to obtain the resonance curves shown in Fig. 2. The rheological constants derived from these measurements are presented in Table I.

An interesting series of measurements was performed on dilute sols of an aluminum soap

[3] J. Miles, J. Acous. Soc. Am. **14**, 183 (1943).

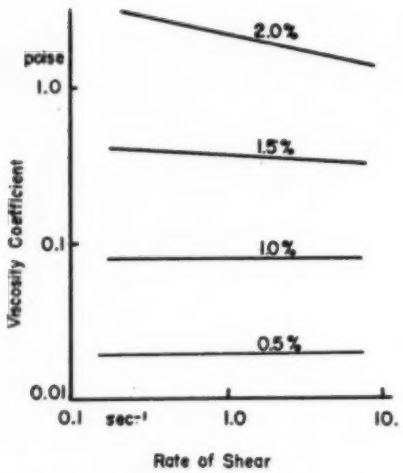


FIG. 4. The viscosity of napalm solutions at various concentrations.

in gasoline. The resonance curves for several concentrations are shown in Fig. 3. The constants calculated from these curves are presented in Table II. The predominant damping at a concentration of 1.5 percent is caused by the series viscosity. Measurements by Goldberg[4] indicate that the damping at concentrations higher than 6 percent is exclusively caused by the parallel viscosity. This means that both the viscosities in series and in parallel with the elastic element grow smaller with decreasing concentration, as might be expected. The transition from parallel to series damping of the elasticity occurs at about 2 percent. It is interesting to note that the concentration at which there is no longer any perceptible change of apparent viscosity coefficient with rate of shear (see Fig. 4) is also the concentration at which the resonance effect disappears.

The variation of shear modulus with molecular weight for a series of fractionated methyl methacrylate polymers is also given in Table II. Although the exact values of the maxima were difficult to determine because of the flatness of the resonance curves, it appears that the shear modulus increases with decreasing molecular weight at concentrations of equal viscosity. This result is in accord with the concept that the elastic properties of such a dilute solution are caused by the stretching of molecules.

TABLE II. Collected elastic data on fluids of low viscosity.

| Fluid studied | | Experimental data | | Calculated constants | | | | | Real constants | | |
|---|---|---|---|---|---|---|---|---|---|---|---|
| | | | | Shear modulus (dynes/cm²) | | | Damping viscosity (poises) | | | | |
| Solute | Solvent | Magnification factor | Resonance frequency (cycles/sec.) | No damping | Series damping | Parallel damping | Series | Parallel | Viscosity of fluid (poises) | Predominant type of damping | Approximate shear modulus (dynes/cm²) |
| 1% napalm (aluminum soap) | gasoline | 1.01 (if any) | 0.6 (?) | 0.4 | 1.6 | 2.6 | 0.46 | 2.3 | 0.02 | Impossible | Not elastic |
| 1.5% napalm | gasoline | 1.29 | 3.5 | 11 | 36 | 18 | 0.76 | 0.88 | 0.8 | Series | 36 |
| 2.0% napalm | gasoline | 1.37 | 4.5 | 18 | 51 | 26 | 0.95 | 0.91 | 2± | Series and parallel | ca. 40 |
| 1% methyl methacrylate (mol. wt. = $32 \times 10^4$) | ortho dichlorobenzene | 1.31 | 5.3 | 25 | 81 | 38 | 1.2 | 1.25 | 2.0± | Series | 80 |
| 1.05% methyl methacrylate (mol. wt. = $32 \times 10^4$) | dichlorodiethyl sulfide (Levinstein HS) | 1.29 | 7.5 | 48 | 160 | 77 | 1.6 | 2.3 | 2.5± | Series | 160 |
| 1.65% methyl methacrylate (mol. wt. = $16 \times 10^4$) | same | 1.09 | 6.0 | 30 | 210 | 75 | 1.6 | 3.5 | 2.0 | Series | 210 |
| 1.95% methyl methacrylate (mol. wt. = $12.4 \times 10^4$) | same | 1.05 | 5.5 | 21 | 210 | 71 | 1.6 | 5.5 | 2.0 | Series | 210 |
| 2.85% methyl methacrylate (mol. wt. = $8.4 \times 10^4$) | same | 1.02 | 5.0 | 21 | 530 | 100 | 3.8 | 9.6 | 3.0 | Series | 530 |
| 4.76% methyl methacrylate (mol. wt. = $4.0 \times 10^4$) | same | 1.00 | none | — | — | — | — | — | 3.0 | | Not elastic |
| Rubber cement | benzene | 1.15 | 0.40 | 0.14 | 0.70 | 0.28 | 0.01 | 0.028 | 1.0 | Parallel | 0.28 |

[4] To be published.

## ACKNOWLEDGMENT

The work reported above was completed in August, 1943 under the sponsorship of N.D.R.C. We wish to thank Dr. E. K. Carver for his helpful advice and suggestions about this problem.


## APPENDIX

### Derivation of the Correction to Shear Modulus Due to Damping

The following discussion is based on the direct electrical analogy, the fundamental definitions of which are listed below:

| *Mechanical Quantity* | *Electrical Analogy* |
|---|---|
| $x$ displacement | $q$ charge |
| $F$ force | $v$ potential |
| $1/G$ reciprocal of shear modulus | $C$ capacitance |
| $n$ viscosity | $R$ resistance |
| $M$ mass | $L$ inductance |
| $v$ velocity | $i$ current |

Because of the equivalence of Hooke's law to the capacity equation, the law of Newtonian viscosity to Ohm's law, and Newton's third law of motion to the equation for an inductance, this direct electrical analogy holds true.

Since sine wave oscillations are applied to the apparatus, the displacement $x$ is related to the amplitude $X$ according to the following equation in which $t$ is the time, $\delta$ is a constant to take care of phase difference, and $\omega=2\pi f$ ($f\equiv$frequency):

$$x_{\text{input}}=X_{\text{input}}\sin\omega t,$$
$$x_{\text{output}}=X_{\text{output}}\sin\omega(t+\delta).$$

By differentiation of the above equations with respect to time, we find that the ratio of the output to the input velocity equals the ratio of the output to the input amplitudes. This ratio is called the magnification factor and is denoted by the symbol $m$.

### Parallel Damping

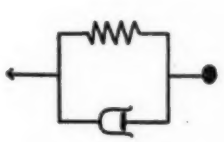

Mechanical model

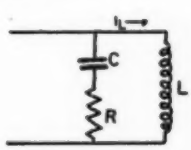


Electrical model

For this model undergoing sine wave oscillations we can set up the following equation for the magnification factor according to the direct electrical analog:

$$m=\frac{i_L}{i}=\frac{R-j/\omega C}{R+j(\omega L-1/\omega C)}. \tag{1}$$

This can be reduced to a more general form by use of $\psi\equiv$the ratio of the observed damped frequency to the free natural frequency of the elastic element, and $d$, a damping coefficient.

$$d=R(C/L)^{\frac{1}{2}} \tag{2}$$

and since the free natural frequency equals $1/(LC)^{\frac{1}{2}}$

$$\psi=\omega(LC)^{\frac{1}{2}}. \tag{3}$$

Then

$$m=\frac{d-j/\psi}{d+j(\psi-1/\psi)} \tag{4}$$

or

$$|m|^2=\frac{d^2+1/\psi^2}{d^2+\psi^2+1/\psi^2-2}. \tag{5}$$

If we differentiate and set $\partial m/\partial\psi$ equal to zero, the condition for a maximum, or resonance, is fulfilled and we find that

$$d^2=2(1-\psi^2)/\psi^4 \text{ at resonance.} \tag{6}$$

Equation (5) gives us the relation between $\psi$ and the physically measurable $m$. If we compute the shear modulus as if there were no damping, we obtain a quantity, $G_0$, according to the equation

$$G_0=k(f')^2.$$

But we really wish to know the true shear modulus

$$G=kf^2$$

where $f'$ is the observed frequency with damping, and $f$ is the free natural frequency.

By definition $\psi=f'/f$:

$$\therefore\quad G=G_0/\psi^2. \text{ (This is Eq. (2) in the text.)}$$

### Series Damping

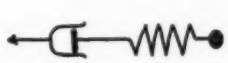

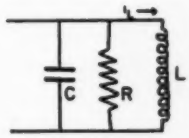


The equation for the magnification factor with the substitutions of $\psi$ and $d$, defined in Eqs. (2) and (3) above, is given below.

$$m=\frac{i_L}{i}=\frac{-j/\psi}{1/d+j(\psi-1/\psi)}, \tag{7}$$

and

$$|m|^2=\frac{(1/\psi)^2}{1/d^2+\psi^2+1/\psi^2-2}. \tag{8}$$

Differentiating with respect to $\psi$ and setting $\partial m/\partial\psi=0$, we find that

$$d^2=1/2(1-\psi^2) \text{ at resonance.} \tag{9}$$

From Eq. (9)

$$m^2=1/[\psi^2(3\psi-4)+1] \text{ at resonance.} \tag{10}$$

This relationship can be used to correct $G_0$ to $G$ as was shown above. Equations (5) and (10) are graphed in Fig. 1.

# On Creep and Relaxation*

B. Gross
*National Institute of Technology, Rio de Janeiro, Brazil*
(Received June 17, 1946)

The creep and the relaxation function of linear systems, for which the principle of superposition is valid, are mutually connected in a simple way. This makes it possible to calculate the distribution function of relaxation times of stress and the distribution function of retardation times of strain, when the relaxation function or the creep function is given. It also allows a transformation formula to be established for the conversion of one distribution function into another. The results of the theory are applied to a detailed discussion of the relaxation process in a particular case.

THE great development in the technique of high polymers has brought a renewed interest in the theory of elastic and dielectric relaxation phenomena. The phenomenological theory of these effects is still based upon the classical work of Boltzmann, Hopkinson, and Volterra. Its recent advance has been made possible by the improvements of the mathematical tools—the Fourier and Laplace transforms, Stieltjes' integral equation, and Heaviside's operational calculus. The classic work on the elastic effect has been carefully reviewed by Leaderman.[1] Modern methods of specification and correlation of the properties of viscoelastic materials were discussed by Alfrey and Doty.[2] The present paper continues in the sense of the phenomenological theory. It treats the relations existing between the creep and the relaxation function, shows how to deduce from them the underlying more fundamental quantities—the distribution functions of retardation time of strain and of relaxation times of stress—and establishes a general transformation formula between these 2 distribution functions.

Permanent deformations shall not be taken into account, because here we are interested only in reversible effects. This does not constitute a serious limitation for the theory; it is possible to deduce from the measured deformation- and load-time curves the corresponding curves, which would be observed, if permanent deformations were absent. Furthermore our considerations are confined to the linear problem. They are entirely based on the assumption that the principle of superposition is valid for creep and for relaxation. On this basis the fundamental relation between the creep and the relaxation function is established.

Even the linear elastic system, under constant strain, does not in general follow the simple exponential law of stress decay, that on theoretical grounds should be expected for a homogeneous material. Soon the hypothesis was formulated that the macroscopic body, that constitutes the object for the measurement, possesses a complex structure, being built up by a multiplicity of different elementary systems, each of them obeying the exponential law and characterized by a proper time constant. The observed curve of decay then represents an integral effect, the linear superposition of the single exponential functions. The distribution function of relaxation times is then more characteristic for a substance than the observed relaxation curve. Wiechert[3] proposed for the distribution function a Gaussian curve; Wagner[4] used the same expression in his theory of the electric after-effect. But *a priori* there seems to be no reason to believe in the existence of a single general law for the distribution function; this function may well have different forms for different materials. Thus the problem arises to deduce the distribution function from the experimental creep and relaxation data. Fuoss and Kirkwood[5] have given an extremely interesting method that allows calcula-

* Publication assisted by the Committee on Inter-American Scientific Publication.

[1] H. Leaderman, *Elastic and Creep Properties of Filamentous Materials and Other High Polymers* (The Textile Foundation, Washington, D. C., 1944).

[2] T. Alfrey and P. Doty, J. App. Phys. **16**, 700 (1945).

[3] E. Wiechert, Ann. d. Physik **50**, 335 (1893).

[4] K. W. Wagner, Ann. d. Physik **40**, 817 (1913).

[5] R. Fuoss and J. G. Kirkwood, J. Am. Chem. Soc. **63**, 385 (1941).

tion of the distribution function of relaxation times, when the admittance function or its real or imaginary part are known. In the field of elastic phenomena, admittance and impedance measurements are not made with the same ease as for dielectrics and they would not lead to the determination of the long time end of the distribution function. Thus one must rely on the interpretation of long time creep and relaxation data. Simha[6] has already shown how to deduce the distribution function of relaxation times, when the creep function is given. Here this problem is treated by a method that is similar to and was suggested by that of Fuoss-Kirkwood; it leads to expressions for the distribution function, which lend themselves readily for analytic or numerical computation.

Parallel with stress relaxation under constant strain goes strain retardation under constant stress. And instead of the first, one can choose the second effect as the adequate basis for a discussion of the structure of the viscoelastic body. Then a reasoning analogous to that outlined above leads to the introduction of the distribution function of retardation times of strain; this derives from the creep function in the same way as does the other distribution from the relaxation function. Thus the problem of its determination is the same and is solved in the same way as the former one.

The two distribution functions are not independent from one another. The present theory establishes the transformation formulae for their mutual conversion. They are expressions which are of a very general scope and well suited for numerical computation.

The results of the general theory are applied to the study of the relaxation process in the particular case in which the creep function is represented by a given analytic expression. To start with, the simple power law is chosen. The corresponding relaxation function is found to be given by a known transcendent, the Mittag-Leffler function, which already has been discussed in detail in connection with various relaxation phenomena. It behaves reasonably at medium values, but does not describe correctly the behavior of the stress for very great values of time, giving too high a value for the amount of stress relaxation. To amend it, an amplitude factor is introduced in the law for the relaxation function, without a modification of the form of the law. With this new expression one calculates backward the creep function, to which it belongs, and gets in this way adequate representations for both the creep and the relaxation function. Then the distribution functions are calculated, and finally the behavior for small times is studied.

[6] R. Simha, J. App. Phys. 13, 201 (1942).

## I. RELATIONS BETWEEN THE CREEP AND THE RELAXATION FUNCTION

### Creep

The deformation, which in a viscoelastic body is produced by the application of a constant load $P_0$, increases with time. It contains a purely elastic, constant component $P_0F/E$, $E$ being the instantaneous value of the modulus of elasticity and $F$ a form factor, and a time-dependent, slowly increasing component $P_0\psi(t)F/E$. $\psi(t)$ is called the creep function. The total deformation under constant load is, therefore, given by

$$y(t)=P_0[1+\psi(t)]F/E. \tag{1}$$

The deformation produced by the application of a variable load $P(t)$ can be calculated with the aid of the principle of superposition

$$y(t)=\frac{F}{E}\left[P(t)+\int_{-\infty}^{t}P(\tau)\varphi(t-\tau)d\tau\right], \tag{2}$$

where

$$\varphi(t)=d\psi(t)/dt \text{ (rate of creep)}. \tag{3}$$

### Relaxation

The load $P(t)$ necessary to produce in a viscoelastic body a constant deformation $y_0$ decreases with time, because the creep of the system gives rise to a phenomenon of stress-relaxation. There is

$$P(t)=y_0[1-\bar{\psi}(t)]E/F. \tag{4}$$

$\bar{\psi}(t)$ is the relaxation function.

The load necessary to produce a variable deformation $y(t)$ can again be calculated with the aid of the principle of superposition

$$P(t)=\frac{E}{F}\left[y(t)-\int_{-\infty}^{t}y(\tau)\bar{\varphi}(t-\tau)d\tau\right], \tag{5}$$

where

$$\bar{\varphi}(t) = d\bar{\psi}(t)/dt \text{ (rate of relaxation).}^{7} \quad (6)$$

### Relations between Creep and Relaxation

The Eqs. (2) and (5) are 2 equivalent expressions of the fundamental experimental fact, on which this theory is based—the validity of the principle of superposition. Their coexistence implies a relation between the creep and the relaxation function. To obtain it easily, substitute $P(t) = \exp(pt)$ in (2) and (5). Since

$$\int_{-\infty}^{t} e^{p\tau}\varphi(t-\tau)d\tau = e^{pt}\int_{0}^{\infty} e^{-p\tau}\varphi(\tau)d\tau, \quad (7)$$

it follows that $y(t) = \text{const.}\exp(pt)$. There results finally

$$\bar{L}(p) + \bar{L}(p)L(p) - L(p) = 0, \quad (8)$$

where

$$L(p) = \int_{0}^{\infty} e^{-pt}\varphi(t)dt, \quad (9a)$$

$$\bar{L}(p) = \int_{0}^{\infty} e^{-pt}\bar{\varphi}(t)dt. \quad (9b)$$

The deduction shows that $p$ may be real positive or complex, but it must not be on the negative real axis, because then the integrals would diverge. If $p$ is purely imaginary, equal to say $i\omega$, $L(i\omega)$ stands for the Fourier integral; if $p$ is real positive, $L(p)$ stands for the Laplace integral. Accordingly, 2 equivalent treatments are possible, i.e., by Fourier transforms or by Laplace transforms. Here we consider only the latter one.

Equation (8) is the fundamental relation, on which depend most of the following considerations. It may be solved with respect to $\bar{L}$ or to $L$:

$$\bar{L}(p) = \frac{L(p)}{1+L(p)}, \quad (10a)$$

$$L(p) = \frac{\bar{L}(p)}{1-\bar{L}(p)}. \quad (10b)$$

[7] Different cases of creep, creep recovery, and relaxation as well as the deduction of the Eqs. (2) and (5) from (1) and (4) are discussed in detail by Leaderman (reference 1). The symbols used by this author are here conserved, but the functions $\varphi$ and $\bar{\varphi}$ are not normalized. This avoids the introduction of the 2 constants $\beta$ and $\bar{\beta}$, which in the present case are not relevant.

With the aid of these equations, it is possible to calculate the rate of creep, when the rate of relaxation is given, or *vice versa*.[8] In both cases, the wanted function is given by an integral equation—the Laplace transform. This must be inverted, when one wishes to obtain the explicit expressions for $\bar{\varphi}$ or $\varphi$. The inversion of the Laplace transform has recently been studied extensively.[9] A very general inversion formula now available is the Bromwich-Wagner or complex inversion formula; this was used by Simha[6] in his calculation of the distribution function of relaxation times. But other methods too may be employed, for instance, those of the operational calculus. And frequently one may find the solution with the aid of a table of Laplace transforms. Therefore, there is here no necessity to write down explicitly the formal expressions for the functions $\varphi$ and $\bar{\varphi}$, so more so as in the present case a more simple way of analysis is possible, based on the implicit relations (10). This is possible, because the functions we are dealing with are very particular ones; they are continuous, continuously decreasing and integrable functions, which in their turn can be represented as Laplace transforms.

## II. THE DISTRIBUTION FUNCTIONS FOR CREEP AND FOR RELAXATION

There are 2 fundamental representations of a viscoelastic body by way of models; the Voigt model and the Maxwell model. Alfrey and Doty[2] have given very recently in this Journal a concise discussion of the properties of these models. We, therefore, can confine ourselves to a summary description.

### The Voigt Model

The Voigt element consists of a spring and a dashpot connected in parallel. Creep under constant stress then follows an exponential law $\beta(1-\exp t/\tau)$, the time constant of which is the retardation time of strain. It indicates the time necessary for the time-dependent component of

[8] Relations of this type are by no means new. For instance, they are already given by J. R. Carson, *Electric Circuit Theory and Operational Calculus* (McGraw-Hill Book Company, Inc., New York, 1926), pp. 51–52.

[9] See for instance, R. V. Churchill, *Modern Operational Methods in Engineering* (McGraw-Hill Book Company, Inc., New York, 1944).

deformation to reach a fraction $(1-e)$ of its final value. The Voigt model of a complex body consists of a multiplicity of Voigt elements with different time constants placed in series. The stress being the same for all, each element takes its share of the total strain. In the limit, the discontinuous system goes over in a continuous one, characterized by the distribution function $F(\tau)$ of retardation times. $F(\tau)d\tau$ is the fraction of the strain, which under constant stress has a retardation time between $\tau$ and $\tau+d\tau$. With the Voigt model, the fundamental experiment is the measurement of strain retardation, or creep, under constant stress. This gives the creep function, which in terms of the distribution function $F(\tau)$ is given by

$$\psi(t)=\beta\left[1-\int_0^\infty F(\tau)e^{-t/\tau}d\tau\right]; \qquad (11a)$$

$F(\tau)$ satisfies the normalizing condition

$$\int_0^\infty F(\tau)d\tau=1. \qquad (12)$$

### The Maxwell Model

The Maxwell element consists of a spring and a dashpot connected in series. Stress relaxation under constant strain follows an exponential law $\bar{\beta}(1-\exp t/\tau)$, the time constant of which is the relaxation time of stress. The Maxwell model of the complex body consists of a multiplicity of such elements placed in parallel. The strain being the same for all, each element takes its share of the stress, according to the value of its time constant. In the limit, the discontinuous system goes over in a continuous one, characterized by the distribution function $\bar{F}(\tau)$ of relaxation times. $\bar{F}(\tau)d\tau$ is the fraction of the stress, which under constant strain relaxes with a time constant between $\tau$ and $\tau+d\tau$. With the Maxwell model, the fundamental experiment is the measurement of stress relaxation under constant strain. This gives the relaxation function, which in terms of the distribution function $\bar{F}(\tau)$ is given by

$$\bar{\psi}(t)=\bar{\beta}\left[1-\int_0^\infty \bar{F}(\tau)e^{-t/\tau}d\tau\right]. \qquad (11b)$$

$\bar{F}$ satisfies a normalizing condition of the type (12).

### The Distribution Functions for Creep and for Relaxation

For the following it is more convenient to work with the functions $\varphi$ and $\bar{\varphi}$. It is easily seen, that these can be represented as

$$\varphi(t)=\int_0^\infty \rho(s)e^{-ts}ds, \qquad (13a)$$

$$\bar{\varphi}(t)=\int_0^\infty \bar{\rho}(s)e^{-ts}ds. \qquad (13b)$$

The functions $\rho$ and $\bar{\rho}$ introduced in this way are related to $F$ and $\bar{F}$ by the equations

$$\beta F(\tau)d\tau=-\rho(s)ds/s, \qquad (14a)$$

$$\bar{\beta}\bar{F}(\tau)d\tau=-\bar{\rho}(s)ds/s, \qquad (14b)$$

$$s=1/\tau. \qquad (14c)$$

We call $\rho$ the distribution function for creep and $\bar{\rho}$ the distribution function for relaxation. By means of Eqs. (14) it is always easy to go over to the "true" distribution functions $F$ and $\bar{F}$. The normalizing constants $\beta$ are determined with the aid of Eq. (12). Equations (14) show that the distribution functions can indeed be represented as Laplace transforms of "primitive" functions $\rho$. The possibility of this representation does not depend on the validity of the 2 models we have discussed, but ensues from the mathematical properties of the functions $\varphi$ and $\bar{\varphi}$. It is a common feature of all linear theories of relaxation phenomena.

## III. DETERMINATION OF THE DISTRIBUTION FUNCTIONS

Experimental evidence gives the functions $\varphi$ and $\bar{\varphi}$. Physically more interesting are the distribution functions $\rho$ and $\bar{\rho}$, because their knowledge may yield information about the structure of the system and the nature of the relaxation mechanism. One way of analysis consists in writing down an analytic expression for the distribution functions, which on theoretical grounds appears plausible and allows the calculation of the creep or the relaxation function, and then the comparison of the calculated and the measured curves. A second method consists in deducing the distribution functions from the ex-

perimentally given set of data. This can be done by an inversion of Eqs. (13).

### Distribution Function for Relaxation from Relaxation Function. Distribution Function for Creep from Creep Function

To obtain the inversion formula in the form needed here multiply both sides of Eq. (13b) by $e^{-pt}$ and integrate from 0 to $\infty$. This gives

$$\int_0^\infty e^{-pt}\bar{\varphi}(t)dt=\int_0^\infty e^{-pt}dt\int_0^\infty \bar{\rho}(s)e^{-ts}ds. \quad (15)$$

The left side, according to Eq. (9b), is equal to $\bar{L}(p)$. On the right side the order of integration can be inverted and the integral over the exponential functions can be evaluated. This gives

$$\bar{L}(p)=\int_0^\infty \frac{\bar{\rho}(s)}{s+p}ds. \quad (16)$$

It is again not necessary for $p$ to be real; it may be complex, but it must not be on the negative real axis. Then (16) is Stieltjes' integral equation, which is inverted by[10]

$$\bar{\rho}(p)=\frac{1}{2\pi i}\lim_{\delta+0}[\bar{L}(-p-i\delta)-\bar{L}(-p+i\delta)]. \quad (17)$$

An analogous expression is obtained for $\rho(p)$.

To demonstrate the validity of (17), substitute in Eq. (16), $(-p-i\delta)$ for $p$. There follows

$$\lim_{\delta+0}\bar{L}(-p-i\delta)=\lim_{\delta+0}\int_0^\infty \frac{\bar{\rho}(s)(s-p)ds}{(s-p)^2+\delta^2}+\lim_{\delta+0}i\delta\int_0^\infty \frac{\bar{\rho}(s)ds}{(s-p)^2+\delta^2}. \quad (18)$$

In the first integral, one can put $\delta=0$, provided Cauchy's principal value is taken. To calculate the second integral, we observe that

$$\lim_{\delta+0}\delta\int_0^\infty \frac{\bar{\rho}(s)-\bar{\rho}(p)}{(s-p)^2+\delta^2}ds=0. \quad (19)$$

Indeed, the value of the integral *without* the factor $\delta$ in front of it is certainly finite even in the limit $\delta=0$; thus the expression *including* this factor disappears for $\delta=0$. But

$$\lim_{\delta+0}\delta\int_0^\infty \frac{\bar{\rho}(p)ds}{(s-p)^2+\delta^2}=\bar{\rho}(p)\lim_{\delta+0}\tan^{-1}(s/\delta)\Big|_{-p}^{\infty}=\pi\bar{\rho}(p). \quad (20)$$

The value of the second integral in (18) is, therefore, $i\pi\bar{\rho}(p)$. And

$$\lim_{\delta+0}\bar{L}(-p-i\delta)=\int_0^\infty \frac{\bar{\rho}(s)ds}{(s-p)}+i\pi\bar{\rho}(p); \quad (21a)$$

analogously.

$$\lim_{\delta+0}\bar{L}(-p+i\delta)=\int_0^\infty \frac{\rho(s)ds}{(s-p)}-i\pi\rho(p). \quad (21b)$$

The difference of both expressions gives $2\pi i\bar{\rho}(p)$.[11]

Equations (21) show that $\lim_{\delta+0}\bar{L}(-p-i\delta)$ and $\lim_{\delta+0}\bar{L}(-p+i\delta)$ are conjugate functions:

$$\lim_{\delta+0}[\bar{L}(-p-i\delta)-\bar{L}(-p+i\delta)]=2i\ Im\lim_{\delta+0}\bar{L}(-p-i\delta), \quad (22a)$$

$$\lim_{\delta+0}[\bar{L}(-p-i\delta)+\bar{L}(-p+i\delta)]=2\ Re\lim_{\delta+0}\bar{L}(-p-i\delta). \quad (22b)$$

$\lim_{\delta+0}\bar{L}(-p-i\delta)$ is equivalent to $\lim_{\epsilon+0}\bar{L}(pe^{-i(\pi-\epsilon)})$; in a shorthand way this is written as $\bar{L}(pe^{-i\pi})$, provided the right meaning is attached to this expression: given $\bar{L}(p)$, $p$ positive; take the value that this function assumes when the argument is rotated through the under half-plan by an angle $-\pi$.[12] Accordingly, we replace the expressions $Im\lim_{\delta+0}\bar{L}(-p-i\delta)$ and $Re\lim_{\delta+0}\bar{L}(-p-i\delta)$, respectively, by $Im\,\bar{L}(pe^{-i\pi})$ and $Re\,\bar{L}(pe^{-i\pi})$. There results finally

$$\bar{\rho}(p)=Im\,\bar{L}(pe^{-i\pi})/\pi, \quad (23a)$$

$$\rho(p)=Im\,L(pe^{-i\pi})/\pi. \quad (23b)$$

The second equation is obtained by a development identical with that given above. When $\varphi$ and $\bar{\varphi}$ are known, $L$ and $\bar{L}$ can be calculated from (9). Then the distribution functions are obtained in a simple way. The deduction shows that the variable $p$ in (23) is equivalent with the variable $s$ of the Eqs. (14). Thus $\rho(p)dp$ and $\bar{\rho}(p)dp$ are, respectively, identic with $\rho(s)ds$ and $\bar{\rho}(s)ds$.

[10] T. J. Stieltjes, "Recherches sur les fractions continues," Ann. de la faculté de Toulouse 8, 1–22 (1894). Cf. D. V. Widder, *The Laplace Transform* (Princeton, University Press, New Jersey, 1941), p. 338. Am. Math. Mo. 52, No. 8 (1945).

[11] The evaluation of $\lim\bar{L}(-p-i\delta)$ is a particular case of the calculus of the boundary values of a function along a given path. For a general solution of this problem see A. Hurwitz and R. Courant, *Funktionentheorie* (Verlagsbuchhandlung, Julius Springer, Berlin, 1929), pp. 333–335.

[12] Employing this terminology we follow E. C. Titchmarsh, *Introduction to the Theory of Fourier Integrals* (Clarendon Press, Oxford, 1937), pp. 317–319, where a discussion of Stieltjes' integral equation is given.

### Distribution Function for Relaxation from Creep Function. Distribution Function for Creep from Relaxation Function

Frequently another type of relation is of interest. From the experimental point of view it is easier to measure the creep function than the relaxation function; but for theoretical reasons one may want the distribution function of relaxation times. This demands a formula that allows deduction of the distribution function for relaxation from the creep function, a problem that has already been discussed by Simha.[6] The particular type of inversion formula (17) makes it easy to solve this problem. By means of this equation, $\bar{\rho}(p)$ is expressed in function of the Laplace transform $\bar{L}(p)$ of $\bar{\varphi}(t)$; this in its turn is given in function of the Laplace transform $L(p)$ of $\varphi(t)$ by (10a). Substitution of (10a) in (17) directly gives, therefore, the wanted relation

$$\bar{\rho}(p)=\frac{1}{2\pi i}\lim_{\delta+0}\left[\frac{L(-p-i\delta)}{1+L(-p-i\delta)}-\frac{L(-p+i\delta)}{1+L(-p+i\delta)}\right]=\frac{1}{2\pi i}\frac{\lim_{\delta+0}L(-p-i\delta)-\lim_{\delta+0}L(-p+i\delta)}{[1+\lim_{\delta+0}L(-p-i\delta)][1+\lim_{\delta+0}L(-p+i\delta)]}. \quad (24)$$

An analogous expression is obtained for $\rho(p)$. Using the relations (22), the formula is transformed in a way similar to that of Eq. (17). There results after simple algebraic transformations

$$\bar{\rho}(p)=-\frac{1}{\pi}\frac{Im\,L(pe^{-i\pi})}{[1+Re\,L(pe^{-i\pi})]^2+[Im\,L(pe^{-i\pi})]^2}, \quad (25a)$$

$$\rho(p)=-\frac{1}{\pi}\frac{Im\,\bar{L}(pe^{-i\pi})}{[1-Re\,\bar{L}(pe^{-i\pi})]^2+[Im\,\bar{L}(pe^{-i\pi})]^2}. \quad (25b)$$

### An Auxiliary Formula

Equations (23) and (25) give the distribution functions in terms of the Laplace transforms of $\varphi$ and $\bar{\varphi}$, not in terms of the creep and relaxation functions themselves. These Laplace transforms are given by (9); when their values $L$ and $\bar{L}$ are known explicitly, the expressions $Im\,L(pe^{-i\pi})$ and $Re\,L(pe^{-i\pi})$ are easily calculated. For many functions, which are here of interest, the integrals can be evaluated in closed form. But in other cases this may not be so. Formulae, which allow to calculate the distribution functions without the previous explicit knowledge of $L(p)$ and $\bar{L}(p)$ are, therefore, of importance. Their deduction shall be discussed in a mathematical paper to be published elsewhere. The result is

$$Im\,L(pe^{-i\pi})=\int_0^\infty e^{-pt}\,Im\,\varphi(te^{-i\pi})dt, \quad (26a)$$

$$Re\,L(pe^{-i\pi})=-\int_0^\infty e^{-pt}\,Re\,\varphi(te^{-i\pi})dt. \quad (26b)$$

The same relations hold for $\bar{L}$ and $\bar{\varphi}$. They apply, when $\varphi$ in its turn is a Laplace transform.

For the application, the experimentally given set of creep or relaxation data must be represented by appropriate analytic functions, and the integrals (26) be calculated. Their evaluation may not always be possible in closed form, but provided the integrand can be written down explicitly, numerical methods can be employed.

## IV. RELATIONS BETWEEN THE DISTRIBUTION FUNCTIONS

The existence of a relationship between the creep and the relaxation function obviously also implies a direct relation between the corresponding distribution functions. For instance, assuming that the distribution function of relaxation times is represented by Wiechert's function, it must be possible to calculate the corresponding distribution function of retardation times, without previously calculating the creep and the relaxation function. To obtain this relation in a general form, we start with Eq. (24). The functions $\lim_{\delta+0}L(-p\mp i\delta)$ are expressed in terms of $\rho(p)$ by means of (21). There results after simple algebraic

transformations

$$\bar{\rho}(p)dp=\frac{\rho(p)dp}{\left[1+\int_0^\infty \frac{\rho(s)ds}{(s-p)}\right]^2+\pi^2\rho^2(p)}, \quad (27a)$$

$$\rho(p)dp=\frac{\bar{\rho}(p)dp}{\left[1-\int_0^\infty \frac{\bar{\rho}(s)ds}{(s-p)}\right]^2+\pi^2\bar{\rho}^2(p)}. \quad (27b)$$

These formulas convert one distribution function into another. They are of a very general scope, well adapted for analytic and numerical computation. Since the integration can be performed by graphical methods it would not even be necessary to represent $\rho$ or $\bar{\rho}$ by an analytic expression. The integrals are principal values, but the singularity at $s=p$ creates no difficulty; the way such integrals are handled has already been discussed in a former paper.[13]

## V. STUDY OF PARTICULAR CREEP AND RELAXATION FUNCTIONS

The simple power law

$$\psi(t)=kt^m, \quad 0<m<1 \quad (28)$$

is one of the functions which most frequently have been proposed as a mathematical expression for experimental creep data. It has the serious fault that it does not reach asymptotically a constant value for very great values of $t$, but yields an ever increasing deformation. But the fact alone that it has survived the many objections raised against it speaks much in favor of it being at least a reasonable approximation to the true fact, valid over a certain interval of time. Thus it is worth while to study the relaxation function that according to this theory is associated with it. The result shall lead us to a generalization of this law that is free of the fault mentioned above.

### The Simple Power Law

The rate of creep is given by

$$\varphi(t)=\beta(t/t_0)^{m-1}. \quad (29)$$

For the following it is convenient to introduce a numerical factor

$$\lambda=\beta t_0\Gamma(m), \quad (30)$$

where $\Gamma(m)$ is the gamma-function $\Gamma(m+1)=m!$[14] Substitution of (29) in (9a) gives

$$L(p)=\lambda(t_0p)^{-m}. \quad (31)$$

Then, according to Eq. (10a), $\bar{L}(p)$ is given by

$$\bar{L}(p)=\frac{\lambda(t_0p)^{-m}}{1+\lambda(t_0p)^{-m}}. \quad (32)$$

To obtain $\bar{\varphi}(t)$, the Laplace transform (9b) must be inverted, with $\bar{L}(p)$ given by (32). There results

$$\bar{\varphi}(t)=-\frac{d}{dt}E_m[-\lambda(t/t_0)^m]. \quad (33)$$

$E_m(t)$ is a known transcendent, the function of Mittag-Leffler, defined by

$$E_m(t)=\sum_{n=0}^{\infty}\frac{t^n}{\Gamma(nm+1)}. \quad (34)$$

The relaxation function is given by

$$\bar{\psi}(t)=1-E_m[-\lambda(t/t_0)^m]. \quad (35)$$

*The deduction* of (33) is easily obtained by the Heaviside operational calculus.[15] Expand $p\bar{L}(p)$ in descending powers of $p$. For the sake of simplicity put $\sigma=\lambda t_0^{-m}$. Then

$$p\bar{L}(p)=\sigma p^{1-m}[1-\sigma p^{-m}+\sigma^2p^{-2m}-\sigma^3p^{-3m}+-\cdots]. \quad (36)$$

Replace, according to the Heaviside rule, $1/p^n$ by $t^n/\Gamma(1+n)$. This gives

$$\bar{\varphi}(t)=\frac{\sigma t^{m-1}}{\Gamma(m)}-\frac{\sigma^2t^{2m-1}}{\Gamma(2m)}+\frac{\sigma^3t^{3m-1}}{\Gamma(3m)}-\frac{\sigma^4t^{4m-1}}{\Gamma(4m)}+-\cdots. \quad (37)$$

Observing that $m\Gamma(m)=\Gamma(m+1)$, Eq. (37) is easily identified with the series expansion of the derivative of the Mittag-Leffler function of argument $\{-\lambda(t/t_0)^m\}$. The inversion of the Laplace transform in the present case can also be obtained by the more orthodox method of the complex inversion theorem. This was shown by Moraes and Schoenberg.[16]

An *asymptotic expansion* valid for great values of $t/t_0$ is also obtained in the Heaviside way. Expand $p\bar{L}(p)$ in ascending powers of $p$.

$$p\bar{L}(p)=p[1-p^m/\sigma+p^{2m}/\sigma^2-p^{3m}/\sigma^3+p^{4m}/\sigma^4-+\cdots]. \quad (38)$$

[13] H. Silva and B. Gross, Phys. Rev. **60**, 684 (1941). The method indicated in this paper has recently been used by S. T. Ma, Phys. Rev. **68**, 166 (1945).

[14] Tables and integral representations of the gamma-function are given by Jahnke-Emde, *Tables of Functions* (B. Teubner, Leipzig, 1933), pp. 86, 96.

[15] Reference 8, p. 28. $\bar{L}(p)$ of the present paper corresponds to Carson's $1/pH(p)$; thus Carson's expansion of $1/H(p)$ corresponds in our case to an expansion of $p\bar{L}(p)$.

[16] A. de Moraes and M. Schoenberg, Ann. Acad. Brasil. Ci. **12**, 137 (1940), Section 4.

Replace $p^n$ by $t^{-n}/\Gamma(1-n)$, discard the term with an integer power in $p$ (because $p^1$ gives $1/t\Gamma(0)$; but $\Gamma(0)=\infty$) and get

$$\bar{\varphi}(t)=-\frac{\sigma^{-1}t^{-m-1}}{\Gamma(-m)}+\frac{\sigma^{-2}t^{-2m-1}}{\Gamma(-2m)}-\frac{\sigma^{-3}t^{-3m-1}}{\Gamma(-3m)}+\frac{\sigma^{-4}t^{-4m-1}}{\Gamma(-4m)}-+\cdots. \quad (39)$$

*The Mittag-Leffler function* is a generalization of the exponential function, with which it is identical, when the parameter $m$ is 1. It is already known to be of importance for relaxation phenomena of various kinds. Several of its mathematical aspects as well as its connection with the theory of nerve conduction have been discussed by Davis.[17] In connection with the theory of the discharge and return voltage curves for absorptive capacitors it has been studied by Castro, who has also availed himself of a very useful approximate representation.[18] For certain integer values of $m$ it can be expressed by elementary transcendents. For small values of $m$ a simple approximation formula exists. There is furthermore $E_m(0)=1$ and $E_m(-\infty)=0$.

Very valuable information about the behavior of the expression (33) is contained in a paper by Cole and Cole.[19] A comparison of their formulae (8) and (10) with the Eqs. (37) and (39) of the present paper shows them to be identical, up to a constant, the parameter $m$ corresponding to Cole's $1-\alpha$. (The Coles write $-nm\Gamma(1-nm)$ for $\Gamma(-nm)$.) This shows, that the Cole's expression for the absorption current is identic with our expression (33) for the rate of relaxation; it allows to use Fig. 1 and Table I of the Cole's paper for computation of the rate of relaxation in exactly the same way as those authors use them for the computation of the dielectric absorption current, and relieves us here of the task to give a plot or tabulate the function $\bar{\varphi}(t)$.

For very small values of $t$, $\bar{\varphi}(t)$ is given by the leading term of (37). Thus, when $t$ approaches 0, $\bar{\varphi}(t)$ tends to $\infty$ in the same way as does $\varphi(t)$

$$t\to 0: \quad \bar{\varphi}(t)=\tilde{\beta}(t/t_0)^{m-1}. \quad (40)$$

For very great values of $t$, $\bar{\varphi}(t)$ is given by the leading term of (39). Observing that $\Gamma(m)\Gamma(-m)=-\pi/m\sin\pi m$,[14] there results

$$t\to\infty: \quad \bar{\varphi}(t)=\frac{m\sin\pi m}{\pi\beta t_0^2}(t/t_0)^{-(m+1)}. \quad (41)$$

Thus when $t$ approaches $\infty$, $\bar{\varphi}(t)$ tends to 0 much more rapidly than does $\varphi(t)$. It follows that the integral taken from 0 to $\infty$ remains finite.

It is known that experimental creep data frequently call for a very small value of $m$. In this case a satisfactory elementary approximation for $E_m(t)$ exists.[18] It allows to write $\bar{\varphi}(t)$ in the form

$$\bar{\varphi}(t)=\beta(t/t_0)^{m-1}\frac{1}{[1+\beta t_0(t/t_0)^m/m]^2}, \quad (42)$$

an expression that shows well the general behavior of the function and its departure from the simple power law.

### The Mittag-Leffler Function

It cannot be expected that these formulae describe correctly the experimental relaxation data for great values of $t$, based as they are on a creep law that admittedly fails for such values. Indeed, an inspection of Eq. (35) shows that $\bar{\psi}(t)$ approaches 1, when $t$ approaches $\infty$. This means, that in the case of stress relaxation under constant strain (Eq. (4)) the stress decays to 0, an absurd result that obviously is a consequence of the infinite increase of the creep function (28). In reality the amount of stress relaxation is only a rather small fraction of the total stress. To get a relaxation function that fulfills this condition it is not necessary to modify the general form of the relaxation law (35). It is sufficient to postulate that the amplitude of the function is not 1, but smaller than 1. Thus one must introduce an amplitude factor $a<1$, writing

$$\bar{\psi}(t)=a[1-E_m\{-(t/t_0)^m\}]. \quad (43)$$

A comparison with Eq. (4) shows the significance of $a$; $1-a$ represents the relation between final load $P(\infty)$ and initial load (or stress) $P(0)$.

$$1-a=P(\infty)/P(0). \quad (44)$$

We, therefore, are led to believe that Eq. (43) is an adequate analytic expression for the relaxation function. Now one has to calculate the creep function to which it belongs.

The rate of relaxation is now given by

$$\bar{\varphi}(t)=-a\frac{d}{dt}E_m[-(t/t_0)^m]. \quad (45)$$

The corresponding Laplace transform $\bar{L}(p)$, according to (32) and (33), is

$$\bar{L}(p)=a\frac{(t_0p)^{-m}}{1+(t_0p)^{-m}}. \quad (46)$$

[17] H. T. Davis, *The Theory of Linear Operators* (The Principia Press, Bloomington, 1936).
[18] F. M. de Oliveira Castro, Zeits. f. Physik **114**, 116 (1939).
[19] K. S. Cole and R. H. Cole, J. Chem. Phys. **10**, 98 (1942).

Substitution of (46) in (10b) gives

$$L(p)=\frac{a}{1-a}\frac{(1-a)(t_0p)^{-m}}{1+(1-a)(t_0p)^{-m}}. \quad (47)$$

Therefore,

$$\varphi(t)=-\frac{a}{1-a}\frac{d}{dt}E_m[-(1-a)(t/t_0)^m]. \quad (48)$$

Both the creep and the relaxation function are now represented by the same general law; they differ only by the values of the parameters. This is very satisfactory; it brings out the experimental fact that those functions are of the same type. By an appropriate choice of $a$, $t_0$, and $m$, a great variety of experimental curves can be represented, varying from the simple power law to the exponential function. The asymptotic expressions (40) and (41) and the approximation formula (42) now apply to creep and to relaxation; they must only be completed by the corresponding amplitude factor. The numerical analysis of creep and relaxation data can be performed by the methods given by Cole and Cole[19] and already mentioned above. But it cannot be the purpose of this paper to enter into details of numerical computation.

The problem could have been approached from the side of the creep function too. The expression (33) is in itself a generalization of the simple power law, coinciding with it for small values, but converging more rapidly at great values, of $t$. This would suggest the possibility of introducing it as a suitable substitute for the power law. In the corresponding electric case, Cole and Cole[19] proceeded in an analogous way, when they represented the dielectric absorption current by such an expression.

### A Functional Relation between Creep and Relaxation Function

Since $\varphi(t)$ and $\bar{\varphi}(t)$ are given by the same general law, a direct relation between them is readily established. It follows from Eqs. (48) and (45) that

$$\bar{\varphi}(t)=(1-a)^{(m-1)/m}\varphi\left[\frac{t}{(1-a)^{1/m}}\right]. \quad (49)$$

This possibility of direct computation of relaxation data from creep measurements should be of particular interest for technical applications.

### The Distribution Function

The distribution function of relaxation times, that belongs to the relaxation function (43) is easily calculated. Since the Laplace transform $\bar{L}(p)$ of $\bar{\varphi}(t)$ is known explicitly, Eq. (23) applies directly. Replace in (46) $p^m$ by $(pe^{-i\pi})^m$. Then

$$\bar{L}(pe^{-i\pi})=\frac{a}{1+(t_0p)^m(\cos\pi m-i\sin\pi m)}. \quad (50)$$

To get $\bar{\rho}(p)$ one has to take the imaginary part of this expression. Thus

$$\bar{\rho}(p)dp=\frac{1}{\pi}\frac{a\sin\pi m\,dp}{(t_0p)^m+(t_0p)^{-m}+2\cos\pi m}. \quad (51)$$

The distribution function has its maximum at $p=1/t_0$. Introducing a new variable

$$u=\log_e 1/t_0p \quad (52)$$

normalizing, and observing that $p=1/\tau$, one gets

$$\bar{F}(\tau)d\tau=\frac{1}{2\pi}\frac{\sin\pi m}{\cosh um+\cos\pi m}du. \quad (53)$$

The distribution function of retardation times is given by the same law, but while for relaxation $u=\log_e\tau/t_0$, there is for creep

$$u=\log_e\{\tau/t_0(1-a)^{1/m}\}.$$

$\bar{F}(\tau)d\tau$ as given by Eq. (53) is easily identified with the distribution function that Cole and Cole[20] have obtained for dielectric relaxation by the Fuoss-Kirkwood method.[5] These authors have discussed in detail the behavior of the function and compared it with the Wiechert-Wagner distribution.

### The Behavior for Small Times

The rates of creep and of relaxation as given by the Eqs. (45) and (48) become infinite at $t=0$, while theoretical expectations let us expect them to be finite. The study of the behavior for

[20] K. S. Cole and R. H. Cole, J. Chem. Phys. 9, 341 (1941). Coles' parameter $1-\alpha$ corresponds to the parameter $m$ of the present paper.

small times should, therefore, be carried out with a class of functions that remain finite for $t=0$. An adequate representation for this interval would be

$$\bar{\varphi}(t)=\beta(c+t/t_0)^{m-1}, \quad c\ll 1. \tag{54}$$

The Laplace transform of this function cannot be written down explicitly. Thus one has to rely on the Eqs. (26). Here we shall confine ourselves to the discussion of the distribution function for relaxation. To obtain it, replace in Eq. (54) $t$ by $te^{-i\tau}$ and take the imaginary part of the expression $\bar{\varphi}(te^{-i\tau})$. This gives

$$Im\ \bar{\varphi}(te^{-i\tau})=\begin{cases}0 & \text{for } t<ct_0,\\ \beta \sin\pi(1-m)\ (t/t_0-c)^{m-1} & \text{for } t>ct_0.\end{cases} \tag{55}$$

The expression (55) is substituted in (26a). The integrand being 0 for $t<ct_0$, the integral now runs from $ct_0$ to $\infty$. By a change of variable, the integral is reduced to a gamma-function; the final result is[21]

$$\bar{\rho}(p)dp=\frac{\beta t_0}{\pi}\Gamma(m)\ \sin\pi(1-m)\frac{e^{-c(t_0p)}}{(t_0p)^m}dp. \tag{56}$$

This distribution must be compared with (51). Here we are concerned only with small values of $t/t_0$, i.e., small values of $\tau$. Since $p=1/\tau$, this means, that we must consider only values of $(t_0p)$ very much greater than $c$. For such values, the distribution (51) decreases like $1/(t_0p)^m$, while the new distribution (56) decreases like $e^{-c(t_0p)}/(t_0p)^m$, i.e., much more rapidly than the former one. Practically, this signifies an exponential cut-off of the distribution function for small relaxation times.

I am very indebted to the Director of the Institute, Professor E. L. da Fonseca Costa, who made this study possible.

[21] This result can be found in tables of Laplace transforms; see for instance, Carson (reference 8), p. 39, formula (e). Here the deduction is outlined, because it is a good example for the application of Eq. (26).

# Parallel Plate Optics for Rapid Scanning*

S. B. Myers**
*Radiation Laboratory, Massachusetts Institute of Technology, Cambridge, Massachusetts*

(Received August 28, 1946)

Rapid scanning using a paraboloid antenna is unsatisfactory; rapid movement of the antenna is mechanically impractical, while motion of the feed near the focus requires long focal length for good optical results. Another attack on the problem is to place the feed between parallel plates which produce a line source near a bifocal reflector. The energy flows along the geodesics of the mean surface between the parallel plates; the problem of shaping the plates so that a circular feed motion produces an oscillating beam at the line source becomes a problem in differential geometry and the calculus of variations. If the mean surface is assumed to consist of two developable surfaces joined along part of their boundaries, the unique solution of the optical problem is a circular disk along the edge of which the feed moves, joined to a section of a 60° cone which is straightened out at the large end to obtain a straight line source. This is the RCA solution of the problem. If the surface is assumed to consist of a surface of revolution which provides a feed circle, and attached to it a circular disk a diameter of which is the aperture, under certain natural restrictions no exact solution of the optical problem is possible, but several approximate solutions exist. Dielectric introduced between the plates of such a surface of revolution scanner effects a great improvement in the optics.

## INTRODUCTION

RAPID scanning by means of movement of a paraboloid antenna is mechanically impractical. If the paraboloid is kept fixed, and the source of energy moved near the focus, the optical results are not satisfactory except with an extremely long focal length. Another approach to the problem is the following. If the energy feed be placed between two curved parallel plates, experiment has shown that the energy

* This paper is based on work done for the Office of Scientific Research and Development under Contract OEMsr-262 with the Massachusetts Institute of Technology.

** Now at the University of Michigan.

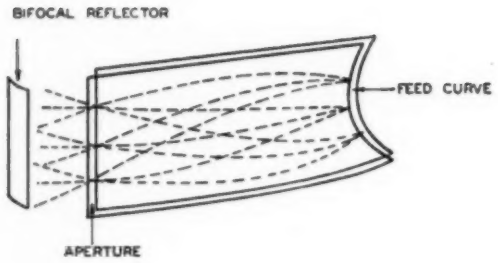


FIG. 1.

will flow along geodesics of the mean surface between the plates; if the parallel plates can be shaped so that a motion of the feed will produce an oscillating beam at a straight aperture, the latter will serve as a line source for a nearby bifocal reflector and the desired scanning is possible. For best illumination it is desirable that the normal ray from every point on the feed curve pass through a fixed point on the aperture; also, it is mechanically desirable that the feed curve be a circle. (See Fig. 1.)

A directed beam will be produced at the aperture by a fixed feed 0 if the phase errors at the aperture vary linearly with length along the aperture. The simplest way to accomplish this is to shape the parallel plates so that the mean surface is planar near the aperture, and the wave fronts are straight (near the aperture). This latter condition implies that the geodesics from 0 are parallel near the aperture. We are thus led to the following geometric problem. To find a surface $S$ containing a straight line $C_2$ and planar near $C_2$, and containing a curve $C_1$ (preferably a circle), with the property that the geodesics issuing from each point 0 of $C_1$ meet $C_2$ at a constant angle (which varies as 0 moves on $C_1$); further, the geodesics normal to $C_1$ must all meet on $C_2$.

This problem involves differential geometry and the calculus of variations. As yet it is not known whether a surface exists which meets all these requirements. Further, additional stringent restrictions as to size and shape of the antenna are usually imposed in any practical application. In this paper we discuss several approximate solutions of the problem, which seem suitable for application.

In Section 2 we take up a solution discovered by RCA; it yields perfect scanning optics (i.e., produces an oscillating beam at the aperture), but fails to meet the illumination requirement. The mean surface consists of a circular disk along the edge of which the feed moves, and a section of a 60° cone which is straightened out at the large end to obtain a straight line aperture (see Fig. 2). It is the only known surface which solves the optical problem exactly, and it is shown here that it is the unique method of joining two developable surfaces so as to obtain such optics. In Section 3, the "surface of revolution" solution is studied. Here the mean surface consists of a surface of revolution which provides a feed circle, and attached to it a circular disk a diameter of which is the aperture (see Fig. 3). Such a solution satisfies all requirements except the optical conditions. It is proved that these optical conditions cannot be satisfied exactly by any such surface if the radius of the surface is bounded by the radii of the feed circle and aperture disk. An investigation of the problem of minimizing the optical errors reveals that by shaping the surface in any one of several simple ways these errors can be made very small. In Section 4 it is shown that this same solution can be improved by use of dielectric between the parallel plates.

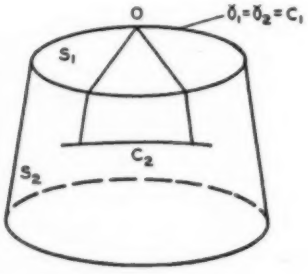


FIG. 2.

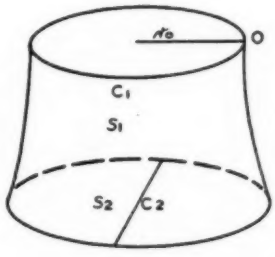


FIG. 3.

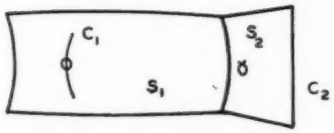


FIG. 4.

## 1. SURFACES AND GEODESICS[1]

Let a surface $S$ be given by equations $x=x(u, v)$, $y=y(u, v)$, $z=z(u, v)$. From the usual formula

$$ds^2=dx^2+dy^2+dz^2=A(u, v)du^2 +2B(u, v)dudv+C(u, v)dv^2$$

is obtained the expression for the length of a curve $u=u(t)$, $v=v(t)$.

$$s=\int (Au'^2+2Bu'v'+Cv'^2)^{\frac{1}{2}}dt =\int F(u, v, u', v')dt.$$

A geodesic may be defined as a shortest arc joining its endpoints. Using $s$ as parameter, the geodesics on $S$ are solutions of the equations

$$\frac{d}{ds}\left(\frac{\partial F}{\partial u'}\right)=\frac{\partial F}{\partial u},$$

$$F(u, v, u', v')=1.$$

Along a geodesic $g$, the geodesic curvature is zero (geodesic curvature of a curve $g$ at a point $P$ is by definition the curvature of the projection of $g$ on the tangent plane to $S$ at $P$).

Two fundamental properties of geodesics needed here are: (1) through every point on a surface and in every direction there is a unique geodesic, (2) if a constant length is measured off on geodesic rays through a point 0 the locus (geodesic circle) thus obtained is perpendicular to the rays through 0 (in other words, wave fronts from a point source are normal to the rays from the source). It can be shown that a geodesic crossing a sharp bend in a surface must make equal angles with the bend on both sides.

A developable surface is one which can be deformed locally onto a plane without stretching or tearing, thus preserving lengths. This is equivalent to the identical vanishing of the Gauss curvature. The fundamental form for a developable is the same as for the plane, $ds^2=du^2+dv^2$ or in polar coordinates, $dr^2+r^2d\theta^2$. Examples of developables are cylinders and cones. Two developables $S_1$ and $S_2$, $S_1$ containing a curve $C$ and $S_2$ containing a curve $C'$, can be joined along $C$, $C'$ as common curve without deforming $S_1$ if the curvature of $C$ at each point is greater than the geodesic curvature of $C'$ at the corresponding point. The geodesics on a developable become straight lines when the surface is developed onto a plane.

[1] See, for example, L. P. Eisenhart, *A Treatise on the Differential Geometry of Curves and Surfaces* (Ginn and Company, New York, 1909).

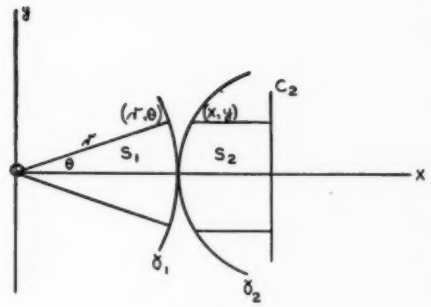


FIG. 5.

## 2. THE RCA SOLUTION

We take up the problem of finding a surface $S$, formed by joining two developables $S_1$ and $S_2$ along a common edge $\gamma$ (see Fig. 4), with the property that $S_1$ contains a curve $C_1$ and $S_2$ a straight line segment $C_2$ such that all geodesics from one point 0 of $C_1$ to the points of $C_2$ have equal lengths (this is equivalent to the condition that all these geodesics be perpendicular to $C_2$), and all geodesics from each point of $C_1$ near 0 to the points of $C_2$ have lengths which vary linearly with length along $C_2$ (this is equivalent to the condition that these geodesics meet $C_2$ at constant angle).

Let $S_1$ and $S_2$ be two developables joined along a common edge $\gamma$. Suppose each developable is developed into planar form, the curve $\gamma$ becoming two curves $\gamma_1$ and $\gamma_2$. Let 0 be a point in $S_1$ and let $\gamma_1$ and $\gamma_2$ be in contact at the foot of the normal from 0 to $\gamma_1$. Using coordinates as shown in Fig. 5, let the polar equation of $\gamma_1$ be $r=r(\theta)$. Now

$$ds^2=dr^2+r^2d\theta^2 \text{ along } \gamma_1,$$
$$ds^2=dx^2+dy^2 \text{ along } \gamma_2.$$

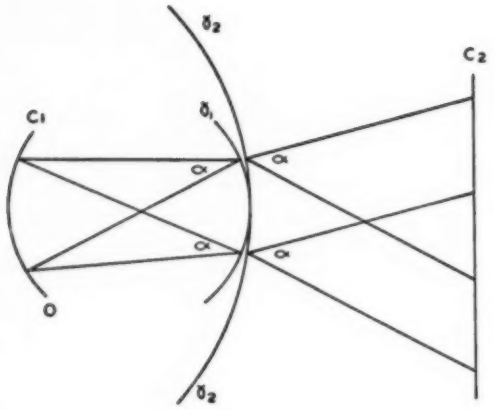


FIG. 6.

If the aperture $C_2$ is to be a wave front for rays from 0 when $\gamma_1$ and $\gamma_2$ are made to coincide, we must have $x=r(\theta)$ along $\gamma_2$. Hence $dx=dr$, $dy=rd\theta$ and the cartesian equations of $\gamma_2$ are

$$x=r(\theta),$$
$$y=\int_0^\theta r(\theta)d\theta. \tag{1}$$

If $C_2$ is to continue to cut the rays from the source 0 at equal angles as 0 moves along a feed curve $C_1$, then each pair of points on $C_1$ must subtend a constant angle $\alpha$ at all points of $\gamma$. Therefore $\gamma_1$ is a circle passing through each pair of points of $C_1$; hence $C_1$ and $\gamma_1$ are parts of the same circle $r=2a\cos\theta$. From (1) it follows that $\gamma_2$ has equations

$$x=2a\cos\theta$$
$$y=2a\sin\theta$$

and is a circle whose radius is double that of $\gamma_1$ (see Fig. 6).

If one-half of the circle $\gamma_2$ is made to coincide with $\gamma_1$, leaving $S_1$ fixed, the surface $S_2$ is deformed into the lateral surface of a cone inclined at a 60° angle to the circular disk $S_1$ (see Fig. 2). The aperture $C_2$ is now a curve on the side of a cone, but the figure can be deformed so that $C_2$ becomes straight in space. As the feed 0 rotates through a central angle $\beta$ on $C_1$, the beam issuing from $C_2$ tilts through an angle $\beta$.

This is the RCA solution. It furnishes the unique method of joining two developables so as to get exact scanning optics and is the only known method of obtaining such optics. However as 0 moves along $C_1$ the illumination pattern along $C_2$ changes, since the rays normal to $C_1$ do not pass through the same point of $C_2$.

### 3. SURFACE OF REVOLUTION SCANNER

A promising type of surface $S$ is composed of a surface of revolution $S_1$ with a base disk $S_2$ attached to it along a circular cross section (see Fig. 3). The feed curve $C_1$ is a circular cross section of $S_1$ and the aperture $C_2$ is the diameter of $S_2$. All the geodesics normal to $C_1$ pass through the center of the aperture, so that the illumination requirement is satisfied. Symmetry properties of $S$ show that if the geodesics from one point 0 of $C_1$ meet $C_2$ at a constant angle, so will the geodesics from any other point of $C_1$. We will show that such perfect optics are impossible if the radius of the surface is bounded by the radii of $C_1$ and $S_2$, and will investigate the question of shaping the surface so as to minimize the optical errors.

If $S_1$ is formed by rotating the curve $y=y(r)$ about the $y$ axis we obtain[2]

$$ds^2=dr^2+r^2d\theta^2+dy^2=(1+y'^2)dr^2+r^2d\theta^2,$$
$$y'=\frac{dy}{dr},$$
$$s=\int\left((1+y'^2)\left(\frac{dr}{dt}\right)^2+r^2\left(\frac{d\theta}{dt}\right)^2\right)^{\frac{1}{2}}dt.$$

The equations of geodesics on $S_1$ can be integrated once to give

$$r^2(d\theta/ds)=h,$$

where $h$ is a constant along each geodesic. But if

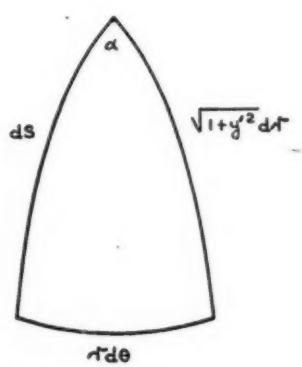


FIG. 7.

[2] Cf. Eisenhart, reference 1, pp. 205–206.

we denote by $\alpha$ the variable angle at which a geodesic meets a meridian, it is easy to see (Fig. 7) that

$$d\theta/ds = \sin\alpha/r.$$

Therefore along a geodesic $r\sin\alpha = h$. Since

$$\cos\alpha = (1+y'^2)^{\frac{1}{2}}\frac{dr}{ds},$$

we find that along a geodesic

$$r^2\left[1-(1+y'^2)\left(\frac{dr}{ds}\right)^2\right]=h^2.$$

Let 0 be the point on $C_1$ such that the plane through 0 and the axis of the surface is normal to the aperture $C_2$, let $g$ be a geodesic issuing from 0, and suppose that at 0 $r=r_0$ and $\theta=0$. Let $r_1$ be the radius of the base circle, $s_1$ the length of $g$ from 0 to the base circle, and $\alpha_0$, $\alpha_1$ the initial and final values of $\alpha$ on $g$ (see Fig. 8). Then

$$\left.\begin{aligned} s_1 &= \left|\int_{r_0}^{r_1}\frac{(1+y'^2)^{\frac{1}{2}}rdr}{(r^2-h^2)^{\frac{1}{2}}}\right|,\\ \theta_1 &= h\left|\int_{r_0}^{r_1}\frac{(1+y'^2)^{\frac{1}{2}}dr}{r(r^2-h^2)^{\frac{1}{2}}}\right|,\\ \alpha_1 &= \arcsin\frac{h}{r_1}. \end{aligned}\right\} \qquad \text{(A)}$$

As $g$ enters the base disk, it becomes a straight line, whose perpendicular distance from the center of the aperture is $h$. Since the meridian geodesic from 0 meets the aperture at right angles, the problem of obtaining perfect optics is that of making all geodesics from 0 be normal to the aperture $C_2$; that is, we want $\theta_1=\alpha_1$ (see Fig. 9).

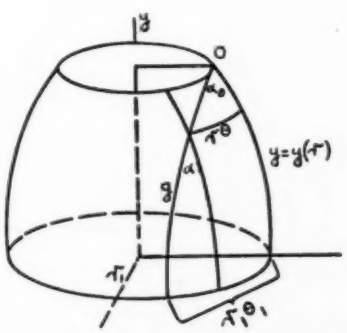


FIG. 8.

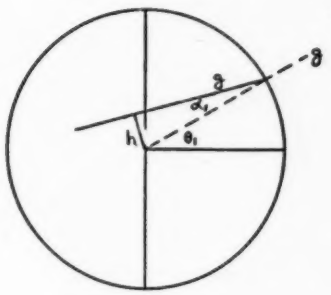


FIG. 9.

If $\theta_1-\alpha_1$ is expanded in a series about $h=0$, we obtain

$$\theta_1-\alpha_1=\sum_{n=1}^{\infty}A_{2n-1}\frac{h^{2n-1}}{2n-1}\frac{1\cdot3\cdot5\cdots(2n-1)}{2^{n-1}(n-1)!(2n-1)},$$

where

$$A_{2n-1}=(2n-1)\left|\int_{r_0}^{r_1}\frac{(1+y'^2)^{\frac{1}{2}}dr}{r^{2n}}\right|-\frac{1}{r_1^{2n-1}}.$$

We now prove the impossibility of $\theta_1=\alpha_1$ for all $h$ by showing that

$$A_{2n+1}>\frac{A_{2n-1}}{\bar{r}^2},$$

where $\bar{r}$ is the larger of $r_0$, $r_1$, so that it is impossible that $A_{2n-1}=0$ for all $n$.

Let $F(r)=(1+y'^2)^{\frac{1}{2}}$. If $r_1>r>r_0$,

$$A_{2n+1}=(2n+1)\int_{r_0}^{r_1}\frac{Fdr}{r^{2n+2}}-\frac{1}{r_1^{2n+1}}$$

$$>(2n-1)\int_{r_0}^{r_1}\frac{Fdr}{r_1^2r^{2n}}-\frac{1}{r_1^{2n+1}}=\frac{A_{2n-1}}{r_1^2}.$$

If $r_0>r>r_1$,

$$A_{2n+1}=(2n+1)\int_{r_1}^{r_0}\frac{Fdr}{r^{2n+2}}-\frac{1}{r_1^{2n+1}}$$

$$=(2n+1)\int_{r_1}^{r_0}\frac{(F-1)dr}{r^{2n+2}}-\frac{1}{r_0^{2n+1}}$$

$$>(2n-1)\int_{r_1}^{r_0}\frac{(F-1)dr}{r_0^2r^{2n}}-\frac{1}{r_0^{2n+1}}=\frac{A_{2n-1}}{r_0^2}.$$

This proof can also be carried through for the case of a contour curve of the more general type $r=r(t)$, $y=y(t)$ provided that the upper and lower radii $r_0$ and $r_1$ are extreme values of $r$.

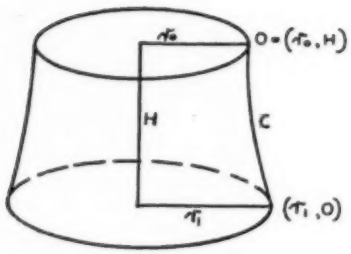


FIG. 10.

If $r_1 > r_0$,

$$A_{2n+1} = (2n+1)\int_{t_0}^{t_1} \frac{\left[\left(\frac{dr}{dt}\right)^2 + \left(\frac{dy}{dt}\right)^2\right]^{\frac{1}{2}} dt}{r^{2n+2}}$$

$$-\frac{1}{r_1^{2n+1}} > \frac{A_{2n-1}}{r_1^2}.$$

If $r_0 > r_1$,

$$A_{2n+1} = (2n+1)\int_{t_0}^{t_1} \frac{\left[\left[\left(\frac{dr}{dt}\right)^2 + \left(\frac{dy}{dt}\right)^2\right]^{\frac{1}{2}} + \frac{dr}{dt}\right] dt}{r^{2n+2}}$$

$$-\frac{1}{r_0^{2n+1}} > \frac{A_{2n-1}}{r_0^2}.$$

Thus we have proved the existence of phase errors at the aperture, provided that $r$ remains between $r_0$ and $r_1$ on the surface.

The size of these errors depends on the contour curve $C$, the upper and lower radii $r_0$ and $r_1$, and the height $H$. For fixed $r_1$, $H$ the phase errors approach zero as $r_0 \to \infty$. But practical considerations restrict $r_0$, $r_1$, $H$. In view of applications the following problem is formulated.

For fixed $r_0$, $r_1$, $H$ what is the contour curve $C$ which maximizes the amount of the aperture for which the phase errors remain less than a pre-assigned amount?

The length of a geodesic from 0 to the aperture is easily computed to be

$$s_1 + r_1 \frac{\cos\theta_1}{\cos(\theta_1 - \alpha_1)},$$

where $s_1$, $\theta_1$, $\alpha_1$ are given by Eqs. (A). The phase errors are given by the difference between this length and the length of the meridian ray from 0 to the aperture.

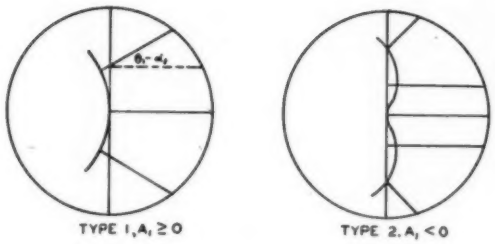


FIG. 11.

The maximizing problem stated above seems too difficult to approach directly, and we replace it by the problem of maximizing the amount of the aperture for which the angular error $|\theta_1 - \alpha_1|$ remains less than a pre-assigned amount. This in turn we replace by the following first approximation (see Fig. 10).

What is the curve $C: y = y(r)$ in the $(r, y)$-plane which furnishes a minimum value to $A_3$ among all curves of the form $y = y(r)$ joining $(r_0, H)$ to $(r_1, 0)$ and making $A_1 = 0$? ($A_1$ and $A_3$ as before are the first terms occurring in the expansion of $\theta_1 - \alpha_1$.)

The graph of a wave front is either of two types shown in Fig. 11, depending on whether $A_1 \geqq 0$ or $A_1 < 0$.

The problem just formulated is equivalent geometrically to flattening the wave front of Type 1 at its center as much as possible. Analytically, we are led to an isoperimetric problem[3] in the calculus of variations—to find the curve $y = y(r)$ which belongs to the class of curves joining $(r_0, H)$ to $(r_1, 0)$ and making

$$\left|\int_{r_0}^{r_1} \frac{(1+y'^2)^{\frac{1}{2}} dr}{r^2}\right| - \frac{1}{r_1} = 0,$$

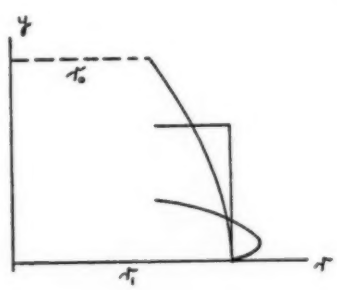


FIG. 12.

[3] See, for example, O. Bolza, *Vorlesungen über Variationsrechnung* (B. G. Teubner, Leipzig, 1933), Chapter 10.

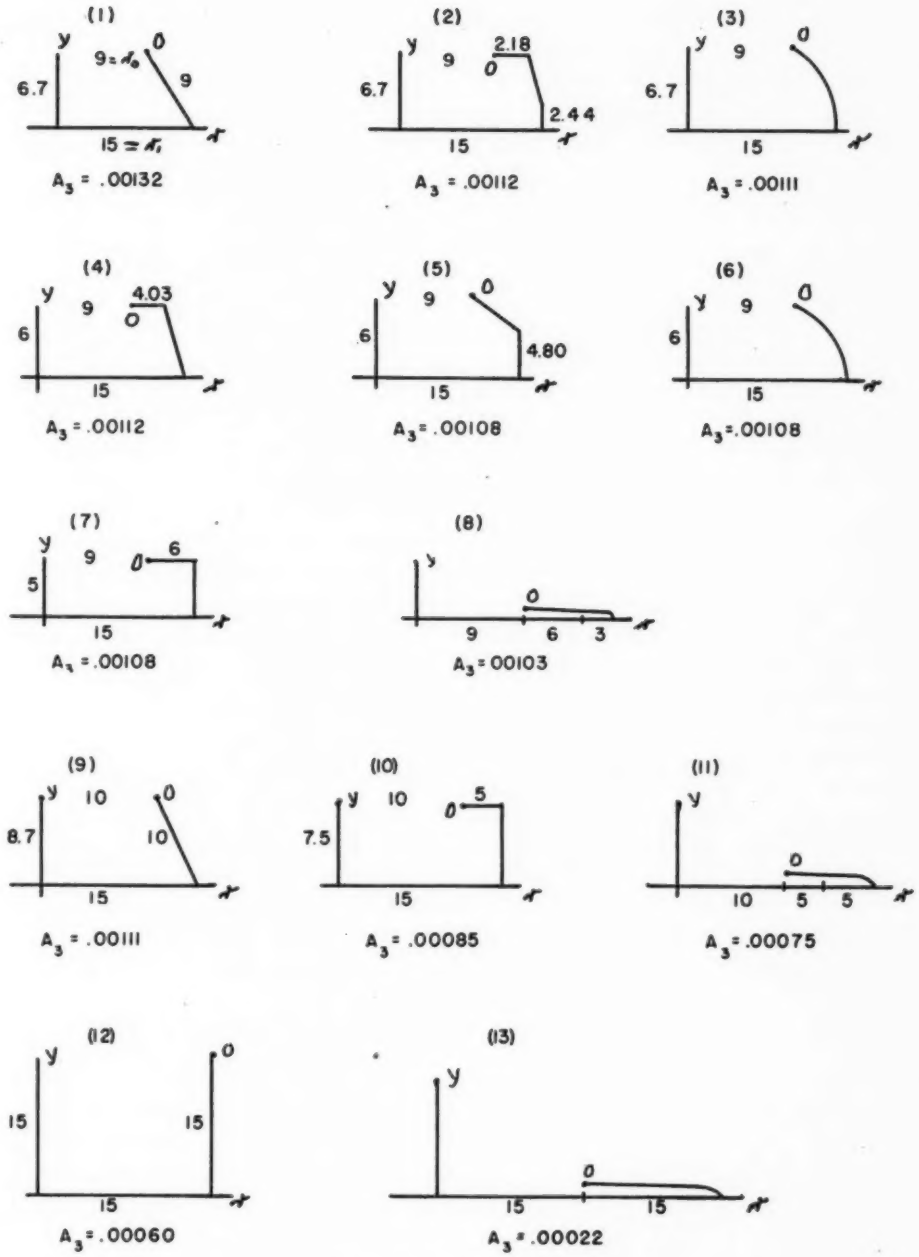


FIG. 13. (Arbitrary units.)

and minimizes

$$\left|\int_{r_0}^{r_1}\frac{(1+y'^2)^{\frac{1}{2}}dr}{r^4}\right|-\frac{1}{3r_1^3}$$

in that class of curves. The Euler-Lagrange equation for this problem is

$$\frac{d}{dr}\left[\frac{y'}{r^4(1+y'^2)^{\frac{1}{2}}}+\frac{\lambda y'}{r^2(1+y'^2)^{\frac{1}{2}}}\right]=0,$$

where $\lambda$ is a constant (Lagrange multiplier). Upon integration we obtain

$$y=\left|\int_{r_0}^{r}\frac{dr}{\left(\left(\frac{1+\lambda r^2}{kr^4}\right)^2-1\right)^{\frac{1}{2}}}\right|, \qquad \text{(B)}$$

where $k$ is a constant. To determine $\lambda$, $k$ we have

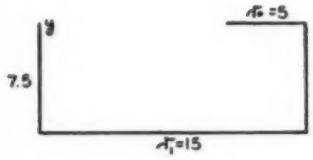


FIG. 14.

the equations

$$\left|\int_{r_0}^{r_1} \frac{dr}{r^2\left(1-\left(\frac{kr^4}{1+\lambda r^2}\right)^2\right)^{\frac{1}{2}}}\right| = \frac{1}{r_1},$$

$$\left|\int_{r_0}^{r_1} \frac{dr}{\left(\left(\frac{1+\lambda r^2}{kr^4}\right)^2-1\right)^{\frac{1}{2}}}\right| = H.$$

By approximate integration, these equations can be solved in any numerical case and the curve (B) found graphically. Figure 12 shows the curve (B) for $r_0, r_1$ fixed, with $r_0 \leqq r_1 \leqq 2r_0$, and for various $H$. As $H$ decreases toward zero, the value of $A_3$ furnished by the curve (B) decreases. Figure 13 illustrates this fact and the fact that the optics improve as $r_0$ increases. In each drawing of the table $A_1=0$. In (3), (6)–(8), (10), (11) the contour curve is of the minimizing type (B). For the cylindrical type of surface (7), (10), (12) we have

$$0=A_1=\int_{t_0}^{t_1}\frac{(r'^2+y'^2)^{\frac{1}{2}}dt}{r^2}-\frac{1}{r_1}=\int_{r_0}^{r_1}\frac{dr}{r^2}$$

$$+\int^{H}\frac{dy}{r_1^2}-\frac{1}{r_1}=\frac{1}{r_0}-\frac{2}{r_1}+\frac{H}{r_1^2},$$

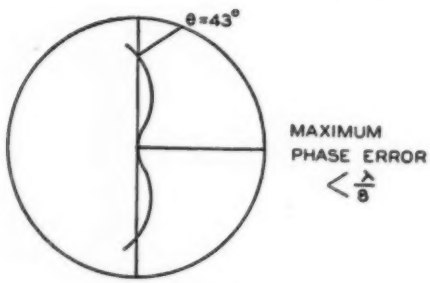


FIG. 15.

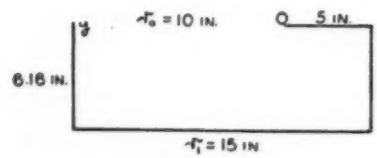


FIG. 16.

so that

$$H=r_1^2\left[\frac{2}{r_1}-\frac{1}{r_0}\right].$$

The limiting degenerate case $H=0$, $r_1=2r_0$ is illustrated by (8), (11), (13), and is a Schmidt circular reflector.

One particular application has already arisen for which $r_0$, $r_1$, $H$ were severely restricted. The wave-length to be used was $\lambda=1.25$ cm, $r_1$ was assigned as 15 inches, $r_0$ was to be $\leqq 10$ inches (for mechanical reasons). Due to lack of space no contour curve which forced the curve (B) to bulge out beyond $r_1$ was allowable, so that it was necessary that $H$ be $\geqq r_1^2(2/r_1-1/r_0)$. The cylindrical case (10) (see Fig. 14) seemed the most practicable. Computation of path lengths for this case shows that the phase errors at the aperture remain less than $\lambda/8$ for approximately $\frac{2}{3}$ of the aperture. If the height $H$ of the cylinder is lowered slightly, the effect is to destroy the equation $A_1=0$, and change to $A_1<0$ and a wave front of Type 2. The height can be adjusted ($H=6.16$ inches) so that the extremum points on the wave front are $\lambda/8$ off the aperture (see Figs. 15, 16). In this case the phase errors remain less than $\lambda/8$ for approximately $\frac{3}{5}$ of the aperture. If the allowable error were $\lambda/4$, by adjusting $H$ to 5.55 inches the phase errors would remain less than $\lambda/4$ for almost 7/10 of the aperture.

## 4. SURFACE OF REVOLUTION WITH DIELECTRIC

If dielectric is introduced into part of the region between the parallel plates of a surface of revolution scanner of the type described in the previous section (see Fig. 17), various degrees of improvement in the optics can be obtained. For

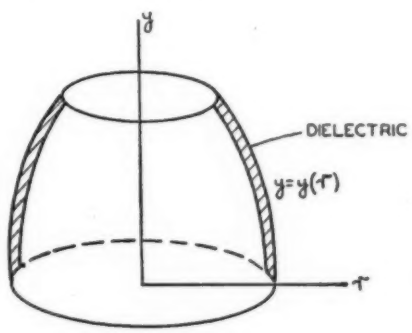


FIG. 17.

example if dielectric of index of refraction $\mu(r)$ is used as shown in Fig. 17, the result is a discontinuity in $\alpha$ at the base disk. Introducing optical length $s$ along a geodesic we obtain

$$s_1=\left|\int_{r_0}^{r_1}\frac{\mu^2 r(1+y'^2)^{\frac{1}{2}}dr}{(\mu^2r^2-h^2)^{\frac{1}{2}}}\right|,$$

$$\theta_1=\left|h\int_{r_0}^{r_1}\frac{(1+y'^2)^{\frac{1}{2}}dr}{r(\mu^2r^2-h^2)^{\frac{1}{2}}}\right|,$$

$$\alpha_1=\arcsin\frac{h}{r_1}$$

where $\alpha_1$ is the angle the geodesic makes with a radius of the base immediately *after* emerging into the base.

The series for $\theta_1-\alpha_1$ becomes

$$\theta_1-\alpha_1=\sum_{n=1}^{\infty}\frac{h^{2n-1}}{2n-1}B_{2n-1}\frac{1\cdot3\cdot5\cdots(2n-1)}{2^{n-1}(n-1)!(2n-1)},$$

where

$$B_{2n-1}=\left|(2n-1)\int_{r_0}^{r_1}\frac{(1+y'^2)^{\frac{1}{2}}dr}{\mu^{2n-1}r^{2n}}\right|-\frac{1}{r_1^{2n-1}}.$$

If $\mu=1.6$, and these results are applied to the case considered at the end of Section 3, Fig. 18 shows the type of improvement obtainable. The last two figures show that if we allow $r_0>r_1$, an extremely high degree of optical accuracy is obtainable. Of course, the feasibility of the use of dielectric depends on the amount of absorption of energy that occurs.

This paper is a condensation of a laboratory report based on work done at the Radiation Laboratory, Massachusetts Institute of Technology, during the summer of 1944. The physical motivation of the problems considered, as well as some of the mathematical development, is due to L. J. Chu, C. V. Robinson, and R. C. Spencer. For obvious reasons, the emphasis is on approximate solutions suitable for practical use rather than the general solution of the mathematical problems involved.

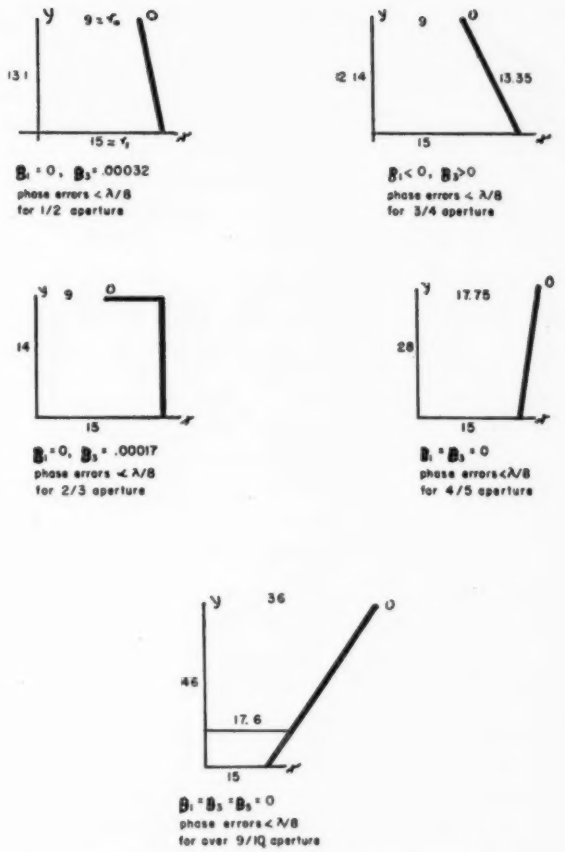


FIG. 18. (Units are inches; $\lambda=1.25$ cm.)

# Space Charge Frequency Dependence of Magnetron Cavity*

W. E. Lamb, Jr. and M. Phillips†
*Columbia Radiation Laboratory, Columbia University,** New York, New York*
(Received July 15, 1946)

The effect on the resonant frequencies of a magnetron cavity produced by the presence of a thin layer of charge surrounding the cathode is investigated theoretically. The corresponding experimental procedure is the "cold impedance testing" of a magnetron with a hot cathode in the presence of a magnetic field and a low d.c. cathode-anode voltage. A small amplitude theory is used, based on the single stream steady state. The correction to the frequency of the empty cavity due to a thin cloud of charge surrounding the cathode is given by a resonance-like formula about the "cyclotron frequency," $eB/2\pi m$. In the "Rising-Sun" tube the curve of $\nu$ *vs.* $\nu_c$ for constant d.c. voltage is asymmetric, apparently because of the presence of the "zero" mode. The validity of the theory is limited to low level oscillations, but the comparison of theory with experimental results seems to support the existence of the single stream steady state for non-operating magnetrons.

## I. INTRODUCTION

THE investigation reported here was undertaken with a view to the use of a non-operating magnetron structure as a tuning device. The tuning unit could either be built into the magnetron to be tuned, utilizing an auxiliary cathode coaxial wth the working cathode, or be coupled externally as an accessory tuner. Since any one of a great variety of coupling possibilities will introduce further complexities, however, and since the validity of the theory is limited to low level oscillations, we shall consider primarily the effect of space charge on the resonant frequencies of the magnetron cavity. The results can be applied to tuning if coupling considerations are taken into account, but in themselves describe the results of cold impedance testing a magnetron with the cathode hot, in the presence of a magnetic field, and with a d.c. voltage below that needed for operation. Our considerations also appear to throw some light on general magnetron theory. The perturbation of circulating space charge has been investigated by Blewett and Ramo[1] and Brillouin.[2] In both these papers it is assumed that the cathode radius is very small in comparison with other dimensions of the apparatus, an assumption not justified for modern magnetrons. Furthermore, their investigations are concerned only with the charge cloud itself, not its effect on anode block frequencies. It has already been pointed out[3] that in reference 1 the neglect of the effect of the constant magnetic field on the perturbations of the electron motion is not justifiable.

A small amplitude theory for magnetrons has been given by Bunemann,[3] who makes use of a velocity potential, analogous to that used in hydrodynamics. The r-f velocity potential is considered as a small perturbation of the d.c. velocity potential associated with the single stream steady state. The impedance presented at the boundary of the charge cloud is computed and, in principle, matched to that of the remainder of the cathode-anode space.

Although some question has been raised[4] as to the stability of the single stream steady state (also sometimes called the Hull or Brillouin steady state) we shall, like Bunemann, take it as our starting point. The validity of a small amplitude theory as applied to a magnetron under operating conditions need not concern us here, since we make no attempt to describe self-sustained oscillations. It turns out that there is very little further complication in handling perturbations of the fields themselves, instead of the velocity potential, while there are advantages

* Publication assisted by the Ernest Kempton Adams Fund for Physical Research.
† At Brooklyn College, Brooklyn, New York.
** This paper is based on work done under OSRD contract OEMsr-485.
[1] Blewett and Ramo, Phys. Rev. **57**, 635 (1940); J. App. Phys. **12**, 856 (1941).
[2] L. Brillouin, Phys. Rev. **60**, 385 (1941) and **62**, 166 (1942).
[3] O. Bunemann, C.V.D. Report, Ref. Mag. 37 (1944), unpublished.
[4] For example, F. Bloch, NDRC Div. 15: RP-295, 411–175 (May 25, 1945), unpublished.

in using the fields for the purpose of matching to the anode cavities. Also the theory of the zero mode, of interest in "rising sun" tubes, appears naturally in our formulation, while Bunemann's hydrodynamical analogy failed to show it. This was caused by his neglect of the vector potential, and setting the curl of the electric field equal to zero. Only in the discussion of boundary conditions at the cathode do we need refer to a velocity potential.

An analysis of the limitations of our theory, and the difficulties involved in satisfying the usual cathode boundary conditions, is undertaken in the concluding section of the present paper.

## II. GENERAL METHOD

We shall use a fixed set of coordinates, $r$, $\theta$, $z$, and assume that the tube is sufficiently long that the dependence on $z$ can be neglected. The unperturbed fields, charge density, and velocity of the single stream steady state are, in rationalized m.k.s. units:[5]

$$\mathbf{E}_0=(m/e)(\omega_c^2/4)(1-b^4/r^4)\mathbf{r}, \tag{1}$$

$$\rho_0=(m/e)(\epsilon_0/2)\omega_c^2(1+b^4/r^4), \tag{2}$$

$$\mathbf{v}_0=-\omega_c/2(1-b^2/r^2)r\hat{\theta}, \tag{3}$$

where $\omega_c=eB_0/m$, the "cyclotron" angular velocity, $b$ is the cathode radius, and $B_0$ the externally applied magnetic field in the $z$ direction. The equation of motion for an electron at a fixed point in space, correct to the first order in the perturbation $(m/e)d\mathbf{v}/dt=\mathbf{E}+\mathbf{v}\times\mathbf{B}$, becomes

$$(m/e)d\mathbf{v}_0/dt+(m/e)d\mathbf{v}_1/dt$$
$$=\mathbf{E}_0+\mathbf{E}_1+\mathbf{v}_0\times\mathbf{B}_0+\mathbf{v}_1\times\mathbf{B}_0+\mathbf{v}_0\times\mathbf{B}_1. \tag{4}$$

The single stream steady state satisfies the zero-order equation, so that the perturbation equation becomes

$$\partial v_1/\partial t+(\mathbf{v}_0\cdot\nabla)\mathbf{v}_1+(\mathbf{v}_1\cdot\nabla)\mathbf{v}_0$$
$$=(\mathbf{E}_1+\mathbf{v}_1\times\mathbf{B}_0+\mathbf{v}_0\times\mathbf{B}_1)(e/m). \tag{5}$$

The first-order field equations are

$$\mathrm{curl}\mathbf{E}_1=-\mu_0\dot{H}_1, \tag{6}$$

$$\mathrm{curl}H_1=\epsilon_0\dot{E}_1+\rho_0\mathbf{v}_1+\rho_1\mathbf{v}_0, \tag{7}$$

where $\rho_1=\mathrm{div}\mathbf{E}_1$. It will be noted that the zero-order quantities do not satisfy the zero-order curl$H$ equation; but since $\rho_0\mathbf{v}_0$ gives a correction to the applied magnetic field which is of order $v_0^2/c^2$, the neglect of this term is consistent with a non-relativistic calculation.

If the time and angular dependence of all quantities is given by the factor $\exp i(n\theta-\omega t)$, where $n$ is the mode number, the field equations in component form become

$$i\omega\mu_0H=(1/r)(\partial/\partial r)(rE_\theta)-inE_r/r, \tag{8}$$

$$inH/r=-i\omega\epsilon_0E_\theta+\rho_0v_r, \tag{9}$$

$$-\partial H/\partial r=-i\omega\epsilon_0E$$
$$+\epsilon_0v_0/r\{\partial(rE_r)/\partial r+inE_\theta\}+\rho_0v_\theta. \tag{10}$$

The equations of motion take the form

$$-i\omega v_r+(v_0/r)inv_r=(e/m)E_r+v_\theta\omega_c+(e/m)v_0\mu_0H, \tag{11}$$

$$-i\omega v_\theta+(v_0/r)inv_\theta+v_r\partial v_0/\partial r=(e/m)E_\theta-v_r\omega_c. \tag{12}$$

Here the subscripts denoting perturbation fields and velocities have been dropped, only the zero subscripts being retained.

Equations (11) and (12) may be solved for $v_r$ and $v_\theta$ in terms of the fields, and substituted in the field equations. These may then be combined to give a single second-order differential equation in $E_\theta$, or $E_r$. This equation is too complicated to be very useful without extended numerical integration, but for the limiting case of thin layers of charge on the cathode conclusions as to the effect on the resonant frequencies may be easily drawn.

The boundary condition at the cathode demands that the tangential component of the electric field be equal to zero, and the differential equation for $E_\theta$ admits of a solution in powers of $(r-b)=y$, starting with the first power. For a very thin charge cloud, $E_\theta$ varies as $y$. The first-order $y$ dependence of the other field quantities can then be found by making use of the field equations. This approximation breaks down for frequencies too near the cyclotron frequency, since the coefficients of higher powers of $y$ contain the factor $(\omega_c^2-\omega^2)$ in the denominator.

To justify the use of this approximation we may investigate the radius of the charge cloud under steady conditions. One has only to demand

[5] Reference 2, part I, sections 2 and 3.

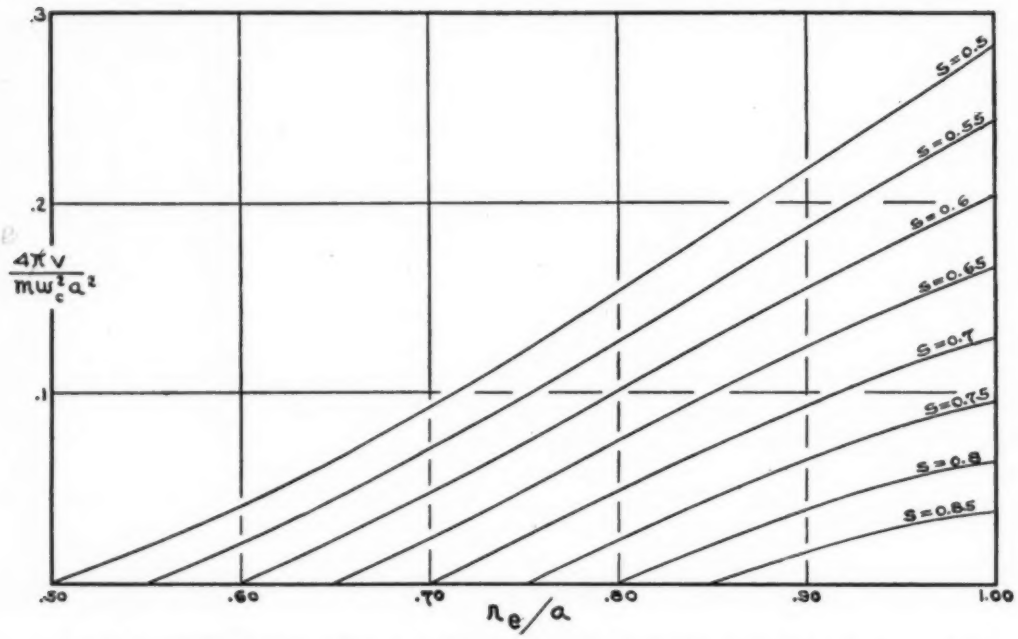


FIG. 1. A plot showing the radius of the boundary of the single stream steady state charge cloud as a function of applied cathode-anode voltage, for cathode diameter to anode diameter ratios ranging from 0.5 to 0.85.

that the fields be continuous across the boundary of the cloud, at $r_e$, and that the total difference of potential between cathode and anode is the applied voltage. The equation for the applied voltage is

$$V=(m/e)(\omega_c^2/8)r_e^2[(1-b^2/r_e^2)^2 +2(1-b^4/r_e^4)\ln(a/r_e)]. \quad (13)$$

Here $a$ is the inside radius of the anode. A plot of $4eV/m\omega_c^2a^2$ against $r_e/a$ has been made for a variety of $b/a$ ratios (Fig. 1), but for low voltages the relation between $y_e$ and $V$ is linear, and well represented by the simple formula

$$y_e/b=(e/m)(V/\omega_c^2b^2)/\ln(a/b).$$

For $\omega_c$ of the order of $10^4$ megacycles, as it is for the experimental tests made, $y_e/b$ is seen to be extremely small, of the order of $10^{-3}$.

### III. APPLICATION TO MODES WITH $n\neq 0$

If $n$ is not equal to zero it is justifiable to neglect the last term of Eq. (11), and to assume that the curl of **E** equals zero. This corresponds to a similar simplification in Bunemann's theory. Even under the simplifying assumptions the exact equation for $E_\theta$ is very cumbersome, although it can be derived in a straightforward way as indicated above. For large $nb/y$ it becomes fairly simple, especially if written in terms of the variable $\eta$, defined by $r/b=\exp(\eta/n)$:

$$(\omega'^2-\omega_c^2)d^2(rE_\theta)/d\eta^2+2\omega_c^3/\omega' d(rE_\theta)/d\eta =[2\omega_c^4/\omega'^2+(\omega'^2-\omega_c^2)](rE_\theta). \quad (14)$$

Here

$$\omega'=\omega+n\omega_c(1-b^2/r^2)/2=\omega+\eta\omega_c.$$

All terms of first order in $\eta$ are kept, in Eq. (13), but not in $\eta/n$, i.e., the effects of curvature alone are neglected, an approximation justified for fairly large $n$. Away from $\omega_c$, $y=0$ or $\eta=0$ is not a singular point, and the power series solutions start with $y$ or a constant. This is also true of the more complicated exact equation, awkward as it is to write down. For the plane magnetron, with a time and $x$ dependence given by $\exp i(\kappa x-\omega t)$, the corresponding equation is

$$(\omega\omega'-\omega_c^2)d^2E_x/dy^2+2\kappa\omega_c^2/\omega' dE_x/dy =(2\omega_c^4/\omega'^2+(\omega\omega'-\omega_c^2))\kappa^2E_x, \quad (14a)$$

where $\omega'=\omega+y\kappa\omega_c$.

The impedance[6] presented by the charge cloud at its boundary, correct to the first order in the

[6] See, for example, S. A. Schelkunoff, Bell Sys. Tech. J. **17**, 17 (1938), or J. A. Stratton, *Electromagnetic Theory* (McGraw-Hill, Book Company, Inc., New York, 1941), p. 282.

thickness of the charge layer outside the cathode, is then easily computed directly from Eqs. (8) to (12) above. If $E_\theta = \mathcal{E}y/b$, $\mathcal{E}$ being inserted as a constant to supply the right dimensions, then from (8) $E_r = \mathcal{E}/in$

from (12)

$$v_\theta = (e/m)iE_\theta/\omega = (e/m)iy\mathcal{E}/\omega b,$$

from (11)

$$v_r = \frac{i}{\omega}(e/m)E_r + \frac{i\omega_c}{\omega}v_\theta,$$

and from (9)

$$H = (\mathcal{E}/in)(i\omega E_r + \omega_c^2 m v_r/e)$$

$$= b\epsilon_0\mathcal{E}(\omega_c^2 - \omega^2)/in^2\omega.$$

$$\therefore \quad Z_{el} = E_\theta/H = \frac{in^2y}{b^2\epsilon_0\omega}\frac{\omega^2}{\omega_c^2 - \omega^2}$$

$$= i(\mu_0/\epsilon_0)^{\frac{1}{2}}\frac{n^2}{bk}\frac{y}{b}\frac{\omega^2}{\omega_c^2 - \omega^2} \text{ ohms}, \quad (15)$$

where

$$k = \frac{2\pi}{\lambda} = \frac{\omega}{c}.$$

Since it is approximately $ny\omega^2/b(\omega_c^2 - \omega^2)$ which enters as an expansion parameter, this expression may be considered valid for $ny/b < (\omega_c^2 - \omega^2)/\omega^2$. The failure of $E_r$ to satisfy the conventional condition at the cathode corresponding to space charge limited emission will be discussed later.

To determine the resonant frequencies of the magnetron when the cathode is surrounded by the sheath of space charge this impedance is used as a boundary condition instead of the simple demand that $E_\theta = 0$ in the usual method.[7, 8]

We shall confine our attention to the symmetric anode. The equation for matching the fields at the openings to the anode cavities[9] for the $n$th mode is:

$$\cot kL = \frac{N\Theta}{\pi}\sum_{m=n+lN}^{\infty}\frac{J_m'(ka) + \alpha_m N_m'(ka)}{J_m(ka) + \alpha_m N_m(ka)} \times \left(\frac{\sin m\Theta}{m\Theta}\right)^2, \quad (16)$$

[7] H. Goldstein, "Resonant modes of magentron cavities," NDRC Div. 14, Report No. 493 (Dec. 14, 1943).

[8] N. Kroll and W. E. Lamb, Jr., "Resonant modes of the "rising sun" anode," NDRC Div. 14, Report No. 323 (Oct. 25, 1944).

[9] Cf. Goldstein, reference 7, p. 9.

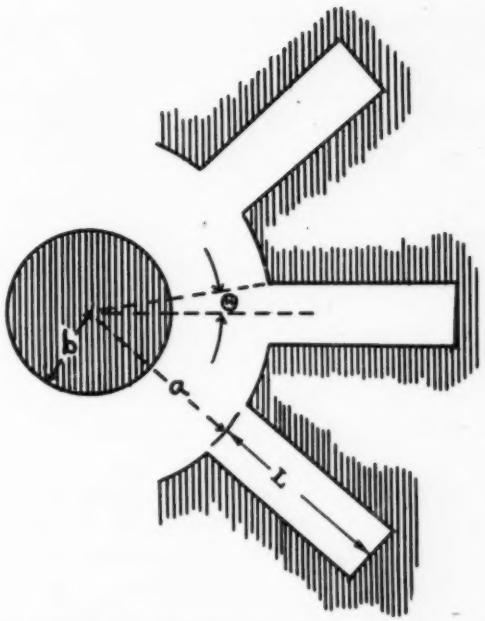


FIG. 2. Partial section of symmetrical anode magnetron. $b$ is the cathode radius, $a$ the inside radius of the anode, $L$ the length of a slot, and $\Theta$ is half the angle subtended by each slot.

where $2\Theta$ is the angular aperture of the cavities, $a$ is the anode radius, and $L$ is the length of the anode slots, as shown in Fig. 2. $\alpha_m$ is the parameter arising from the presence of the cathode or the cathode charge layer boundary condition. It has been shown that a consideration of the cathode radius in an empty cavity introduces very little change in the frequency except for the lowest mode numbers, and that for any $n$ the preponderance of the effect arises from the fundamental. This should remain true for the effect of thin layers of charge on the cathode. For this reason we may neglect all harmonics and determine $\alpha_n$ by simply matching the electron impedance at the edge of the cloud to that given by the solution for a cylindrical cavity. Furthermore, since $kb \ll 1$ for most tubes we may substitute for each Bessel and Neumann function the first term in its power series expansion about the origin.

The matching then involves using

$$H \simeq J_n(kr) + \alpha_n N_n(kr),$$

$$E \simeq -i\mu_0\omega/k[J_n'(kr) + \alpha_n N_n'(kr)],$$

so that

$$Z_{\text{cavity}} = E_\theta/H = \frac{i\sqrt{\mu_0}}{\sqrt{\epsilon_0}}\frac{J_n'(kr) + \alpha_n N_n'(kr)}{J_n(kr) + \alpha_n N_n(kr)} \quad (17)$$

is determined by the condition $Z_{el}=Z_{cavity}$ at the boundary of the space charge, i.e.,

$$\frac{n^2y_e}{kb^2}\frac{\omega^2}{\omega_c^2-\omega^2}=-\frac{J_n'(kr_e)+\alpha_nN_n'(kr_e)}{J_n(kr_e)+\alpha_nN_n(kr_e)}, \quad (18)$$

where $r_e=b-y_e$ is the radius of the charge cloud. It follows that

$$\alpha_n=-\frac{J_n'(kr_e)}{N_n'(kr_e)}\left\{1+\frac{2ny_e}{b}\frac{\omega^2}{\omega_c^2-\omega^2}\right\}$$

$$=\left(\frac{kb}{2}\right)^{2n}\frac{\pi}{n!(n-1)!}\left\{1+\frac{2ny_e}{b}\frac{\omega^2}{\omega_c^2-\omega^2}\right\}. \quad (19)$$

This expression for the boundary condition parameter is to be compared with the corresponding expression in the absence of the layer of space charge,

$$\alpha_n=-\frac{J_n'(kb)}{N_n'(kb)}=\left(\frac{kb}{2}\right)^{2n}\frac{\pi}{n!(n-1)!}. \quad (20)$$

The matching equation at the anode radius, from which the resonant frequencies of the whole resonating cavity are determined, becomes

$$\cot kL=\frac{N\Theta}{\pi}\sum_{m=n+lN}^{\infty}\left(\frac{\sin m\Theta}{m\Theta}\right)^2\frac{J_m'(ka)}{J_m(ka)}$$

$$\times\left\{1+2\left(\frac{b}{a}\right)^{2m}\left(1+\frac{2my_e}{b}\frac{\omega_c^2}{\omega_c^2-\omega^2}\right)\right\}. \quad (21)$$

This is to be compared with Eq. (15), of reference 4, *viz.*,

$$\cot kL=\frac{N\Theta}{\pi}\sum_{m=n+lN}^{\infty}\left(\frac{\sin m\Theta}{m\Theta}\right)^2\frac{J_m'(ka)}{J_m(ka)}$$

$$\times\left\{1+2\left(\frac{b}{a}\right)^{2m}\right\}. \quad (22)$$

From the fact that $(ny_e/b)(\omega^2/(\omega_c^2-\omega^2))$ appears as a small quantity in the solution of our differential equation for $E_\theta$ it is not permissible to use this correction for $\omega_c=\omega$, but if $y_e$ is sufficiently small (21) may be valid for frequencies very near the cyclotron frequency. It is seen that the maximum tuning predicted safely by Eq. (21) will be of the order of the correction to the frequency caused by the finite cathode.

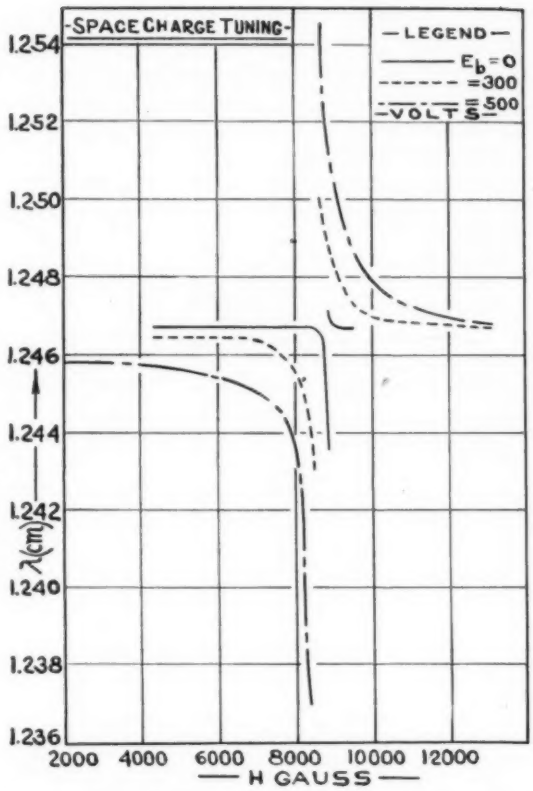


FIG. 3. Wave-length of rising-sun magnetron cavity as a function of magnetic field for cathode-anode voltages shown in the legend.

For $\omega_c<\omega$, i.e., for low magnetic fields, it will be in the direction of cancelling the cathode effect, decreasing the resulting resonant wave-length. For modes of higher $n$, where the fields at the center are small, there will be no appreciable effect; none, at least, which can be predicted with confidence from Eq. (21).

Some preliminary measurement of the tuning effects of the space charge layer about a magnetron cathode were made by Mr. B. Hildebrand of this laboratory. A number of 1.25-cm wave-length magnetrons were "cold impedanced" with a hot cathode in the presence of an axial magnetic field and d.c. radial electric field. The resonant wave-length was measured as a function of the applied fields. The r-f used was obtained from a local oscillator and had an intensity of a few milliwatts. The voltages used were insufficient to allow appreciable leakage current and back bombardment of the cathode, except at the lower magnetic fields. No detectable r-f of microwatt intensity was generated by the magnetrons,

which were designed for pulsed operation at well over 10 kv.

Figure 3 shows the resonant wave-length ($\pi$ mode) of a rising sun magnetron cavity as a function of magnetic field for three values of d.c. voltage, 0, 300, and 500 volts. Within the limits of the field calibration, the sharpest tuning effects occur as expected at the cyclotron frequency. The tuning observed for zero anode voltage may be ascribed to the thermal motion of the electrons, for no tuning was observed with five volts of reversed potential.

These experiments are being continued with better cavity geometry and more careful control of cathode emission. A quantitative comparison between theory and experiment will be made when more complete data are available.

If one tries to make more rigorous use of the equation for $E_\theta$ in determining the impedance of the charge cloud, the first correction is a displacement of the singularity toward higher frequencies by an amount of the order of magnitude of $ny_e\omega/b$. The singularity in terms of $B_0$ is shifted toward lower magnetic fields according to the equation

$$\omega_c' = \omega_c\left(1+\frac{3}{2}\frac{ny_e}{b}\right).$$

Experimentally this means that the singularity in the curves of $\omega$ against $B_0$ should be displaced slightly as the d.c. potential and thus the thickness of the charge cloud is increased. The experiment is not conclusive on this point.

## IV. THE ZERO MODE

The case of the zero mode, of importance in rising sun tubes,[8] is somewhat different. This mode corresponds to a circular current in the tube. Here curl$E$ is not equal to zero, and the correction term in the magnetic field, $v_0B_1$, must also be kept. The absence of any dependence on $\theta$ makes the equations simpler, however, and if the layer of charge is sufficiently thin to justify the assumption that the magnetron is plane the differential equation for $E_\theta$ becomes

$$[1-k_c^2y^2/(1-\gamma^2)]d^2E_\theta/dy^2-\frac{2k_c^2y}{1-\gamma^2}dE_\theta/dy -k_c^2(1-\gamma^2)E_\theta=0, \quad (23)$$

where $k_c=\omega_c/c$, $\gamma=\omega/\omega_c$.

This equation somewhat resembles Legendre's equation, and is satisfied by a power series containing only odd powers of $y$, but again the solution is not valid for $\omega=\omega_c$, since the coefficient of $y^3$ is $k_c^2(2+(1-\gamma^2)^2)/6(1-\gamma^2)$. Also,

$$E_r=\frac{i[E_\theta+ydE_\theta/dy]}{\gamma(\gamma^2-1)}. \quad (24)$$

To obtain a charge cloud impedance which does not depend critically on the frequency, it is necessary to take account consistently of the second term in the expansion in $y$. Working to this order also involves taking into account the deformation of the boundary layer. If a point on the surface of the charge cloud differs from its unperturbed value by an amount $\delta$, the value of $H$ to be used in matching differs from that inside the cloud by the contribution of the surface current, $\rho_0v_0\delta$.

To compute the impedance presented at the edge of the cloud we need

$$E_\theta\sim y+\frac{k_c^2y^3}{3(1-\gamma^2)},$$

$$H=\frac{1}{i\mu_0\omega}\frac{dE_\theta}{dy}-\rho_0v_0\delta.$$

Since $r_e=$constant$+\delta$, it follows that $\delta=iv_r/\omega$, evaluated at $r=r_e$. Since $v_r=i\omega\epsilon_0E_r/\rho_0$,

$$H=1/i\mu_0\omega[1-k_c^2y^2/(1-\gamma^2)] \quad (25)$$

and

$$Z_{el}=i\left(\frac{\mu_0}{\epsilon_0}\right)^{\frac{1}{2}}ky[1+2k_c^2y^2/(1-\gamma^2)]. \quad (26)$$

The coefficient of the resonance term would be affected by including corrections to be caused by the current and the relativistic change of mass with velocity, and so is not to be interpreted too literally. This impedance is to be matched to that of the cylindrical part of the cavity, for which the dominant term is

$$Z_{cav}=i\left(\frac{\mu_0}{\epsilon_0}\right)^{\frac{1}{2}}\frac{J_1(kr)+N_1(kr)}{J_0(kr)+N_0(kr)}. \quad (27)$$

$$\therefore\quad Z_{cav}=\pi\left(\frac{kr_e}{2}\right)^2\left[1-\frac{2y}{r_e}\left(1+\frac{2}{3}\frac{k_c^2y^2}{1-\gamma^2}\right)\right]. \quad (28)$$

The zero-order Bessel and Neumann functions need not be expanded if use is made of the relation $J_0(x)N_1(x)-N_0(x)J_1(x)=-2/\pi x$, so that the approximations are as valid as those for modes with $n$ not equal to zero.

Matching at the anode radius leads to the equation

$$\cot kL=-\frac{N\Theta}{\pi}\frac{J_0(ka)}{J_1(ka)}\times\left\{1+\left(\frac{b}{a}\right)^2\left[1-\frac{2y}{b}\left(1+\frac{2}{3}\frac{k_c^2y^2}{1-\gamma^2}\right)\right]\right\}. \quad (29)$$

The effect of the charge cloud is thus always such as to cancel the cathode correction, by an amount which is larger for $\gamma<1$ than for $\gamma>1$.

It will be noticed that all amplitudes of vibration of the charge go to zero at the cathode, so that there is here no difficulty about satisfying the conventional boundary conditions. From the curl$H$ equation,

$$\frac{1}{r}\frac{\partial H}{\partial\theta}=0=\epsilon_0E_r+\rho v_r,$$

it appears that insofar as it is legitimate to neglect any $z$ dependence there is no emission at any time directly into this mode. Nevertheless, where the mode exists, by virtue of its mixture with the $\pi$ mode of rising sun tubes, for example, the tuning effect owing to its presence will be important for the same reason that a consideration of the cathode size is important, because the fields are large near the center of the cylindrical space. This effect probably accounts for the lack of symmetry in the frequency curves found in the cold test experiments carried out with rising sun tubes. Apart from the critical frequency dependence there is a correction in the presence of zero mode excitation which varies linearly with the depth of the charge cloud, and always tends to cancel the effect of the finite radius.

## V. CATHODE CONDITIONS AND VALIDITY OF THE THEORY

The linear equations used in the small amplitude theory preclude the imposing of the usual boundary conditions at the cathode if the mode number is different from zero. The two-power series solutions of the differential equation for any field quantity begin with the zero and first powers of $y$, respectively, and the field equations lead to the conclusion that if $E_\theta$ varies as the first power of $y$, then $E_r$ has a term independent of $y$. Thus if one demands that $E_\theta$ and $v_\theta$ are zero at $r=b$, one cannot also demand that $E_r$ and $v_r$ are zero at that radius, the usual condition for space charge limited emission. Taken seriously, this would mean that the radial field at the cathode is alternatively positive and negative, with the same $\exp\{i(\omega t-n\theta)\}$ dependence as other perturbation quantities. In other words the cathode is here defined merely as a surface on which the tangential field is zero.

Quite apart from a consideration of cathode conditions the small amplitude theory might not be expected to hold all the way into the cathode. In the impedance matching at the edge of the cloud we were interested only in the ratio of the perturbation fields, not their absolute magnitudes, but it might be expected that the theory would break down for $E_r$ of the order of $E_\theta$. The assumption that $|E_r|<E_\theta$ would mean, in terms of distances, that $\delta$, the amplitude of radial oscillations of the electrons is subject to the condition $\delta<y$, and that the small amplitude theory would not be valid for distances less than $y_1\sim\delta$.

The reasons for demanding the strict observance of space charge limitation of any possible emission in the absence of equilibrium conditions are not entirely clear, and in our own case there is no total current, and hence possibly no emission. Nevertheless, in view of the large part played by conventional cathode conditions in magnetron theory, it was thought feasible to attempt to match solutions of the exact equations to the fields predicted by the small amplitude theory at some distance $y_1<y_e$.

The hydrodynamical formulation has the advantage of added elegance and formal simplicity over the expansion of the field quantities and velocities separately, so that we choose this method of presentation similar to that used by Cherry.[10] Fixed coordinates may be used if the vector potential is included, which also enables us to include in the description the motion corresponding to the zero mode of the cavity.

[10] General Theory of the Magnetron, Council for Sci. and Ind. Research, Rept. MUM1, Sydney (April 1, 1943).

Let $m\mathbf{v}+e\mathbf{A}=-\text{grad}\psi$. The proof that curl $(m\mathbf{v}+e\mathbf{A})=0$ is maintained (if there is no $H_n$) has been given, e.g., by Gabor.[11]

If $\mathbf{B}=\text{curl}\mathbf{A}$ and $\mathbf{E}=-\text{grad}\phi-\dot{A}$, the equation of motion leads to

$$e\phi=-mv^2/2+\psi=-\frac{(\text{grad}\psi+e\mathbf{A})^2}{2m}+\psi. \quad (30)$$

The fields, velocities, and charge density may be written in terms of $\psi$, the hydrodynamical potential or "stream function," and $\mathbf{A}$. We then demand that $E_{\tan}$ and $\mathbf{v}$ be zero on the cathode, and that $B_{\tan}$ and $\rho\mathbf{v}$ be finite. For an infinitely long cathode there is no normal component of $B$. These conditions mean that if there is any emission the charge density is infinite at the cathode surface, so that this surface is a "front" in the language of hydrodynamics.

If $\psi$ and $\mathbf{A}$ are now expanded in powers of $y$, with coefficients subject to the above condition, there follow limitations on the lowest allowed power of $y$, as well as relations between the coefficients of successive powers.

For the formal relations which must be borne in mind it is convenient to set up a system of right-handed cartesian coordinates, with $x$ in the direction of $-\hat{\theta}$. In addition to (30) and the definition of $\psi$ these relations are:

$$B=\partial A_y/\partial x-\partial A_x/\partial y=\text{curl}\mathbf{A}, \quad (a)$$

$$E_x=-\frac{\partial\phi}{\partial x}-A_x, \quad (b)$$

$$E_y=-\frac{\partial\phi}{\partial y}-A_y, \quad (c)$$

$$\epsilon\rho=\text{div}\mathbf{E}=-\frac{\partial^2\phi}{\partial x^2}-\frac{\partial^2\phi}{\partial y^2}-\frac{\partial A_y}{\partial y}-\frac{\partial A_x}{\partial x}, \quad (d)$$

and

$$\text{div}\mathbf{A}=-\mu_0\epsilon_0\dot{\phi}=\frac{\partial A_x}{\partial x}+\frac{\partial A_y}{\partial y}, \quad (e)$$

$$\epsilon_0\dot{\rho}+\text{div}\rho\mathbf{v}=0. \quad (f)$$

The Lorentz condition (e) shows that there are only two, not three, independent series, which we can take as $\psi$ and $A_x$. Consideration of (a), remembering that $B$ must be finite but not identically zero on the cathode, leads to

$$A_x=-[B_0+\alpha_x(\theta, t)]y+\text{higher terms in } y.$$

If $\psi=\psi_l(\theta, t)y^l+\text{higher terms in } y$, the vanishing of $v_y$ on the cathode means that $l>1$, but $l=2$ leads to $v\sim y$, $\rho=\text{const.}$, and no emission. To obtain emission the introduction of fractional powers is necessary. The conditions are satisfied by $l=5/3$, so that

$$\psi=\frac{3}{5}\psi_5(\theta, t)y^{5/3}+\frac{3}{6}\psi_6(\theta, t)y^{6/3}+\frac{3}{7}\psi_7(\theta, t)y^{7/3}+\cdots$$

is a convenient form for the series. It follows that

$$\rho v_r=\frac{\epsilon_0}{m^2e}\frac{2}{9}\psi_5^3(\theta, t)+0(y^1)+\cdots. \quad (31)$$

$\psi$ is then determined by the emission, and $A_x$ by the value of $B$ on the cathode, arbitrarily. As Cherry has pointed out, $E_y\sim y^1$, $E_\theta\sim y$, $v_r\sim y^1$, $v_\theta\sim y$, $\rho\sim y^{-1}$, for small $y$.

The apparent arbitrariness of the emission, determining $\psi_5$, is closely related to the question of convergence, a fact which has not been pointed out by previous authors. The coefficients $\psi_6$, $\psi_7$, etc., may be determined by substituting in the continuity equation and collecting terms in the same power of $y$. It turns out that $\psi_6\sim\dot{\psi}_5/\psi_5$ and that $\psi_7$, $\psi_8$, etc., also go to infinity as $\psi_5$ goes to zero. Thus the series fails if the emission is ever equal to zero, or changes sign. This seems to indicate that the standard conditions for space charge emission, derived historically for steady constant currents, are not appropriate to the discussion of oscillations of emission about zero. This may correspond to Brillouin's finding a double stream, and not a single stream, in the case of final current.[12] An exact solution, involving emission, contradicts the single stream assumption for the cathode layer. So long as the oscillations are small, however, Brillouin found no indication that the double stream produced at the cathode extends far into the charge cloud.

An attempt was made by us to work out the single stream hydrodynamical theory on the strict basis of no emission under saturation conditions. This is formally easy: the stream func-

[11] Gabor, Proc. I.R.E. **33**, 792 (1945).

[12] App. Math. Panel 129.3R, p. 30 *et seq.* and p. 51.

tion $\psi$ is then zero, and all quantities can be expressed in terms of **A**. $E_\theta$ and $v_\theta$ vary as the first power of $y$, as before, but $E_r$ and $v_r$ now also vary as $y$ for small $y$, with a finite charge density at the cathode. No Fourier analysis in the time is possible, however, so that the solutions cannot be matched to those of the linear equation.

The question of the stability of the single stream steady state under a periodic perturbation thus involved the cathode conditions very intimately. Those proofs of instability which are based on the assumption of ideal equilibrium cathode conditions seem to us of doubtful validity. In the absence of knowledge of the nature of the cathode surface, and the applicability of the demand that $E_r=0$, the qualitative experimental verification of theoretical results whose existence depends on there being such a steady state seems as good a way as any of testing the matter. It would remain to show that our results do indeed depend on the existence of a single stream steady state.

While it is impossible to make a general and categorical answer to this question, the observed resonance curves indicate a resonance frequency dependence which does depend on the existence of a magnetic field and the attendant circulation of the charge, and not merely on the charge density. This is easily shown. Maxwell's equation can be set up for a charge cloud of cylindrical symmetry, having the density $\rho=\epsilon_0\omega_c^2 m/e$. For a thin sheath of static charge about the cathode the resulting equations can be solved, and the impedance looking into the sheath can be computed. For this case

$$Z_{e1}=-i\left(\frac{\mu_0}{\epsilon_0}\right)^{\frac{1}{2}}\left\{\frac{n^2 y}{b^2}\frac{c}{\omega}\left(\frac{\omega^2}{\omega^2-\omega_c^2}\right)^{\frac{1}{2}}\right\}, \quad (32)$$

corresponding to the results in the plane case well known in the theory of the ionosphere.[6] It is seen that at $\omega=\omega_c$ the impedance matching breaks down, and there is a change from reactive to resistive impedance. Contrary to this prediction the experimental curve, Fig. 3, shows a typical resonance pattern.

If, on the other hand, the effect of the applied magnetic field on the motion is taken into account, but not the zero-order velocity, the field equations and the equations of motion lead to

$$Z_{e1}=i\left(\frac{\mu_0}{\epsilon_0}\right)^{\frac{1}{2}}\frac{n^2 y}{b^2}\frac{c}{\omega}\frac{\omega^2-\omega_c^2}{\omega^2-2\omega_c^2}. \quad (33)$$

This is again ruled out by the experimental results. Thus the experiments indicate a perturbation of circulating individual electrons, and constitutes evidence for something like the single stream steady state.

Another solution of the stationary state problem has been given recently by Gabor,[13] who introduces "ergodic disorder," retaining conservation of energy and angular momentum for each individual electron. This is in reality an infinite stream steady state. It is interesting to see the differences and similarities between this solution and the one we have used. Gabor's method depends on the existence of a non-zero velocity of emission, although the assumption of equilibrium conditions means zero field at the cathode. If the initial velocity $u_0$ is small the tangential velocity at any point in the swarm of electrons is distributed about the $v_0$ of the single stream steady state, the width of the distribution being just $2au_0/r$, while there are small random velocities in the $r$ and $z$ directions to preserve the energy intact. The value of the saturation density arrived at by Gabor[14] also agrees with that of the single stream steady state for a thin layer about the cathode, although this is not true for thick clouds. Unfortunately the kinetic energy of an electron in a thin cloud is not in general much greater than the thermal energies corresponding to the cathode temperature, so that this agreement must not be taken too seriously. The same kind of difficulties as to how such a state is set up occur here as with the single stream steady state.

[13] D. Gabor, Proc. Roy. Soc. **183**, 357 (1945).
[14] Reference 13, Eq. (28.1).

# The Reduction of Microphonics in Triodes

A. H. WAYNICK
*Ordnance Research Laboratory, School of Engineering, The Pennsylvania State College, State College, Pennsylvania*
(Received September 6, 1946)

An analysis is presented showing the effect of grid displacement on the plate current of a planar triode. This is defined in terms of a new parameter called the motional transconductance. The analysis indicates that a useful mechanical displacement indicator may be constructed by moving the grid and noting the change in plate current. The analysis also indicates that the effect of certain modes of grid displacement on the plate current may be eliminated under conditions which are stipulated. Since microphonic effects are, in great part, caused by the mechanical motion of grid structures, the analysis indicates how microphonism may be reduced. It is shown that the electrical transconductance is large under these conditions, for the case investigated, so that the tube functions normally as an amplifier. Preliminary experimental results for comparison with the theory are presented.

## INTRODUCTION

A RECENT patent[1] describes an electron tube whose plate current is varied by displacement of the grid, relative to the rest of the tube structure, while holding the applied tube potentials at constant values. The grid is mechanically connected through a vacuum-tight member so that it may be moved by the application of suitable forces to the tube envelope.

The following analysis was initially carried out to determine the feasibility of this idea when it had been determined that this type of tube had not been reduced to practice. The patent disclosure itself did not prove this.

The analysis indicates the plate current variations that may be expected in terms of a parameter called the motional transconductance. Inspection of the relation giving this parameter shows that, under suitable conditions, the effect of grid displacement on the plate current vanishes. This suggests a method of design, or mode of operation, by which the microphonism of a tube may be reduced since, as is well known, most of the microphonic difficulties encountered in tubes are caused by the mechanical movement of the grid. Design and operation relations are developed for this case.

Preliminary experiments are then described which indicate that the theory is fundamentally correct.

[1] "Microphonic Electron Tube," issued to J. Rothstein, November 27, 1945, U. S. Patent No. 2,389,935.

## THEORY OF A PLANAR TRIODE[2]

Consider a planar triode as illustrated in Fig. 1. Here $K$ is the cathode; $A$ is the anode; and $G$ is the grid structure. The grid is assumed to be made of equi-distant parallel rods having a radius $R$ and a rod center spacing of $1/n$.

The distance $dg$ is the cathode-grid center distance. The distance $dp$ is the cathode to plate distance. The distance $dq$ is the cathode to an equivalent plate distance, of an equivalent diode, which would give the same space-charge-free off cathode field intensity as the triode with the grid removed. The plate current obtained with the equivalent diode is the same as that obtained with the triode.

By a suitable conformal transformation of Fig. 1, the triode amplification factor, $\mu$, can be

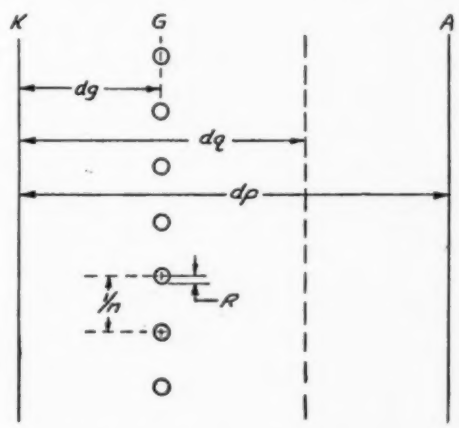


FIG. 1. Notation for planar triode theory.

[2] See W. G. Dow, *Fundamentals of Engineering Electronics* (John Wiley & Sons, Inc., New York, N. Y., 1937), Chapter 2.

determined by electrostatic theory utilizing the quantities enumerated above.[3] The relation is

$$\mu=\frac{2\pi n(dp-dg)-\log_e \cosh 2\pi nR}{\log_e \coth 2\pi nR}$$

and applies with sufficient accuracy when $R<1/10n$.

For $2\pi nR<1$, $\cosh 2\pi nR\rightarrow 1$ and $\log_e \cosh 2\pi nR \rightarrow 0$. Similarly,

$$\coth 2\pi nR=\frac{\cosh 2\pi nR}{\sinh 2\pi nR}\rightarrow\frac{1}{2\pi nR}$$

since $\sinh 2\pi nR\rightarrow 2\pi nR$. Hence, we can write

$$\log_e \coth 2\pi nR=\log_e\frac{1}{2\pi nR},$$

and the above relation becomes

$$\mu=\frac{2\pi n(dp-dg)}{\log_e\dfrac{1}{2\pi nR}}. \tag{1}$$

For the space-charge-free case with an equivalent diode plate voltage of $Eg+Ep/\mu$ the equivalent diode spacing has been found to be[4]

$$dq=dg\left[1+\frac{1}{\mu}\frac{dp}{dg}-\frac{\mu+2}{2\pi n\mu dg}\log_e \cosh 2\pi nR\right].$$

Under the conditions given above, the last term may be set equal to zero leading to

$$dq=dg\left[1+\frac{1}{\mu}\frac{dp}{dg}\right]. \tag{2}$$

As an approximation, Child's Law for the space charge limited equivalent diode may be written:[5]

$$Ip=\frac{2.33\times 10^{-6}A}{dq^2}\left(Eg+\frac{Ep}{\mu}\right)^{\frac{3}{2}}. \tag{3}$$

Where $A$ is the equivalent diode plate area, equal to the actual triode plate area, $Eg$, the triode grid-cathode voltage, $Ep$, the triode plate-cathode voltage, and $Ip$ is the total plate current in milliamperes.

As abbreviations write

$$K=\frac{1}{2\pi n}\log_e\frac{1}{2\pi nR},$$

$$K'=2.33\times 10^{-6}A. \tag{4}$$

Substituting (1) and (2) into (3) in view of (4) yields

$$Ip=\frac{K'\left[Eg+\dfrac{KEp}{(dp-dg)}\right]^{\frac{3}{2}}}{\left[dg+\dfrac{Kdp}{(dp-dg)}\right]^2}\text{ ma} \tag{5}$$

for the total plate current of the triode in terms of triode parameters.

The triode transconductance is defined as

$$Sp\equiv\left(\frac{\partial Ip}{\partial Eg}\right)_{Ep=\text{constant}}\text{ in }\frac{\text{ma}}{\text{volt}},$$

where, for the present case, other tube parameters are also held constant.

Carrying out of the indicated differentiation on (5) yields

$$Sp=\frac{\frac{3}{2}K'\left[Eg+\dfrac{KEp}{(dp-dg)}\right]^{\frac{1}{2}}}{\left[dg+\dfrac{Kdp}{(dp-dg)}\right]^2}\frac{\text{ma}}{\text{volt}}. \tag{6}$$

We wish to compare the effect of a grid displacement for constant $Eg$, $Ep$, and other parameters with (6). Consequently, we define a mechanical transconductance as

$$Mp\equiv\left(\frac{\partial Ip}{\partial dg}\right)_{\text{other parameters constant}}$$

$$\text{in }\frac{\text{ma}}{\text{unit grid displacement}}.$$

Carrying out of the indicated differentiation on (5) yields, after suitable rearrangement of

[3] F. B. Vodges and F. R. Elder, "Formulas for the amplification constant for three element tubes," Phys. Rev. **24**, 683 (1924).

[4] See reference 2, page 44, Eq. (111).

[5] C. D. Child, "Motion of positive ions," Phys. Rev., **32**, 498 (1911).

TABLE I. Dimensions of an RCA 6A3.

| |
|---|
| Radius of grid wire $= R = 0.00225$ in. |
| Grid wire center spacing $= 1/n = 0.055$ in. |
| Grid wires per inch $= n = 18.2$. |
| Grid cathode distance $= dg = 0.045$ in. |
| Plate cathode distance $= dp = 0.090$ in. |
| Plate area (4, ½ sections) $= A = 4.22$ in.$^2$. |

terms,

$$Mp = Sp\left\{\frac{KEp}{(dp-dg)^2} - \frac{4}{3}\frac{\left[Eg+\frac{KEp}{(dp-dg)}\right]\left[1+\frac{Kdp}{(dp-dg)^2}\right]}{\left[dg+\frac{Kdp}{(dp-dg)}\right]}\right\} \quad (7)$$

in milliamperes/unit grid displacement.

From a comparison of $Sp$ with $Mp$, it should be possible to determine the relative effectiveness of the two methods of obtaining plate current variations.

## MAGNITUDE OF THE MOTIONAL TRANSCONDUCTANCE FOR A TYPICAL TUBE

In order to compare the above theory with handbook data, and to determine the magnitude of $Mp$, an RCA 6A3 was selected as a typical tube whose characteristics could be easily determined. One of these tubes was taken apart, and the dimensions appearing in Table I were determined.

The 6A3 is comprised of two tube structures in parallel enclosed in a common envelope. Each structure has an $M$ type filamentary cathode. The grid and plate electrodes are nearly rectangular in form. Consequently, the tube is treated as though it were four planar triode structures in parallel in the above table.

The tube parameters of interest, shown in Table II, were obtained from handbook curves[6] for $Ep = +200$ volts and $Eg = -30$ volt. The voltage values indicated were chosen so that

[6] RCA Tube Handbook HB-3, Vol. 1–2, Tube Division, Radio Corporation of America, Harrison, New Jersey.

TABLE II. Tube factors of 6A3. $Ep = +200$ volts, $Eg = -30$ volts.

| Factor | Handbook data | Theoretical | Equation No. |
|---|---|---|---|
| $\mu$ | 4.25 | 3.8 | (1) |
| $Sp$ | $6\frac{\text{ma}}{\text{volt}}$ | $7\frac{\text{ma}}{\text{volt}}$ | (6) |
| $Mp$ | | $3.6\frac{\text{ma}}{\text{in.}\times 10^{-3}}$ grid displacement | (7) |

the point on the tube surface under consideration lies on a plane region of the surface. This point also constitutes a compromise between the space-charge-free assumption involved in Eq. (2), and the space-charge-limited case involved in Eq. (3).

The parameters given in Table I were substituted in the relevant theoretical relations, under the voltage conditions mentioned above, and the theoretical values of Table II determined.

In view of the accuracy of the measurements in Table I, and the approximations employed in the theory, the results indicated in Table II with respect to the first two factors are considered satisfactory. We may conclude, therefore, that the value of $Mp$ obtained is correct to within about the same accuracy without experimental verification.

## CONDITIONS FOR THE MOTIONAL TRANSCONDUCTANCE BEING EQUAL TO ZERO

Inspection of Eq. (7) indicates there are several interesting facts concerning the magnitude and sign of $Mp$ under certain conditions. For $Eg$ negative and $Ep$ positive, as is the case for normal amplifiers, the magnitude and sign of the bracket factor vary somewhat as follows. For

$$|Eg| > \frac{KEp}{(dp-dg)},$$

the right-hand term of the bracket factor is negative and large so that the bracket factor is positive and large. Since $Sp$ is positive, $Mp$ is positive and large. For

$$|Eg| < \frac{KEp}{(dp-dg)}, \quad (8)$$

the right-hand term of the bracket factor be-

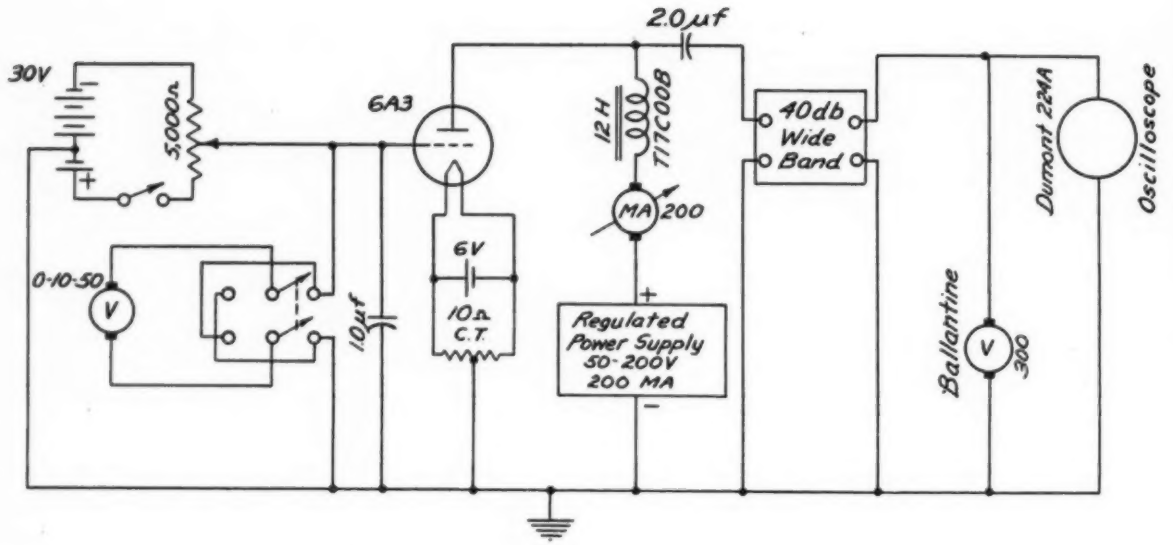


FIG. 2. Schematic diagram of the experimental arrangement.

comes positive and larger as the $|Eg|$ decreases to zero; and as $Eg$ subsequently becomes positive. Hence, the bracket factor passes through zero, when the second term equals the first term, and then goes negative and larger in magnitude as the $|Eg|$ decreases to zero; and as $Eg$ subsequently goes positive. Since $Sp$ remains positive, $Mp$ passes through zero and becomes negative and large in magnitude.

It is well known that, for triodes, $Sp$ increases monotonically as $Ip$ increases. Further, that $Ip$, for fixed positive $Ep$, increases as the $|Eg|$ decreases for $Eg$ negative and continues to increase as $Eg$ goes through zero and becomes positive for normal maximum positive values.

Hence, we can conclude that, in practice, $Mp$ may be zero or small in the normal operating voltage range of triodes where $Sp$ is large so that the tube will still amplify normally as far as electrical fluctuations in grid voltage are concerned.

Since microphonic effects are known to be caused, in great part, by mechanical motion of the grid rods, it is evident that microphonics may be reduced or eliminated by operating a tube, or designing a special tube, under the conditions for $Mp$ to be zero or small.

## EXPERIMENTAL ARRANGEMENT

A simple experiment was set up to check Eq. (7) by mechanically driving a tube and measuring the resulting "microphonic" output signal. Inspection of Eq. (7) indicates that this may be done most easily by varying $Eg$, with $Ep$ fixed, so that the only other variable is $Sp$. This varies in a known manner in terms of $Ip$, which in turn is a known function of $Eg$ for $Ep$ constant.

The schematic diagram of the experimental arrangement is shown in Fig. 2. A 6A3 was operated with battery filament supply to permit

TABLE III. Dominate driving frequencies of microphonic output for a 6A3 and other data. $Ep = +100$ volts; $Eg = -10$ volts; $E_f = 6$ volts; volts across speaker = 1.0.

| Case | Driving frequency for maximum output c.p.s. | Frequencies at which the output is 3 db down from the maximum output c.p.s. | Remarks concerning the output wave form |
|---|---|---|---|
| Transverse Excitation | | | |
| 1 | 194 | 192– 202 | Very complex wave form |
| 2 | 310 | 309– 317 | Symmetrical complex wave form |
| 3 | 359 | 357– 361 | Fair sine wave |
| 4 | 465 | 461– 470 | Good sine wave |
| 5 | 549 | 548– 550 | Excellent sine wave |
| 6 | 938 | 883– 985 | Extremely complex wave form with multiple resonances |
| 7 | 2100+ | 2095–2115 | Good sine wave |
| Longitudinal Excitation | | | |
| 8 | 355 | 351– 359 | Complex wave form |
| 9 | 469 | 461– 471 | Good sine wave |
| 10 | 544 | 542– 546 | Good sine wave |
| 11 | 722 | 719– 742 | Extremely complex wave form |
| 12 | 948 | 943– 952 | Fair sine wave |
| 13 | 2090 | 2065–2095 | Secondary maximum at 2070 c.p.s. |

hum-free operation. The grid bias was varied by means of the potentiometer across the grid bias battery and its magnitude determined by the grid voltmeter. A.c. pick-up in the grid circuit was avoided by grounding the grid at a.c. by means of the 1-mfd condenser.

The plate supply was a heavy duty, electronically regulated power supply whose output voltage was adjustable over the limits indicated. A voltmeter, not shown in the figure, was connected from plate to ground to indicate the plate voltage. A 12-henry heavy duty choke was used as a plate load in order to obtain a low value of d.c. drop in the plate load over the large range of d.c. plate currents employed.

The resulting "microphonic" output voltage developed across the plate load was impressed, through the 2-mfd d.c. blocking condenser, across the input of a stable, wide band amplifier having a voltage gain of 40 db. The output of the amplifier was indicated by a Ballantine model 300 voltmeter and was also observed on an oscilloscope screen. The no signal output of the circuit was well below the minimum signal measured.

The mechanical arrangement employed is shown in Fig. 3. The output of a sine wave audio oscillator was impressed across the voice coil of a small dynamic speaker. The oscillator output was measured by a Ballantine voltmeter and was held constant throughout the experiment at 1 volt.

Two types of mechanical excitation were employed. As shown in Fig. 3A, the transverse case, the tube was placed on a heavy table top so that the grid planes were parallel with the table top. The speaker was placed on top of the tube envelope so that the speaker diaphragm was pressed tightly against the tube. The speaker was then taped to the table top so that it would maintain this position. It is evident that mechanical excitation of the tube for this case will result in grid rod displacement perpendicular to the plane of the grid.

Figure 3B illustrates the mounting used for the longitudinal case. For this arrangement mechanical excitation of the tube will result in grid rod displacement in the plane of the grid or parallel to the longitudinal axis of the tube.

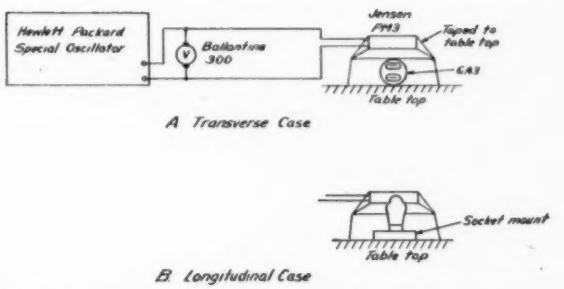


FIG. 3. Mechanical layout of the experimental arrangement.

## EXPERIMENTAL PROCEDURE AND RESULTS

The experimental procedure involved setting the driving oscillator at some constant output voltage and varying the frequency of the oscillator while observing the "microphonic" output on the oscilloscope. The magnitude of the output was highly frequency-sensitive in that the output would vary by as much as 40 db in passing through a frequency range of a few cycles. It is considered that these variations in output are associated with mechanical resonances of the tube structure; and, in particular, with mechanical resonances of the grid rods.

In some frequency ranges the output wave form was greatly dependent on the excitation frequency, indicating complex modes of vibration. In other cases the output wave form was sinusoidal and only the amplitude of the output signal was frequency dependent.

For the particular tube tested, it was found that there were seven dominant frequency ranges for the transverse case and six for the longitudinal case in the excitation frequency range of 100 c.p.s. to 10,000 c.p.s. These are tabulated in Table III below with other relevant information such as a statement concerning the observed wave form and an estimate of the width of the dominate frequency range in terms of the frequencies at which the output signal amplitude, as measured by the Ballantine voltmeter, are 3 db down from the output at the frequency of maximum output. In obtaining these data, the following were held constant: $E_f = 6$ volts, $Ep = +100$ volts, volts across speaker $= 1.0$, and $Eg = -10$ volt. The magnitudes of $Ep$ and $Eg$ were found to effect the output amplitude and wave form, as discussed below, but not the frequency at which the maximum output was obtained.

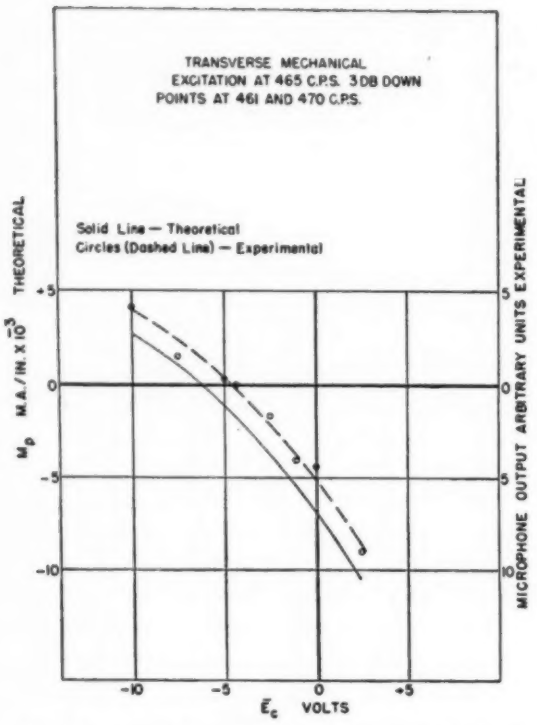


FIG. 4. An experimental check of Eq. (7) with $\bar{E}_c$ as the variable and sine wave mechanical excitation normal to the grid plane.

An experimental check of Eqs. (7) and (8) was then attempted in the following manner. With the driving oscillator accurately set at a frequency of maximum "microphonic" output, as indicated by the output Ballantine voltmeter, the grid bias was varied and the "microphonic" output as a function of grid bias determined. $Ep$ was carefully held constant at +100 volts. This value of plate voltage was chosen so that the plate dissipation rating of the tube, 15 watts, was not exceeded at the largest positive grid bias voltage used during the experiment. The latter was +2.5 volts.

Many very interesting factors were noted; some of which are summarized below:

1. With $Eg$ varied in the voltage range from −10 volts to +2.5 volts a minimum was noted in the "microphonic" output for the following cases of Table III. For transverse excitation 4 cases, number 1, 3, 4, and 7. For longitudinal excitation 1 case, number 11. This factor is discussed in greater detail below.

2. For the transverse case 2 and longitudinal case 8 the "microphonic" output increased as $Eg$ was varied from −10 volts to +2.5 volts in about the same amount that $Sp$ increased.

3. For the remaining cases the "microphonic" output decreased in varying amounts as $Eg$ was varied from −10 volts to +2.5 volts.

4. For many cases, and in particular for case 6, oscilloscope examination of the output signal indicated that one component of a complex vibration spectra minimized as in 1, while other components did not.

In view of the above, it was assumed that cases 4 and 9 probably represented the gravest mode of vibration of the grid rods so that these cases are studied in detail below. Upon completion of the experiment, an attempt was made to observe the vibration of the grid rods under a low power microscope while the tube structure was vibrated under conditions similar to those of Fig. 3A. This experiment failed since the amplitude of vibration was too small to be detected with the apparatus used.

Considering case 4 of Table III, the experimental results obtained are tabulated in Table IV below.

The results of Table IV are plotted as circles on Fig. 4. The solid line of this figure was obtained by substituting the tube parameters of Table I and the experimental parameters of Table IV in Eq. (7) and solving for $Mp$. To do this, $Sp$ was calculated from Eq. (6) under the same conditions.

It is evident that the shape of the experimental curve closely approximates that of the theoretical curve. Considering the type of measurements involved, this is considered a rather good check with the theory in spite of the displacement of the two curves. In addition, the following should be noted:

1. The theoretical value of $Eg(=\bar{E}_c)$ for $Mp=0$

TABLE IV. Experimental results for transverse case with driving frequency of 465 c.p.s. $Ep=+100$ volts; $Eg=\bar{E}c$ = variable; $E_f=6$ volts; volts across speaker = 1.0. 3 db down points 461 c.p.s. and 470 c.p.s.

| $\bar{E}c$ volts | Output volts | Normalized output volts | 11 X normalized output for scale factor | Driving frequency for maximum output c.p.s. |
|---|---|---|---|---|
| −10 | 0.49 | 0.37 | 4.09 | 465 |
| − 7.5 | 0.36 | 0.13 | 1.44 | 465 |
| − 5 | 0.14 | 0.02 | 0.22 | 465 |
| − 4.3 | 0.12 | 0 | 0 | 465 |
| − 2.5 | 0.27 | 0.15 | 1.65 | 465 |
| − 1 | 0.49 | 0.37 | 4.08 | 465 |
| 0 | 0.52 | 0.40 | 4.40 | 465 |
| + 2.5 | 0.94 | 0.82 | 9.00 | 465 |

is $-6.2$ volts under the conditions of the experiments. This compares with the experimental value of $-4.3$ volts.

2. When $Mp$ changes sign the phase of the "microphonic" output voltage should shift 180°. This was noted experimentally although not indicated on the figure.

3. Most of the residual output signal near and at the minimum value of output is at the second harmonic of the driving frequency.

4. The maximum range in output signal variation greatly exceeded that of the example in some cases. As an example, in case 7 the range of maximum to minimum signal, as a function of $\bar{E}_c$, was over 30 db.

The theory does not cover the case of displacement of the grid rods in the grid plane. Experimentally, this case is probably complicated by phase relations between the vibrations of adjacent grid rods and by transverse components of the resulting vibrations. Experimental results for this case, case 9, are plotted in Fig. 5 as circles to illustrate the results obtained. As noted, the driving frequency is nearly the same as for case 4. The absolute magnitude of the output signal for $Eg=-10$ volts was nearly the same in both cases. This is not considered significant, however, since there is not reason to believe that the driving forces for the two cases are the same.

## CONCLUSIONS

1. The method of utilizing the displacement of the grid relative to the rest of the tube structure to obtain plate current variations which are a function of the displacement, and hence of the mechanical force causing the displacement, is feasible from an electronic standpoint.

2. Microphonism of tubes, under certain conditions, may be reduced as indicated by the theory developed and in terms of two factors or a combination thereof:

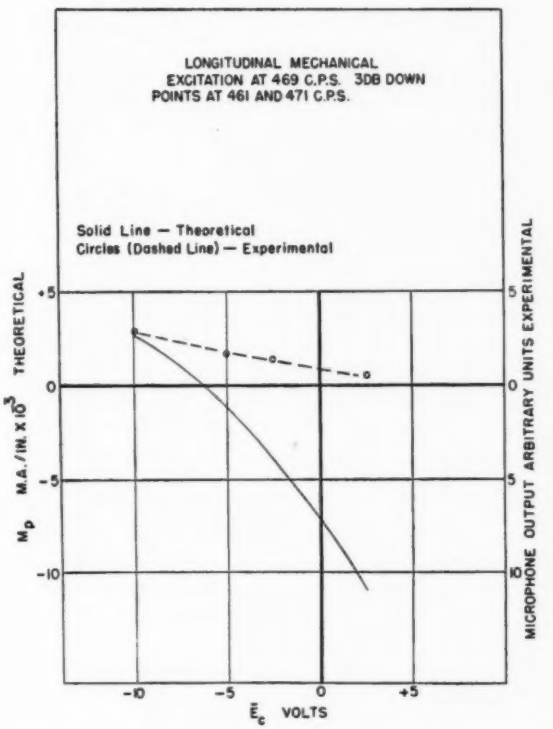


FIG. 5. Similar to Fig. 4 with mechanical excitation approximately in the grid plane.

(a) By designing a tube for minimum $Mp$ given the operating potentials or (b) for a given tube to select the optimum operating potentials so as to obtain a minimum $Mp$.

In view of the latter, it may well be advantageous to operate the input stage of a high gain automatic volume controlled amplifier with fixed bias to reduce microphonics even though the flatness factor of the system may be decreased.

The above is thought to be interesting and useful, but from the practical standpoint further theoretical work should be done for the cylindrical triode and multi-grid tube cases. The construction of a planar triode whose grid can be moved relative to the cathode and plate should also be attempted. It is hoped that further work along these lines can be carried out in the future.

# The Effect of Hydrostatic Pressure on the Fracture of Brittle Substances

P. W. BRIDGMAN
*The Physics Laboratory, Harvard University, Cambridge, Massachusetts*
(Received November 11, 1946)

An arrangement is described permitting the fracture of brittle materials under the action of tensile stress superposed on hydrostatic pressure. The hydrostatic pressures range up to 30,000 kg/cm². The tensile stress superposed on the pressure required to break Pyrex glass is a strong function of the material by which pressure is transmitted to the lateral surface of the glass, but in all cases of fracture produced at pressures above 25,000 kg/cm² the net stress at fracture was compressive, that is, tensile fracture takes place against the direction of the stress. Beryllium and phosphor bronze lose the brittleness which characterize them at atmospheric pressure and fracture in tension under pressure after marked plastic deformation. Carboloy remains brittle in tension under pressure, but its tensile strength may increase by a factor of three. NaCl elongates plastically in tension under pressure with no obvious disturbance of the optical homogeneity. Pipestone remains completely brittle under pressure and of very low strength. In simple compression combined with hydrostatic pressure Pyrex glass increases greatly in strength. Single crystal $Al_2O_3$ under the same conditions exhibits plastic slip on the basal plane without fracture. In the discussion the importance of the condition of energy release as a factor controlling fracture is emphasized. The Griffith conception of fracture as resulting from stress concentration at the ends of microscopic cracks is consistent with many qualitative aspects of the situation, but probably cannot be carried through quantitatively.

## INTRODUCTION

IN a number of previous papers[1] I have described the effect of hydrostatic pressure in increasing the ductility of substances like mild steel under the action of tensile forces. In this paper the experiments are extended to a number of materials ordinarily brittle, like glass.

The effect of pressure is investigated on both compressive and tensile strength. Measurements of compressive strength may be made straightforwardly, but the tensile tests require a special technique. Under ordinary conditions there are technical difficulties in making tests on substances like glass with the conventionally shaped tension specimen, because of the effect of stress concentration at the corners of the specimen, resulting in capricious fracture. Most fortunately it turns out that a technique which is simply adapted to the application of tension under hydrostatic pressure at the same time uses specimens of such a shape that the difficulty from stress concentration disappears, making the investigation of the tensile properties under pressure much easier than at atmospheric pressure.

The experiments on tension to be described in the following are in a certain sense an extension of experiments made long ago on what I called the "pinching-off" effect.[2] In these experiments rods of glass or other brittle substances passed completely through the pressure vessel, emerging through stuffing boxes, the part within the vessel being exposed to hydrostatic pressure. On raising pressure high enough, the glass rod fractured by a clean tensile breaks at some place inside the pressure vessel. These experiments were mostly qualitative in nature, and no attempt was made to get consistent values for the pressure required to produce fracture. The chief result from these experiments was to emphasize that it is possible to have tensile fracture across a plane across which there is no stress component. This is, from the point of view of some of the traditional conceptions of fracture, a highly paradoxical thing. The conclusion which I drew from these experiments has, therefore, understandably been met with considerable scepticism in some quarters, and with the attempt to explain away the phenomenon as caused by various secondary effects. For a long time I have had it in mind to make a more exact study of the "pinching-off" effect. A few years ago I found, in some unpublished experiments, that the precise pressure at which the "pinching-off" fracture is produced in glass is

[1] P. W. Bridgman, J. App. Phys. **17**, 201 and 692 (1946). Rev. Mod. Phys. **17**, 3 (1945).

[2] P. W. Bridgman, Phil. Mag. p. 63 (July, 1912).

extraordinarily sensitive to surface conditions. This indicated the necessity for a more elaborate investigation of the whole effect. With these new experiments, this extended examination is now possible. We have now two degrees of freedom in the stress system, whereas formerly there was only one. Formerly the set-up was such that the longitudinal component of stress was continually zero, and the two equal lateral components were increased until fracture occurred. Now, the longitudinal component and the two equal lateral components may be independently varied, so that fracture may be studied over a much wider range of conditions. The paradox that characterized the "pinching-off" effect is now carried much further, for now tensile fractures can be produced across planes on which the stress is a *compressive stress* so high as to be beyond any possible experimental error. Thus, to mention only a single example, tensile fracture has been produced in glass under a mean hydrostatic pressure of 26,000 kg/cm² with a superposed tension of 11,000 kg/cm², so that the net stress across the plane on which the tensile break occurred was a compressive stress of 15,000 kg/cm².

## THE METHOD

The method and the general nature of the problems encountered may be indicated by means of a highly idealized mental experiment. Figure 1 represents a compound tension specimen consisting of a central cylinder $A$ of the brittle substance to be tested, and of two "pull" pieces $B$ with shoulders and the same small diameter as the specimen, mounted together in the thin cylindrical sheath $C$ which is attached by solder or otherwise to the pieces $B$ at $D$ in such a way as to be liquid tight. The whole compound specimen is immersed completely in a liquid, to which any desired hydrostatic pressure is applied, and, superposed on the hydrostatic pressure, a tensile force is then applied to the pull pieces $B$. The situation is idealized by supposing that the pull pieces are infinitely strong, that the lateral contraction of $A$ and $B$ under the complete stress system is the same, so that their diameters continue to be the same, and that the sheath $C$ has negligible longitudinal strength, offers zero friction on its inside surface, and is infinitely stiff so

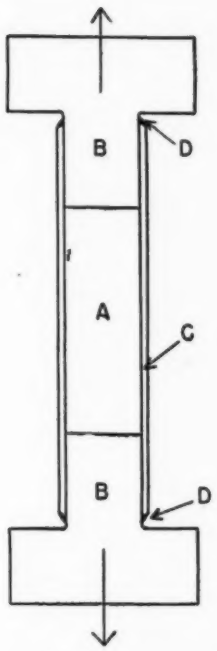


FIG. 1. Tension specimen, $A$, with steel pull pieces, $B$, and sheath, $C$, as used in combining hydrostatic pressure and tension.

that it cannot be pushed by the external pressure into any cracks which might be formed on the surface of $A$ or $B$. We now inquire what will happen if the pressure is first raised to some high value, at which it is kept constant, and the tension is then increased indefinitely. It is evident in the first place that the compound specimen cannot separate at the surface of separation between $A$ and $B$ as long as the tension is less numerically than the pressure. For if incipient separation should start at this surface, the surfaces of separation would be pushed back into contact by the pressure, which is greater than the tension. All the more, if separation cannot occur at surfaces already free between $A$ and $B$, it cannot occur in the material of the solid rod $A$. That is, under a hydrostatic pressure, $P$, the tensile strength of the material $A$ is, under these conditions, at least as high as the pressure $P$. Ideally, it seems impossible to place any limit to this behavior, so that by increasing indefinitely the hydrostatic pressure the tensile strength may also be indefinitely increased. This means that the numerical value of the pressure coefficient of tensile strength approaches unity under these conditions. This in itself is highly anomalous. It

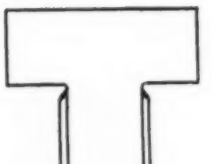

FIG. 2. Modification of arrangement of Fig. 1 in which the tension is concentrated in a neck, permitting the fracture in tension of the stronger materials.

is a matter of experience that the pressure coefficient of most physical properties of substances like glass is of the order of magnitude of perhaps $10^{-5}$, if the unit of pressure is taken as the kilogram per square centimeter. Yet here we have the necessity for a coefficient $10^5$ times as high. The situation is also anomalous when considered from the point of view of strain. Under combined tension and pressure the specimen $A$ elongates, and we have apparently the necessity for an indefinitely great elongation with no fracture. To say that beyond a certain point the specimen will receive plastic set on release of stress does not relieve the paradox of the situation while the stress is in action.

This idealized experiment, leading to such paradoxical conclusions, may be made the basis of the actual experiment, and also suggests the direction in which the experimental results may be expected to go, which is indeed the direction of paradox. In practise the pull pieces $B$ may be made of heat-treated steel, and the specimen $A$ made of the brittle substance under examination, such as glass or brittle alloy or what not. The sheath $C$ may be made of copper, a few thousandths of an inch thick. We now see at once that we have a method of applying tension to a brittle specimen without shoulders or regions of stress concentration on the specimen itself. The pull pieces $B$ may be re-used from experiment to experiment, so that the preparation of the specimen could not well be simpler. In the simple form shown in Fig. 1 any tension can be applied up to the magnitude of the pressure itself, assuming that there are no limiting complications in practise. These complications do, in fact, occur, since the copper is not infinitely rigid, and would eventually blow into the surface of separation between $A$ and $B$ before tension reaches its theoretical upper limit. This difficulty may be avoided by artificially fashioning a neck on the tension specimen, as shown in Fig. 2. The neck may be easily made of such proportions that there is no harmful stress concentration in the neighborhood. By making the neck of suitable dimensions, any tensile stress may be applied in this manner, without grips, to any material up to the fracture point, whether that is above or below the surrounding hydrostatic pressure. This arrangement has been used, for example, in testing the tensile strength of Carboloy under pressure, the tensile strength being much higher than the highest hydrostatic pressure that was applied.

The material of the sheath is a vital factor in the result, for not only may it be blown between the surface of separation of $A$ and $B$, but it may also be blown into any incipient cracks which appear in the surface of the specimen $A$. One would anticipate, therefore, that the measured tensile strength would be a strong function of the surface conditions, as exemplified by the material of the sheath. This did indeed prove to be the case. Various materials were tried. In practise the sheath sometimes was made compound, still keeping copper over the surface of separation of $A$ and $B$, but replacing the central part by some other substance such as lead or rubber, which must naturally be attached in such a way as to prevent access of liquid. It would have been desirable if conditions could have been pushed to the limit by permitting contact between the liquid and the specimen all over its lateral surface, while preventing entry of the liquid into the interface between $A$ and $B$, but no feasible way of doing this presented itself. As it was, a sufficiently wide range of external conditions was attained by the use of copper, lead, and rubber to

indicate the general nature of what might be expected.

The arrangement indicated in Figs. 1 and 2 has points of resemblance to an arrangement probably first used by Richart, Brandtzaeg, and Brown[3] in studies of the effect of compound stresses on concrete and later by Balsley[4] working with Griggs on minerals. Both these investigators used straight cylindrical steel pull pieces, attached to the specimen by a sheath. The pull pieces were taken out of the pressure chamber through stuffing boxes, and on the outside were subjected to an independent compressive stress, which, as it varied from greater to less than the internal hydrostatic pressure was capable of exposing the specimen to a superposed stress either of compression or tension. There are technical difficulties with this arrangement, however. The stuffing boxes have to be accurately aligned and are not capable of as wide a pressure range as that used here. The maximum pressure in the Illinois experiments was 300 kg/cm², and in those of Balsley 10,000 kg/cm². Neither of these experimenters used necked specimens in order to permit raising the tension to values exceeding the hydrostatic pressure, but there is no reason why necked specimens should not be used with externally projecting pull pieces.

During the war Gurney and Rowe[5] in England made a large number of measurements of the pinching-off effect (which they describe as fracture by "radial" pressure) on glass and several plastics, and in a number of instances used necked specimens, thus permitting any desired tensile stress depending on the dimensions of the neck. These experiments were limited, however, because of the extension of the specimen itself through stuffing boxes, to hydrostatic pressures not greater than the "pinching-off" pressure of the straight cylindrical specimen.

In addition to the effect of one-sided tension, the effects of one-sided compression were also studied under pressure. These experiments were perfectly straightforward, and the details need not be specially indicated, for there is no such complication as with the tension specimens, but the stress may be applied to simple cylindrical specimens by compressing between platens. The specimen may be imbedded in lead or other suitable soft material when it is desired to prevent access of the transmitting liquid.

The various other details of the experiment, such as methods of applying and measuring the force, were the same as in my previous experiments, and the details have already been sufficiently described. An improved method of measuring the deformation was used in these present experiments, which has not yet been described in print. This employed a new insulating plug with seven terminals and a potentiometer method, which permitted measurement of the changes of dimensions from the inside of the pressure vessel, instead of from the outside, as hitherto. However, since these deformations during the action of stress are to play no role in the following, the description of this new arrangement can be deferred until the compressibility measurements in which it played an essential role are described.

## THE EXPERIMENTS

### Tensile Tests

#### *Glass*

The experiments on glass were made on Pyrex, all specimens being taken from the same batch. Five experiments were made in all. In the first a copper sheath was used 0.016 inch thick over the junction between steel and glass, turned down to a thickness of 0.005 inch over the central part of the glass. No extravagant precautions were taken with the glass, which was 0.44 inch long and 0.12 inch diameter. The lateral surface was the natural surface of the rod as provided commercially. The ends were lapped by hand with a fine carborundum stone perpendicular to the axis. Care was taken not to chip the edges. This specimen was exposed to a pressure of 27,000 kg/cm², and then a superposed tension added up to 19,000 kg/cm², when separation occurred between glass and one steel pull piece. The glass was undamaged, as was found by dissolving off the copper sheath in acid. The pull pieces were found to be too soft, and under this tension received a permanent elonga-

[3] F. E. Richart, A. Brandtzaeg, and R. L. Brown, Bull. No. 185 (1928), Eng. Exp. Stat. Univ. Ill.

[4] J. R. Balsley, Trans. Am. Geophys. Un. Part II, 519 (1941).

[5] C. Gurney and P. W. Rowe, Royal Aircraft Establishment, Farnsborough, Rep. No. Mat. 5 (May, 1945), and Rep. No. Mat. 8 (November, 1945).

tion of 1.5 percent. This flow of the steel may have been responsible for the separation. The glass received no measurable permanent change of dimensions.

In the next experiment, copper ferrules were used over the surface of separation of glass and steel, but the central part of the glass was covered with a soft Neoprene tube, extending over the copper ferrules. At a hydrostatic pressure of 25,000 kg/cm² and a superposed tension of 5900 kg/cm², making the net compressive stress in the glass 19,100 kg/cm², this failed by a tensile break at the edge of the copper ferrule. On removing the ferrules from the glass, the glass fell apart into several disks separated from each other by clean tensile breaks. In this experiment the edges of the ferrules were comparatively thick, and it seemed probable that the fracture was in some way connected with a discontinuity of stress at the edge. The experiment was accordingly repeated, but with the edges of the copper ferrules feathered down to vanishing thickness. At a hydrostatic pressure of 25,300 kg/cm² and a superposed tension of 11,400, failure occurred at the interface. The entire central portion of the glass, where it had been exposed to the Neoprene, was separated into thin disks, still hanging lightly together. In the fourth experiment, copper ferrules again guarded the surface of separation of glass and pull pieces, and the central part of the glass was covered with a heavy lead sheath, soldered to the copper, The central part of the glass was necked down by grinding and polishing from .120 to 0.106 inch in order to concentrate the tensile stress at the center and locate the fracture. Under a hydrostatic pressure of 28,000 kg/cm² this broke in clean tensile fracture across the smallest diameter of the neck under an average superposed tensile stress at the neck of 15,500 kg/cm². Tensile fracture, therefore, occurred here against a net compressive stress of 12,500 kg/cm². The lead was melted off, and the copper dissolved off in aqua regia. An additional tensile break appeared on thus stripping the specimen, and the entire mass of the remaining glass was copiously fissured with fine disking cracks, the glass still hanging lightly together. In the fifth experiment, the glass was necked down at the center from .120 to 0.080 inch by grinding, polishing, and fire polishing to remove the last trace of mechanical cracks. The glass, together with the pull pieces, was mounted in a heavy straight copper sheath 0.21 inch in diameter, which was then collapsed tightly around the neck in the glass by a preliminary exposure to 8000 kg/cm², and then turned down to a thickness of 0.005 inch over the neck. Under a hydrostatic pressure of 27,000 kg/cm², this failed by a clean tensile break across the neck at an average superposed tension at the neck, corrected for the strength of the copper, of 24,500 kg/cm². This makes fracture to have occurred at a net compressive stress of 2500 kg/cm².

### *Carboloy*

Tests were made on Carboloy of grade 999, which is the grade containing the smallest quantity of binder furnished by the General Electric Company. To increase the stress the specimen was necked by grinding with diamond. Two unsuccessful preliminary experiments were made in which the strength of the Carboloy was not estimated high enough and the neck diameter accordingly was not made small enough. In two final experiments the area at the neck was made somewhat less than one quarter the area at the ends. In the two final experiments hydrostatic pressure was raised to 27,000 kg/cm². In the first of the two, there was a leak at the maximum load, suddenly throwing an uncontrolled and unmeasured increment of tension on the sample, under which it fractured. The best estimate of the superposed tensile load at the neck at fracture was somewhere between 56,000 and 60,000 kg/cm². In the second, there was no mishap and tensile fracture occurred at a superposed tension at the neck of 54,500 kg/cm². In both cases the break was a clean fine-grained tensile break square across the narrowest part of the neck, with no evidence whatever of any plastic flow in the neck, and no trace of the little shearing rim around the edge of the break that is almost always found in hardened steel.

The tensile strength under 27,000 is thus between two and three times as high as any value that has ever been recorded for any grade of Carboloy at atmospheric pressure by the method of the bending of slender rods. It was a surprise that there was no evidence of plasticity. Under one-sided compressive stress this grade of

Carboloy permits plastic shortening up to at least 10 percent.

### *Beryllium*

Beryllium as ordinarily obtained commercially, even in the purest form, breaks at atmospheric pressure in tension with no appreciable elongation and with tensile strength not more than 2000 kg/cm². Being a crystalline material it was anticipated that under hydrostatic pressure it might exhibit a degree of plasticity. The first experiment with beryllium, which was kindly furnished by Professor John Chipman of the Massachusetts Institute of Technology, employed steel pull pieces, by the same technique as used for glass and Carboloy. The specimen was necked to 0.7 of the full diameter, and mounted in a copper sheath, collapsed around it as in the last experiment on Pyrex. Under a pressure of 27,500 kg/cm² this broke at the neck with a further reduction of area at the neck of 48 percent, thus showing the anticipated ductility under the action of pressure. The neck at the break was very jagged, and the contour was finely corrugated around the periphery in an unusual way. The superposed tensile stress at fracture was 7900 kg/cm², on the original area of the neck. Two other experiments were made with beryllium, in which the conventional shaped tensile specimens were used, like Fig. 1, entirely fashioned out of a single bar. Mr. Charles Chase skillfully found how to fashion the beryllium rod with a Carboloy tool. In these two experiments the beryllium was directly exposed to the action of the pressure transmitting liquid, a mixture of iso-pentane and commerical "pentane." In the first experiment the specimen pulled apart at the shoulder under a hydrostatic pressure of 23,000 kg/cm². This was evidently the effect of stress concentration. There was, however, measurable extension in the body of the specimen. In the second specimen, the fillet at the shoulder was given a larger radius and the center of the specimen was further necked down to localize the break. Under a pressure of 18,000 kg/cm², this broke across the center of the neck with a coarse granular break, with a 20.6 percent reduction of area, and a maximum superposed tensile stress of 5400 kg/cm² calculated on the original area.

There would seem to be no reason to think that the transmitting liquid exercises any effect in the case of this material. It would appear that increasing hydrostatic pressure progressively raises the ductility and the tensile strength.

### *Phosphor Bronze*

For commercial welding a bronze is used consisting of 93 percent copper and 7 percent phosphorus. Under atmospheric conditions this material as ordinarily supplied in the cast condition is coarsely crystalline and completely brittle. It was of interest to find whether ductility is imparted by pressure. Three experiments were made. The specimens were made in one piece from the commercial cast rod, and were exposed to direct contact with the pressure liquid. The first two of these were not pulled to fracture, the ductility proving to be greater than anticipated, so that the dimensions originally given did not permit extension to fracture. The first of these was pulled under 22,000 kg/cm² to a reduction of area of 12.6 percent, and the second under 29,000 kg/cm² to 18.5 percent reduction. The elongation of both these specimens was uniform, necking not having yet started. The maximum superposed tensile load on the second specimen was 8700 kg/cm². In the third experiment the original specimen was turned down further over the central portion, to locate the break. Under a hydrostatic pressure of 29,900 kg/cm² this broke with an 80.2 percent reduction of area. The break was a burnished shearing break at approximately 45° across the narrowest part of the neck. The load at fracture was not obtained.

A control run on a similarly shaped specimen at atmospheric pressure yielded, as expected, a completely brittle fracture at the bottom of one fillet.

### *$Al_2O_3$ (Synthetic Sapphire)*

The Linde Air Products Company has recently developed a method of making single crystal rods of $Al_2O_3$, which have found various industrial uses. One of these rods was tested in tension, and I am much indebted to the Linde Company for making the specimen available. The hexagonal axis was oriented, as determined by the Linde laboratory, at an angle of 20° with the length of the specimen. It was mounted with steel pull pieces, copper ferrules, and Neoprene over the

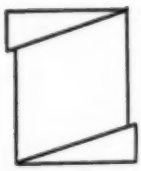

FIG. 3. Schematic indication of the manner of fracture of Pyrex glass in simple compression when supported by hydrostatic pressure.

central part. The central part was necked down by grinding with fine diamond powder from an original diameter of 0.100 to 0.070 inch, in order to locate the break. Although the final grinding was with the finest powder on hand, about No. 500, fine scratches were visible on the surface of the ground part. This material as ordinarily supplied is by no means as perfect as the crystals which are formed in nature, but usually there are imperfections visible to a low power glass in the form of minute bubbles irregularly scattered through the interior. The specimen used for this test was unusually perfect in this respect, however, and showed no such visible imperfections. This was pulled at a pressure of 24,700 kg/cm². At a superposed tensile load of 4900 kg/cm² it fractured on a plane perpendicular to the axis, not at the neck, nor at the edge of the copper ferrule, but at a place where the diameter was the full original diameter, situated about half-way between the edge of the ferrule and the neck. The conclusion forced by this is that the material is very inhomogeneous. The neck withstood without fracture a stress of 10,200 kg/cm² at the same time that the ruptured part was giving way under 4900. The surface of the break itself was not homogeneous. About half the area of the break was a mirror-like plane, with fine ripple marks around the edge, but the remainder of the section had a mat appearance, perhaps caused by the presence of bubbles too small to see with the hand glass.

### *Pipestone (Catlinite)*

This material, an iron-rich clay-stone, has a typical composition: $SiO_2$ 57.4, $Al_2O_3$ 25.9, $Fe_2O_3$ 8.7, $H_2O$ 7.4, MgO and CrO trace. Mechanically it seems to be an exceedingly fine-grained cemented aggregate. I have used it extensively for the insulation of electrical leads into the high pressure chamber, and in this usage it is capable of supporting high shearing and compressive loads without appreciable flow. When it does yield in this usage it disintegrates to a fine powder. Advantage was taken of the new technique to study its behavior in tension, it being quite impossible to make the conventional tension tests at atmospheric pressure. The specimen used was a single straight cylinder 0.180 inch in diameter and 0.438 inch long, mounted between steel pull pieces in a copper sheath turned to a thickness of 0.005 over the central part. At a pressure of 27,400 kg/cm², this failed on a clean tensile plane well within the central portion of the specimen, and with a reduction of diameter at the break of not more than 0.0005 inch. The superposed tension at fracture was only 430 kg/cm². There was no evidence of the copper sheath being blown into the fracture, but the copper was cleanly sheared through at the break. In view of experience with other materials, such a negligibly small effect of pressure on tensile properties was hardly anticipated. It is doubtless connected with the unusual mechanical composition of this material.

### *NaCl*

Under normal conditions at atmospheric pressure rocksalt breaks brittlely in tension on one of its numerous cleavage planes. It is well known, however, that under special conditions, as when properly supported or when in aqueous solution, it may be made to support plastic deformation. Two tests were made of the effect of hydrostatic pressure. Both specimens were cut from the same natural crystal, with one of the natural cleavage planes perpendicular to the length. They were used in the form of straight cylinders, mounted between steel pull pieces. The first was used with a copper sheath 0.007 inch thick over the central part, and the second with copper ferrules and lead over the central portion. The first was pulled under a hydrostatic pressure of 29,800 kg/cm² to a reduction of area of 20 percent under a superposed "true" tension as calculated on the final diameter, of 520 kg/cm². At the necked part there was no loss of optical homogeneity—no evident slip planes or other evidence of crystal structure, and the cross section remained round. The second specimen, with lead sheath, was pulled under 29,300 kg/cm² pressure. The experiment was

terminated by leak, which prevented the measurement of the tension, but the specimen necked down to a reduction of area of 14.6 percent. Again the specimen retained its perfectly homogeneous appearance.

Voigt[6] experimented on the effect of gas pressures up to 60 kg/cm² exerted by $CO_2$ on the tensile strength of NaCl. He found that up to this pressure the superposed tensile load required to fracture was independent of pressure, and that the fracture continued to be a clean brittle break with no trace of plastic flow. Break occurred on the cleavage planes, and the superposed stress to cause fracture was 57 kg/cm². Evidently his pressures were not high enough to bring about the plasticity which is exhibited at higher pressures. It is to be noted that Voigt's tensile strength was only one-tenth of the stress which at high pressure produced only flow without fracture.

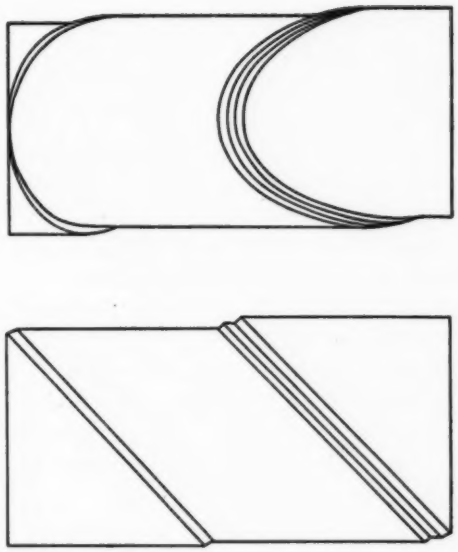

FIG. 4. The slip planes developed in single crystal $Al_2O_3$ under simple compressive stress when supported by hydrostatic pressure.

## Compressive Tests

### *Glass (Pyrex)*

Two experiments were made on glass of the same origin as that of the tension tests. The first specimen was 0.235 inch long and 0.125 inch in diameter. It was compressed in the regular way between Carboloy platens, after soldering into a lead sheath to prevent contact with the pressure liquid. Compressive load was applied at a hydrostatic pressure of 28,000 kg/cm². At an additional compressive load of 18,900 kg/cm² the capacity of the grid to measure compressive stress was reached, and the experiment had to be discontinued. The glass was found undamaged except for a slight chipping around one edge. In the second experiment, the specimen was made smaller, 0.131 inch long and 0.069 inch diameter. The method of mounting was as before. Compressive load was applied under a hydrostatic pressure of 28,000 kg/cm². The specimen failed under a superposed compressive load of 47,000 kg/cm², calculated on the original area. The lead sheath maintained the fragments in approximate position; when the sheath was removed the specimen was found with the appearance suggested in Fig. 3. Two wedge-shaped regions on the ends had slipped sidewise on planes at an angle with the axis of about 65°; the material in these wedges was completely comminuted to a fine powder, opaque and white. The central portion was filled with conchoidal fracture surfaces; the fragments were much larger than at the ends and were transparent.

It is to be noticed that the effect of hydrostatic pressure is markedly greater in increasing the compressive strength of glass than in increasing its tensile strength.

### *$Al_2O_3$*

A number of tests were made on material of the same origin as that of the tensile tests. The results on this material were very capricious, and would hardly merit description here if it were not for one remarkable feature. Four specimens were tested at atmospheric pressure as controls. The crushing strengths of these were 40,000, 8000, 12,000, and 38,300 kg/cm², respectively. Three specimens tested under hydrostatic pressures of 23,800, 25,300, and 22,200 kg/cm² failed completely at additional superposed compressive loads of 18,300, 7700, and 9200 kg/cm², respectively. The failure of these specimens under pressure was remarkable in that it was not catastrophic, but was preceded by a long period of yield under approximately constant compressive load, as in a tension specimen that shows

[6] W. Voigt, Göttinger Nachrichten 521 (1893).

high plastic extension. Another experiment was, therefore, made in which the experiment was terminated before the final failure, so as to permit examination of the specimen. This was exposed to 24,000 kg/cm² hydrostatic pressure and a superposed simple compression of 6300 kg/cm². The appearance was as indicated in the sketch, Fig. 4, which I owe to the kindness of Mr. McCandless, of the Linde Air Products Company. The slip planes, which were inclined at approximately 45° to the compression axis, were identified by Mr. McCandless as the basal 0001 plane of the crystal. This is *not* the plane of cleavage when a sapphire rod is broken at a neck by tension-plus-bending. The cleavage plane under these conditions is $10\bar{1}1$. It may be that in this case fracture occurred on 0001 because it by accident happened to coincide with the plane of maximum resolved shear. It would seem, therefore, that under sufficiently high supporting hydrostatic pressure internal slip without fracture is possible in a *crystalline* substance as brittle under normal conditions as sapphire. The crystal structure obviously plays a decisive role; no tendency to plastic flow has ever been found in glass.

The maximum compressive strength found under pressure in the experiments above is much less than that previously found under pressure for $Al_2O_3$ of other origin.[7] For this, compressive strengths as high as 70,000 kg/cm² have been observed. The difference is doubtless connected in some way with fine scale inhomogeneities. There seemed to be no correlation between the compressive strengths obtained in these new experiments and the crystal orientation.

*Note added on reading proof January 17, 1947.*

I have just found similar slip bands in *tension* on the basal plane, at angles of 45° and 30° to the length, when the specimen is enclosed in a copper sheath.

### *Sintered Carbides*

A number of observations have been made on these materials incidentally in the course of explorations for materials best suited for the construction of high pressure vessels. It has already been stated that Carboloy (tungsten carbide cemented with cobalt) will support plastic shortening in simple compression when supported by high hydrostatic pressure. The pistons of the piezometers used in measuring compressions to 100,000 kg/cm² are made of Carboloy, and because of this, considerable work has been done in examining the behavior of the piston material. In general the grades of Carboloy containing small percentages of cobalt are best suited for pistons. I have used the grades known as 905, and lately exclusively 999. Shortenings in simple compression up to 10 percent have been observed at hydrostatic pressures around 30,000 kg/cm². Carboloy does not work harden when it yields plastically in compression, but the shortening continues proportionally to time. Compressive stresses as high as 150,000 kg/cm² have been obtained in Carboloy for a short time. The rate of yield under these conditions is, however, so high as to make the use for pistons infeasible. My pistons in the compression measurements have seldom been carried above 110,000, and more usually are not carried above 105,000. Under these stresses the total plastic shortening of the pistons is something of the order of one quarter of a percent for a duration of maximum stress of fifteen minutes. There is considerable variation in piston material of ostensibly the same composition, and it pays to make a preliminary examination in order to pick out the best pieces.

It is not inconceivable that other materials than Carboloy would be better adapted for standing high compressive stress when supported by hydrostatic pressure, even though the material might not be so well adapted for ordinary conditions of use. The natural direction in which to seek for improvement is in diminishing the amount of binder, since it would appear that the plastic flow takes place in the binder. A cursory examination was made of some of the more obvious or easy possibilities, but with no improvement. In fact, none of the materials tried approached Carboloy in performance; doubtless we went too far in the direction of minimizing the binder. In this exploration I was fortunate to obtain the cooperation of Mr. deWald, who has specialized in the subject, and who prepared the specimens for me at Massachusetts Institute of Technology, where he enjoyed the facilities of the Department of Metallurgy. The following materials were tried with the following results.

[7] P. W. Bridgman, J. App. Phys. **12**, 461 (1941).

(1) A mixture of 97 percent TaC, 2 percent VaC, and 1 percent $Mo_2C$ with no binder. Under a pressure of 23,000 kg/cm² this failed with a completely brittle fracture under a superposed compressive stress of 36,000 kg/cm².

(2) WC with 0.25 percent Co as binder. Under 25,000 kg/cm² this failed brittlely under 47,500 kg/cm² superposed compressive stress.

(3) TaC with 0.25 percent Ni as binder. Under 25,000 kg/cm² hydrostatic pressure this failed brittlely under 30,700 kg/cm² superposed compressive stress.

There is room for much more work on this subject. In particular, systematic investigation should be made of the effect of varying the grain size and the time and temperature of sintering.

## DISCUSSION

This should be regarded as a first paper on this subject, in which the general nature of the effects is suggested; there is obviously need for much more investigation in detail, both with a wider range of materials and a wider range of stress conditions.

Perhaps the most important single result is to emphasize the reality of a condition of fracture which may often be disregarded. This is: fracture cannot occur unless the process of fracture is an energy releasing process. The reason that in the idealized experiment with which we started our exposition tensile fracture could not occur until the superposed tension reached a value at least equal to the ambient hydrostatic pressure was merely that fracture under these conditions was not an energy-releasing process. For if fracture were to occur, the work done against the hydrostatic pressure would be greater than the work received from the force producing the tension. The fact that fracture occurs in the actual experiment under tensions less than the hydrostatic pressure, that is, against a net compressive stress, is a consequence of the difference between the ideal and the actual case. This difference is in the lateral conditions. In the ideal case, there was an infinitely rigid sheath shielding the lateral surface from entry by the pressure liquid if a crack should appear. In the actual case, the sheath is not infinitely rigid, and if the external pressure is high enough, the sheath may be forced into incipient cracks, and this is an energy-releasing process. According to this view, tensile fracture of a brittle substance in a medium carrying hydrostatic pressure starts on the external surface. This view is confirmed by the extreme sensitiveness of tensile fracture under these conditions to the surface conditions. Thus in the case of glass, we may have fracture by the "pinching-off" effect at a pressure of 1500 kg/cm² if the external medium is water, and at a pressure of 3000 or 4000 if the medium is oil, or otherwise expressed, fracture at superposed tensions of 1500 and 3000 or 4000, respectively. But if the external medium is Neoprene or lead or copper we have seen that tensile fracture occurs at superposed tensions of 5900, 15,500, and 24,500 kg/cm², respectively. There is a specific effect of hydrostatic pressure concealed in this comparison, but this effect does not obscure the main result. The surface conditions at glass are doubtless complicated, and at least in the case of water involve a chemical factor as well as a purely mechanical factor, since it is known that water is forced by pressure into the surface layers of glass. Brittle substances thus differ essentially from the substances which flow plastically before yielding in tension which have been made the subject of previous study. In the case of these ductile substances, fracture starts in the interior on the axis, where the tensile stress is a maximum, because of the stress redistribution produced by the necking itself, and always at values of the tensile stress materially higher than the ambient hydrostatic pressure. Fracture under these circumstances is again an energy-releasing process, because although work is done against the external pressure when a cavity appears in the inside, nevertheless the work received from the tensile stresses more than compensates because of their greater intensity. The fact that fracture starts at the inside explains the consistency of the results on fracture of ductile substances as contrasted with the capriciousness of the results for a brittle substance like glass.

From the point of view of energy release it is easy to understand the very much greater strength of glass to compressive stresses when supported by hydrostatic pressure than to tensile stresses. In the experiments above under a hydrostatic pressure of 27,000 or 28,000 kg/cm² the maximum superposed tensile stress supported was 24,500 kg/cm² (copper sheath), whereas a superposed compressive stress of 47,000 was observed. When fracture occurs under tensile stress combined with hydrostatic pressure two processes

occur, both energy-releasing. The force producing the tension does work, and the pressure does work, because when tension is released the volume of the specimen decreases. But when fracture occurs under one-sided compressive stress, only one of the processes is energy-releasing. The force producing the compressive stress again does work during the fracture, but, since the volume increases on release of compressive stress, work is done against the pressure by the fracture.

From the point of view of energy release there is no particular significance as to whether the superposed tensile stress under which fracture occurs is greater or less than the hydrostatic pressure, that is, whether the tensile fracture occurs against a net tensile or compressive stress. For in either case the process of fracture may be resolved into two components, both energy-releasing. The significant thing is the lateral conditions, and the extent to which the surrounding hydrostatic pressure may follow through into any crack which appears, doing work in the process. In the case of ductile materials, when a crack appears on the surface the propagation is by a process of slip, which is not energy-releasing for the pressure, so that the fracture does not spread.

Both the strong dependence on the surface conditions in brittle fracture under hydrostatic pressure and the condition of energy release emphasize that there can be no single criterion of fracture in terms of stress and strain at a point only.

The actual experimental conditions differ from those of the idealized experiment in another important respect than the rigidity of the sheath, namely in the molecular structure of the specimen under test. In the idealized experiment, the material was thought of as structureless, and capable of indefinite and microscopically homogeneous distortion, as in the mathematical equations of elasticity theory. Actually, the material is composed of molecules, which have a certain impenetrability preventing indefinite approach, so that when strain is pushed too far individual molecules must be forced out of their positions by a series of discrete operations. It is doubtless something of this sort that is responsible for the remarkable separation of the glass tension specimens into thin disks, often, but not invariably, observed after simultaneous exposure of glass to pressure and tension. As tension increases, lateral contraction increases, and there must ultimately come a time when some of the molecules are brought into such close contact that they are forced out of their normal positions into neighboring spaces that have been opened by the simultaneous longitudinal extension. This process of molecular transfer is irreversible. When stress is released these displaced molecules act like internal wedges, distending the structure, which eventually fractures as in tension when stress is reduced far enough. A similar sort of thing has been found in other situations; fracture on release of stress would appear not to be uncommon. A somewhat similar state of affairs may be brought about in glass if foreign molecules are forced into the interior at the surface. Thus disking was almost always found in glass after a failure by the pinching-off effect in water as the transmitting medium.

The question has been much discussed of the great discrepancy between the experimental values of fracture stress and those calculated theoretically from various points of view. These considerations may have some bearing on this question. Strength in tension for a brittle substance we have seen to be an indeterminate matter, depending on the surface conditions. Under hydrostatic pressure breaking strengths in tension may be expected, with proper surface conditions, up to at least the magnitudes of the hydrostatic pressure. With pressures of the magnitude reached in these experiments, this is bringing the breaking stress up within reach of the theoretical values. In compression, dependence on the surface conditions is not to be anticipated, because the surface action that would take place at fracture is not energy releasing. Very large values of compressive strength can be reached, as for example 47,000 kg/cm$^2$ in Pyrex glass against some 2000 under ordinary conditions, or an increase of some 25-fold, again getting within sight of theoretical expectations.

It seems probable that the increases in compressive strength brought about by hydrostatic pressure are much greater for glass-like substances than for crystals. This is caused by the interlocking of the molecules in a glass, which is accentuated by pressure, making relative dis-

placement more difficult. The effect is analogous to the very large increase of viscosity under pressure observed in some liquids with complicated molecules. In a crystal, on the other hand, the regular structure provides the possibility of internal slip. The plastic distortion of the crystal of $Al_2O_3$ is a case in point. The behavior of a crystal under compression is doubtless a highly specific property of the kind of crystal; I have never been able to produce measureable flow in crystalline quartz, although experiments on the collapsing of negative crystals show that some flow must be present.

Certain of the points emphasized here recall the point of view of Poncelet in a paper in Volume VI of Alexander's *Colloidal Chemistry*. Poncelet regards brittle fracture in tension as originating at the surface, and also emphasizes the role played by the "particulate" structure of ordinary matter as distinguished from the homogeneous isotropic structure assumed in the mathematical theory of elasticity.

Rowe and Gurney[8] have concluded from their experiments on the fracture of glass under "radial" pressure (my "pinching-off" effect) that Griffith's theory of fracture is essentially correct. According to this theory an actual specimen of glass is filled with minute crevices, with corners so sharp that under ordinary tensile load there may be stress concentrations at the corners by as much as a factor of 600. The breaking strength of geometrically perfect glass would thus be of the order of 6,000,000 p.s.i., which is of the order of the theoretical value, whereas the strength of an actual piece of glass is of the order of only 10,000 p.s.i. Under radial pressure fracture starts at the surface cracks. Rowe and Gurney have shown that assuming stress concentrations of 600, failure under radial pressure would be expected to occur at a pressure very approximately equal numerically to the ordinary breaking stress in tension, and this does in fact approximately agree with their experimental results. I think it must be admitted that qualitatively the Griffith point of view has considerable to recommend it. The strong dependence of fracture on surface conditions, for example, is consistent with its picture.

Qualitatively, Griffith's picture would lead to the expectation of pressure coefficients of tensile strength of completely sheathed brittle material of the order of magnitude of unity, and this also agrees with the experimental results above, and again indicates a real value in Griffith's point of view. It would not be easy to make a more precise calculation of the exact coefficient to be expected for completely sheathed specimens, however, because of the complicated nature of the surface conditions, and various other over-simplifications discussed in the next paragraph.

I question, however, whether other considerations do not play a vital role and whether the Griffith's picture is not much over-simplified. For instance, the surface conditions are in fact complicated, and involve chemical as well as purely mechanical factors, as shown by the very great effect of pressure media such as water or alcohol as contrasted with the oil used by Rowe and Gurney. Again, the ordinary concepts of stress and strain are carried down to a fineness of scale where there are stress concentrations of 600, whereas stress and strain are properly macroscopic concepts. At this scale of magnitude, the conditions of fracture are applied in the form that fracture occurs when the maximum tension reaches a critical value, irrespective of the other components of stress and independent of the strains. This condition of fracture does not seem to me to have any greater plausibility on the microscopic scale than on the macroscopic scale. The assumption of such a criterion amounts, among other things, to postulating that a pure hydrostatic pressure exerts no specific effect on the fracture properties of a substance. This is certainly not the case for ductile substances, as shown by my experiments on the enormous increase of the ductility of steel under pressure. The same thing is shown by the experiments of Rowe and Gurney themselves on plastics, which under their conditions of radial pressure tolerated an elongation before fracture eighteen times greater than under normal conditions. These results can properly be described as an increase of ductility under pressure. If plastic materials have their properties thus drastically altered by hydrostatic pressure it would seem to be only reasonable to expect some effect also on brittle substances. This is strongly suggested by the great increase of strength to simple compressive stresses found above for glass under high pressure.

[8] C. Gurney and P. W. Rowe, Second reference under 5.

The high tensile strength acquired by Carboloy under pressure is worthy of notice. The tensile stress at fracture is much higher than the surrounding hydrostatic pressure in the case of this material, so that the net stress at fracture is a tension. It is not necessary in this, or similar cases, therefore, to suppose that surface conditions play any role in the process, and the increase of strength may be a specific effect of pressure. The absolute value of the tensile strength, between 50,000 and 60,000 kg/cm², is not far from that which has been observed in steel, pulled to the limit of ductility and strain-hardened under pressure. A possible explanation of the effect in Carboloy is that it is associated with the cementing film of cobalt on the surface of each grain of carbide; the cobalt becomes ductile under pressure and strain-hardens in a way similar to steel.

A question that naturally presents itself in connection with these experiments is under what conditions does a substance lose its brittleness and become ductile under pressure? In order to deal with this question it is necessary to consider the concept of brittleness itself. It is not uncommon to speak of a brittle fracture, and in fact this usage has been followed in this paper. Such usage, however, employs a specialization and extension of meaning, because "brittle" properly does not refer to the process of fracture, but to what comes before the fracture. If the substance fractures before it receives permanent set, as shown by a permanent change of dimensions on release of stress, then the substance is brittle; if the substance fractures after it has received permanent set, then it is plastic or ductile. So far as the act of fracture itself is concerned it may be characterized as a shearing fracture or a tensile fracture, but not as a brittle fracture. When a brittle fracture is spoken of, what is meant is the fracture of a brittle substance. But strictly, from this point of view, all fractures might be spoken of as brittle, for a plastic substance which has been work-hardened to the limit and then fractures is, when at the point of fracture, a brittle substance. There is thus a considerable verbal element in the concept of brittle. Furthermore, the concept is not sharp, because if measurements are increased in sensitiveness plastic flow may be discovered before fracture where formerly with rougher measurements none appeared. In practise all that can be meant is fracture with no noticeable preliminary distortion.

In answer to our question as to what substances lose their brittleness under pressure, it may now be said that as a rough qualitative matter a crystalline substance, particularly if it is cubic, is more likely to become measureably plastic under pressure than an amorphous substance like glass. The observed plasticity of crystalline $Al_2O_3$ described in this paper lends plausibility to this statement. The limits are not sharp, however, and there is enormous variation in the numerical magnitude of the effect, as illustrated by the variation from soft steel to beryllium. In fact, even in the case of quartz crystal or glass an infinitesimal amount of flow must exist in principle, as shown by the spontaneous breakage of these materials under some circumstances a long time after exposure to high pressure.

## Addendum and Erratum: the Thermoluminescence and Conductivity of Phosphors*

[J. App. Phys. 17, 743 (1946)]

ROBERT C. HERMAN AND CHARLES F. MEYER
*Applied Physics Laboratory, Johns Hopkins University, Silver Spring, Maryland*

(Received November 21, 1946)

IN a recent paper with the above title,[1] the variations in the luminescence and conductivity of zinc sulphide type phosphors during infra-red illumination were discussed. The solutions given for the differential equations describing these processes are valid only in the case in which the retrapping of electrons is negligible. Recently, Klasens and Wise[2] derived the solution for the

* A portion of the work described in this paper has been supported by the Bureau of Ordnance, U. S. Navy, under contract NOrd-7386.

[1] R. C. Herman and C. F. Meyer, J. App. Phys. 17, 743 (1946).

[2] H. A. Klasens and M. E. Wise, Nature 158, 483 (1946).

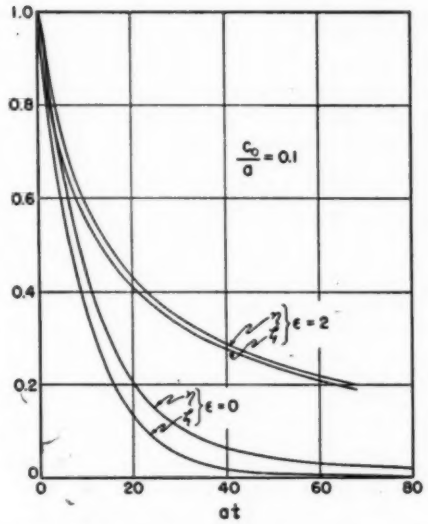


FIG. 1. The fraction of empty luminescent centers, $\eta$, and the fraction of trapped electrons, $\zeta$, *versus at* for $c_0/a=0.1$ and $\epsilon=0$, 2.

special case in which the cross section for capture of a conduction electron into a trap is equal to the cross section for capture into an empty luminescent center or hole. At the present time we are obtaining general solutions to this problem by means of a differential analyzer and wish to indicate some of the preliminary results.

The general solutions of Eq. (1) in reference 1 involve the following parameters[3]: $\epsilon$, the ratio of the cross sections for electron capture into empty traps and empty luminescent centers or holes and the parameter $c_0/a$, where $c_0=\sigma I_0/h\nu$, and $a=AN_1$. In Fig. 1, the fraction of empty luminescent centers, $\eta$, and the fraction of trapped electrons, $\zeta$, are plotted *versus at* for $\epsilon=0$ and 2 with the time $t$ in seconds. The corresponding variations of the luminescent intensity, $I$, proportional to $\xi\eta$, are plotted in Fig. 2. The

[3] Note that $A=\sigma V$, where $\sigma$ is the cross section for capture into a hole, $V$ the velocity of a conduction electron; $I_0$ is the intensity of the incident infra-red light, and $N_1$ the number of electrons per cm³ trapped originally.

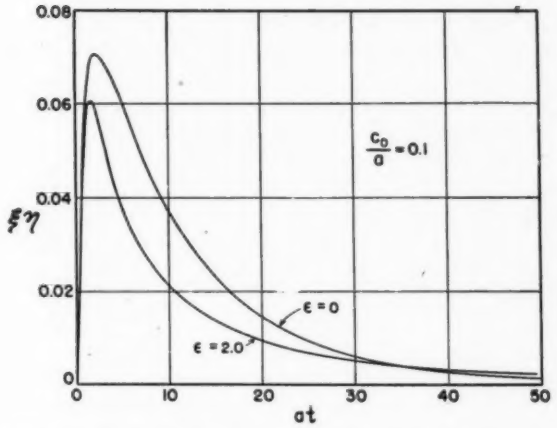


FIG. 2. The variations of $\xi\eta$, proportional to the luminescent intensity, *versus at* for $c_0/a=0.1$ and $\epsilon=0$, 2.

behavior of $\xi$, which is proportional to the current $i$, can be obtained from Fig. 1 since $\xi=\eta-\zeta$.

We take this opportunity to point out that Eq. (12) in our recent paper[1] should be written as follows:

$$\eta^{-1}=\exp(y-a/c_0) - (a/c_0)[Ei(-y)-Ei(-y_0)]\exp y$$

where $y=(a/c_0)\exp(-c_0t)$, $y_0=a/c_0$, $a=AN_1$, and $\eta=n_0/N_1$. This modifies Fig. 4 of the original paper in the manner shown for $\epsilon=0$ in Figs. 1 and 2 of this note. The conclusions drawn from Fig. 5 remain unaltered.[1]

More detailed information on the effect of the retrapping of electrons on the luminescence and conductivity of phosphors during infra-red illumination as well as on the phenomenon of thermoluminescence will be published in the future.

We express our appreciation to Drs. G. C. Munro and D. T. Sigley of the Applied Physics Laboratory for their interest in this problem and thank the differential analyzer staff of the Moore School of Electrical Engineering, University of Pennsylvania for their cooperation.

# Letters to the Editor

## On the Action of Cutting Oils

G. P. Brewington
*Lawrence Institute of Technology, Detroit, Michigan*
December 5, 1946

Ernst and Merchant[1] have studied the efficiency (cutting ratio) of a number of cutting fluids on several metals and, for aluminum, have attempted to relate various physical properties of these fluids with observed cutting performance. They conclude ". . . that no relationship whatever appears to exist between the physical property and the cutting ratio." Even though the data given either in the paper referred to in reference 1 or in other sources are not as extensive as desired, it appears that some relationship does exist.

Those materials having a high cutting ratio appear to belong to that group of compounds having a sulfur (−SH) or chlorine in a low state of valence at the end of a short chain hydrocarbon. This would suggest that some of the higher valences of the sulfur and chlorine become active in the strong force fields known to exist at the newly formed surfaces of the work and chip, with the result that the molecule then adheres to the surface, thus reducing its activity and tendency to seize. The element fluorine exhibits only one valence but does form an analogous group of compounds similar to those of chlorine; it should be interesting, therefore, to compare the cutting ratios of these two fluids. The results obtained from cutting measurements on aluminum using a series of alcohols as cutting fluids may be due to a more common type of chemical action. If certain assumptions in the use of thermochemical data can be granted, the methanol-aluminum surface reaction must be sufficiently energetic to remove completely an aluminum atom, while the higher alcohols tend to attach themselves, through the −OH radical, to the surface and form a monomolecular film. It would appear that an approach somewhat different from that used by Ernst and Merchant could be found in the surface energy studies of Bartell *et al.*[2]

The literature in the field of cutting oils is largely in the form of advertising and, while quite readily available, does not yield much quantitative information. Apparently innumerable experiments have been performed and reported only by word of mouth. Among such is a statement of high success associated with the use of a small stream of dry HCl gas playing on the cutting edge of a tool cutting steel. Should the HCl gas be as good as reported, and the cutting ratio as a function of cutting speed curve, as observed by Ernst and Merchant,[1] change materially, some indication as to the role of diffusion of the active agent in cutting phenomena might be obtained. Certainly the mobility of HCl gas would be much higher than that of larger organic molecules dissolved in liquids. It also should prove very interesting, if further data were available, to attempt to correlate the "cutting ratio" of various fluids with electron configurations of the active end of the molecule.

The cutting process viewed from any angle is extremely complicated and anyone who attempts to single out one phenomena for consideration is on dangerous ground. Assuming however, for this discussion, that tool failure at least depends on fatigue, which frequently can be associated with oscillation or standing wave phenomena, the varying force experienced by a tool tip must set up a standing wave pattern, possibly of ultrasonic frequencies, in the tool itself. This would suggest that the tool shape, particularly in carbide tools, should be such as to offer less opportunity for well-developed standing wave patterns to become established. One isolated unintentional experiment, reported verbally to the author, in which an "irregular chunk" of carbide brazed in a tool gave very good life, tends to suggest that other than the conventional form of tools might be further investigated.

The author wishes to thank Mr. H. A. Montgomery, president of the H. A. Montgomery Oil Company, for first suggesting that a problem, somewhat related to that discussed above, should be studied and also to Mr. W. Woijtowicz for many discussions of similar phenomena.

[1] "Surface Treatment of Metals," Symposium, Am. Soc. Metals (1940).
[2] Am. Chem. Soc. **56**, 2205 (1934); J. Phys. Chem. **40**, 881, 889, 895 (1936).

## Approximation for Absorption Displacement in X-Ray Diffraction by Highly Absorbing Cylindrical Samples

Zigmond W. Wilchinsky
*Esso Laboratories, Standard Oil Company (N. J.), Baton Rouge, Louisiana*
November 18, 1946

In an article by Warren[1] treating displacement of diffracted x-rays caused by absorption in cylindrical samples, it was shown that for very high absorption, the displacement $\Delta S$ on the film is given by

$$\Delta S=(1+R/D)r\cos\theta\left\{\frac{\sin 2\theta-2\theta\cos 2\theta}{4\sin\theta+4\cos^2\theta\ln\tan\left(\frac{\pi}{4}-\frac{\theta}{2}\right)}\right\}, \quad (1)$$

where $R$ is the radius of the Debye camera used, $r$ is sample radius, and $D$ is the distance from the sample to the point

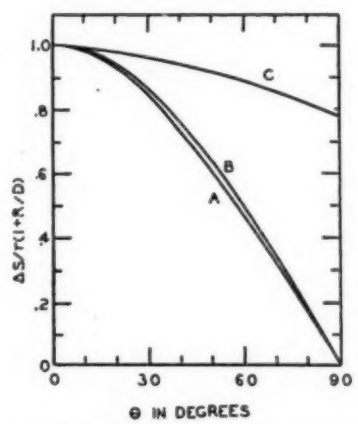


Fig. 1. Comparison of exact expression curve *A* with approximation curve *B*. Ratio of *A* to *B* is shown in *C*.

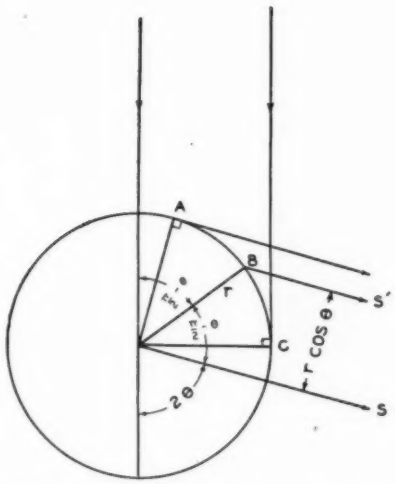


FIG. 2. Diffraction of a parallel x-ray beam from the surface of a highly absorbing cylindrical sample. By virtue of the above construction, $B$, the center of arc $ABC$ lies on the bisector of the supplement of $2\theta$ giving the above relationship among the angles.

from which the beam diverges. The purpose of this note is to point out that an approximation useful for general work is simply

$$\Delta S = (1+R/D)r\cos\theta. \qquad (2)$$

This approximation is compared with Eq. (1) in Fig. 1. It can be noted that the approximation is best for small values of $\theta$. As $\theta$ increases, the magnitude of the departure increases at first, goes through a maximum, then decreases to zero at $\theta=90°$. The fractional departure however, increases steadily as can be gathered from curve $C$ which is the ratio of (1) to (2), or simply the bracket in (1). At $\theta=90°$, curve $C$ attains the value $\pi/4$.

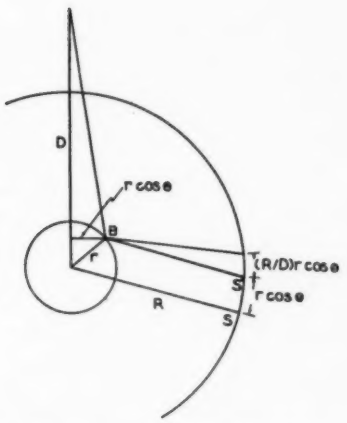


FIG. 3. Additional displacement caused by beam divergence.

A physical interpretation of the approximation (2) can be obtained with the aid of Fig. 2. First consider a parallel incident beam. For the right half of the sample, only the surface generated by moving $ABC$ parallel to the sample axis is capable of contributing to the diffraction corresponding to $\theta$. *Assuming* that the center of gravity of the diffracted beam coincides with the ray diffracted from $B$ the center of arc $ABC$, we find that $S'$ is displaced parallel to the ideal position $S$ by an amount $r\cos\theta$.

If the beam diverges from a point distant $D$ from the sample (see Fig. 3), the angle of divergence of the ray to $B$ is very nearly $(r/D)\cos\theta$. Therefore at the film, the ray diffracted from $B$ is deviated by an amount $R(r/D)\cos\theta$, in addition to the quantity $r\cos\theta$ for the parallel case; the sum of the two effects is Eq. (2).

[1] B. E. Warren, J. App. Phys. 16, 614 (1945).

# Here and There

### New Appointments

J. H. Dillon, formerly with the Firestone Tire and Rubber Company, is now director of research of the Textile Research Institute, Inc., and of The Textile Foundation.

Frank M. Clark, insulation expert at the Pittsfield Works of the General Electric Company's Apparatus Department and assistant engineer of the Works Laboratory there, has been named technical consultant on insulation of the entire Apparatus Department.

W. Ewart Williams, English scientist now residing in the United States, has been appointed a consulting physicist on the research and engineering staff of Bausch and Lomb Optical Company.

### Awards

The Medal of Freedom, the nation's second highest decoration for civilian achievement in wartime, was awarded recently to two members of the staff of the National Bureau of Standards: Lauriston S. Taylor, chief of the X-Ray Section, and Fred L. Mohler, chief of the Atomic Physics Section. Mr. Taylor was also awarded the Bronze Star Medal.

### Electron Jubilee Celebrations

The fiftieth anniversary of the discovery of the electron by the British physicist, Sir Joseph Thomson, will occur this year. To mark this jubilee and to demonstrate the tremendous influence such an advance in pure physics may have on the life of the community, the Institute of Physics and the Physical Society are jointly arranging a series of meetings and other functions to take place on September 25 and 26, 1947, in London. A special exhibition which will remain open to the public for several weeks will be held at the Science Museum, South Kensington, and will show the development of the vast range of modern industrial equipment from its earliest experimental origins.

### Radio Engineering Show in March

The Annual Radio Engineering Show, a part of the 1947 National Convention of The Institute of Radio Engineers, will be held in Grand Central Palace, New York, March 3–6, 1947. The displays will be strictly of an engineering nature—transmitter equipment, instruments, component parts, and radio direction and location devices.

### Commemoration Program at Argonne National Laboratory

Major General Leslie R. Groves and Enrico Fermi were the principal speakers at the anniversary program held December 2 at the Museum of Science and Industry in Chicago, commemorating the initial operation of the first self-sustaining nuclear chain reaction.

### Research Physicists and Engineers Needed by NACA

The following statement was issued recently by the National Advisory Committee for Aeronautics:

"Physicists and engineers with research experience in problems related to aeronautics are needed by the National Advisory Committee for Aeronautics. Areas of research include the following: electronics, electrical measurements, servomechanisms, optics, interferometry, spectroscopy, electron or x-ray diffraction, mechanics of static or moving bodies, thermodynamics, aerodynamics, hydrodynamics, gas dynamics, metallurgy, lubrication, heat engines, mathematics, and other fields.

"The work of the NACA is to solve the fundamental problems of flight. This work is accomplished by means of basic research, consisting of experimental investigations and the development of theories needed for the prediction and explanation of aeronautical phenomena. The information obtained from this basic research is disseminated through publications to the field of aeronautics, where its application leads finally to the design and development of the nation's aircraft.

"This work is carried forward at three laboratories. The Langley Memorial Aeronautical Laboratory, Langley Field, Virginia, and the Ames Aeronautical Laboratory, Moffett Field, California, were constructed for, and are principally devoted to aerodynamic studies of the problems of flight and aircraft structures. Both are devoting a major portion of their work to fundamental problems of transonic and supersonic flight. Langley is also doing advanced research on the problems of guided missiles.

"The Aircraft Engine Research Laboratory, Cleveland, Ohio, is specifically designed for aircraft propulsion research. At the present time, the Cleveland facilities are primarily devoted to research investigations of the turbo jet, turbo propeller, ram jet, and rocket type power plants.

"Applications for positions or requests for further information should be addressed to the personnel officer of one of the laboratories."

## Calendar of Meetings

**February**

| | |
|---|---|
| 15 | American Geophysical Union, Pasadena, California (Section of Hydrology) |
| 16–19 | American Institute of Chemical Engineers, Louisville, Kentucky (regional meeting) |
| 20–22 | Optical Society of America, New York, New York |
| 22 | American Mathematical Society, New York, New York |
| 24–25 | Inter-Society Color Council, New York, New York (Joint Meeting with the Technical Association of the Pulp and Paper Industry on the 25th) |
| 24–27 | Technical Association of the Pulp and Paper Industry, New York, New York |
| 24–28 | American Society for Testing Materials, Philadelphia, Pennsylvania |

**March**

| | |
|---|---|
| 2–5 | American Society of Mechanical Engineers, Tulsa, Oklahoma |
| 3–6 | Institute of Radio Engineers, New York, New York |
| 17–21 | American Institute of Mining and Metallurgical Engineers, New York, New York |
| 22–27 | American Society for Metals, Oakland, California |
| 28 | Institute of Aeronautical Sciences, Cleveland, Ohio |

**April**

| | |
|---|---|
| 4–5 | American Physical Society, Southeastern Section, Salisbury, North Carolina |
| 9–11 | Society of Automotive Engineers, New York, New York (Aeronautic Meeting) |
| 14–18 | American Chemical Society, Atlantic City, New Jersey |